H2 TECHNOLOGY CONSULTING

H2 Technology Consulting, LLC
kgross@h2techconsulting.com
tel: (510) 468-7515

Recommended Best Practices for Characterizing Engineering Properties of Hydrogen Storage Materials

Karl J. Gross, H2 Technology Consulting LLC
Bruce Hardy, of Savannah River National Laboratory

We gratefully acknowledge assistance and financial support from the U.S. Department of Energy Office of Energy Efficiency and Renewable Energy Hydrogen Storage Program.

National Renewable Energy Laboratory Contract No. 147388
Contract Technical Monitor: Dr. Philip Parilla

List of Figures

List of Tables

Recommended Reading

This document is not meant to be a thorough review of the leading work in this field, but rather an overview and series of instructive examples of important issues concerning the measurement of the kinetic properties of hydrogen storage materials. The following resources are a good place to find more detailed information on the key topics.

1 Hydrogen Storage

The book "Solid-state hydrogen storage: materials and chemistry", edited by Walker.[1]

The book "Hydrogen Storage Materials (Materials Science Forum)" edited by Barnes.[2]

The review article "Hydrogen-storage materials for mobile applications" by Schlapbach and Züttel.[3]

European Commission Joint Research Centre Institute for Energy (JRC) Scientific and Technical Reports by D. P. Broom, "Hydrogen Sorption Measurements on Potential Storage Materials".[4]

2 Hydrides

The book "Hydrides" by Wiberg and Amberger.[5]

3 Metal Hydrides

The book "Metal Hydrides" edited by Muller, Blackledge, and Libowitz.[6]

The book "Transition Metal Hydrides" edited by Dedieu.[7]

The review article "A panoramic overview of hydrogen storage alloys from a gas reaction point of view" by Sandrock.[8,9]

4 Off-board Regenerable Hydrogen Storage Materials

The article "Ammonia–borane: the hydrogen source par excellence?" by Frances H. Stephens, Vincent Pons and R. Tom Baker.[10]

The chapter "Aluminum Hydride" by Ragaiy Zidan in the book, "Handbook of hydrogen storage: New Materials for Future Energy Storage".[11]

5 Physisorption Storage

The review article “Hydrogen adsorption and storage on porous materials” by K.M. Thomas.[12]

6 Thermodynamics

The review article “Materials for hydrogen storage: current research trends and perspectives” by A.W.C. van den Berg and C.O. Arean.[13]

The article “Heat of Adsorption for Hydrogen in Microporous High-Surface-Area

Materials” by B. Schmitz, U. Muller, N. Trukhan, M. Schubert, G. Ferey, and M. Hirscher.[14]

“Perry's Chemical Engineers' Handbook” by R. H. Perry and D. W. Green.[15]

B. N. Roy (2002). Fundamentals of Classical and Statistical Thermodynamics. John Wiley & Sons. ISBN 0-470-84313-6.[16]

F. Reif (1965). "Chapter 5 – Simple applications of macroscopic thermodynamics". Fundamentals of Statistical and Thermal Physics. McGraw-Hill. ISBN 0070518009.[17]

7 Engineering Thermal Properties

“Basic Heat Transfer”, by M. Necati Özişik.[18]

“A Heat Transfer Textbook”, 4th edition by J.H. Lienhard IV and J.H. Lienhard V.[19]

"The thermal conductivity of liquids and dense gases," by E. McLaughlin.[20]

“Heat transfer—a review of 1985”, “1993”, “1999”, “literature”, by E.R.G Eckert et al.[21,22,23]

“Convection in Porous Media”, by Donald A. Nield, Adrian Bejan.[24]

“Springer Handbook of Metrology and Testing”, by Czichos, H. and Saito, T. and Smith, L.M. and Smith, L.E., (2011), Springer.[25]

“A Practical Introduction to Differential Scanning Calorimetry”, by Paul Gabbott, in the book “Principles and Applications of Thermal Analysis” [26]

Section 6: Measurements of Engineering Thermal Properties of Hydrogen Storage Materials

1 Introduction

Knowledge of the thermal performance properties of materials is critical in the engineering design of materials-based scaled-up hydrogen storage systems. Thermal properties such as thermal conductivity and heat capacity have a large impact on the performance, cost and efficiency of the storage system. Engineered systems will rely heavily on the ability not only to modify the material and system's thermal properties, but also on our ability to measure these properties accurately and in a manner that is highly representative of how the materials will behave in a full-scale system.

For this reason, it is absolutely critical that the measured thermal properties of hydrogen storage materials accurately represent the materials as they will be used in the actual real world application. Many hydrogen storage materials themselves undergo significant thermal property changes as a function of preparation, capacity, and cycling. Additionally, important thermal properties such as thermal conductivity and heat capacity are strongly dependent on the environmental conditions (operating temperature, presence of hydrogen gas, pressure of hydrogen, mobility of gaseous hydrogen….) in the storage system. Therefore, it is recommended that these material properties measurements be performed on the materials as they will be used in the application: For reversible materials, measurements should be made after the materials have been cycled to a point that they have achieved steady-state performance and under different capacity conditions (fully discharged, half capacity and fully charged conditions). For all hydrogen storage materials (solids and liquids), thermal properties should ideally be measured in situ under the applicable conditions of hydrogen pressures and temperatures found during storage system operation. While these conditions are not typical of standard thermal properties measurements and potentially difficult to perform, measurements under any other conditions will bring into question the validity of the data in predicting the performance of the materials in a real application.

Heat transfer in a media is customarily divided into 3 different modes of energy exchange: 1) Conduction, 2) Convection, and 3) Radiation. In real applications, all of these modes typically contribute to heat transfer to one degree or another and it is not

possible to completely isolate one mode from another. However, for most materials-based hydrogen storage systems, heat transfer occurs primarily through conduction, and the contributions from convection and radiation are often neglected. For this reason, the principal focus of this document will be on the measurement of the thermal conductivity of hydrogen storage materials. An exception to this is that convective heat transfer is the principal mode of heat transfer for cooling (or heating) fluids that are used in complete storage systems. In addition, advanced storage bed modeling includes the convective heat transfer of hydrogen gas entering or leaving the storage bed. Thus, convection plays an important role in system modeling and will be briefly discussed in that regard.[27,28]

This section of the Best Practices document provides a review of measurement techniques currently being used for measuring thermal properties of hydrogen storage materials. As this has not been done extensively in the hydrogen storage field, this section also includes an evaluation of common thermal property measurement methods used in other applied materials fields that may be appropriate for hydrogen storage materials. The main focus of this section is to clarify problem areas in these measurements and to establish common methods and best practices. The following key aspects (and difficulties) of thermal property measurements are covered herein:

Thermal conductivity measurements:

The relative impact of a thermal conductivity of hydrogen storage materials on total system performance. How thermal conductivity data is used in the engineering design of the storage system. What types of data are currently available, useful, and not available but needed.

Heat capacity measurements:

The importance of a materials heat capacity with respect to system performance.

Topics covered:

- Appropriate methods for measuring thermal conductivity and heat capacity of different hydrogen storage materials (reversible hydrides, off-board regenerable, and physisorption hydrogen storage materials). These will include both solids and liquids over a wide range of operating temperatures (77K to 500K).
- An evaluation of the accuracy or issues related to the accuracy of different measurement techniques when applied to hydrogen storage materials.
- The ability to make measurements under hydrogen at typical application pressures.

- Methods and the importance of performing measurements at specific materials hydrogen storage concentrations.
- The ability to perform simple and accurate measurements on materials that require controlled environments (airless setup or inert gas glove box operations).
- The validity of translating measurements on small samples to full systems scale performance.
- The impact on the measurement technique of materials being in loose powder, compressed powder, bulk compact forms or a liquid.
- The ability to generate useful data for modified materials including the use of additives, designed materials morphology, or incorporated thermal enhancement components and structures.
- The impact on thermal conductivity changes due to cycling or, in the case of off-board regenerable materials, decomposition.

The impact of many of the same issues listed above, including sample form, additives and cycling.

Heat Transfer

The following is a brief introduction to the general concepts of the thermal properties of materials. For a detailed review of thermodynamics and the measurement of thermodynamic properties of hydrogen storage materials, please refer to Section 5, Thermodynamics of the Best Practices document "Recommended Best Practices for the Characterization of Storage Properties of Hydrogen Storage Materials".[29,30]

Energy transfer by heat flow cannot be measured directly. However, heat transfer has physical meaning as it relates to the measurement of temperature distribution. The study of heat transfer is often presented in terms of three distinct modes: Conduction, Convection and Radiation. In practice, the distribution of heat in a material or system is typically controlled by a combination of these three modes of heat transfer. As a consequence, measurements to evaluate heat flow will generally be effected by all three physical modes of heat transfer. Under special conditions (such as solid samples, vacuum, etc.) it may be possible to reduce the measurement to one or two modes of heat transfer to gain more insight into the predominant mechanism. As mentioned above, this document focuses primarily on conduction as it most directly relates to hydrogen storage materials R&D. However, we present here a brief overview of convection and radiation as well.

Thermal Convection

Convection heat transfer is the transfer of heat resulting from the bulk motion of a fluid. In hydrogen storage systems convection heat transfer arises from the flow of hydrogen through the storage media, the flow of a heat transfer fluid through tubes or other passages within the storage vessel, flow of gas over pelletized storage media and a number of other processes. Convection due to hydrogen flow within the storage media bed is best modeled using an energy transport equation formulated in terms of enthalpy and coupled with appropriate equations for mass and momentum transport. Convective heat transfer for heat exchange tubes or other passages within the storage vessel are typically modeled by using correlations for the Nusselt number to obtain the convection heat transfer coefficient. The Nusselt number (Nu ≡ hL/k) represents the ratio of the rates of convection to conduction within the fluid. Here L is a characteristic length, h is the convection heat transfer coefficient of a fluid, and k is the thermal conductivity of the fluid.

Thermal Radiation

Thermal radiation becomes important for storage systems operating at temperatures that greatly differ from the ambient. This situation occurs for cryo-adsorption systems, especially in dormancy calculations. For dormancy heat loss, thermal radiation is the predominant mechanism for heat transfer across vacuum insulation on the exterior of the pressure boundaries. In cryo-adsorption systems thermal radiation from the bed into piping will also contribute to heat transfer from the media. However, proper design of piping and other penetrations will minimize this form of parasitic heat transfer. The majority of thermal radiation heat transfer is thus characterized by the geometry and emissivity of the surfaces that bound the evacuated part of the insulation.

Thermal Conductivity

1 Thermal Conductivity – Importance

The thermal conductivity measurement of hydrogen storage materials is an important parameter in the design and ultimate performance of an on-board fuel system. Since material-based storage systems (e.g. metal hydrides or adsorbents) depend on the hydrogen binding energy, the temperature and pressure operating conditions need to be maintained within a desired range to maximize the storage density of the system. In particular, the uptake of hydrogen by the material can be significantly reduced due to the increase in temperature during fueling from the heat of absorption/adsorption, the compression work, and the inlet hydrogen gas. Typically, these material-based systems

incorporate a heat exchanger within the material bed for managing the temperature during fueling and hydrogen delivery. The thermal conductivity properties have a direct influence on the heat exchanger design. If the thermal conductivity is incorrectly measured too low, the heat exchanger could be over-designed which adds unnecessary weight, cost, and complexity. If the thermal conductivity is incorrectly measured too high, the heat exchanger will underperform which will increase the fueling times and reduce storage capacity along with the transient response of the material. This situation is made more complex by the variation in effective thermal conductivity that will be experienced in practice due to the hydrogenation process and the fluctuating concentration of hydrogen and bed temperature, as will be detailed later in section 6.1.1 for example. It is not uncommon for hydrogen storage materials to have poor heat conduction properties. As a counter-measure, material enhancements (e.g. graphite) can be added to the material to form a composite to increase their thermal conductivity. These enhancement materials typically displace the storage material, which results in a decrease in the system storage capacity and an increase in the system weight. Therefore, it is important to accurately measure thermal conductivity to minimize the amount of the enhancement materials.

2 Theory

Thermal conductivity, k (or sometimes denoted as λ), is the property of a material's ability to conduct heat. It appears primarily in Fourier's Law for heat conduction. A critical property to be determined for materials based hydrogen storage systems, is the bulk effective thermal conductivity. In this case, "bulk" refers to measurement of thermal conductivity on a volume of material that is significantly larger than that of an individual particle. The Effective thermal conductivity (k_{eff}) incorporates all forms of heat transfer (versus Thermal Conductivity (k) which is strictly for heat transfer by conduction of homogeneous materials). Effective thermal conductivity is the value that is determined for the combined system including hydrogen gas and storage materials. It is also the appropriate term for solids that are not homogeneous or uniform (powders, porous media…). A material's actual thermal conductivity (k) may not only be difficult to measure but is most likely not representative of the thermal properties of the material in a hydrogen storage application. The challenge of determining k_{eff} (versus k) is that it is dependent on a wider range of system variables including interstitial gas type and pressure.

2.1 Thermal Conductivity of Solids

Conduction is the mode of heat transfer in which energy exchange takes place from a region of high temperature to a region of low temperature by the kinetic motion or direct impact of molecules, as in the case of a fluid at rest, and by the drift of electrons,

as in the case of metals.[18] In conduction, the heat flows through matter itself, as opposed to its transfer by the bulk motion of the matter as in convection, or by thermal radiation.

In solids, heat transfer by conduction is due to the combination of vibrations of the molecules in a lattice or phonons as well as by the energy transported by free electrons. In gases and liquids, conduction is due to the collisions and diffusion of the molecules during their random motion.

Thermal Conductivity of solids must be derived from experimental measurements since they depend on many factors that are difficult to measure or predict. For example in crystalline materials, the phase and crystallite size are important. In porous solids, the thermal conductivity is highly dependent on void fraction, pore size and the fluid contained in the pores (e.g. gaseous or liquid H_2, etc.)

Heat: As a form of energy, heat has the unit joule (J) in the International System of Units (SI). However, in many applied fields in engineering the British Thermal Unit (BTU) and the calorie are often used. The standard unit for the rate of heat transferred is the watt (W), defined as joules per second.

The total amount of energy transferred as heat is conventionally written as Q for algebraic purposes. Heat released by a system into its surroundings is by convention a negative quantity (Q < 0); when a system absorbs heat from its surroundings, it is positive ($Q > 0$).

Heat Flow: Heat transfer rate, or heat flow per unit time, is denoted by

Equation 1

$$\dot{Q} = \frac{dQ}{dt}$$

Heat Flux: Heat flux is defined as rate of heat transfer per unit cross-sectional area, resulting in the unit watts per square meter and will be denoted by its direction in this text (i.e.: Q_x for heat flux in the direction x, or Q_r for radial heat flow).

Thermal Conductivity: Thermal conductivity is a property of a conducting medium and, like the viscosity, is primarily a function of temperature.[31] Thermal conductivity k *(sometimes given by the symbol λ),* in ($W \cdot K^{-1} \cdot m^{-1}$), describes the ability of a material to transfer heat. This transfer of heat is defined by Equation 2 (This equation is called Fourier's law):

Equation 2

$$Q_x = -kA\frac{\mathrm{d}T}{\mathrm{d}x}$$

where Q_x is the heat transfer rate in the x direction, in W; A is the area normal to direction of heat flux, in m^2; dT/dx is the temperature gradient in the x direction, in $K \cdot m^{-1}$, and k is the thermal conductivity, in $W \cdot K^{-1} \cdot m^{-1}$. The negative sign indicates that the flux is down the gradient, and it can be shown from irreversible thermodynamics that the coefficient k is always positive.

Multiplied by a temperature difference (in kelvins, K) and an area (in square meters, m^2), and divided by a thickness (in meters, m), the thermal conductivity predicts the rate of energy loss (in watts, W) through a piece of material. Thermal conductivity and conductance are analogous to electrical conductivity ($A \cdot m^{-1} \cdot V^{-1}$) and electrical conductance ($A \cdot V^{-1}$).

In its most simple form, the measurement of thermal conductivity of a solid involves applying heat to one end of a sample of a uniform shape and measuring Q_x and dT/dx to determine k by means of Equation 2.

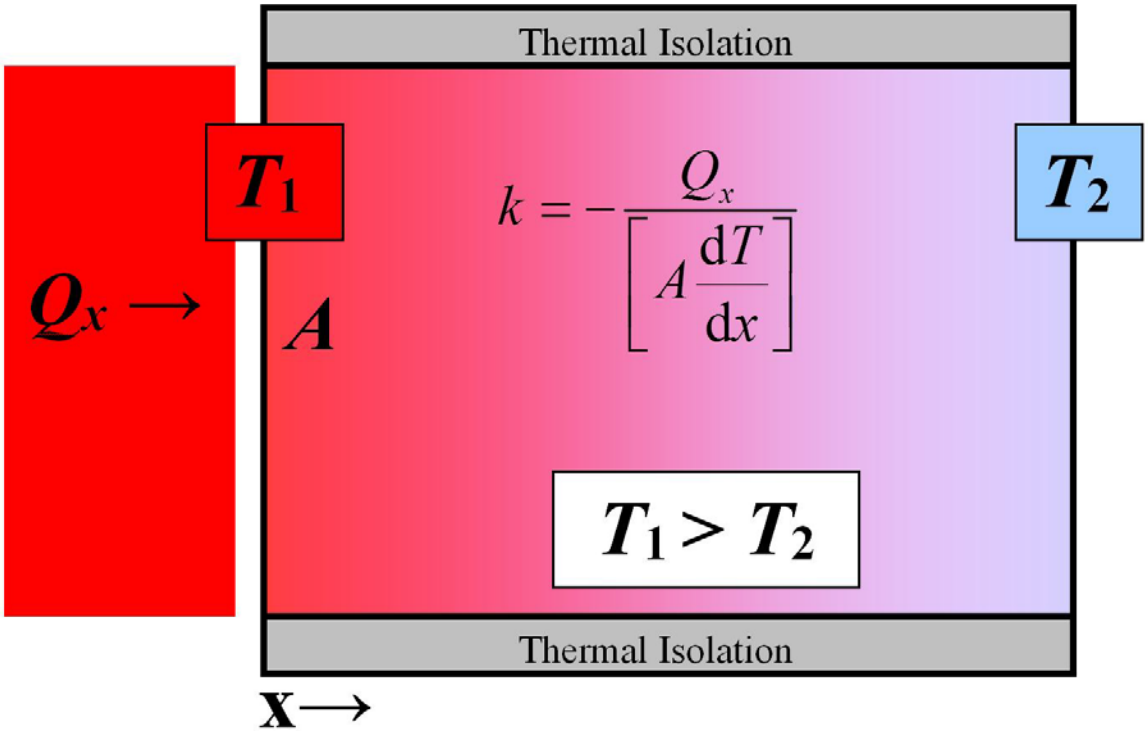

Figure 1. Schematic diagram a simple thermal conductivity measurement of a solid.

Thermal resistivity: is the inverse of thermal conductivity and is usually presented in units of kelvin-meters per watt ($K \cdot m \cdot W^{-1}$). For a fixed amount of material, thermal conductivity and thermal resistivity are expressed as the object's thermal conductance and thermal resistance respectively. Depending on the use, however, there are differing definitions for these terms.

Conductance: In scientific use, thermal conductance is the quantity of heat that passes in unit time through a plate of particular area and thickness when its opposite faces differ in temperature by one degree kelvin.

Heat transfer coefficient: is another related term that is the quantity of heat that passes in unit time through unit area of a plate of particular thickness when its opposite faces differ in temperature by one degree kelvin. The reciprocal is thermal insulance.

Resistance: ($K \cdot W^{-1}$) is the reciprocal of thermal conductance. When thermal resistances occur in series, they are additive. For example, when heat flows through two components each with a resistance of 1 $K \cdot W^{-1}$, the total resistance is 2 $K \cdot W^{-1}$.

Working in units of thermal resistance greatly simplifies design calculations. An example of a typical engineering design problem involves the selection of an appropriately sized heat sink for a given source of heat. The following formula can be used to estimate the performance:

Equation 3

$$R_{hs} = \frac{\Delta T}{P_{th}} - R_s$$

where R_{hs} is the maximum thermal resistance of the heat sink to ambient, in $K \cdot W^{-1}$ or $°C \cdot W^{-1}$, ΔT is the temperature difference (temperature drop), in K or °C, P_{th} is the thermal power (heat flow), in watts, and R_s is the thermal resistance of the heat source, in $K \cdot W^{-1}$ or $°C \cdot W^{-1}$.

For example, using Equation 3, if a component produces 100 W of heat, and has a thermal resistance of $0.5°C \cdot W^{-1}$, what is the maximum thermal resistance of the heat sink? Suppose the maximum temperature is 125°C, and the ambient temperature is 25°C; then the ΔT is 100°C. The heat sink's thermal resistance to ambient must then be $0.5°C \cdot W^{-1}$ or less.[30]

Transmittance: incorporates the thermal conductance of a structure along with heat transfer due to convection and radiation. It is presented in the same units as thermal conductance and is sometimes known as the composite thermal conductance. The term U-value is synonymous with transmittance.

Effective Thermal Conductivity: There are three basic modes of heat transfer which can occur through a given medium: conduction, convection, and radiation (Transmittance). The Effective Thermal Conductivity (k_{eff}) is a property of a system (solid materials, liquids and gasses) that incorporates a material's ability to transfer heat by all modes into a single coefficient.

Because Thermal Conductivity is a property of a homogeneous material, technically, it is the thermal resistance of an inhomogeneous sample that should be reported or an Effective Thermal Conductivity (resistance/sample thickness). Note, however, that it is common in building materials that the term is used for materials that contain a continuous mixture of two or more substances (for example air and insulation or air and concrete) provided the size of any particles is less than a tenth of the specimen thickness. ***Thus, because hydrogen storage materials are typically powders containing void spaces and often a mixture of compounds, measured values should be reported as Effective Thermal Conductivity (or the inverse Thermal Resistance).***

To summarize:

Thermal Conductance = kA/L, measured in $W \cdot K^{-1}$.

Thermal Resistance = $L/(kA)$, measured in $K \cdot W^{-1}$ (equivalent to: $°C \cdot W^{-1}$) .

Heat Transfer Coefficient = k/L, measured in $W \cdot K^{-1} \cdot m^{-2}$ (also known as Thermal Admittance).

Thermal Insulance = L/k, measured in $K \cdot m^2 \cdot W^{-1}$.

Thermal Conductivity vs. Thermal diffusivity:

The property governing the flow of heat through a material at steady state is the thermal conductivity k. The property governing transient heat flow is the thermal diffusivity, α. They are related by:

Equation 4 $$\alpha = k/\rho C_p$$

or

Equation 5 $$k = \alpha \rho C_p$$

where ρ is the density, C_p the specific heat, and ρC_p is the volumetric specific heat. All three properties vary with temperature. Both Thermal Conductivity and Diffusivity span almost five orders of magnitude for all materials. The highest Thermal Conductivities are found for diamond, silver, copper, and aluminum and the lowest are highly porous materials like firebrick, cork, and aerogels in which Thermal Conductivity is limited partly by entrapped gas in the material's pores.

Equation 5 indicates that the ratio of Thermal Conductivity to Thermal Diffusivity is equal to the volumetric specific heat. The volumetric specific heat is roughly the same for most solid materials ($\rho C_p \approx$ *3.0 X* 10^6 *J·m*$^{-3}$*·K*$^{-1}$*).* The reason for this is that, in general, a solid containing N atoms has $3N$ vibrational modes. Each mode (in the classical approximation) absorbs a thermal energy of $k_B T$ at the absolute temperature T where k_B is Boltzmann's constant ($k_B = R/N_A$ = 1.3806488(13)×10^{-23} J·K^{-1} where N_A is Avogadro's constant). Thus, the vibrational specific heat is $C_p \approx C_V = 3Nk$. On a volumetric basis, the volume of N atoms is ($N\Omega$) m^3, where Ω is the volume per atom. For nearly all solids, Ω lies within a factor of two of 1.4x10^{-29} m^3 giving an approximate volumetric specific heat for most materials of:

Equation 6 $$\rho C_p \approx 3.0\ N k_B/N\Omega = 3k/\Omega = 3.0\ X\ 10^6\ J\cdot m^{-3}\cdot K^{-1}$$

This relationship between α, k_B, and ρC_p is shown in Figure 2 for a host of common materials. It is, however, notable that there are materials that deviate from this approximation and have a lower-than-average volumetric specific heat. For some materials, such as diamond, the volumetric specific heat is low because the Debye temperature lies well above room temperature. In this case heat absorption is not classical. That is, some modes do not absorb $k_B T$, leading to specific heat that is less than $3Nk$.

The largest deviations are found for porous solids such as foams, low-density firebrick, and wood. Their low density means that they contain fewer atoms per unit volume and, consequently, ρC_V is low. The result is that, although foams have low Thermal Conductivities (and are widely used for insulation because of this), their Thermal Diffusivities are not necessarily low. That is; they may not transmit much heat, but they reach a steady state temperature quickly. This may be an important consideration in the development of low density, high-surface area materials for hydrogen storage by physisorption.

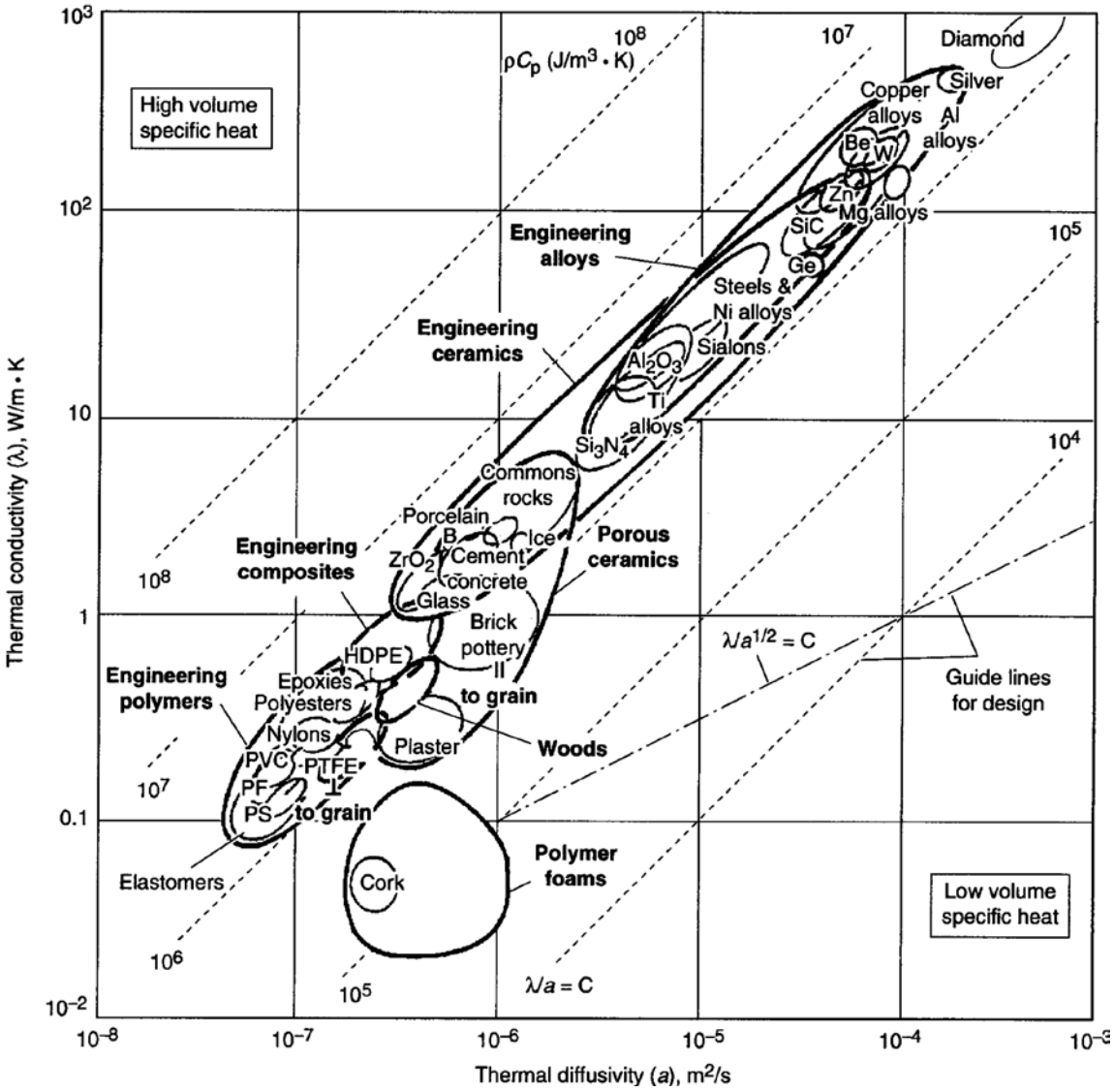

Figure 2. Thermal conductivity plotted versus thermal diffusivity. The contour lines show the volume specific heat, ρC_p. All three properties vary with temperature; the data here are for room temperature.[32]

2.2 Thermal Conductivity of Liquids and Gases

Because of the importance of two-phase (liquid-gas) heat transfer processes in many processes, thermal conductivity of the saturated liquid and vapor are of great importance. It is difficult, however, to measure the thermal conductivity at saturation and thus single-phase measurements are generally used to extrapolate to saturation conditions.

The theory of thermal conductivity of solids was fairly straightforward. In fluids the case is not as simple. If one applies a temperature gradient to a fluid, either gas or liquid initially at rest, it will lead to a density gradient. The resulting density gradient creates a buoyancy force that is opposed by viscous resistance of the fluid leading to mechanical non-equilibrium. This produces bulk convective motion of whole portions of the fluid. As a result, experimental measurements of the thermal conductivity of gases and liquids are considerably more difficult than with solids. However, measurement methods do exist and if conducted with great care, can provide valid results.[20]

2.3 Thermal Conductivity of Porous Materials

For thermal conductivity of porous material there is a valuable discussion in a book by Parrott and Stuckes.[33] They notably point out that the overall conductivity cannot exceed the volume average of the components, and cannot be above the value obtained from the volume average of the resistivities. In the case of pores in solids the second limit is not useful, since pores have almost infinite resistivity.

Many different models have been proposed for predicting the thermal conductivity of porous materials based on microstructural parameters (such as porosity and pore size) and the thermal conductivities of the solid and "porous" components.[34] Many of these come from the study of refractory or insulating materials. Three of the more detailed theories include those of Russell[35], Frey[36], and Bruggeman[37].

Russell derived the effective thermal conductivity of a dry porous material from the properties of its component gas and solid for a distribution of uniform pores of cubical shape arranged in a simple cubic lattice. He assumed parallel heat flow and neglected convection across the pores. Russell's equation for the thermal conductivity of the porous material,[35] $k_{Russell}$, is given by Equation 7:

Equation 7

$$k_{Russell} = k_{solid} \frac{\nu p^{2/3} + 1 - p^{2/3}}{\nu(p^{2/3} - p) + 1 + p - p^{2/3}}$$

Where:
k_{solid} = thermal conductivity of the solid material,
k_{pore} = thermal conductivity of the pores in the porous material = f(k_{cond}, k_{rad}),
$\nu = k_{pore}/k_{solid}$,
p = porosity = $(\rho_{powder} - \rho_{material})/\rho_{powder}$,
ρ_{powder} = density of the solid material present in the porous material, and
$\rho_{material}$ = density of the porous material.

The theory of Frey[36] relies on the same variables as that of Russell and can be written as:

Equation 8

$$k_{Frey} = k_{solid} \frac{\nu(1 - p^{1/3} + p) + p^{1/3} - p}{\nu(1 - p^{1/3}) + p^{1/3}}$$

Finally, the theory of Bruggeman[37] can be written as:

Equation 9

$$k_{Bruggeman} = k_{solid}[\nu + (1-p)(1-\nu)(\frac{k_{Bruggeman}}{k_{solid}})^{1/3}]$$

While Equation 7 and Equation 8 are directly solvable for $k_{Russell}$ and k_{Frey}, respectively, a solution for $k_{Bruggeman}$ in Equation 9 can be obtained only by an iterative process. One approach is to use initial starting values of $k_{Russell}$ obtained from Equation 7 in applying the iterative method to solving Equation 9.[34]

In the above equations, there are two contributions to the conductivity of the pores within the porous materials: conduction and radiation; convection within and between the pores is not considered in these models. Assuming that the conduction and radiation contributions are acting in the same direction, these two components of the pore conductivity are simply added together to obtain a final value at any given temperature. The contribution due to conduction is simply input using tabulated values for the thermal conductivity of the gas in the pores as a function of temperature and pressure. For spherical pores, a model developed by Loeb[38] can be used to estimate the radiation contribution to the overall pore thermal conductivity as follows:

Equation 10

$$k_{rad} = \frac{16}{3} r \sigma E T^3$$

where
r = pore radius,
σ = Stefan-Boltzmann constant [5.669 x 10^{-8} $W \cdot m^{-2} \cdot K^{-4}$)],
E = emissivity of solid material (assumed to be 0.9 here), and
T = absolute temperature (K).

Loeb also developed a similar equation for laminar and cylindrical pores, where the factor of 16/3 used Equation 10 for spherical pores is replaced by a factor of 8 and the radius of the pore, r, is replaced by one half of the largest (gap) dimension in the

direction of heat flow.[38] Thus, to be able to employ such an analysis to hydrogen storage materials it is important that the average pore size and shape is well understood. In many cases this requires extensive measurements of pore size distributions and examinations of pore shapes using methods such as SEM.

2.4 Thermal Conductivity of Packed Particle Beds

The effective thermal conductivity of a packed particle bed can be described by three distinct gas pressure regimes.[39]

1) ***Low pressure regime (generally << 1 bar):*** characterized by molecular or rarified gas transport in interparticle spaces. The gas plays very little role in heat transfer and, therefore, thermal properties of the bed are not strongly dependent on pressure in this regime.
2) ***Intermediate pressure regime:*** characterized by the transition between molecular and continuum transport within the void spaces. Thermal properties are strongly affected by gas pressure in this regime.
3) ***High pressure regime:*** characterized by continuum gas transport within the void spaces. In this regime, the gas pressure has no further influence on the thermal properties of the bed.

The pressure range from each regime is determined by the characteristics of the material, including pore size and the size of void spaces between particles in the bed. The pressure at which the gas behavior changes from the transition (Intermediate pressure regime) to continuum (High pressure regime) is known as the *Critical Pressure*.

Note that because of the operating pressure of most on-board hydrogen storage applications (> 1 bar) , heat and mass transfer take place in the Intermediate- and High-pressure regimes.

According to Oi et al. heat transfer in a metal-hydride packed-particle bed occurs through one or more of six modes.[40] These are:

1) Heat conduction at the points of contact between particles,
2) Heat conduction through a thin hydrogen ‘film’,
3) Heat radiation between particles,
4) Heat conduction through the body of each particle,
5) Heat conduction through the hydrogen in larger void spaces,
6) Heat radiation between vacant spaces.

A generalized resistance model for packed beds was developed by Yagi and Kunnii [41] that was later adapted for metal hydride beds.[40,42,43,44] Heat transfer by radiation can be neglected for most (low and moderate temperature) hydrogen storage application.[40,42,43, 45 , 46] A general resistance model for the effective thermal conductivity (K_{eff}) of a metal hydride bed is given by: [39]

Equation 11

$$K_{\text{eff}} = K_{\text{H}_2}\left[\phi_{\text{v}} + \frac{1-\phi_{\text{v}}}{\gamma + \frac{2}{3}\left(\frac{K_{\text{H}_2}}{K_{\text{p}}}\right)}\right]$$

where K_{H_2} is the thermal conductivity of hydrogen gas, K_{p} is the thermal conductivity of the solid metal hydride, ϕ_{V} is the void fraction of the bed and γ is a constant relating conduction to the effective length of the average particle diameter. This constant is difficult to predict as it is a function of particle contact angle, shape, and roughness. The model was used by Oi et al. to predict the thermal conductivity of a typical metal hydride bed depending on the thermal conductivity and porosity of different hydride powders.[40] The results were values of K_{eff} that ranged from 0.5 to 2 $W \cdot m^{-1} \cdot K^{-1}$ for typical materials.

While resistance models are good for making rough estimates of bed performance, more accurate numerical models are now more commonly used. One of these is the model developed by Zehner, Bauer, and Schünder based on spherical particles in a cylinder of fluid (hydrogen).[47,48] The effective thermal conductivity (K_{eff}) of a bed is calculated using the equation:

Equation 12

$$K_{\text{eff}} = K_{\text{H}_2}\left\{\begin{array}{l}(1-\sqrt{1-\Psi})\cdot\Psi\cdot\dfrac{1}{\Psi-1+\dfrac{1}{K_{\text{H}_2}}} \\ \quad + \sqrt{1-\Psi}\cdot[\varphi\cdot K_{\text{p}} + K_{\text{pgp}}\cdot(1-\varphi)]\end{array}\right\}$$

where K_{H_2} is the thermal conductivity of hydrogen gas, ψ is the void fraction, ϕ is the flattening coefficient that defines the contact quality, K_{p} is the thermal conductivity of the particle, and K_{pgp} is an expression for the thermal conductivity at the particle-gas-particle interface. The expression for K_{pgp} includes the particle diameter and describes the contribution of the fluid to the contact quality between particles.

The above model has been used to calculate effective thermal conductivities (K_{eff}) for a hydride bed as a function of hydrogen pressure, particle thermal conductivity, particle diameter, and void fraction (Figure 3).[39]

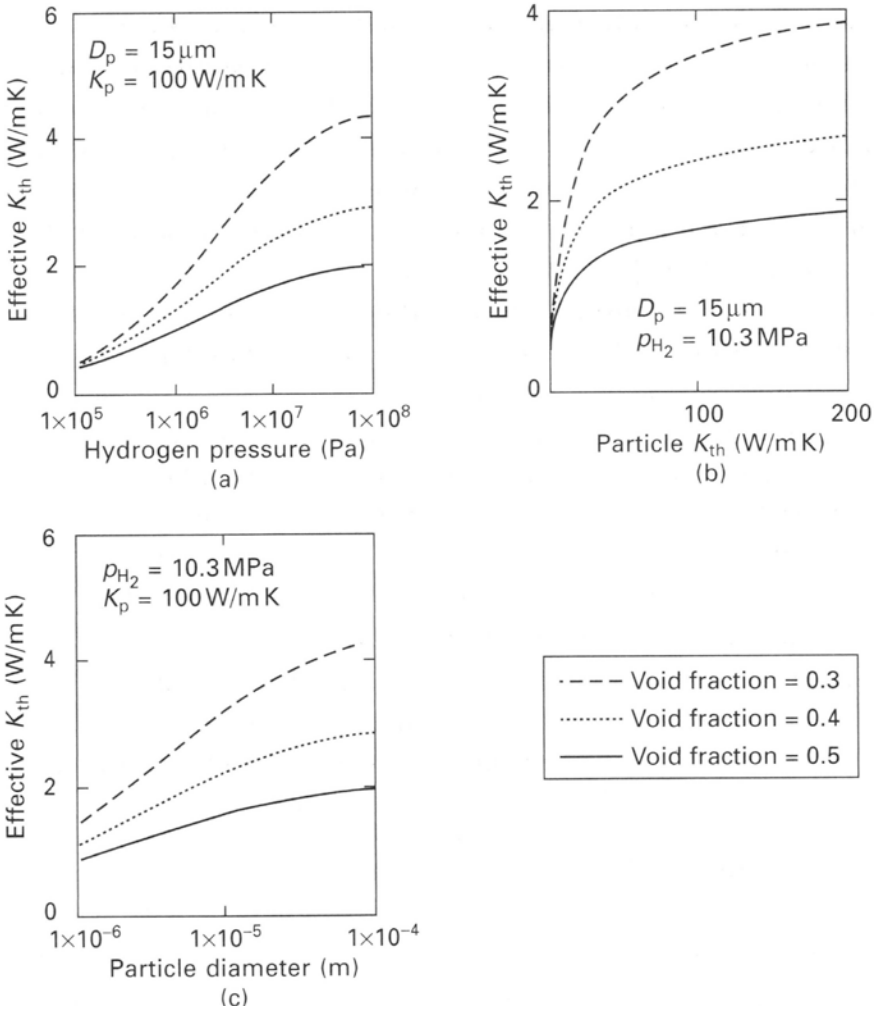

Figure 3. Calculated effective thermal conductivity of a packed particle bed as a function of void fraction, a) hydrogen pressure, b) particle thermal conductivity, and c) particle dimensions.[39]

It was found that, in general, higher pressures up to the critical pressure and lower void fractions lead to increased conductivity. It was also found that, the effective thermal conductivity was less sensitive to the deformation factor and contact flattening (indication the area of contact between particles) than other variables. Above about 50 $W \cdot m^{-1} \cdot K^{-1}$ the particle conductivity does no longer has a large influence on K_{eff} due to the dominance of porosity and particle to particle contact. Larger particle diameters were shown to lead to higher K_{eff} because of the reduction in particle-to-particle contact and the increase in thermal transport of the gas as the void spaces transition to the

continuum regime. Perhaps the most important finding was that K_{eff} in such packed particle hydrogen storage beds is limited to a maximum of about 5 $W \cdot m^{-1} \cdot K^{-1}$ regardless of improvements in the thermal conductivity of the particles (hydride materials). Thus, greater improvements in heat transfer will require novel approaches to materials and systems designs.

In their study specifically on sodium-alanate materials, Dedrick et al. found that sintered-solid alanates' thermal transport properties were very similar to those of the packed particle beds.[39]

3 Thermal Contact Resistance

Thermal contact resistance is the inverse property of thermal contact conductance which is the heat conduction between solid bodies in thermal contact. The degree of thermal conductivity between two bodies in contact is given by a value known as the thermal contact conductance coefficient, h_C.

When two solid objects come into contact heat will flow from the hotter object to the colder object. This is illustrated in Figure 4 where A is the mass of the hot object and B is the cool object. In this steady state example it is assumed that heat Q (or specific heat q = Q/m) flows into A from the left maintaining this surface at temperature T_1 and out of B on the right maintaining a surface temperature T_3.

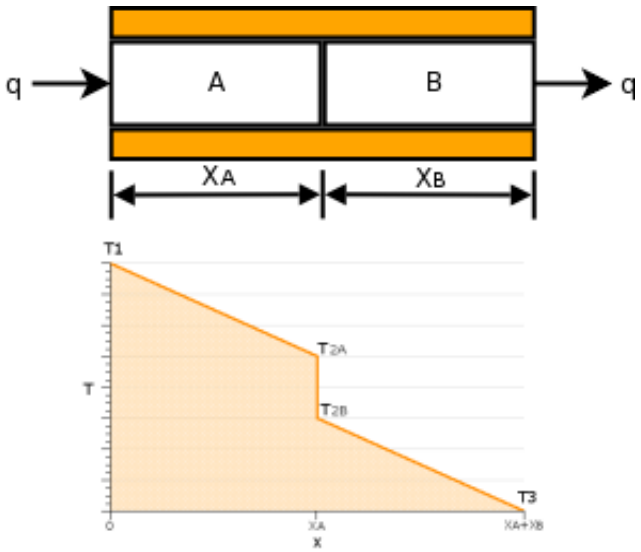

Figure 4. Heat flow between two solids in contact and the temperature distribution.[49]

Each object will have a temperature gradient within the object. At the interface between the two objects a temperature drop is generally observed. This temperature drop is a result of the thermal contact resistance existing at the surface between the two objects. Thermal contact resistance is defined as the ratio between this temperature drop and the average heat flow across the interface.[50]

According to Fourier's law, the heat flow between the bodies is given by (Equation 2):

Equation 13

$$Q_x = -kA\frac{\mathrm{d}T}{\mathrm{d}x}$$

Where *Q* is the heat flow, k is the thermal conductivity, *A* is the cross sectional area, and dT/dx is the temperature gradient in the direction of flow. For this one-dimensional steady state example the heat flow between the two contacting objects A and B, is given by:

Equation 14

$$Q_x = \frac{T_1 - T_3}{\Delta x_A/(k_A A) + 1/(h_C A) + \Delta x_B/(k_B A)}$$

Thus, heat flow is dependent not only on the thermal conductivities of the bodies in contact, k_A and k_B, but also on the contact area A, and the thermal contact resistance, $1/h_C$, which is the inverse of the thermal conductance coefficient, h_C.

Thermal contact resistance is a complex property of the materials and surrounding and may involve more than one mechanism. Some of the factors that have a strong effect on thermal contact resistance are:

1. Contact pressure,
2. Surface roughness,
3. The presence or absence of one or more gases or fluid in the area around the interface between contacting surfaces,
4. Surface deformation under pressure, and
5. Contaminants or secondary phases at the surface.

Thermal contact resistance between hydrogen storage materials and the containment vessel or heat-transfer elements (fins, foams…) can have a large impact on the overall heat transfer performance of a hydrogen storage system. There are experimental means (as discussed in later examples) to measure the average value of these contact resistances. Such measured values are of significant importance to the accurate modeling of hydrogen storage prototype systems. However, thermal contact resistance is a particular problem when the storage material is in powder form as it is difficult to quantify or control.

4 Modeling of Thermal Conductivity

An example of modeling of the effective thermal conductivity of the metal hydride bed is the work by Asakuma et al. They used the homogenization method to develop a numerical model describing thermal conductivity as a function of gas type, gas pressure and bed temperature.[51] The homogenization method represents the microstructure within the metal-hydride hydrogen storage bed. The homogenization method may be a powerful tool for the estimation of effective thermal conductivity within a metal hydride bed by considering microscopic behaviors such as the pulverization and the change of the contact area between particles at different hydrogen concentrations.

For the analysis the metal hydride packed bed was considered to be composed of a periodic composite. The periodic structure consists of two domains, solid phase (Ω_s) and gas phase (Ω_g) as shown in Figure 5.

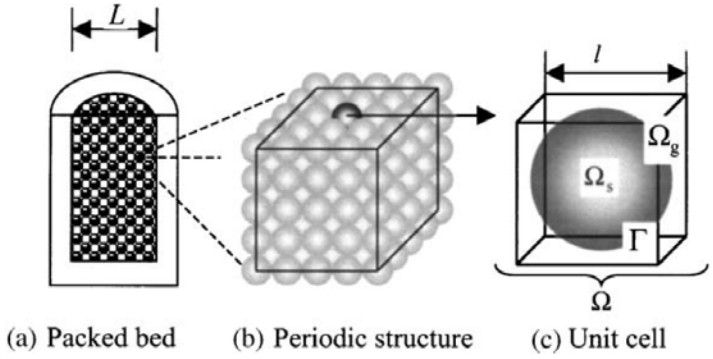

Figure 5. Schematic diagram of homogenization method: (a) packed bed, (b) periodic structure, and (c) unit cell.[51]

The periodic domain Ω is small compared to the characteristic length, L at the macroscopic scale:

Equation 15 $$\varepsilon = l/L << 1$$

where ε is a scale parameter and l and L are the characteristic sizes of the microscopic (particle) and the macroscopic (bed) sample, respectively.

The numerical model was fit to measured data Hahne and Kallweit.[52] This required change in the free parameters of the Biot number, the Knudsen number and the contact area of hydride particles to be able to express the behaviors from the experimental data of precisely.

The Biot number ($\mathbf{Bi} \equiv \mathrm{hL/k}$) is a dimensionless number used in non-steady-state (or transient) heat transfer calculations. It is named after the French physicist Jean-Baptiste Biot (1774–1862), and gives a simple index of the ratio of the heat conduction within a body to convection at its outer surface. This ratio determines whether or not the temperatures inside a body will vary significantly in space, while the body heats or cools over time via convection at its surface. Note that the Biot number has the same mathematical form as the Nusselt number discussed earlier in this document. The difference is that the Biot number uses the thermal conductivity of the solid body, while the Nusselt number uses the thermal conductivity of the fluid.

In general, problems involving small Biot numbers (much smaller than 1) are thermally simple, due to uniform temperature fields inside the body. If the temperature profile within the body is nearly uniform it may be modeled using lumped-capacity analysis, which greatly simplifies the heat transfer calculations. Biot numbers much larger than 1 signal more difficult problems due to non-uniformity of temperature fields within the object as is the case for a metal hydride particle, where the particle can contain both the metallic compound and the hydride.

The **Biot number** has a variety of applications, including use in extended surface heat transfer calculations.

The **Knudsen number** (***Kn***) is a dimensionless number defined as the ratio of the molecular mean free path length λ to a representative physical length scale L. The number is named after Danish physicist Martin Knudsen (1871–1949). The Knudsen number is a dimensionless number defined as:

Equation 16

$$Kn = \frac{\lambda}{L}$$

This length scale could be, for example, the radius of a body in a fluid. For an ideal gas, the mean free path may be readily calculated so that:

Equation 17

$$Kn = \frac{k_B T}{\sqrt{2}\pi\sigma^2 pL}$$

Where, k_B is the Boltzmann constant (1.3806504(24) × 10^{-23}J·K^{-1} in SI units) [$M^1L^2T^{-2}\theta^{-1}$], T is the thermodynamic temperature, [θ^{-1}], σ is the particle hard shell diameter, [L^1], and p is the total pressure, [$M^1L^{-1}T^{-2}$].

Using this model, H_2, He, N_2 and Ar were considered as the filling gases giving the thermal conductive as a function of gas pressure (Figure 6).[51] When the pressure is fairly low, the frequency of collisions between molecules in a micro-region affects the thermal conductivity of the gas. Actually, with the decrease in the pressure, the thermal conductivity of the gas decreases because of the increase in the mean free path of the gas molecules (Smoluchowski effect [53]).

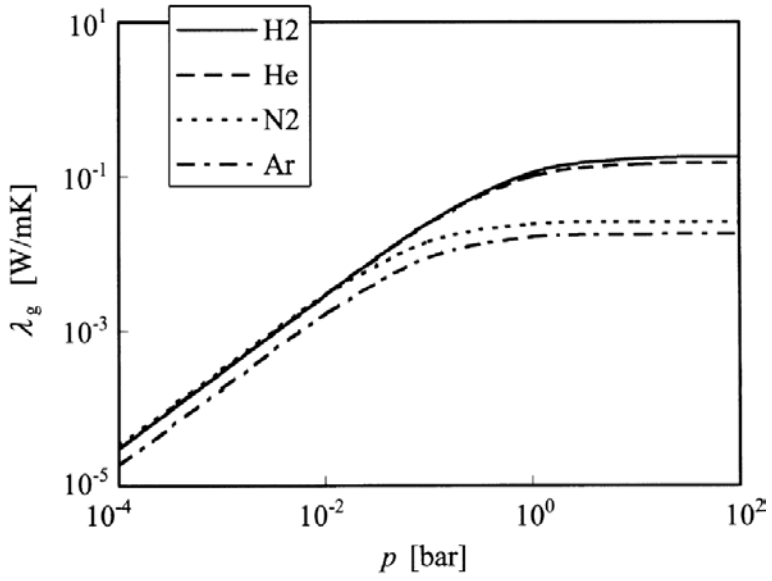

Figure 6. Effect of the pressure on the thermal conductivity of different gases.[51]

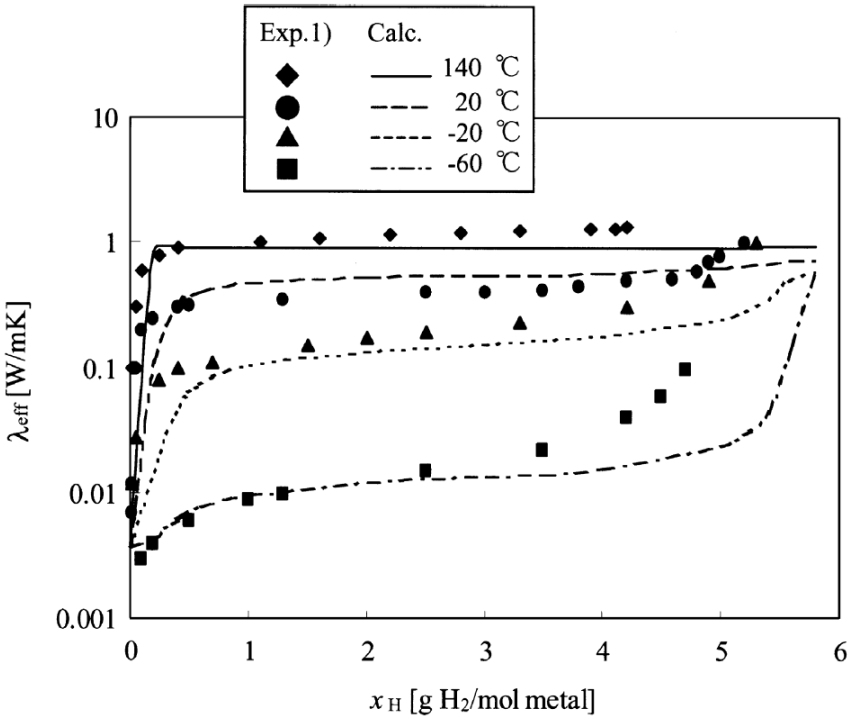

Figure 7. Relation between the effective thermal conductivity and hydrogen concentration for $LaNi_{4.7}Al_{0.3}$: (a) experimental data[52], (b) homogenization method.

The effective thermal conductivity, k_{eff} was evaluated for $LaNi_{4.7}Al_{0.3}H_x$ at several temperatures and hydrogen concentrations. The relationship between concentration and hydrogen pressure at each temperature was taken from experimental pressure concentration isotherms (PCTs) data.[52] The model assumed that the contact area, Biot number and the mean diameter of the pore are constant ($a = 0.0009$, $Bi = 100$, $L = 14.9$ μm as determined by fitting the experimental thermal conductivity data[52] at one temperature). The experimental data and the model results are shown in Figure 7. These results show a good fit to experimental conductivity values at high hydrogen concentration (β-phase) and show that conductivity values at low hydrogen concentration (α-phase) increase rapidly as measured. Good agreement is obtained when the temperature and, thus, the equilibrium pressure are high (p=0.1 bar). However, there are differences at the lower temperature. This can be explained by the change of the contact area because of the material's volume expansion and the change of the thermal conductivity of the metal hydride with temperature.

Heat conduction across a particle bed is a function of both the thermal contact resistance between particles and the thermal conductivity of individual particles. Although generally of minor significance, there are operating conditions for which gas present in the void space can impact conductive heat transfer. Models used to evaluate and design storage systems incorporate the aforementioned components of heat conduction into an effective bed thermal conductivity. Although there are approximate methods for calculating the effective thermal conductivity from the characteristics of the material[54,55] they are subject to significant error. For metal hydride beds, describing the material characteristics is complicated by the fact that the chemical composition and morphology changes with hydrogen uptake. The morphological changes include volumetric expansion which further impacts particle contact, especially within constrained regions such as a tank. Hence, it is more appropriate to measure the bed thermal conductivity directly, recognizing that it will be dependent upon the amount of stored hydrogen, temperature and the effects of boundaries that constrain its expansion. In conjunction with the thermal conductivity within the bed, the thermal contact resistance between the bed and adjacent heat transfer surfaces, such as fins or tubes, must be measured to provide a complete assessment of bed heat transfer. That being said, it should be recognized that bed expansion and contraction with uptake and discharge of hydrogen will affect the extent of contact with heat transfer surfaces and subsequently the thermal contact resistance.

Adsorbent bed thermal conductivity is affected by the same physical phenomena as metal hydrides except that the adsorbent does not undergo morphological changes with hydrogen uptake. However, adsorbents typically operate under cryogenic conditions. In general, at temperatures near 80K the effective thermal conductivity of adsorbents is significantly different from its value at 298K. Further, the change in bed thermal conductivity with respect to temperature may be more profound at temperatures below 150K. As for metal hydrides it is advisable to directly measure the bed thermal conductivity as a function of temperature.

Both metal hydrides and adsorbents typically have very low thermal conductivities, which has led to consideration of modifications to the storage media to increase its thermal conductivity. These include addition of material to increase thermal conductivity and/or structuring of the material into compacted forms that improve contact between particles and heat transfer surfaces.

5 Thermal Conductivity Measurement Methods

5.1 Standards

- ASTM Standard C 177, “Standard Test Method for Steady-State Heat Flux Measurements and Thermal Transmission Properties by Means of the Guarded-Hot-Plate Apparatus”.
- ASTM Standard E1225-04, "Standard Test Method for Thermal Conductivity of Solids by Means of the Guarded-Comparative-Longitudinal Heat Flow Technique".
- ASTM C518, “Standard Test Method for Steady-State Thermal Transmission Properties by Means of the Heat Flow Meter Apparatus”.
- ASTM E1530 – 06, “Standard Test Method for Evaluating the Resistance to Thermal Transmission of Materials by the Guarded Heat Flow Meter Technique”.
- ASTM Standard D5334-08, "Standard Test Method for Determination of Thermal Conductivity of Soil and Soft Rock by Thermal Needle Probe Procedure".
- ASTM Standard D5930-01, "Standard Test Method for Thermal Conductivity of Plastics by Means of a Transient Line-Source Technique".
- ASTM Standard E1461 - 07 “Standard Test Method for Thermal Diffusivity by the Flash Method”.
- ASTM Standard C1113 / C1113M - 09 “Standard Test Method for Thermal Conductivity of Refractories by Hot Wire (Platinum Resistance Thermometer Technique”).
- ASTM C1363 – 05, “Standard Test Method for Thermal Performance of Building Materials and Envelope Assemblies by Means of a Hot Box Apparatus”.
- ASTM Standard D2717-95, "Standard Test Method for Thermal Conductivity of Liquids"
- ISO 22007-2:2008 "Plastics -- Determination of thermal conductivity and thermal diffusivity -- Part 2: Transient plane heat source (hot disc) method".
- ISO 8301/8302, “Standard Test Technique for Measurements of Insulating Materials Using the Heat Flow Meter/Guarded Hot Plate Method”.

- ISO 8894-1 (EN 993-14), “Determination of Thermal Conductivity; Hot-Wire Method (cross array; $\lambda \leq 1.5$ $W \cdot m^{-1} \cdot K^{-1}$)”.

- ISO 8894-2 (EN 993-15), “Determination of Thermal Conductivity; Hot-Wire Method (cross array; $\lambda \leq 25$ $W \cdot m^{-1} \cdot K^{-1}$)”.

- IEEE Standard 442-1981, "IEEE guide for soil thermal resistivity measurements", ISBN 0-7381-0794-8.

- DIN EN 12667/12939, “European Standard for Measurements of Insulating Materials Using the Heat Flow Meter Method or the Guarded Hot Plate Technique”.

- DIN EN 13163, “European Standard for Characterization of Foam Insulations for Building Applications Using the Heat Flow Meter Method or the Guarded Hot Plate Technique”.

The most recent details for these and other standards may be obtained at:

- ASTM International, www.astm.org, (ASTM International, 100 Barr Harbor Drive, PO Box C700, West Conshohocken, PA, 19428-2959 USA).

- ISO, International Organization for Standardization, http://www.iso.org, (Central Secretariat, 1, ch. de la Voie-Creuse,CP 56, CH-1211 Geneva 2, Switzerland, E-mail: central@iso.org, Tel./Fax. : +41 22 749 01 11 / 733 34 30).

- DIN, Deutsches Institute für Normung e. V., http://www.din.de (DIN Deutsches Institut für Normung e. V., Am DIN-Platz Burggrafenstraße 6, 10787, Berlin, Germany, Tel./Fax. +49 30 2601-0 Fax: +49 30 2601-1231).

5.2 Introduction to Measurement Methods

The measurement of thermal conductivity of materials goes back to the mid-19th century.[56] The original version of the guarded hot-plate insulation test method was developed later in 1912.[57] This measurement method has undergone many improvements and modifications and continues to be the most widely used thermal conductivity measurement method.

There are many different methods to measure thermal conductivity, and the method selected should be appropriate for the general type of material (gas, liquids, solids, powders) and the temperature range for which the material will be used. The following is a list of some common measurement methods that are presented in detail in this document:

- Guarded Hot Plate Method (ASTM C 177)
- Concentric Cylinders Method
- Concentric Spheres Method
- Thermal Probe Method (ASTM D 5334)
- Transient Plane Source (TPS) Method
- Divided Bar Method (ASTM E1225-87)
- Hot-Wire Method (ASTM C1113) for Gases and Liquids
- Flash Method

Figure 8 illustrates the wide range of thermal conductivities for common materials and shows the generally applicable range of thermal conductivity for common measurement methods. For example, for highly conductive ceramics, metals or diamond composites, the Laser Flash method (LFA) is often employed. Whereas, the thermal conductivity of refractory materials is typically determined on large samples using hot wire instruments.

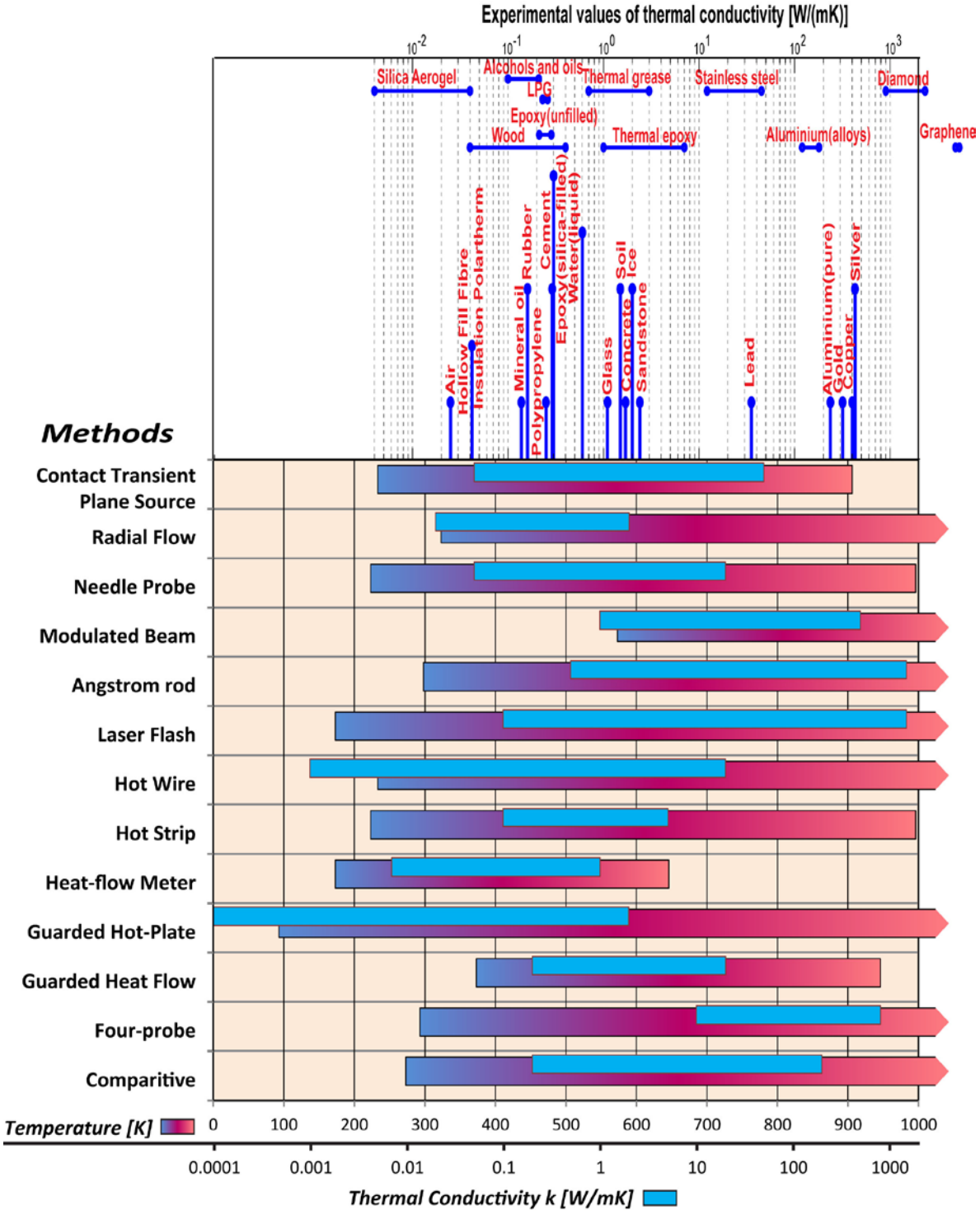

Figure 8. Example materials and common measurement methods for different ranges of thermal conductivity.[58]

5.2.1 Considerations for which measurement method to use?

In general **Thermal conductivity measurements** can be made using steady-state methods (up to 1200K) and pulse methods (in particular over 1500K). For materials that are electrical conductors the sample itself can be self-heated by applying an electric current. Given that most hydrogen storage materials are in powder form, this would not be the most common or recommended measurement technique.

For **Thermal Diffusivity** measurements the transient methods are usually preferred. This is because the measurement of diffusivity requires an accurate recording of the time dependence of temperature following a transient or periodic temperature perturbation at the sample boundary or surface.

Broadly speaking, thermal conductivity is measured by steady-state techniques and thermal diffusivity by transient techniques. However, it is also possible to use some transient techniques in a modified way to measure thermal conductivity.

Due to the wide ranges of thermal property of hydrogen storage materials there is no single measurement method that can be recommended for both Thermal Diffusivity and Conductivity, or that will be applicable to all types of materials. The method used will depend on the type of material and the range of the thermal property being measured over its operational temperature range. The following summarizes important factors that are important in determining what method is used:

- likely range of thermal conductivity to be measured, because low conductivity materials like insulating materials or foams require different methods than for high conductivity materials such as metals,
- measurement temperature range, which is technique dependent,
- whether the material is a solid or a liquid,
- the size, shape, and morphology of the sample (bulk solid or powder),
- whether the sample is air sensitive,
- whether or not the sample needs any in situ pre-treatment (bake-out or hydriding) and, in particular,
- whether the sample will decompose, outgas, or change morphology during the testing procedure.

Table 1 below provides short descriptions of the most commonly used measurement methods.[58]

Method	References	Material Type	T range [°C]	Property range [$W \cdot m^{-1} \cdot K^{-1}$]
Comparative technique	59,60	all solids	0 to 1000	0.2 to 200
A secondary method of thermal conductivity measurement in which steady-state linear heat flow is established in a stack consisting of a specimen sandwiched between two references and surrounded by a cylindrical guard heater.				
Key Requirements: 1) Where possible the thermal conductance of the reference pieces should be similar to that of the test specimen. 2) The surfaces of the test and reference pieces should be flat and parallel. 3) All care should be taken to eliminate or maintain reproducible contact resistances at mating surfaces - vacuum environment not recommended, hydraulic or pneumatic load used to maintain a constant value and use of a suitable thin contacting medium at surfaces if no contamination expected. 4) Definitive attachment of temperature sensors at required positions to test and reference pieces are critical.				
Four-probe technique	61,62,63	metals and metallic alloys	20 to 1600	10 to 800
Thermal conductivity is determined from measurement of the electric resistivity; current and voltage are normally measured with four probes.				
Key Requirements: 1) The sample must be a rod with cylindrical geometry. 2) The diameter must be constant within 20 µm and the material must be homogenous over the length of the rod. 3) The length to diameter ratio should be in the range of 20 (e.g. 100 mm/5 mm) at least for materials with high electrical conductivity. 4) The reason for key requirement 3 is the low voltage drop in the sample. This requires precise voltage measurement. 5) If measurements are required above the melting point then a ceramic crucible tube has to be used with a negligible electrical conductivity, but without any chemical reactivity with the sample material.				
Guarded heat flow method	64,65,66	polymers, rocks, ceramics, foods, some metals and alloys	100 to 300	0.2 to 20
Similar in principle to the heat flow meter method but used to measure much smaller higher conductivity specimens using different calibration materials and cylindrical guard around the test stack.				
Key Requirements: 1) Specimen surfaces must be flat and parallel to less than 0.01 mm. 2) Calibration must be undertaken under the same temperature and pressure conditions as those for the test specimen. 3) Height of test stack should not exceed that of the guard cylinder. 4) Temperature control of surface plates to be 0.1K.				

Guarded hot-plate	67,68,69	solid, opaque, homogeneous, composites, insulation materials	-180 to 1000	0.0001 to 2
Steady-state linear heat flow established in a large flat sample (usually in two nominally identical pieces) sandwiched between a controlled and guarded central hot plate and cold plates operating at a controlled lower temperature. A well-established absolute technique having high accuracy, especially at ambient temperatures.				
Key Requirements: 1) Specimen pieces flat and parallel within limits provided in ISO Standard 8302 2) Specimen thickness MUST be representative of the bulk material 3) Specimen thickness determines area plate size 4) Specimen thickness must be at least a factor of ten greater than the dimension of the largest material constituent, pore or crystal or imperfection in the material 5) Hard, higher conductivity materials must be instrumented separately with temperature sensors to help minimize contact resistances between surfaces and to provide representative specimen surface temperatures.				
Heat-flow meter method	70,71,72	insulation materials	-100 to 200	0.007 to 1.0
A secondary steady-state method using a similar configuration to the guarded hot plate but normally using one large self-guarding specimen in conjunction with a heat flux transducer and with the apparatus calibrated with one or more reference materials or transfer standards.				
Key Requirements: 1) Not suitable for materials that are hard and have a thermal conductivity in excess of 0.3 $W \cdot m^{-1} \cdot K^{-1}$). 2) Specimen flat and parallel within limits specified in Standard ISO 8301; the thickness and area size limits are the same as those for the guarded hot plate. 3) Temperature control of plate surfaces needs to be ± 0.1K. 4) Heat flux transducer made from highly stable materials – its stability and reproducibility over the temperature range of continuous operation is the CRITICAL factor. 5) Calibration of apparatus must be undertaken under the same conditions as for the test material. 6) Regular apparatus calibration, in accordance with guidelines provided in the test standard, to verify stability.				
Hot-box apparatus either guarded or calibrated (thermal resistance)	73, 74, 75, 76, 77, 78, 79	systems containing insulation, wood, masonry, glass and other materials and products used for the building envelope	-20 to 40	Thermal conductance range of 0.2 to 5 ($m^2 \cdot K \cdot W^{-1}$)
Not generally used for materials but for measuring the steady-state thermal transmission properties (U-value) or the thermal conductance of building envelope components and systems. A large specimen is placed between a hot and a cold chamber operating at fixed temperatures, humidity and air flow conditions. A guarded metering box is attached to the central section of the specimen in the guarded hot box while in the calibrated version a well-insulated much larger box is calibrated with a transfer standard.				
Key Requirements: 1) Ensure that the metering section is truly representative of the inhomogeneous construction being measured. 2) Ensure that sufficient temperature sensors are used in appropriate positions on the specimen surfaces and in the air opposite, in order to provide representative area- weighted temperatures of each.				

3) Good attachment of temperature sensors on the specimen surfaces is critical. For the guarded box ensure that all power sources (fans etc.) within the guard section are considered for inclusion in the measurement of the total power.				
Hot strip method	80, 81, 82, 83,84	glasses, foods ceramics, etc.	-50 to 500	0.1 to 5
Very similar in principle to the hot wire method but uses a narrow thin metal foil pressed directly between two specimen pieces as the power source.				
Key Requirements: 1) Choose the most suitable technique, based on material size availability, for the thermal conductivity range and temperature range of measurement. 2) Prepare specimen surfaces carefully and use applied load to reduce the effects of contact resistances in the test stack. 3) Choose carefully the input power levels and times of experiment and selection of time windows to use in the analysis of the response curves. 4) Use high precision experimental hardware and fully automated data collection, analysis and display system. 5) If property relationships are to be used to derive a property ensure that the test material is one in which heat transmission is predominantly due to solid conduction mechanisms. 6) Verify the performance with appropriate available reference materials.				
Hot wire method		refractory materials, many solid types including earth minerals, glasses, plastics granules and, powders, plus fluids and gases	-40 to 1600	0.001 to 20
Three forms available, either a single or crossed resistive wire or two parallel wires a small distance apart. A quasi-steady state method where the thermal properties are obtained from the temperature v. time response due to a heat flux generated by the wire embedded in the specimen. The curve is analyzed in accordance with a model based on a solution of the time-dependent heat equation under a particular set of boundary conditions. In principle an absolute method.				
Key Requirements: Same as Hot strip method				
Laser flash method	85,86,87	metals, polymers, ceramics	-100 to 3000	0.1 to 1500
Thermal diffusivity is determined from an analysis of the temperature rise v. time response induced by absorption of a pulse of laser energy.				
Key Requirements: 1) The specimen faces must be flat and parallel. 2) In the case of inhomogeneous materials, only specimens with small inhomogeneities (grains or pores etc. <0.05 thickness) can be measured because of small specimen dimensions (in order that the specimen is representative of the material). 3) The specimen must be opaque to the laser wavelength, otherwise non opaque specimens have to be coated. 4) The specimen thickness must be chosen according to the laser pulse width and the expected thermal diffusivity.				

Angstrom method	88,89,90	Metals, alloys, graphite, ceramics	25 to 1300	above 0.5
A long thin (0.3 - 0.9 mm diameter,100 - 300 mm long) radiating rod, tube or bar of a good conducting material, assumed to behave as a semi-infinite medium, is heated at one end by a sinusoidal heat source with a period of typically 100 to 150 s. Temperature sensors are attached at two or more positions along the rod axis. Thermal diffusivity is determined from the resulting velocity and amplitude decrease using one of a number of solutions to the mathematical model.				
Key Requirements: 1) Heat loss from the surface has to be minimized or corrected. 2) A surface coating is required if contact-less heating and/or temperature detection is used. 3) The length of the specimen must be large in comparison to its diameter.				
Modified Angstrom method	91,92,93	diamond, semiconductors, metals, ceramics and polymer multi-layered composites	-100 To 500	Covers a range of six orders of magnitude
The partially masked blackened surface of a thin rectangular specimen is irradiated by uniform chopped light at fixed frequencies and the ac temperature excursion on the opposite face monitored as the specimen is moved in small increments. The in-plane thermal diffusivity is then determined from the linear amplitude decay and phase shift curves.				
Modulated beam technique	94 , 95 , 96 , 97	metals, polymers, ceramics	300 to 2000	1 to 500
Thermal diffusivity is determined from the temperature modulation induced by absorption of the modulated light beam from a xenon lamp or other source.				
Key Requirements: 1) The specimen faces must be flat and parallel. 2) Non-opaque specimens have to be coated to prevent absorption of the modulating beam and radiation from the sample material. 3) Both sides of the specimen could be coated with a thin layer of graphite to optimize emission of thermal radiation. 4) Measurements must be performed at different modulation frequencies, depending on specimen thickness and thermal diffusivity. The disagreement of resulting thermal diffusivity values, measured at different frequencies, is a clear indication of measurement uncertainties caused by not correctly maintaining the same experimental conditions (inhomogeneous heating, absorption of specimen radiation in the bulk etc.).				
Needle probe	80,81,82, 83,84	soils, minerals, solid and molten polymers and foods, rubber, particulates, powders	-50 to 500	0.05 to 20
A modification of the hot wire technique whereby the heat source and temperature measurement sensor(s) are together sealed into a long thin tube which is then directly embedded in the specimen or fixed in grooves cut across the matching surfaces of two specimen pieces. Can be used for in situ measurements. Some versions use reference materials for calibration although in principle the technique is an absolute one.				
Key Requirements: 1) Choose the most suitable technique, based on material size availability, for the thermal conductivity range and temperature range of measurement. 2) Prepare specimen surfaces carefully and use applied load to reduce the effects of contact resistances				

in the test stack.
3) Choose carefully the input power levels and times of experiment and selection of time windows to use in the analysis of the response curves.
4) Use high precision experimental hardware and fully automated data collection, analysis and display system.
5) If property relationships are to be used to derive a property ensure that the test material is one in which heat transmission is predominantly due to solid conduction mechanisms.
6) Verify the performance with appropriate available reference materials.

Photo-thermal methods	98,99,100	small specimens of most solid material types	-50 to 500	0.1 to 200. Methods also very useful in a qualitative NDT mode

Intensity modulated light is directed onto the specimen surface and the run-time behavior of the resultant thermal waves is detected. The amplitude and phase change are evaluated as a function of the modulation frequency using appropriate models to obtain the thermal diffusivity or thermal conductivity.

Key Requirements:
1) Specimen faces must be flat and parallel.
2) The thermal properties of the substrate must be known for two-layer systems.
3) Non-opaque films must be coated.

Pipe test method (radial flow)	101 , 102 , 103	insulation such as calcium silicates, mineral and refractory fiber blankets, cellular plastics, foamed glass, microporous block and powder products	50 to 800	0.02 to 2, depending on material type and temperature

Similar in principle to the guarded hot plate but using a long cylinder or tubular specimen wrapped around a central heater with end guard heaters and employing radial heat flow to measure thermal conductivity and thermal transference.

Key Requirements:
1) Ensure that the pipe insulation fits around the heater correctly so that no air gaps exist between the insulation and heater surfaces - this is critical, especially with insulation supplied in preformed hemispherical sections.
2) Adjustment of spacing of heater windings to attain temperature uniformity of central pipe.
3) Select best way of attaching temperature sensors to the type of insulation to be measured.
4) Maintain apparatus in an enclosed draft-free environment to minimize fluctuations of air temperature.

Contact transient methods: Plane source with pulse transient	80,81,82, 83,84	polymers, rocks, ceramics, some alloys, thermal insulations, liquid samples such as water, oils, molten polymers	-40 to 400	0.05 to 50

Multi-property version of contact transient. A heat pulse generated during an appropriate time through a metal foil on one face of the specimen and the temperature response measured by a sensor attached to the other specimen surface.

Key Requirements:
1) Choose the most suitable technique, based on material size availability, for the thermal conductivity

range and temperature range of measurement. 2) Prepare specimen surfaces carefully and use applied load to reduce the effects of contact resistances in the test stack. 3) Choose carefully the input power levels and times of experiment and selection of time windows to use in the analysis of the response curves. 4) Use high precision experimental hardware and fully automated data collection, analysis and display system. 5) If property relationships are to be used to derive a property ensure that the test material is one in which heat transmission is predominantly due to solid conduction mechanisms. 6) Verify the performance with appropriate available reference materials.				
Contact transient methods: Plane source with step-wise transient	80,81,82, 83,84	soils, minerals, solid and molten polymers and foods, rubber, particulates, powders, some building materials	-40 to 400	0.05 to 50
Similar to the pulse transient with a heat flux generated for an appropriate time.				
Key Requirements: 1) Choose the most suitable technique, based on material size availability, for the thermal conductivity range and temperature range of measurement. 2) Prepare specimen surfaces carefully and use applied load to reduce the effects of contact resistances in the test stack. 3) Choose carefully the input power levels and times of experiment and selection of time windows to use in the analysis of the response curves. 4) Use high precision experimental hardware and fully automated data collection, analysis and display system. 5) If property relationships are to be used to derive a property ensure that the test material is one in which heat transmission is predominantly due to solid conduction mechanisms. 6) Verify the performance with appropriate available reference materials.				
Sub-second techniques	104 , 105 , 106,107	electrical conductors only	700 to 3300	50 to 400
Thermal conductivity is determined from the power balance obtained during the cooling part of the rapid heating and cooling of a thin wire. The heat dissipated by the specimen is lost by radiation and conduction.				
Key Requirements: 1) Specimen must be an electrical conductor. 2) Specimen must be homogeneous and isotropic. 3) Specimen must be cylindrical and a long thin-rod approximation must be possible. 4) There must be a blackbody hole in the specimen tube to allow pyrometric temperature measurements.				

Table 1. Common thermal conductivity or thermal diffusivity measurement methods.[108]

5.2.1 Common Thermal Properties Measurement Q&As

The following is a series of commonly asked questions and answer that present important considerations in making thermal conductivity and diffusivity measurements.[109]

A1. What is the connection between thermal conductivity and thermal diffusivity?
Thermal conductivity (k) and thermal diffusivity (α) are related by $k = \alpha \cdot \rho \cdot Cp$, where ρ is density and Cp is specific heat capacity. At high temperatures, or when the material is available only in small sizes, α, ρ and Cp are often measured to determine k.

A2. What is the physical difference between thermal conductivity and thermal diffusivity?
Thermal conductivity (k) is a property that determines HOW MUCH heat will flow in a material, while thermal diffusivity (α) determines HOW RAPIDLY heat will flow within it. A homely example is to imagine holding a poker that is suddenly put into a fire. How hot you feel at the handle end is determined by the poker's thermal conductivity and how quickly you feel the heat is determined by its thermal diffusivity.

A3. How can I test loose-fill insulating materials?
The insulating material is blown (or cured depending on material type) into a frame of rigid material and a bottom with a thin material with negligible resistance. The blowing is carried out according to instructions (e.g. manufacturer, standard) so as to obtain the intended fiber distribution, weight and density.

A4. Is it possible to measure the thermal resistance/conductivity of products with air cavities?
Yes it is possible but heat flow direction and size of the cavities must be considered. The heat flow in a cavity is by radiation, convection and conduction. If convection occurs, the convection pattern/type will mainly depend on heat flow direction, temperature and size of the cavity.

A5. Why can I see different thermal conductivity values for foamed plastics?
If the product is manufactured with a blowing agent that has a lower thermal conductivity than air and it gradually leaves the product, the thermal conductivity will increase with time. The long-term change in thermal resistance will depend on the gas type, gas permeability and thickness of the product and type of covering (if any). For slabs an aged value is stated.

A6. Is it possible to calculate thermal conductivity with knowledge of the density?
An approximate estimation is possible. The equation lambda = a + b*density + c/density can be used for low density material. The third term represents the radiant heat transfer, which is considerable for low densities. For higher densities the equation lambda = a +

b*density + c*density² is often used. The constants a, b, c are usually calculated from several measurements.

A7. How can one perform a measurement on a moist material?
Measurement of moist materials is complicated, time-consuming and must be carried out by experienced personnel. Measurement causes normally a redistribution of moisture in the material which leads to two types of problem: A) Redistribution of moisture. The test is carried out on a specimen with a moisture distribution that is no longer uniform. B) Redistribution of the moisture simultaneously induces phase changes. These effects must be well known or negligible during the test. Small temperature gradients do not guarantee that phase-change effects will be negligible.

A8. Is it possible to measure thermal conductivity on components of unusual size and shape?
In situ measurements are often not possible. Thermal conductivity measurement devices need special geometries which usually differ from that of ordinary objects. In the case of small components thermal diffusivity measurements are recommended, with samples of 8 mm diameter or so.

A9. What are the reasons to measure thermal diffusivity instead of thermal conductivity?
In order to calculate thermal stress during rapid temperature change you need the thermal diffusivity of the material. Other reasons are: 1) Only small samples in the range of 8 mm diameter and 2 mm thickness are available, 2) the temperature is higher than 1000°C which is the upper limit for thermal conductivity measurements.

A10. What are the most frequently used methods to measure thermal diffusivity or thermal conductivity?
There is no universal method to measure thermal diffusivity or thermal conductivity. Basically, thermal conductivity is determined by steady state methods and thermal diffusivity by transient methods. The choice of a measurement method depends on many criteria such as sample geometry, temperature range, type of material, magnitude of thermal conductivity / diffusivity, uncertainty, etc.

A11. Does the thermal conductivity / diffusivity of all materials have same temperature dependence?
The variation of these thermal properties with temperature depends on the type of material. In the same temperature range the values of thermal conductivity / diffusivity can decrease for some materials and increase for others.

A12. Is it possible to extrapolate the thermal conductivity of a material beyond the temperature range for which the measurements are made?

The variation of thermal conductivity / diffusivity is not monotonous in a wide temperature range. Thermal diffusivity and thermal conductivity sometimes vary sharply with temperature, especially at low temperatures and in the vicinity of phase transition (Curie point of iron for example). So thermal properties values should not be extrapolated outside the temperature range for which the measurements are made.

A13. What are the most accurate measurement methods?
Measurement methods can be divided into two categories: absolute methods and comparative methods. An absolute method allows one to perform a measurement that is directly traceable to the primary SI units (such as temperature, time, length, voltage, weight, etc.) without the use of an external reference of the same quantity. For comparative methods, the thermal conductivity / diffusivity measurement is carried out by comparison with reference materials that were beforehand characterized by an absolute method. So, absolute methods give smaller uncertainties of measurement than with comparative methods.

A14. In the laser flash method, why should the specimen be opaque to the laser beam?
Laser flash method is based on the comparison of experimental curves with a mathematical model that assumes that the energy of the beam is absorbed at the surface of the specimen. If the specimen is not opaque at the wavelength of the beam, then the energy pulse is absorbed inside it. Then the boundary and initial conditions of the mathematical model are different from experimental conditions. This leads to a wrong estimation of thermal diffusivity. This problem can be avoided by coating the specimen or by using a laser having a suitable wavelength (CO2 laser for example).

A15. Is it possible to measure thermal diffusivity of a multilayered material by laser flash method?
Usual methods that estimate thermal diffusivity from experimental curves assume that the specimen is homogeneous. Thermal diffusivity of multilayered materials can be estimated by these methods if the number of layers is high enough to consider the specimen as homogeneous. This assumption is valid if the same thermal diffusivity values are obtained for specimens having different thicknesses. For multilayered materials which cannot be considered as homogeneous (specimen consisting of 2 or 3 layers for example), a specific mathematical model describing the thermal behavior of the considered specimen should be used.

A16. What are the problems in measuring thermal conductivity using pulse methods?
The problems are not due to the experimental apparatus which is relatively simple, but the complexity of evaluation of thermal conductivity from thermal profiles inside the specimen. This requires a large matrix computation.

A17. Why do thermal conductivity/diffusivity measurement devices need special specimen geometry?

The uncertainty of thermal diffusivity / conductivity measurements depends on how well the theoretical model corresponds with the measurement set-up, in particular the validity of the assumptions concerning sample geometry (shape, size, thickness/diameter ratio, parallelism of specimen faces, etc.).

A18. What is the thermal equivalent of Ohm's law?
There is a close analogy between the flow of electricity (electrons) and heat. Heat flux Q corresponds to the electric current I. Temperature difference corresponds to voltage (potential difference). Thermal resistance corresponds to the electrical resistance. Thermal resistance is connected with thermal conductivity through geometrical parameters (area and length). Applying this model one can solve thermal problems in the same way as when analyzing electrical circuits.

A19. What is the principle of thermal diffusivity measurement?
The methods of measuring thermal diffusivity rely on analyzing the temperature response of the specimen subjected to transient thermal conditions. The transients can be caused by a pulse, a periodically varying heat flow or a monotonic heating regime.

5.2.2 In situ Measurements

An important consideration for hydrogen storage materials is whether-or-not the goal is to test the thermal properties of the material under operational conditions. Specifically, under a hydrogen atmosphere, steady state conditions or during hydrogen uptake or release, and possibly at different hydrogen contents. For physisorption materials this will likely mean making measurements at low (e.g. 77K) temperatures, and, for many hydrides, at elevated temperatures (20 to +300°C). Ideally, one would like to be able to control the hydrogen overpressure and control the charge or discharge of the material. Such in situ measurements present many technical challenges, requiring a controlled hydrogen atmosphere measurement cell that is able to withstand temperature extremes and elevated pressures. For many of the thermal conductivity measurement techniques this would impose gas-tight feed-through for electrical control and measurement lines adding to the technical complexity of the device. An example of one approach to overcome these complexities was the use of the needle probe method combined with a cylindrical pressure vessel to contain the sample materials.[110] The thermal conductivity probe was sealed into the bottom of the vessel and positioned in the center of the sample material (see Figure 23). The hydrogen pressure, content, and temperature of the vessel could be controlled by external means. The advantage of this simple design is that only one feed-through for the thermal conductivity measurement device (which was came sealed in a stainless steel tube) was needed. While the needle probe method has its own set of strengths and weaknesses, like all methods, it points to the importance of considering simplicity of design as a factor in making successful measurements.

5.2.3 Steady-State vs. Transient Techniques

These measurement methods can be divided between steady-state and transient techniques. Steady-state techniques are appropriate for material application where the temperature of the material does not change with time and data analysis is straightforward. However, this is unlikely to be the case for most hydrogen storage systems which operate by changing temperatures. The transient methods perform measurements during the process of heating up the sample.

Re-arranging Equation 2, thermal conductivity is defined as:

Equation 18 $$k = - (Q_x/A)/(dT/dx)$$

where Q_x is the heat transfer rate in the x direction, in W; A is the area normal to direction of heat flux, in m^2; dT/dx is the temperature gradient in the x direction, in $K^{-1}\cdot m^{-1}$, and k is the thermal conductivity, in $W\cdot K^{-1}\cdot m^{-1}$. The negative sign indicates that the flux is down the gradient, and it can be shown from irreversible thermodynamics that the coefficient k is always positive.

Q_X/A is the heat flux which creates the thermal gradient, dT/dx. Thus, as demonstrated earlier in Figure 1, the measurement of thermal conductivity involves the measurement of the heat flux and temperature difference. The most difficult part of the measurement is usually associated with the measurement of heat flux.

The measurement of the heat flux is referred to as absolute when it is measured directly, as for example, by measuring the electrical power going into the heater). Thermal conductivity measurements are referred to as comparative when the heat flux measurement is done indirectly by comparison.

In addition to these two main methods, other secondary methods usually transient in nature, can also yield thermal conductivity.

In general, the entire heat flux must flow through the sample (and the references, in the comparative case) in the direction of the measured temperature difference. Therefore, the heat losses or gains must be minimized as close to zero as possible in all other directions. To some degree, this can be accomplished with packing insulation around the sample, or, at higher temperatures, where such simple solutions become inefficient, with installation of a "guard". If the guard is controlled to have the identical temperature gradient as the sample, then errant heat flow will be minimized.

The configuration of a given measurement system and of the specimen itself is influenced most prominently by the magnitude of the thermal conductivity. When the thermal conductivity is high, the specimens are usually "long" (for example, in the form of cylinders). When the conductivity is low, the specimens are usually "flat" (for example, in the form of plates or disks). When the specimen conductivity is high, the heat flux is usually fairly high so that a long specimen in the direction of flow helps establish a reasonably high temperature gradient which can then be accurately measured.

On-the-other-hand, when the specimen conductivity is low and the heat flux is correspondingly low, only a relatively small thickness is required to generate a large accurately measurable gradient. With low specimen heat flux, lateral losses are of concern, thus thin samples with large surface areas a help to minimize heat loss in the non-measuring directions. In some flat-plate cases, the surfaces of the sample not in the direction of heat flow are surrounded by pieces of the same sample material to provide self-guarding.

In general, however, the magnitude of the sample's conductivity relative to the insulated surroundings should be as high as possible. This becomes more critical as the temperature range of measurements increase. In some measurement techniques, done at very high temperatures, the lateral losses are allowed to be high, but they are accounted for quantitatively in the conductivity measurement.

The following is a summary of some of the current methods used for measuring Thermal Conductivity. The first section discusses the all-important question of the various ways that heat flux can be measured.

5.2.1 Example of One Common Measurement Approach for Hydrogen Storage Materials

One common method for determining the thermal conductivity of hydrogen storage materials is to calculated it from measurements of thermal diffusivity α ($m^2 \cdot s^{-1}$), the specific heat capacity C_p ($J \cdot kg^{-1} \cdot K^{-1}$), and finally the density ρ ($kg \cdot m^{-3}$)of a sample of the material.

Thermal diffusivity measurements are can be performed with a thermal flash (e.g. xenon) diffusivity instrument. The instrument should be calibrated prior to the sample measurement. This can be done using an iron standard. Hydrogen storage materials are often in powder form, however, for flash diffusivity measurements, solid sample are require and so, it is common to form pellets of the material for these measurements. To

avoid transmittance and improve light absorption, the lower (flash side) surfaces of the samples are typically coated with graphite. It has also been noted that it has been necessary to apply a thin layer of silver paint to the top surfaces of pellet samples to prevent them from fracturing during measurements.[111] The specific heat capacity measurements are commonly performed using differential scanning calorimetry (DSC). Again, calibrations of the instrument should be performed prior to measurements and this can be done using, for example, a sapphire standard. The density is often simply determined as a bulk parameter (packing density) from the mass and physical dimensions of each material sample.

The thermal conductivity $\boldsymbol{k}$ is then (Equation 5).

Equation 19 $$k = \alpha \rho C_p$$

5.3 Heat Flux Measurement Methods

The determination of thermal conductivity under steady state conditions typically requires the precise measurement of temperatures at sample boundaries and the heat flux across the sample. Temperature measurement can be achieved by a variety of direct measurement sensors or (in the case of cryogenic measurements) by assuming the sample interface is at the boiling point temperature of the cryogen employed. However, the measurement of heat flux is not always as straight forward. The following are the most common methods for the determination of the heat flux through a material.

5.1 Axial Flow Methods

Axial flow methods have been around for a long time and have produced some of the most consistent, highest accuracy results reported for a variety of applications in the literature. It is often used for measurements at cryogenic temperatures. The sample and instrument are symmetrical along the axial direction to provide (in principle) On-dimensional steady-state axial heat flow. The flow of heat is created through the specimen from the electrical heater mounted at one end and a heat sink at the other. The heat flux in through the sample is calculated from the power dissipation of the electrical heater.

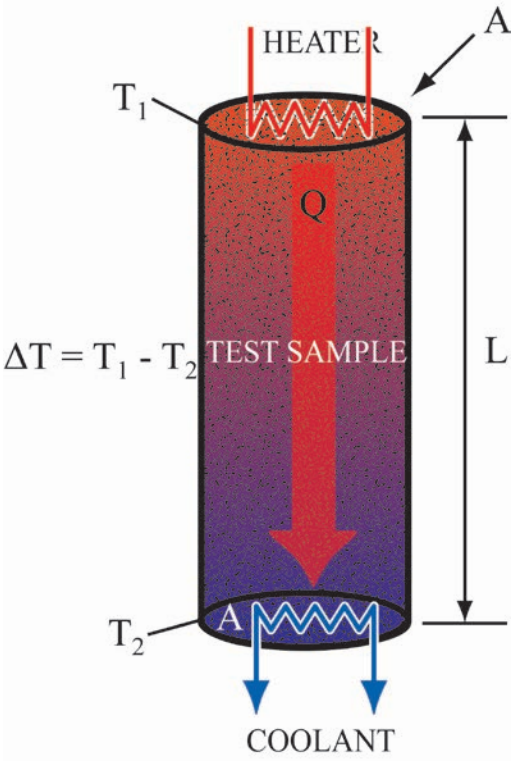

Figure 9. Simple schematic of axial heat flow method.

From Equation 2 the heat flow through the sample *Q* becomes:

Equation 20 $$Q = k\,A\,\Delta T / L$$

Where k is the thermal conductivity, A is the surface area in the axial direction of the sample, ΔT is the temperature change from one end to the other in the sample, and L is the length of the sample. The heat flux Q can be measured either directly or indirectly as described in the next two sections. Thus, the thermal conductivity, k, can be determined by measuring Q, ΔT, A, and L.

The reduction of radial heat losses in the axial heat flow is the key issue in making accurate measurements. While these losses may be minimal at low temperatures, they become significant and more difficult to control for sample temperatures above room temperature. For accuracy, it is important to pay attention to experimental parameters such as the ratio of effective sample conductance to lateral insulation conductance (the higher the better). Additionally, the quality of thermal guarding is very important. Note that, as with many of heat flow measurement techniques, the Axial Heat Flow method

can only measure the thermal conductivity of homogeneous materials. This measurement technique is not normally suitable for samples that have either discrete layers or inclusions.

An example illustration of an axial heat flow instrument is presented in the figure below.

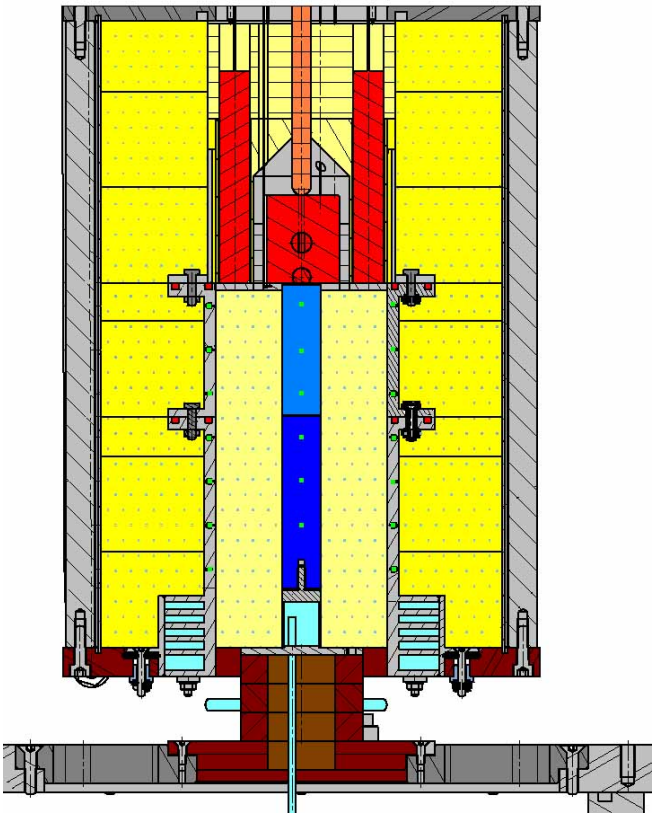

Figure 10. Example schematic of an Axial Heat Flow measurement device.[112]

5.1.1 Direct Power Measurement

One of the most common ways to determine heat flux through a sample is to measure the power supplied to a heater that creates a temperature gradient in the sample. This is mostly used in sub-ambient environments. Instruments of this type require very precise knowledge of the electrical power feeding the heater. Any losses from the heater surfaces can have a major effect on the results. Unfortunately, because of parasitic heat losses, the direct measurement of heating power is not trivial and can lead to highly inaccurate thermal conductivity values when large heat leaks are present.

5.1.1 Comparative Thermal Conductivity Methods

In comparative thermal conductivity measurements a standard material with a known thermal conductivity and precise thickness is placed in series with the sample to be measured (Figure 11). The heat flux through the standard material can be calculated fairly accurately by measuring the temperatures on each side of the standard materials.

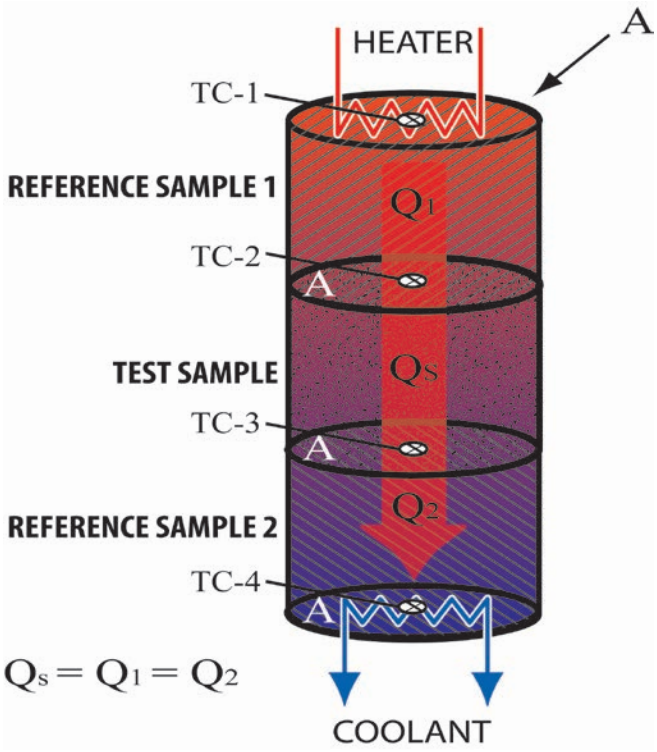

Figure 11. Schematic of comparative thermal conductivity measurement configuration.

Without significant heat loss in other directions, the heat flux across the sample will the same as that determined for the standard materials. By knowing the thermal conductivity of the standard reference materials the heat flow Q across the sample can be determined indirectly without the need to accurately measure the heat input by the heater. Thus, the reference samples combined with temperature sensors on either side act as heat metering (or measuring) sensors.

5.1.2 Boil-off Calorimetry Method

In Boil-off calorimetry, the sample is placed between a heat source and a cold source which is in direct contact with an enclosed and thermally isolated cryogenic liquid. The heat source increases the temperature of the hot side of the sample to above the boiling point of the liquid. The cryogenic liquid maintains a constant temperature (the boiling point of the liquid) at the sample. Heat transferred through the sample causes the cryogenic liquid to evaporate (boil-off). The flow rate of the release gas vapor is measured and knowing the heat of evaporation can be converted into heat flow (and heat flux knowing the cross-sectional area of the sample.

Several systems have been designed based on this principle for measuring thermal conductivity and cryogenic temperatures. For example, Fesmire et al. developed guarded hot plate and concentric cylinder cryostats using boil-off calorimeters for cryogenic thermal conductivity measurements. Two of the instruments incorporated direct power measurements and comparative thermal conductivity measurements in addition to the boil-off heat flux measurements.[113] The advantage of this is that the heat flux could be measured directly from the heat source, comparatively through the standard materials, and through boil-off on the cold side of the instruments. This provided 3 independent measurements of heat flux.

One of the disadvantages of Boil-off calorimeters is that, in using a cryogen for the cold side, the temperature of the measurement is generally limited to the liquification temperature of that cryogen. This either creates a very large ΔT or a very limited average temperature range which can only be modified by changing one cryogen for another. Another issues is that it is difficult with such designs to limit heat leaks on the cryogenic side of the device that contribute to a boil-off rate of the liquid that may not accurately represent heat flux through the sample. Additionally, using boil-off calorimetry to make measurements at liquid hydrogen and liquid helium temperatures may be impractical due to economic and safety factors.

5.2 Guarded or unguarded heat flow meter method (ASTM C518, E1530).

This method involves the use of a flux gauge. The flux gauge is very similar, in purpose, to the references in the comparative cut bar method. In practice, the reference plate material of the flux gauge has a very low thermal conductivity and, therefore, it can be made very thin. Flux gauges can be constructed from just about any material and any thickness depending on the material's thermal conductivity. Common requirements for all flux gauges are that the reference material used for the measuring section be stable, not affected by the thermal cycling, and that the gauge materials thermal conductivity be calibrated using an accurate independent system.

Typically, a large number of thermocouple pairs are located on both sides of the reference plates. These thermocouples are connected differentially to yield directly an electrical signal that is proportional to the differential temperature across the plate. In its most simple form the sample's thermal conductivity k_S is determined by:

Equation 21

$$k_S = k_R \left(\frac{\Delta T_1 + \Delta T_2}{2\Delta T_S} \right)$$

Where k_R is the known thermal conductivity of the reference material in the flux gauge, ΔT_1 and ΔT_2 are the temperature differences across two identical reference materials in the flux, and ΔT_S is the temperature difference in the axial direction between the two ends of the sample.

This type of flux gauge is mostly used with instruments testing very low thermal conductivity samples, such as building insulations. Since many of the hydrogen storage materials have very poor thermal conductivities, this may be an appropriate method for such materials. A very large variety of testing instruments use this heat flow meter method.

5.3 Guarded Hot Plate Method (ASTM C 177)

The guarded hot plate method of testing thermal conductivity was the first to become a nationwide standard (ASTM C 177).[114] The method is an excellent method of testing the effective thermal conductivity of solids under certain conditions. It is a widely used and versatile method for measuring the thermal conductivity of insulating materials. The method typically requires sample that are rather large samples (e.g. a pair of 6.0 inch square specimens, up to 2.0 inch thick for insulating materials). This may be problematic for some hydrogen storage materials that can only be produced in small quantities.

The method attempts to create unidirectional heat transfer through a pair of identical samples. Then, by adding a known heat flux to a hot plate between then while providing a heat sink at a cold plate on the opposite side of each sample a temperature gradient within each sample is formed. The subsequent temperatures at each side of the samples are measured when the system reaches steady state. Using the heat flux, sample thickness and surface areas, and temperature measurements, Fourier's unidirectional heat conduction equation (Equation 2) can then be applied to easily calculate an effective thermal conductivity for the samples.

One of the first systems for the measurement of insulating materials was described in a 1920 publication by Van Dusen.[115] Figure 12 shows a diagram of a similar version of the NBS 200mm guarded-hotplate apparatus.

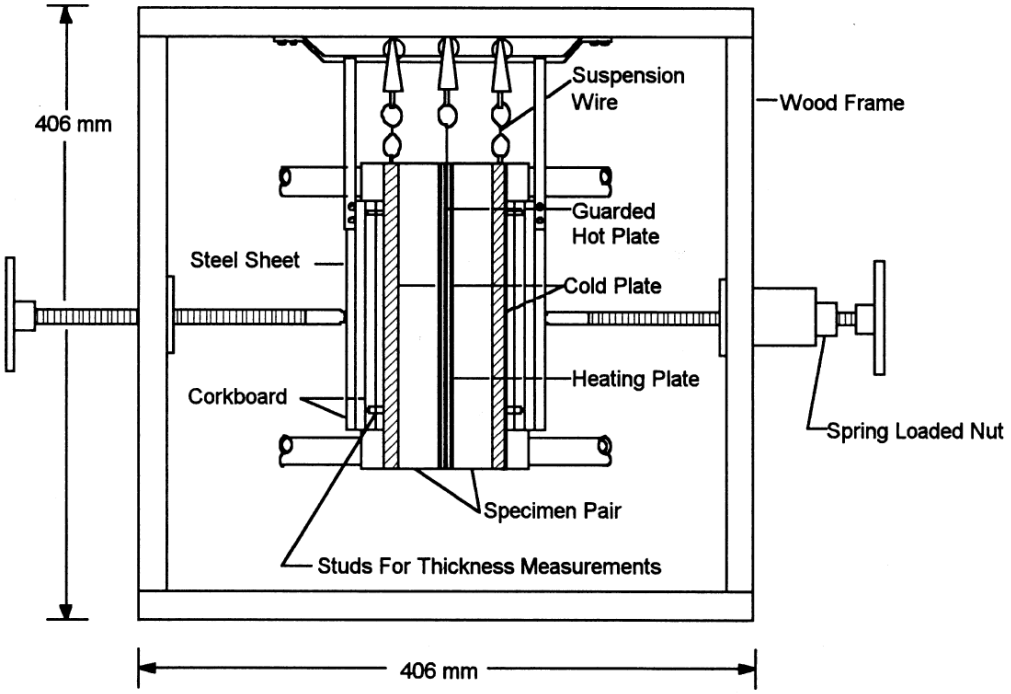

Figure 12. Schematic of NBS 200 mm guarded-hot-plate apparatus (1928 version).[114]

In this type of device, a flat, electrically heated metering section supplies the planar heat source over the hot face of the sample(s) and is controlled through differential thermocouples. The most common measurement configuration is a symmetrical setup where the heater assembly is sandwiched between two samples. The opposite side of each material sample is covered by cooling plates. The cooling plates are generally air or water cooled. This installation is then surrounded by an insulated thermal shield or guard that causes the heat to flow only uni-axially rather than towards the sides of the test cell. Ideally, the pair of samples is well matched (i.e., nearly identical) so that the differences between samples for both ΔT_X and L are quite small. The thickness and surface areas of the specimens should be measured very precisely. A schematic of a guarded hot plate apparatus is shown in Figure 13.

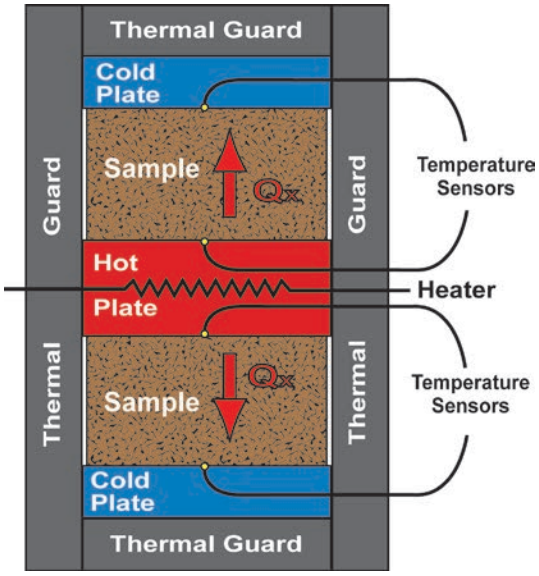

Figure 13. Schematic of basic guarded hot plate design.

This is an absolute method of measurement. It requires: the establishment of steady-state conditions, and the following measurements:

- measurement of the unidirectional heat flux in the metered region,
- measurement of the temperatures of the hot and cold surfaces,
- measurement of the thickness of the sample(s), and
- measurement of any other parameter which may affect the unidirectional heat flux through the metered area of the specimen.

Measurement systems based on this method can be divided into three different categories:

1. apparatus working around room temperature,
2. apparatus working below room temperatures (down to about -180°C), and
3. apparatus working at high temperature (600°C or above). A given apparatus is most often best adopted for measurement in one of these temperature ranges.

Typically, in more advanced systems the heat metering section of the hot plate is surrounded on all lateral sides by a guard heater sections and possibly additional auxiliary heaters on the opposite side of each sample. In the single sided configuration, the heat flow is passing through a single sample and the back of the main heater acts as a guard plane creating an adiabatic environment. This can also be done by replacing the second sample in a double-sided instrument with a known insulating material. A diagram showing a single sided mode in an advanced double-sided Guarded Hot Plate

configured with metered heating section is shown in Figure 14a.[116] Figure 14b illustrates heat flow at the gaps at the edge of the metered heating section. Figure 14c shows a diagram of an advanced system with a heater in the guard plate adjacent to the metering heater section, and Figure 14d provides the temperature profile for double- and single-sided mode of operation of the apparatus in c. The actual designs of guarded hot plates may differ markedly from the schematic design shown in the figure. This basic design was selected to illustrate the differences in temperature profiles that can arise when equipment designed for operation in a double-sided mode is used in a single-sided mode. Designs of actual guarded hot plates should be reviewed using this example as a guide to assess what problems they may have in either mode of operation.

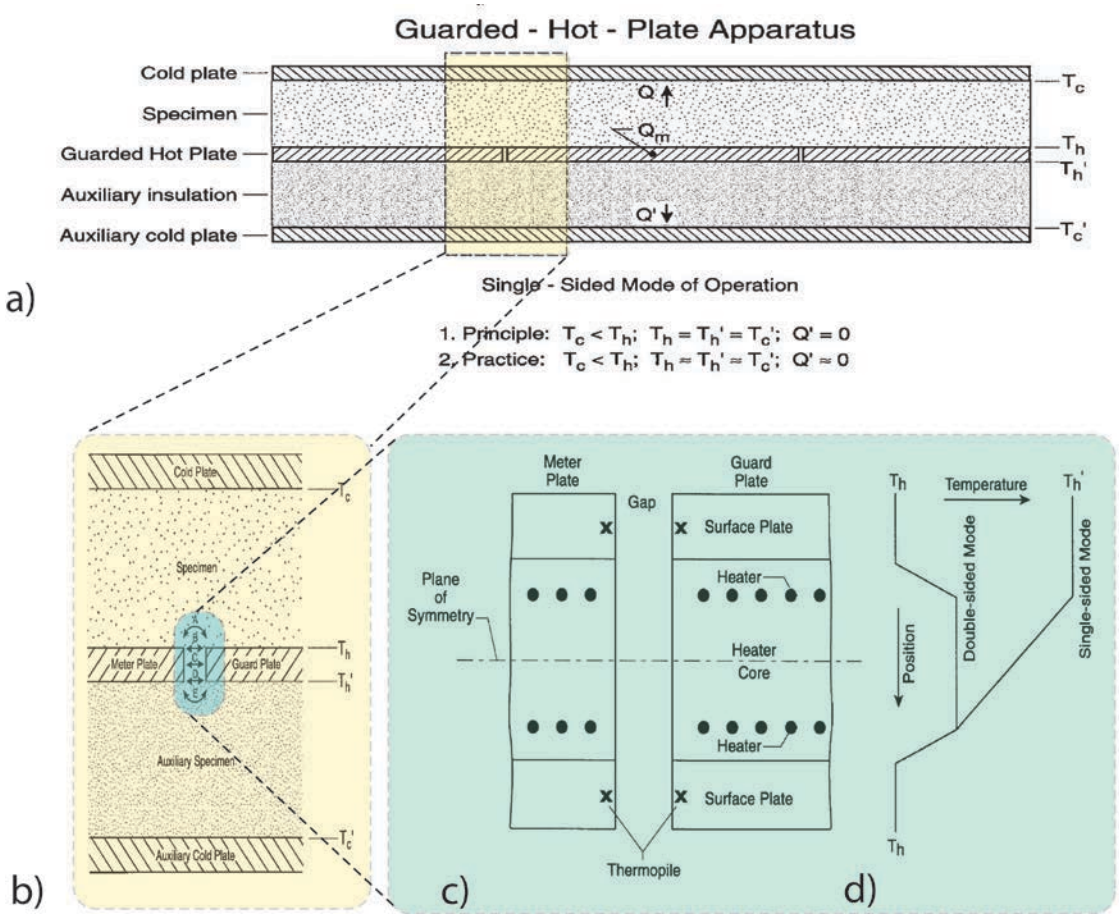

Figure 14. a) Schematic diagram of an advanced single-sided mode of operation Guarded-Hot-Plate apparatus, b) Diagram illustrating heat flows at gap region, c) Diagram of (hypothetical) Guarded-Hot-Plate with distributed heat source, and d) Corresponding temperature profile for double- and single-sided mode of operation.[116]

In the case of double-sided Guarded-Hot-Plate operated in single sided mode the samples effective thermal conductivity can be determined as follows, where

A = meter area of hot plate [m^2],
Q = heat flow through meter section of test sample [W],
C = thermal conductance of specimen [$W \cdot m^{-2} \cdot K^{-1}$)],
R = thermal resistance of specimen [$m^2 \cdot K \cdot W^{-1}$],
k = thermal conductivity of specimen [$W \cdot m^{-1} \cdot K^{-1}$)
r = thermal resistivity of specimen [$m \cdot K \cdot W^{-1}$]
L = specimen thickness [m],
T_c = surface temperature of cold plate [K],
T_h = surface temperature of hot plate in contact with the sample [K], and the primes indicate values for the auxiliary insulation side of the measurement apparatus.

The heat flow through the specimen is given by

Equation 22 $$Q = Q_m - Q'$$

where Q is the heat flow through meter section of specimen, Q_m is the measured power input to meter plate and Q' is the heat flow through meter section of auxiliary insulation.

Q' is determined from the known thermal conductance t of the auxiliary insulation material and the measured temperature gradient across the insulation according to

Equation 23 $$Q' = C' A (T'_h - T'_c)$$

where: C' is the know thermal conductance of the auxiliary insulation at a temperature corresponding to $(T'_h - T'_c)/2$. Both Q_m and Q' should be measured and determined in accordance with ASTM C 177.

Thus having determined Q, the thermal properties of the sample are given by

Equation 24 $$C = Q / A (T_h - T_c)$$

Equation 25 $$R = A (T_h - T_c)/Q$$

Equation 26 $$k = (LQ) / A (T_h - T_c)$$

Equation 27 $$r = (A (T_h - T_c))/(LQ)$$

When operated in a single-sided mode, half of the heat flow through the test specimen comes from the heater on the front side of the guarded hot plate, half from the backside heater. The second temperature profile in Figure 14d illustrates the variation in spatially averaged temperature through the guarded hot plate when operated in the single-sided mode with the same heat flux through the test specimen as above. The temperature drop across the insulating layer on the front side is the same as it was in the double-sided mode, since the total heat flow through that layer is the same in each case. However, the heat flow from the heater on the backside of the hot plate must pass through the heater core region, resulting in a significant temperature drop. In some guarded hot plate designs, the heater core is thick enough, and its thermal conductivity low enough, that the temperature drop across the guarded hot plate (T_h' - T_h) is a significant fraction of the temperature drop across the test sample. In such cases controlling the guard heater so that the thermopile produces a zero output may not ensure that there is a temperature balance between the meter and guard plates. If it does not, significant errors may occur in the determination of the heat flow through the test sample due to extraneous heat flows across the gap, across the portions of the test specimen, or the auxiliary specimen in the proximity of the gap.

The guarded hot plate method, although very effective for many practical tests on insulating materials, is difficult to apply to powders. This is because containing the powder within the apparatus is much more difficult than installing a solid specimen. Any mechanical supports used would create a heat leak and make material thermal conductivity much harder to calculate. Therefore, other configurations which may be more conducive to loose powders should be examined for most hydrogen storage materials (which typically consist of powders). An exception may be powders that have been pressed into compacts. However, one should consider whether the compacts in the as measured state will be representative of the hydrogen storage material after many cycles.

5.4 Radial Heat Flow Method

One-dimensional heat flow thermal conductivity measurements can be performed by means of other geometries besides the flat-plate geometry of the guarded-plate method. For example, the guarded radial method promotes one-dimensional radial heat flow by minimizing undesired axial (i.e., longitudinal) heat flows. An early version of such

a device was developed in the 1960s.[117] This was a ceramic-core apparatus for the measurement of thermal conductivity of granular materials from 100°C (373K) to 1100°C (1373K). A schematic diagram of the horizontal cross section this apparatus is shown in Figure 15.

For this cylindrical geometry, the algebraic form of Fourier's heat conduction equation for one-dimensional heat flow is:

Equation 28

$$Q = 2\pi L\bar{k}\frac{-(T_a - T_b)}{ln(b/a)}$$

where L is the length of the test section, T_a is the temperature at radius a, T_b is the temperature at radius b, and $\bar{k}$ corresponds to the thermal conductivity at $\overline{T}$ given by: $\overline{T} = ½(T_a + T_b)$.

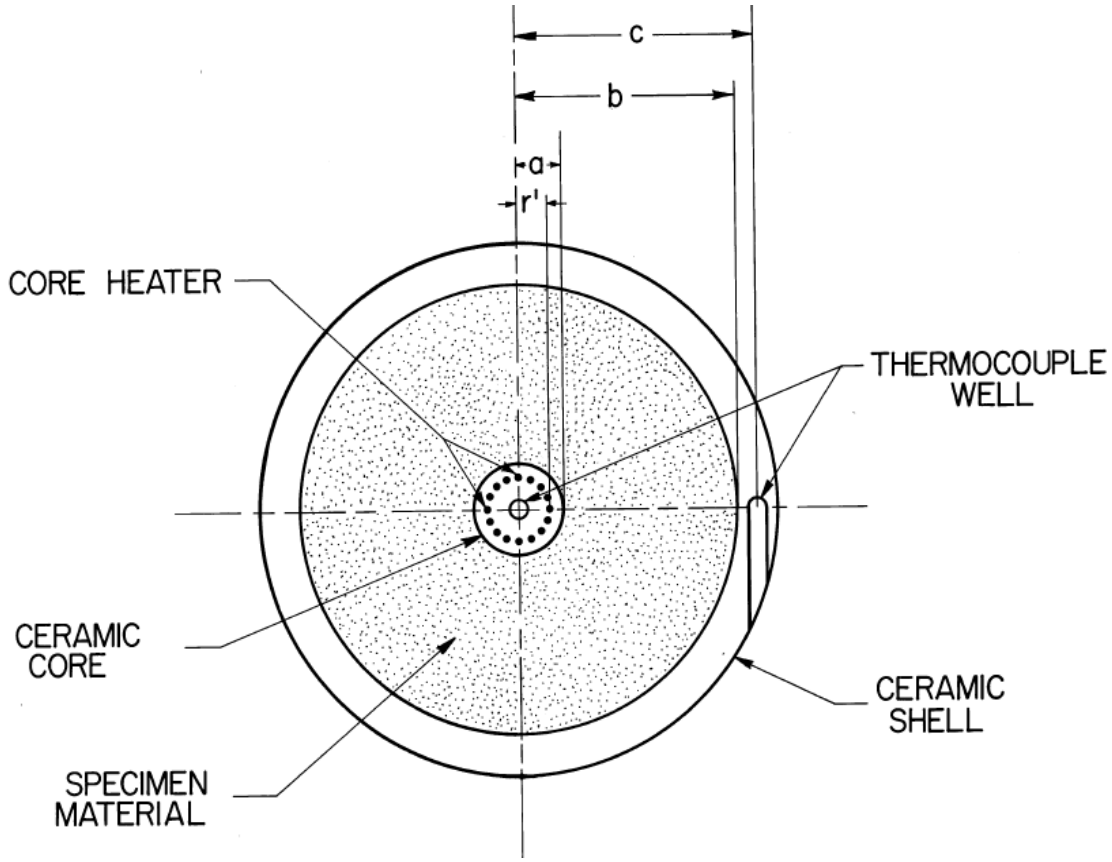

Figure 15. Horizontal cross-section of ceramic core (CC) apparatus for granular insulation materials.[114,118]

5.5 Concentric Cylinders Method

Two configurations which have proven to be suitable for low thermal conductivity powder sample measurement are the concentric cylinder and concentric sphere methods. The concentric cylinder method has been used effectively to measure the thermal conductivity of insulating materials at cryogenic temperatures. [119,120] It is a method that has been used for such measurements as early as 1926.[121]

Most commonly a concentric cylinder measurement system consists of a liquid cooled outer cylinder and an electrically heated inner cylinder with powder filling the annular space between the two. The material space can then be evacuated or filled with gas to a controlled pressure. Ideally, the concentric cylinder apparatus should maintain a uniform heat flux in the radial direction only. Typically, the mechanical supports at the top and bottom of the device to retain the inner cylinder act as heat leaks creating a temperature gradient along the inner cylinder. For this reason, the apparatus is designed to be very long with respect to its radius. This allows for a fairly uniform temperature along a sufficient length of the cylinder.

An example illustration of such a system used for measuring the effective thermal conductivity of insulating materials over large cryogenic temperatures is show in Figure 16.[119]

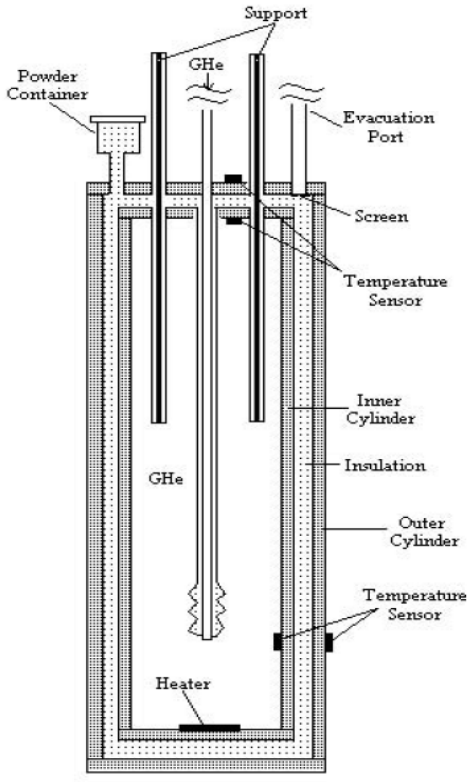

Figure 16. Vertical cross-section of an example concentric cylinder apparatus for powder insulation materials.[119]

The following is a description from Barrios of the particular equipment used for these insulation materials measurements.[119] This instrument consisted of two closed, concentric copper cylinders. The inner cylinder is the hot cylinder (HC), and the outer cylinder is the cold cylinder (CC). The cylinders were suspended by insulating rods. An electric heater was fixed between a copper plate and the bottom of the HC to ensure good thermal contact with the HC. Temperature sensors were mounted on the side and top of the HC and the CC.

One simple option for measurements was to immerse the CC in LN2 and recording the temperature of the HC over time. The limitations of this technique is that it is very time consuming and only provided thermal conductivity measurements down to roughly 80K. The use of lower temperature cryogens is not especially practical as these must be refilled frequently. A second option was the use of a single stage cryocooler capable of reaching ca. ~20K. The cryocooler coldhead must have good thermal contact with the CC of the measuring apparatus for the experiment to perform effectively. In this particular study, flexible, tinned copper braids were used to form a thermal link between the cryocooler coldhead and the CC while allowing for thermal contraction/expansion. In order to allow the experiment to reach its minimum temperature, the cryocooler and the measurement apparatus must be well insulated from any outside heat sources. Insulation of the apparatus from its surroundings was accomplished by: a) the installation of two radiation shields between the measurement apparatus and the top plate, and b) placing the entire apparatus inside of a high-vacuum insulated cryostat with a liquid nitrogen thermal shield.

Pressurized gaseous helium is used in the HC to ensure a uniform temperature. The pressure in the annular space (insulation space) and outside the CC may vary. Therefore each cylinder must be vacuum sealed so as to prevent gaseous conduction or convection between the cylinders. Also, ports must be provided to all spaces to allow for pressurizing and/or vacuum pumping. All ports and wiring feeds directly connected to the apparatus are connected by solder, welded, or stycast and are tested individually to assure that they are leak tight. To ensure that the vacuum pump connected to the insulation space is not contaminated with insulation powder, a fine screen is placed where the vacuum port meets the top of the CC. Because the cylinders must be opened and closed relatively frequently, indium O-rings seals are fit into grooves set into the top and bottom of each cylinder and compressed to form a leak tight seal.

It is important to recognize that, axial heat leakage can still be problematic when using the concentric cylinder method. Convective heat transfer and temperature gradients when measuring under a gas pressure may also create temperature gradients in the axial direction. In addition these effects may be a function of pressure, adding further complexity to the analysis of in situ thermal conductivity of hydrogen storage materials.

The calculation of effective thermal conductivity at cryogenic temperatures from the closed concentric cylinder configuration shown in Figure 16 can be derived as follows.[119] The initial step of a cryogenic measurement is the cool-down of the system from ambient temperature to cryogenic temperatures. This cool-down can be modeled by the lumped capacitance method based on convection heat loss causing a decrease in the internal energy of a body. This is given by:

Equation 29

$$q = hA(T - T_{\infty}) = -mc(T)\frac{\partial T}{\partial \tau}$$

where *h, A*, and *c(T)* represent the convection heat transfer coefficient, the heat transfer area of the body, and the specific heat of the body, respectively. The requirement to be able to derive estimates for heat loss within 5% accuracy using the lumped capacitance method is:

Equation 30

$$\frac{h(V/A)}{k_{Cu}} < 0.1$$

where k_{Cu} and V are the thermal conductivity and volume of the body (the copper cylinder in the present example). For the present insulation materials example, heat transfer is modeled as conduction, rather than convection. Therefore, the following substitution must be made for h

Equation 31

$$h = \frac{k_{ins}}{z}$$

where k_{ins} and z represent the effective thermal conductivity and thickness of the sample, respectively. This may be a reasonable representation for many hydrogen storage materials (Hydrides, some low thermal conductivity physisorption materials such as aerogels…). Note however that this is correct for the materials only and not for material plus hydrogen as would be found in normal operating conditions. Using this conduction model, Equation 30 then becomes

Equation 32

$$\frac{k_{ins}V}{k_{Cu}A \cdot z} < 0.1$$

Using the lumped capacitance method, the solution to Equation 29 is

Equation 33

$$\frac{T - T_\infty}{T_o - T_\infty} = e^{-\left(\frac{k_{ins}(T)\cdot A}{z\cdot m\cdot c(T)}\right)\tau}$$

where T_∞ represents the temperature of the outer cylinder. T_o and T represent the initial temperature and temperature after time τ of the inner cylinder, as seen in Figure 17.

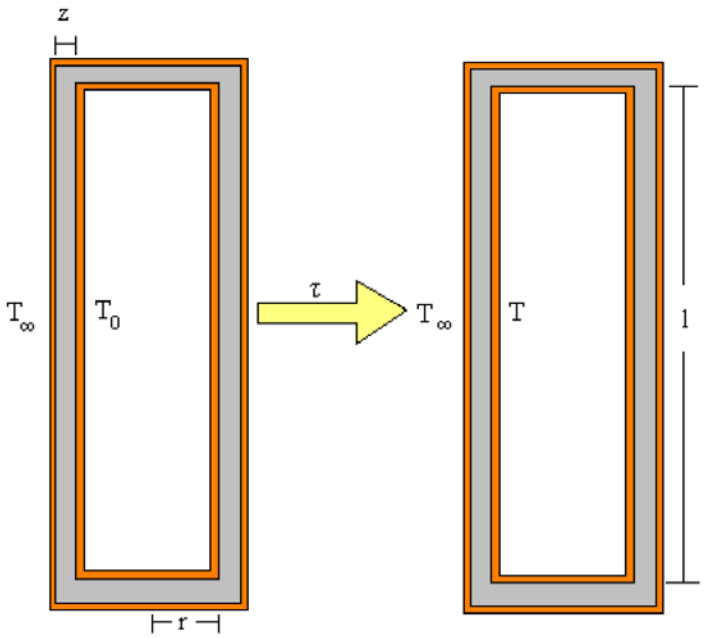

Figure 17. Schematic representation of temperature change in time in cylindrical measurement system.[119]

Solving for k_{ins} yields:

Equation 34

$$k_{ins}(T) = \frac{-z\cdot m\cdot c(T)}{A\cdot\tau}\ln\left(\frac{T - T_\infty}{T_o - T_\infty}\right)$$

Here it must be noted that the above derivation assumes that the specific heat of the cylinder material and thermal conductivity of the sample are independent of temperature. Note that this does not hold true over large temperature ranges. For this reason temperature increments of 10K or less should be sampled, and the resulting calculations use an average heat capacity for each temperature range. In turn, the thermal conductivity data will also be the average thermal conductivities for each range. While not performed in this example, it may also be possible to perform the calculations including a temperature dependent function for heat capacity in the solution of Equation 29.

The second part of the experimental measurements of the present example was to collect data under steady-state conditions. Fourier's law of heat conduction was used to calculate the thermal conductivity in this second part of the experiment:

Equation 35

$$q = -k(T)A\frac{dT}{dx}$$

Fourier's law of Equation 35 $q = -k(T)A\frac{dT}{dx}$ applies to one dimensional heat conduction. In the present case, however, the heat flux will be in the radial and axial directions. Therefore, the calculated data must be considered approximate. With this approximation, the solution of Equation 35 is

Equation 36

$$q = -k(T)A\frac{(T_i - T_o)}{z}$$

Solving for thermal conductivity $k(T)$

Equation 37

$$k(T) = -\frac{zq}{A(T_i - T_o)}$$

The measurement can be more accurately modeled in cylindrical coordinates. In this case the heat transfer rate in the radial direction becomes

Equation 38

$$q_r = -2\pi rlk\frac{\partial T}{\partial r}$$

where l and r represent the length and radius of the cylinder, respectively. With the boundary conditions $T=T_i$ at $r=r_i$ and $T=T_0$ at $r=r_0$ where i and o denote inner and outer surfaces, Equation 38 becomes

Equation 39

$$q_r = -2\pi lk \frac{(T_i - T_o)}{\ln(r_o/r_i)}$$

From, Equation 35 the heat transfer rate through the top and bottom of the cylinder is

Equation 40

$$q_z = -2\pi r^2 k \frac{\partial T}{\partial z}$$

Based on Equation 36 the heat flow in the axial direction becomes

Equation 41

$$q_z = -2\pi r^2 k \frac{(T_i - T_o)}{z}$$

where z is the thickness of the sample insulation material. The steady state heat flow in this example measurement is illustrated schematically in Figure 18.

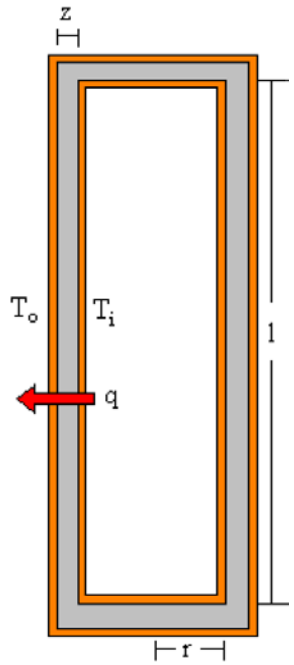

Figure 18. Schematic illustration of heat flow in the Concentric Cylinders Guarded Hot Plate method.[119]

Due to symmetry and the cylindrical boundary of the material region it can be assumed that there is negligible heat transfer in the angular (θ) direction. Therefore the total heat transfer rate through the sample is

Equation 42

$$q_{tot} = -2\pi lk\frac{(T_i - T_o)}{\ln(r_o/r_i)} - 2\pi r^2 k\frac{(T_i - T_o)}{z}$$

5.6 Concentric Spheres Method

End effects and the need for guard plates associated with the concentric cylinder and guarded hot plate methods can be eliminated using the concentric sphere method developed by Nayak and Tien for thermal measurements of cryogenic insulation.[122] A schematic illustration of their concentric sphere apparatus is shown in Figure 19. Thin nylon supports minimize the heat leak between cylinders, making it essentially negligible. The temperature of the outer sphere is maintained by adjusting the cryogen level on the copper stem at the bottom of the outer sphere and the heating power of the stem heaters. This design allows any initial temperature between the temperature of the cryogen and ambient temperature to be reached. To perform a measurement, the insulation sample space is evacuated, and the heater on the inner sphere is powered to create a temperature difference between the spheres.

The concentric sphere method is a novel approach to measuring the effective thermal conductivity of powders while reducing errors generated by the geometry of the measurement system. However, due to the expense of manufacturing spheres and other ease of use considerations the concentric sphere method has not been widely used.

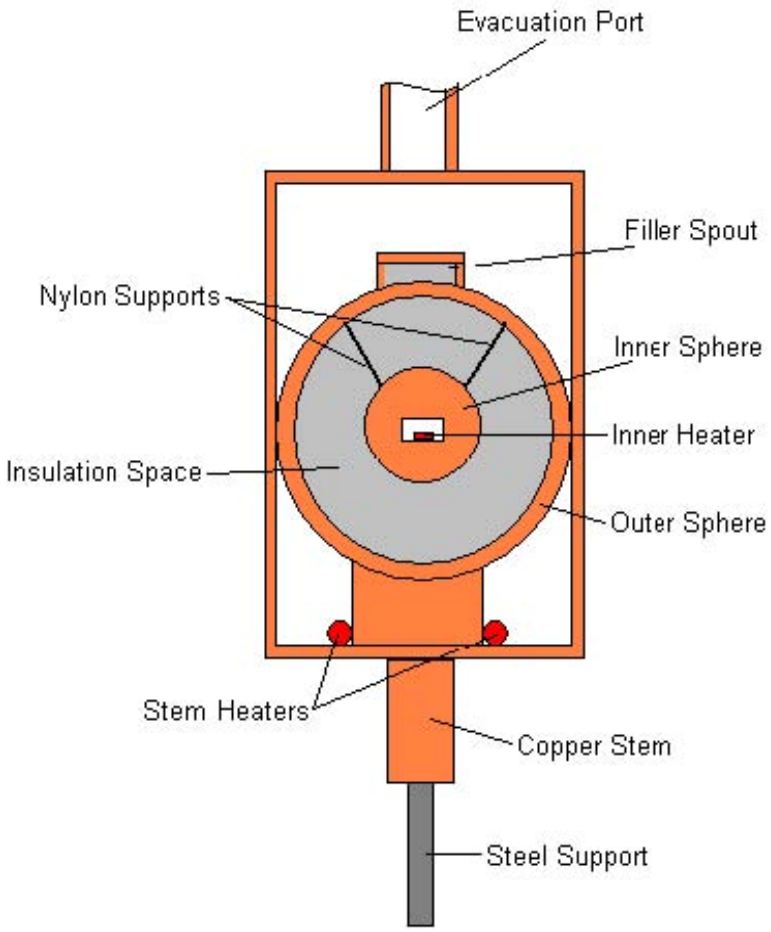

Figure 19. Schematic illustration of concentric sphere apparatus.[119]

5.7 Divided Bar Method (ASTM E1225-87)

The Divided Bar or comparative cut bar (ASTM E1225-87 Test Method) is perhaps the most widely used method for axial thermal conductivity testing. In this method heat flux is passed through both a known sample (reference material with a well-known thermal conductivity) and the test sample. The thermal conductivity of the sample can be determined by comparing the respective thermal gradients between the two materials. The thermal gradients will be inversely proportional to their thermal conductivities. Typically, the test sample is, in fact, sandwiched between two reference samples of a material to further account for minor heat losses that are very difficult to eliminate Figure 20.

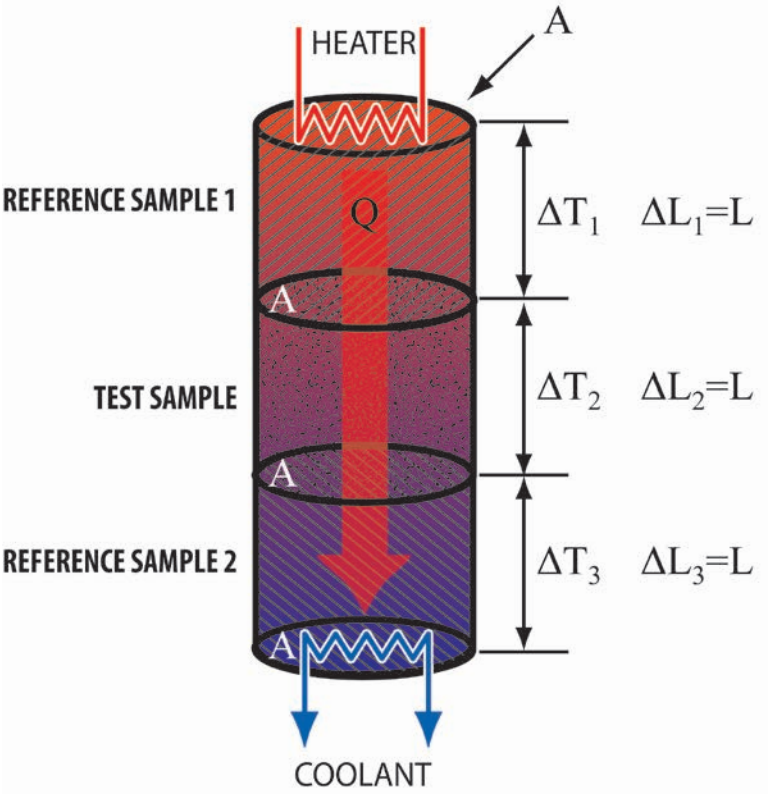

Figure 20. Schematic of Divided Bar method with the sample placed between two measurement references composted of a standard material of known thermal conductivity.[123,124]

The actual instrumental setup may vary depending on the temperatures and pressures needed as well as sample sizes. However, in the most general setup, a specimen of unknown thermal conductivity is placed between two references (usually brass plates) with known thermal conductivity. The sample is coated using a thermal grease and a pliable metal foil to eliminate interfacial thermal contact resistance between the sample and references. Typically the measurement device is setup in the vertical orientation with the hot brass plate at the top and the cold brass plate at the bottom. This is because by heating from the top down avoids errors that would be cause by excessive thermal convection rather than conduction within the sample if it were heated from the bottom. Thermocouples are fixed at positions along the sample and both references. The differential temperatures across the references are used to calculate the rate of heat flow through the two reference-material sections of known conductivity. The Divided Bar method is a steady-state measurement method, thus, temperature readings are taken after the sample has attained equilibrium. This occurs when the heat flow is constant over the entire sample. The thermal conductivity is calculated from the heat-flow rate across the sample which is determined from the temperature differentials

across the references and the known thermal conductivity of the reference material. This is given by the one-dimensional Fourier conduction equation:

Equation 43

$$\frac{Q}{A} = k_S \frac{dT}{dx} = k_S \frac{\Delta T_S}{L} = k_R \frac{\Delta T_1 + \Delta T_2}{2} \frac{1}{L}$$

where Q is the rate of heat flow, k_S is the thermal conductivity of the sample, A is the cross-sectional area of the sample through which the heat flows, and dT/dx is the temperature gradient. Experimentally, dT is approximated by ΔT, the finite temperature difference measured across reference 1; ΔT_1 , reference 2; ΔT_2 and the sample ΔT_S , and dx is approximated by L, the distance over which the temperature difference is measured (lengths of both the sample and reference plates). In this simplified derivation, it is assumed that the sample is cut to the same length as the two reference samples. Clearly, precise measurements of the sample contact area and length (as well as those of the references) are critical to making accurate thermal conductivity measurements.

5.8 Guarded-Comparative-Longitudinal Heat Flow Method (ASTM E1225 – 09)

The comparative axial (longitudinal) heat flow method (or for the case of cylindrical samples and meter bars, the cut-bar technique) has been used since the 1930's[125] and more completely studied and developed in the decades following that. [126,127,128,129] The accuracy of the technique independent of uncertainties related to the reference samples have been reported to be better than ± 5%.[130,131] A standard (ASTM E 1225) for the method was developed by the American Society of Testing and Materials (ASTM) in 1987 and revised in 2004.[132] Babelot et al. published studies using a comparative thermal conductivity apparatus in a glove box which may be a necessary approach for highly air and moisture sensitive hydrogen storage materials.[133] Since that time relatively few studies have been published providing detailed analysis of this type of instrumentation.[134] One noteworthy exception was a mathematical analysis in which the guard temperature distribution was matched at the hot and cold ends to produce a compilation of design charts.[135]

The Guarded-Comparative-Longitudinal Heat Flow Method is generally applicable for materials with effective thermal conductivities in the range $0.2 < k < 200$ ($W \cdot m^{-1} \cdot K^{-1}$) and over the approximate temperature range of 90K to 1300K. The method may be used outside these ranges, but with decreased accuracy.

In the guarded-comparative-longitudinal heat flow method, a test sample of unknown thermal conductivity is inserted under load between two other reference materials, of known thermal conductivity, with the same cross section, and known thermal

properties. A metering heater is controlled in such a way as to produce heat flux across the references (meter bars) and sample to produce a steady-state temperature gradient across the sample. This is done using a controlled heater on one end and a cold plate on the other end. The cold plate's lower temperature is usually maintained by circulating a coolant fluid. Temperatures are measured at the interface between the heat source and reference sample, heat sink and reference sample and at the interface between the test sample and reference samples.

A thermal guard system in the instrument helps to reduce radial heat losses from the sample column as much as possible as these heat leaks will produce error in the final results. In ASTM E 1225, two guard temperature schemes are recommended[132]: (1) guard temperature gradient matched to the test stack and (2) isothermal guard with a temperature equal to the average temperature of the specimen. A simple schematic of the set-up of this method a), and the temperature gradients in a system b) are shown in Figure 21.

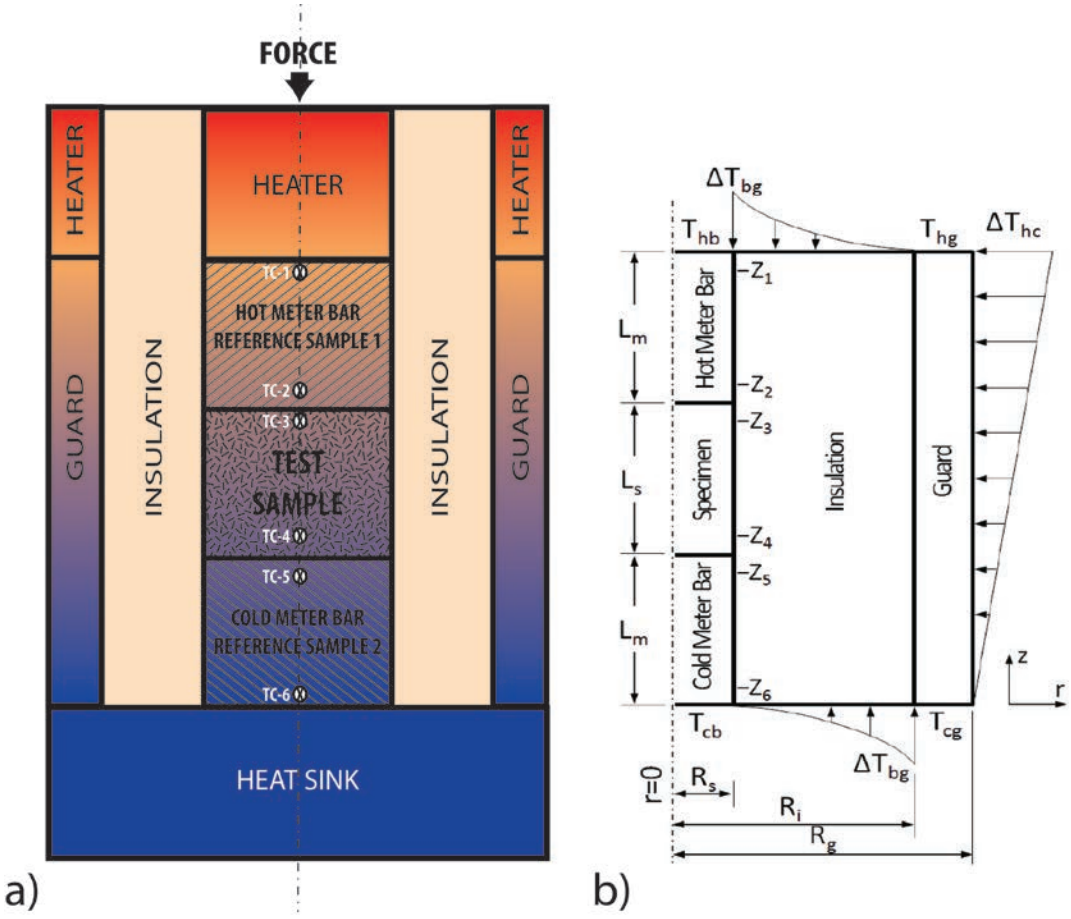

Figure 21. a) Schematic of a comparative-guarded-longitudinal heat flow system showing possible locations of temperature sensors along the stack, and b) a schematic illustration of the temperature gradients in the system[134].

The reference sample together with temperature sensors act as heat flow meters and are often referred to as meter bars. Only two thermocouples for each one of the reference materials is require to calculate the heat flow through the references. However, the use of a third temperature sensor is recommended to test the uniformity of the other two sensors and the data acquisition system.

By measuring the heat flux in the meter bars and the temperature gradient across the test sample, the thermal conductivity of the test sample at its average temperature may be calculated. The heat flux rate per unit area q'' for each of the two reference materials is given by the equations below:

Equation 44

$$q''_{\text{upper}} = k_{\text{RM1}} \frac{T_6 - T_5}{Z_6 - Z_5}$$

Equation 45

$$q''_{\text{lower}} = k_{\text{RM2}} \frac{T_2 - T_1}{Z_2 - Z_1}$$

where the temperatures T and positions Z refer to those in Figure 21.

While the heat flow though each reference material is calculated using average temperatures, the two heat values q upper and q lower should agree with each other to within about ± 10%.

The samples thermal conductivity at the average temperature of (T_3 + T_4)/2 is given by:

Equation 46

$$k_{\text{sample}} = \frac{\left(q''_{\text{lower}} + q''_{\text{upper}}\right) \times \left(Z_4 - Z_3\right)}{2 \times (T_4 - T_3)}$$

However, it is very important to note that this assumes no heat loss to the isolation. In reality there will always be heat leaks and thermal gradients (as shown in Figure 21b) which may significantly impact the measurements. For more accurate measurements these heat leaks should be taken into consideration in a whole system analysis. This can be done using finite element analysis (FEA) of the test instrument and evaluating the FEA model with data collected on test samples of known thermal conductivity.[134] Some results of such an analysis are shown in Figure 22. In this figure calculated measurement error is presented as a function of the difference in temperature between the hot end of the guard and the hot end of the meter bar (ΔT_{BG}). It can be seen that the errors depend on the thermal conductivity of the sample. One important conclusion of the cited study was that the guard temperature gradient has a more dramatic effect on system results than the guard average temperature. It was also found that the system

demonstrated good performance closely following the published values up to 600°C for lower conducting materials. For higher temperatures, the measured values began to deviate more and showed less repeatability.

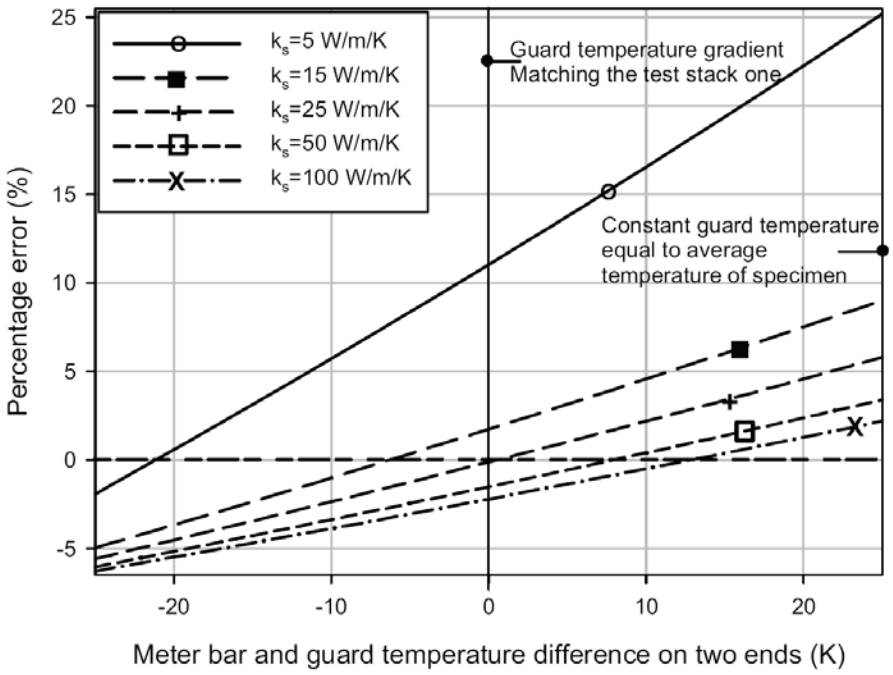

Figure 22. Percentage error yield by calculated and input specimen thermal conductivity with respect to the variation in ΔT_{BG}.[134]

The following important issues regarding the samples to be measured should be considered when using this method:[132]

- The sample can be considered homogeneous if k_{eff}, does not vary with changes of thickness or cross-sectional area by more than ±5 %.
- Samples of composites or heterogeneous materials composed of multiple layers should be significantly wider and thicker than a single layer. The recommendation is for the sample to beat least $20L$ wide and $20L$ thick, where L is the thickness of the thickest layer. Thus, if the diameter or length changes by as much as $0.5L$ the effect on k_{eff} will be less than ±5 %.
- For materials that are non-opaque or partially transparent to infrared radiation, the combined error in k_{eff} due to inhomogeneity and photon transmission should be less than ± 5 %. Measurements on highly transparent solids must be accompanied with infrared absorption coefficient information, or the results must be reported as effective k_{eff} (or apparent, k_A) thermal conductivity.

5.9 Thermal Probe Method (ASTM D 5334)

Thermal Probe Method is generally based on ASTM D 5334 and Blackwell.[136,137] This method is based on transient heat transfer rather than steady thermal gradients and is most appropriate for low thermal conductivity materials.[138]

The method consists of measuring a material's thermal conductivity from the response of a "hypodermic needle" probe inserted in the test sample. The method is particularly conveniently for use with low-conductivity materials that are powders. The probe contains a heater with a thermocouple attached to it. The rate that heat is transferred through the sample is determined from the transient temperature of the constant-power heater in the probe. The temperature history of the heater's surface will take on a characteristic form when a constant current is passed through the heater for a short period of time. At first, the temperature will rise rapidly. Subsequently, as the heat begins to transfer to the material, the rate of temperature increase becomes constant. Finally, the temperature increase at the probe will slow down or stop altogether when the thermal front reaches the outer surface of the sample due to heat loss to the surrounding environment. The thermal conductivity can be calculated from the straight portion of the temperature vs. time curve.

This method has been commonly used to measure low conductivity materials and packed beds.[139,140] For hydrides, this method may be chosen over other methods due to the transient nature of the measurement. Because large long-term temperature gradients are not required, this method is especially well suited for the measurement of low conductivity materials typical of many hydrogen storage materials. Furthermore, measurement-induced physical changes (such as desorption) are minimized due to the relatively short measurement time. Due to the physical configuration and relative simplicity of 'The Thermal Probe Method' it lends itself to testing hydride samples in situ i.e., measurements that are taken when the sample is undergoing dehydrogenation, as identified in, the example 6.1.2 section. It should be noted that in execution a major source of inaccuracy is the thermal mass of the probe which is often not accounted for in the theory. The ratio of the thermal mass of the probe to the thermal mass of the specimen has an impact on the response of the probe. The precision of the probe can be improved by the addition of a calibration factor. This factor is determined by using a reference material of known thermal conductivity which is in a similar range to that of the test specimen, ASTM D5334 ref 75. Figure 23 shows a schematic of a probe and its relation to a test chamber that was used to measure the thermal conductivity of Ti-doped alanates for hydrogen storage.[110]

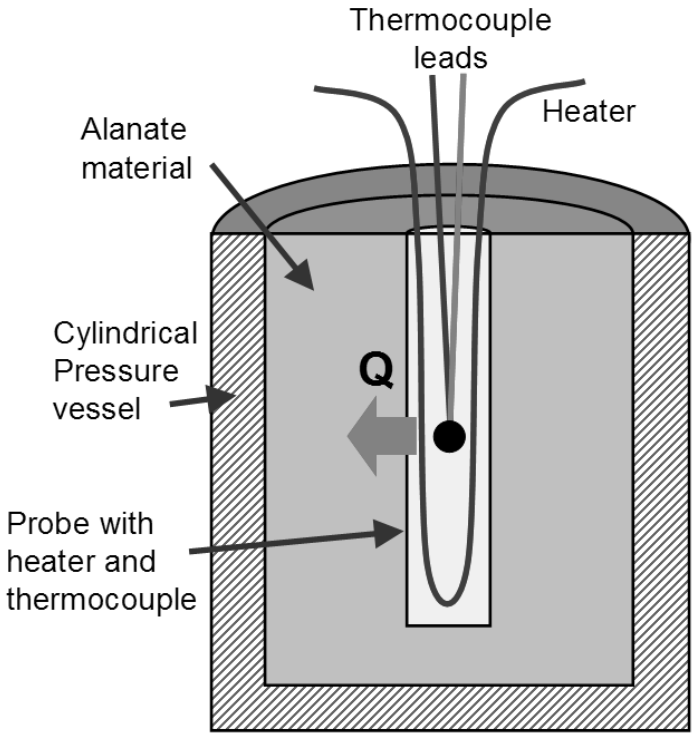

Figure 23. Schematic of transient thermal probe method, not to scale. Probe consists of a heating element and thermocouple. The transient temperature of the probe is related to the thermal properties of the measured material.[110]

The accuracy and repeatability of the thermal probe measurement method was assessed in great detail by Batty.[141] In that analysis, by measuring paraffin wax, Batty found 2% repeatability and 4% overall accuracy for 15 measurements with single probes and 3.3% repeatability and 10.6% overall accuracy for a complete group of measurements with different probes.

When applying the 'Thermal Probe Method' the length-to-diameter ratio must be observed to preserve the theoretical principal of an infinitely long line-heat source and an infinite and homogeneous sized specimen. The limits of the length-to-diameter ratio can be predicted, which enables the calculation of the minimum diameter of specimen. This is advantageous when there is a limited supply of specimen available for testing which could be the case when a range of Hydride mixtures are being explored for their suitability.

When applying the technique to samples that are at the limit of the minimum acceptable diameter that is theoretically allowable the magnitude of the heat flux becomes an important consideration. This is because the magnitude of the power input is specimen dependent and varies with the thermal conductivity of the specimen. If the power input is too low there will be an insufficient temperature response from which to derive the gradient. If the power input is too high, there will be the inclusion of edge effects i.e., the heat flux meets the boundary of the specimen, before the test has been completed.

5.10 Transient Plane Source (TPS) Method

The Transient Plane Source (TPS) method is a transient pulse heating technique used to measure thermal properties of materials including thermal conductivity and thermal diffusivity. Because it is a transient technique, thermal property data can be acquired quickly relative to steady state techniques. The original method, device, and theory was developed in the 1980's by Gustafsson.[142,143] It is based on the Transient Hot Strip (THS) technique for measuring thermal conductivity and diffusivity of a substance.[144,145]

In the THS method, a thin strip of a metal foil is positioned between two identical test samples, or alternatively a thin metal film is deposited on the test sample by vapor deposition. The metal strip (foil or film) acts as both an extended plane heat source and as a temperature sensor. A constant current is passed through the metal strip causing it to heat up. The electrical resistance of the strip is temperature dependent depending on the temperature coefficient for the resistance (TCR) of the strip. Thus, with a constant current, changes in temperature will cause a change in the voltage across the strip. These voltage variations are recorded as a function of time. The mean temperature increase of the strip in turn depends on the thermal properties of the test samples. Therefore, it is possible with such a measurement to estimate the thermal conductivity and diffusivity of the test sample. In order to simplify the models of the system used to calculate the thermal properties, it is assumed that the strip is of infinite length. The response time of the system and, thus, the experimental measurement is very short as it depends on the square of the strip width. This leads to the need to use very sensitive measuring instruments making many such measurements impractical.

By contrast the TPS method utilizes an advanced sensor design to overcome the problems of such transient THS measurements by increases the characteristic time for the measurement. This allows less sophisticated measuring equipment to be used, without reducing the accuracy of the measurement. The TPS sensor consists of a long wire, foil, or film laid down in a pattern in which the sensor strip has a very small width to length ratio within a given small area. The pattern typically consists of a double spiral, or square pattern as illustrated in Figure 24.

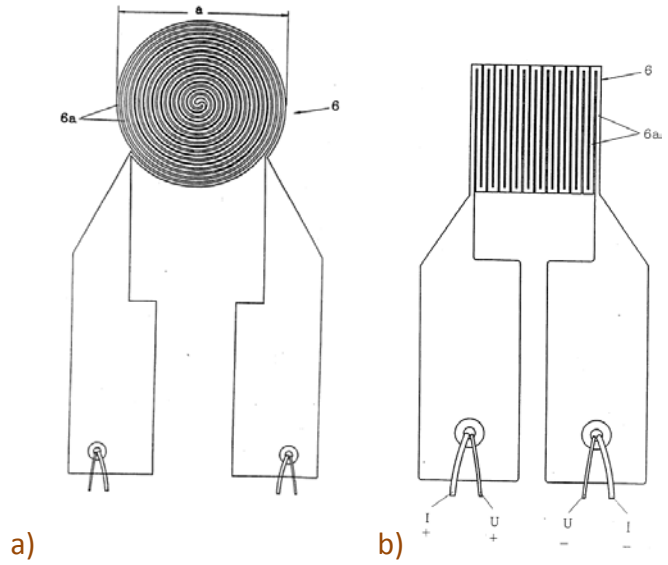

Figure 24. a) Double spiral and b) Square pattern TPS sensors.[142]

An example of an experimental apparatus employing a TPS measurement sensor is shown below in Figure 25.

Figure 25. An image of an example TPS measurement setup.[146]

The geometry of the Transient Plane Source (TPS) sensors enable the time characteristic for the measurements to typically be increased by two orders of magnitude and the resistance by one order of magnitude as compared with the THS method.

The double spiral pattern has often been used for laboratory measurement devices. From a theoretical perspective, the double spiral pattern can be approximated by a series of concentric, equally spaced ring heat sources.[147,148,149] The solution to the thermal response of a material from a single imbedded ring source with an instantaneous heat input can be found in the literature.[150] Assuming radial symmetry in the sample, the characteristic heat conduction equation is:

Equation 47
$$\left(\rho C_p\right)\frac{\partial T}{\partial t} = k_{in}\frac{1}{r}\left(\frac{\partial}{\partial r}\left(r\frac{\partial T}{\partial r}\right)\right) + k_{thru}\frac{\partial^2 T}{\partial z^2} + \sum_{rings} Q_r \delta(r - r')\delta(z)$$

where ρ is the sample's (kg·m^{-3}), C_p is the heat sample's capacity (J·kg^{-1}·K^{-1})), T is the temperature of the sample (K), t is the time of the measurement (s), k_{in} and k_{thru} are the in-plane and through-plane thermal conductivities of the sample (W·m^{-1}·K^{-1}), δ is the Dirac delta function, r' is the radius of one of the ring sources, and Q_r is the power supplied to that ring per unit length of the ring (W·m^{-1}). The total power for each ring is proportional to the circumference of the ring $2\pi r'$, such that the total power supplied for all of the rings is Q (W). The total power Q is the control parameter used in an experimental measurement.

The first term in Equation 47 represents accumulation of thermal energy, the second term radial (or in-plane) heat conduction, the third term axial (or through-plane) heat conduction, and the final term is a heat source.

The sample can be approximated as an infinite domain if the experimental time is much less than the characteristic thermal diffusion time. For an anisotropic material in a cylindrical geometry, the experimental time must meet the following two criteria: $t << \left(D/2\right)^2/\left(\alpha_{in}\right)$ and $t << x^2/\left(\alpha_{thru}\right)$. In these formulas, $\alpha = k/(\rho C_p)$, which is the thermal diffusivity of the material.

The average transient temperature increase of the sensor is simultaneously measured by recording the change in electrical resistance of the sensor and calculating temperature change according to:

Equation 48
$$\Delta T = \frac{1}{\alpha_{TCR}}\left(\frac{R_n}{R_{no}} - 1\right)$$

where ΔT is the change in temperature at time t (K), α_{TCR} is the temperature coefficient of resistance (TCR) of the material ($1 \cdot K^{-1}$) (TCR subscript to distinguish this property from the thermal diffusivity α), R_n is the electrical resistance of the sensor at time t, and R_{no} is the electrical resistance of the nickel at time t=0. The temperature rise in Equation 48 is correlated with the in-plane (l) and through-plane (k) thermal conductivities (k_{in} and k_{thru} respectively) through the solution of Equation 47 giving:

Equation 49

$$\Delta T = \frac{P}{\pi^{3/2} R \sqrt{k_{in} k_{thru}}} F(\tau)$$

where P is the power dissipation in the probe and $F(\tau)$ is a dimensionless function given by an integral of a double series over the number of rings m:

Equation 50

$$F(\tau) = [m(m+1)]^{-2} \int_0^{\tau} \sigma^{-2} \left[\sum_{l=1}^{m} l \sum_{k=1}^{m} k \exp\left(-\frac{l^2 + k^2}{4m^2\sigma^2} \right) I_0\left(\frac{lk}{2m^2\sigma^2} \right) \right] d\sigma$$

For convenience, the mean temperature change of the sensor is defined in terms of the dimensionless variable τ, where $\tau = \sqrt{\alpha_{in} t / R^2}$ or $\tau = (t/\theta)^{1/2}$. The time t, is the time measured from the start of the transient heating, $\theta = a^2/\kappa$ is the characteristic time. The above equations are used to determine the in-plane and through-plane thermal conductivity of the material being tested. For a more detailed derivation of these equations the reader is referred to the publication by He.[151]

In a typical TPS device, the sample is tested by placing it in intimate contact with the heating element of the sensor for a specific length of time (typically 0.8 seconds). A known current is applied to the sensor's heating element, providing a small amount of heat. This results in a rise in temperature at the interface between the sensor and the sample – typically less than 2°C.

The current $\boldsymbol{I}$ generated electrical heat Q in the sensor of resistance R according to:

Equation 51

$$\boldsymbol{Q = I^2 R}$$

Typically, the voltage leads across the sensor are connected to one leg of a Wheatstone bridge circuit acting as a resistance thermometer. The changing voltage across the bridge is used to determine the change in resistance of the sensor which is known to be a linear function of temperature given by:

Equation 52 $$R = R(T_0)[1 + \alpha_{TCR}\Delta T]$$

which is essentially Equation 48 above. The temperature coefficient of resistance, α_{TCR} has the dimensions of an inverse temperature (K^{-1}). The thermal properties of the surrounding sample material determined how much of the electrical heat diffused into the sample with a highly conductive material absorbing more of the input heat than a poorly conductive material. At any given time, the residual heat that had not diffused into the sample material generates a temperature increase in the sensor.

This temperature rise at the interface induces a change in the voltage drop of the sensor element. A typical voltage data chart collected using a commercial instrument is displayed in Figure 26. With proper calibration, the slope of the voltage time chart is inversely proportional to the thermal conductivity of the sample material.

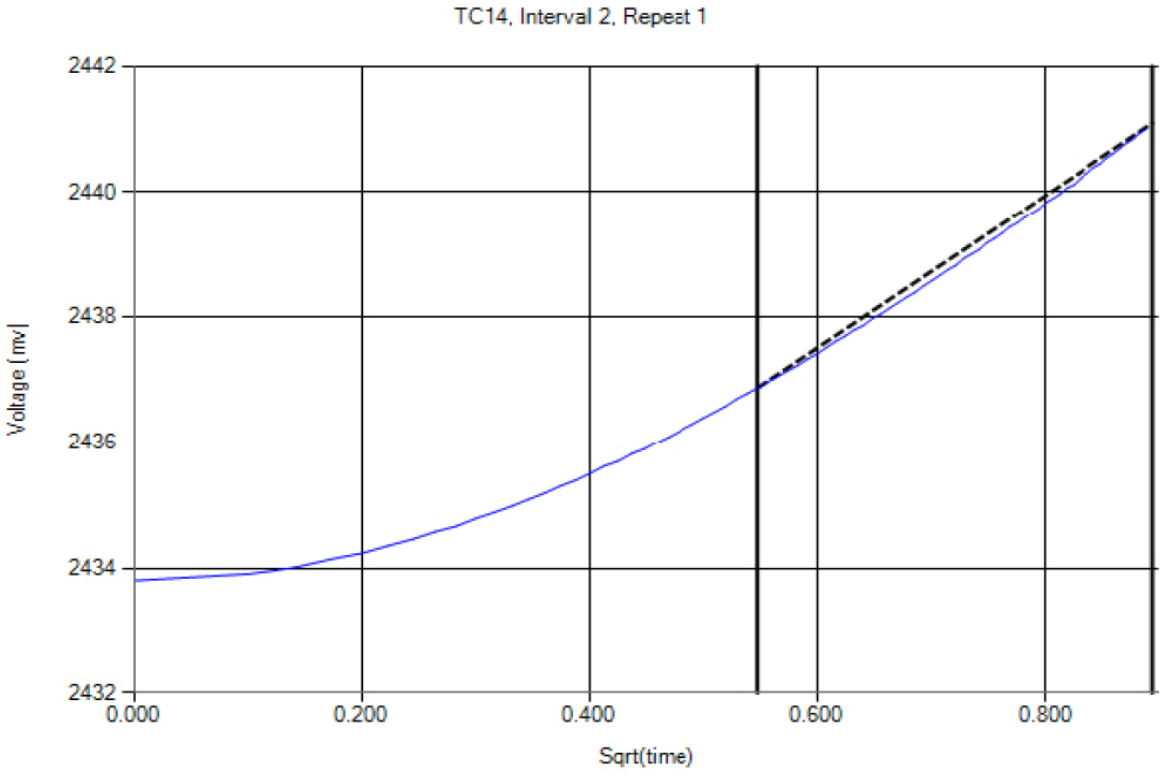

Figure 26. Representative Voltage vs. Square root of time (Sqrt(Time)) plot from a TCi thermal conductivity probe.[152,153]

A recent example of using this method to measure the thermal conductivity of high-pressure hydride hydrogen storage material was the detailed study by Flueckiger.[154] In this work, the transient plane source method was employed in a customized apparatus to measure k_{eff}, α, and C_p of a high pressure metal hydride in situ at pressures up to 275 bar hydrogen. For this experimental work, the TPS sensor was made of nickel wire wound in a double spiral formation, surrounded in Kapton (12.7 µm thick) insulation. The sensor was inserted between two disk shaped samples of the test material (Figure 27).

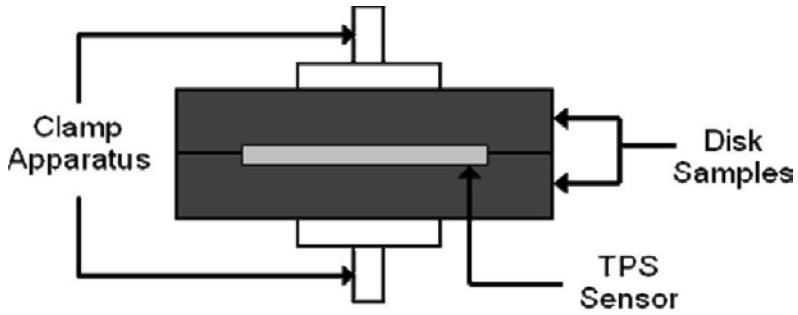

Figure 27. Experimental assembly for TPS measurements on high-pressure hydride hydrogen-storage materials.[154]

At room temperature, the thermal coefficient of resistivity of the nickel wire sensor was approximately α_{TCR} = 0.004693K^{-1}. Because this value depends on the initial temperature, the environmental conditions prior to an experiment had to be precisely determined to ensure an accurate resistivity (and thus temperature) measurement.

By fabricating the nickel wire in a double spiral formation, it could be modeled as a series of concentric rings as described above. For the data analysis the temperature profile for only the sensor itself was needed. Therefore, the sensor's height term was set to zero and the radial term was eliminated by averaging the temperature increase of each ring and dividing by the length of all the rings.

If an experimental temperature profile was generated for a material with known α, the increase in temperature could be plotted against the function given in Equation 50 to yield a linear plot (Figure 28). From Equation 49 the slope of the resulting function was proportional to the material's thermal conductivity. In addition, the y-intercept of the linear curve was dependent on R_{tc} at the interface between the material and the ring sources.

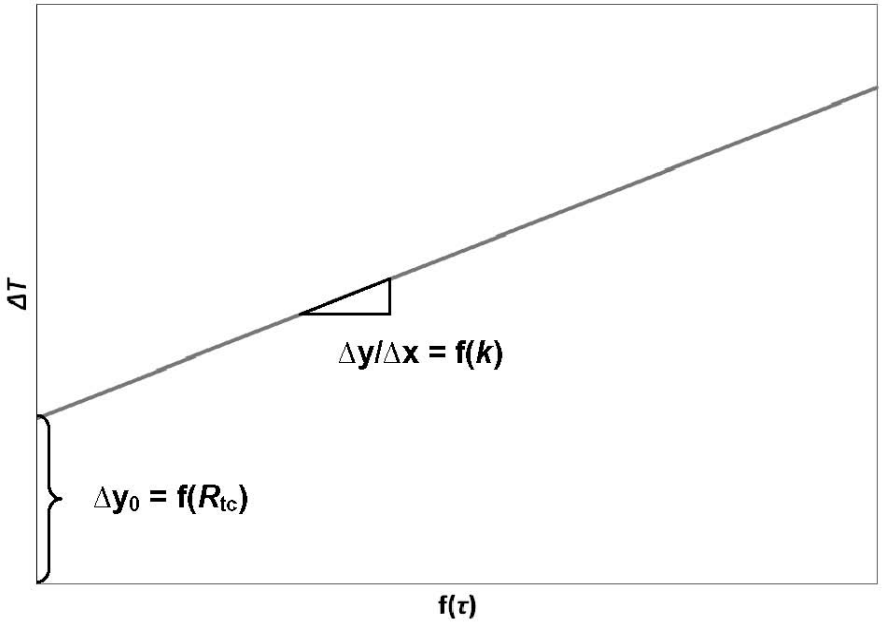

Figure 28. Processed TPS temperature profile.[154]

For analyzing the data from the actual measurements, one major assumption was that the test material was initially under isothermal steady state conditions. If a temperature gradient existed in the material prior to testing, the sensor properties were dramatically affected producing an erroneous temperature profile. To check for this instability, the instrument recorded the temperature variation of the material for 40 seconds prior to every experiment. If this variation included a significant temperature drift, the experimental data was rejected.

Experiments were performed by selecting an appropriate input power to the sensor and test duration. The input power needs to be large enough to generate a sufficient signal to noise ratio for the temperature increase. However, the power should not be so high that a large change in sample temperature occurs, making it difficult to assign the resulting thermal properties to a specific temperature value. In the cited work, repetitions of several trial and error settings were performed to determine an appropriate power setting.

With respect to the duration of each measurement, the appropriate test times varied according to the size of the test samples and the material's thermal diffusivity. Because the analytical solution for determining thermal conductivity assumes that test samples are an infinite medium, the measurements should be stopped before thermal boundary effects impact the data. To be able to satisfy this limitation, the duration should be less than the time necessary for the diffused heat to reach the edge of the samples. The total time of the transient event is proportional to the square of the overall dimension

of the conduction pattern or the distance from the conducting pattern to the nearest free surface of the sample. This can be evaluated in terms of the probe depth:

Equation 53 $$\Delta P = \beta(t_{max}\alpha)^{1/2}$$

where t_{max} is the total time of data recording, α is the thermal diffusivity of the sample and β is a constant which related to the experimental accuracy.[143,155] The probing depth and the sample size are intimately connected in the sense that the shortest distance from any point on the TPS element to the nearest point on any of the free surface of the sample must always exceed the probing depth. If the probing depth value determined by Equation 53 is greater than the true probing depth, boundary effects will be present in the data for the given test duration (t_{max}) and will cause error in the experimental results. For accurate property measurements, Gustafsson et al. reported that the heating time should be roughly equal to the characteristic time: $\theta = a^2/\alpha$ where a is the radius of the sensor.[145] As this time and the theoretical probing depth were both dependent on the material α, an iterative testing process was needed to determine suitable test duration.

By excluding the initial part of the measurement, the influence of the insulting layer, the heat capacity of the sensor, and the contact resistance (possible presence of air pockets between the sensing element and the sample) are all avoided. This is accomplished by deleting a few experimental points at the beginning of the transient recording.[156]

In the current example experiment, once an acceptable temperature profile was generated, α was determined through an iterative procedure. After an estimate value of α was defined; the time points were normalized with respect to $\tau = \sqrt{\alpha_{in} t / R^2}$. Then each of the normalized time points τ were then solved according to Equation 50. This procedure was repeated for different α values until a linear slope with temperature increase was generated. At the correct α (determined through linear regression analysis), the slope was calculated to determine k.

Initial data points are sensitive to the thermal contact resistance (R_{tc}) between the sensor and the test samples, but this sensitivity reduces to zero as the measurement progresses in time. To eliminate this effect, initial data points should be omitted from analysis.[151] To account for the inherent time lag between test initiation and temperature increase, a time correction value was measured and included in the non-dimensional time equation. An evaluation of the accuracy of such measurements was reported by Gustavsson, who found that the typical experimental uncertainty for the thermal diffusivity α was 5 to 10 percent, while experimental uncertainty for the thermal conductivity k was 2 to 5 percent.[145] The uncertainty in determining k was less than that of α, implying that the linear portion of the slope of the processed data used

to determined k did not vary to a significant extent between iterative values of α. It is important to note that the uncertainty in TPS measurements may vary greatly and depends on a number of factors including sensor size and sample properties.

In the work by Flueckiger on measuring the thermal conductivity of high-pressure hydride hydrogen storage materials, potential sensor and sample sizes were evaluated in order to optimize the accuracy the experimental measurements.[154] Commercial TPS sensors were available in sizes from 0.492 to 29.40 mm radius. In this work, the metal hydride was assumed to have a diffusivity of α = 1 ($mm^2 \cdot s^{-1}$). Knowing this, the characteristic time $\theta = a^2/\alpha$ for each sensor radius was determined. By setting the maximum measuring time $t_{max} = \theta$, the probing depth ΔP of sample material could be estimated using Equation 53. This means that the minimum length of the sample rod is equal to the probing depth ΔP and the radius of the sample should be equal to the sensor radius (*a*) plus the probing depth ΔP (with the sample diameter being d = 2 (a + ΔP). The calculated values of the experimental requirements based on sensor size are listed in Table 2.

In the case of this metal hydrides example the time resolution of the data collection equipment was not appropriate for the θ = 0.242 seconds of the 0.492 mm sensor. On-the-other-hand, the largest sensor sizes require substantial volumes of metal hydride to avoid boundary effects during testing. In the custom pressure vessel sample holder that was used, the shortest distance between the sensor and the cavity wall was 12.7 mm, limiting the probing depth to this distance. Also, safety is an important consideration. The pyrophoric metal hydride being tested became a greater safety risk with increasing sample volume. To satisfy the constraints of the TPS method and limit the volume of metal hydride required for analysis, the most appropriate sensor radii were 2.001, 3.189, and 6.403 mm.

***a* (mm)**	**θ (s)**	**ΔP (mm)**	**Sample *d* (mm)**
0.492	0.242	0.804	2.592
2.001	4.004	4.002	12.01
3.189	10.17	6.378	19.13
6.403	41.00	12.81	38.42
9.719	94.46	19.44	58.31
9.908	98.16	19.82	59.45
14.61	213.5	29.22	87.66
29.40	864.3	58.80	176.4

Table 2. Effect of TPS sensor size on test and sample conditions.[154]

In order to test the accuracy of the TPS setup, a preliminary series of measurements were performed on 5 cm diameter stainless steel disks.[154] The experiments included five tests with an unmodified sensor (a = 6.403 mm) and five tests with the sensor customized for the pressure vessel (a = 3.189 mm) under ambient conditions. The averaged results along with literature values are presented in Table 3. The author estimated the uncertainty to be twice the standard deviation of the raw data. The measurements showed a reasonable agreement between the normal and the customized sensor with values from the literature.

Source	k ($W \cdot m^{-1} \cdot K^{-1}$)	α ($mm^2 \cdot s^{-1}$)	C_p ($J \cdot g^{-1} \cdot K^{-1}$)
Commercial TPS Sensor	13.6 ± 0.4	3.56 ± 0.06	0.483 ± 0.018
Custom TPS Sensor	14.0 ± 0.1	3.72 ± 0.11	0.474 ± 0.017
Literature value[157]	13.4 ~ 15.1	3.71 ~ 3.95	0.468 ~ 0.480

Table 3. Thermal properties of SST.[154]

The TPS method requires close contact of the surfaces of the two test samples with the sensor. For the highest accuracy, the two samples should have identical bulk thermal properties. In addition the thermal contact resistance on both sides of the sensor should be equal for accurate measurements. To investigate to what degree differences in thermal contact resistance would affect the results, a set of tests were performed using the stainless steel disks. Measurements were made (and repeated five times) with and without thermal paste (Chemplex 1381) between the stainless steel sample and TPS sensor (a = 6.403 mm).[154] The results indicated that the inclusion of thermal paste did not significantly affect the thermal property measurements of the stainless steel disks. As a result, it was concluded that asymmetric thermal contact resistance does not adversely affect the TPS results.

5.11 Hot Wire Method for Solid Samples (ASTM C1113)

The Hot-Wire methods are most commonly used to measure the thermal conductivity of "refractories" such as insulating bricks and powder or fibrous materials. It is important to note that, because it is essentially a transient radial flow measurement technique, the samples must be isotropic. The technique has also been applied less frequently to measure thermal properties of liquids and gases.

The Hot-Wire method is a transient dynamic technique that consists of applying a current to a one-dimensional heating source (hot wire) and measuring the thermal response of the test material surrounding the heating source.[158] If the heating source is assumed to have a constant and uniform output along the length of test sample, the thermal conductivity can be derived directly from the resulting change in the temperature over a given time interval.

There are several different experimental setups that can be used to implement method. The differences are mainly on how the temperature is measured in the sample.

Standard Cross Technique: Two fine groves are ground across two equally sized material specimens. The two line groves form an identical cross on the surface of each sample. A heating wire is imbedded in one leg of the cross between the samples and the second set of grooves is used for separate thermocouple wires for measuring the temperature of the heating wire (Figure 29). The two different metal wires of the thermocouple are connected at the temperature measuring point in the center of sample where the groves cross and are in direct contact with the heating wire. The reference junction of the thermocouple is either a known temperature source (for example ice water) or is provided by the temperature measurement equipment. The heating wire is typically platinum or Kanthal of 0.1 to 0.4 mm diameter and the Thermocouple (TC) may be welded Type-K Ni-NiCr wires, Type-S Pt/PtRh, or other thermocouple standards depending on the temperature range and accuracy required.

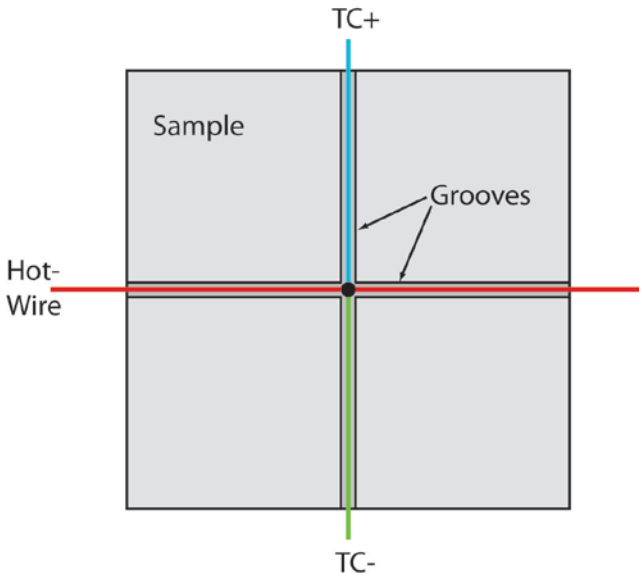

Figure 29. Illustration of Standard Cross setup for Hot-Wire measurement of the thermal conductivity of a sample.

Resistance Technique: in this case, the heating wire acts also as the temperature sensor. The temperature is determined by measuring the change in resistance of the hot wire with temperature based on the four point method for measuring electrical resistance. The four point probe method is an electrical impedance measuring technique that uses separate pairs of current-carrying and voltage-sensing electrodes to make accurate measurements of electrical resistivity (Figure 30). The key advantage of four-terminal sensing is that the separation of current and voltage electrodes eliminates the impedance contribution of the wiring and contact resistances. The accuracy of the technique comes from the fact that almost no current flows in the sense wires, so the voltage drop, V=RI, is extremely low. The temperature is determined from knowing the temperature-resistance relationship for the hot-wire material being used.

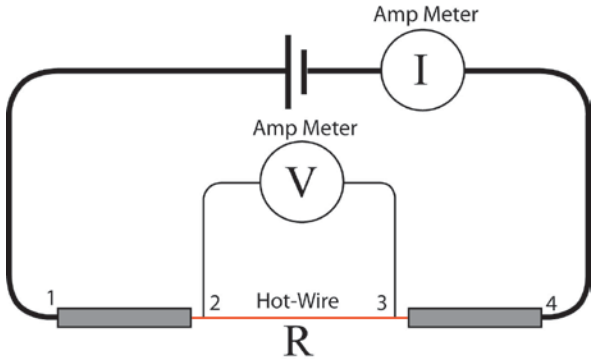

Figure 30. Illustration of the Four-Point electrical resistance measurement of the Hot-Wire (grey). Four-point measurement of resistance between voltage sense connections 2 and 3. Current is supplied via connections 1 and 4.

In the case of electrically conducting sample materials, the heating wire and thermocouple wires, or potential leads, are electrically insulated by non-conducting coating on the wires.

The determination of thermal conductivity is based on the assumption that the hot wire can be modeled as an ideal, infinite thin and long one-dimensional line source of heat. It also assumes that the sample is well represented as an infinite, homogeneous and isotropic material with a uniform initial temperature. For the assumptions to be valid the wire must be much longer that its diameter and the sample must also be significantly thicker than the diameter of the hot wire. The steady heat produced starting at time t = 0 per unit time and per unit length of the heating wire is given by q (W.m^{-1}). This is then radial heat flow around the wire. At radial position r from the heat source (Figure 31) the temperature rise $\Delta T(r,t)$ is given by:

Equation 54

$$\Delta T(r,t) = \frac{q}{4\pi k} \ln \frac{4at}{r^2 C}$$

where k is the thermal conductivity (W.m^{-1}.K^{-1}), a is the thermal diffusivity (m^2.s^{-1}) and C = exp(γ), where γ=0.5772157 is the Euler's constant.

The thermal diffusivity is given by:

Equation 55

$$\alpha = k/\rho C_p$$

where ρ is the density (kg.m^{-3}) and C_p the heat capacity (J.kg^{-1}.K^{-1}) of the test material.

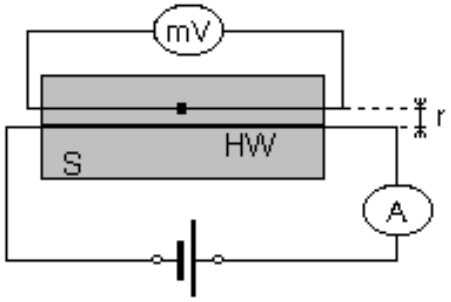

Figure 31. Schematic illustration of the Hot-Wire measurement setup.[159]

Given a sufficiently long time *t* greater than a minimum time t_{min} (initial heating period) and less than t_{max} (heat has reached the exterior surface of the sample) and for a small distance *r*, the factor: $r^2/4at$ << 1. In this regime Equation 54 becomes linear and reduces to:

Equation 56

$$\Delta T(r,t) = \frac{q}{4\pi k} \ln(t).$$

In this regime, one can plot the measured temperature rise $\Delta T(r,t)$ as a function of time. The thermal conductivity k can then be determined from the slope K of the linear portion of temperature rise $\Delta T(r,t)$ vs. natural logarithm of the time (ln$t$) evolution from

Equation 57 $$K = \frac{q}{4\pi K}$$

Where K is the slope $\Delta T(r,t)$ / ln$t$. Figure 32 illustrates an example of the time evolution of a hot wire temperature rise for an ideal case (instant heat up and infinite media) versus the shape and linear portion of a typical measurement curve.

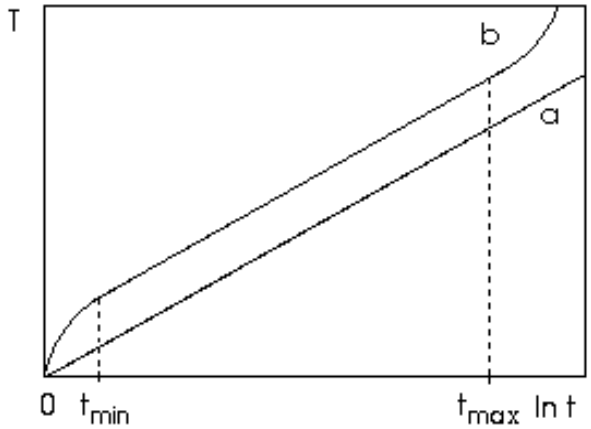

Figure 32. Example of temperature rise curves (a - ideal, b – non-ideal case).[159]

An example of a real measurement made using such a Hot-Wire apparatus is shown in Figure 33.

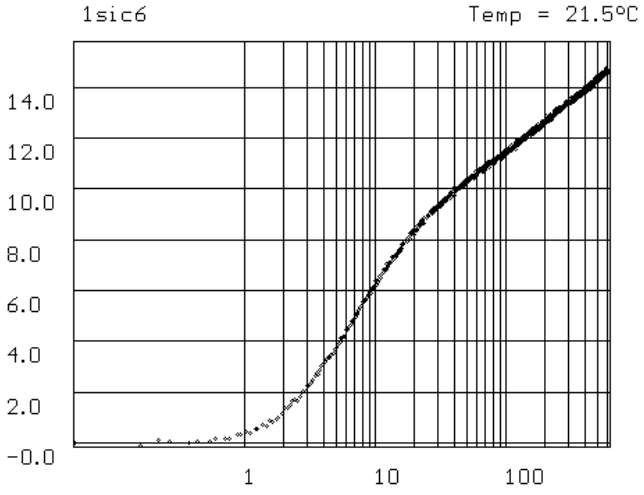

Figure 33. Typical experimental temperature rise vs. time evolution.[159]

Such an apparatus has been used, for example, in performing *in situ* measurements of solid materials in the shape of a (100x100x50 mm) or cylinder (10 mm in diameter and length of 100 mm) as well as sand, powder and granular materials are usually put into cube container of 100x100x100 mm in the temperature range 20 – 1200 ºC.[160]

5.12 Hot-Wire Method (ASTM C1113) for Gases and Liquids

For fluids, the transient Hot-Wire method consists of using a small diameter wire immersed in the fluid sample. The wire is used simultaneously as an electrical resistance heater and as resistance thermometer to measure the resulting temperature rise due to the resistance heating of the wire. The measurement device is composed of a cell containing the fluid and the hot-wire designed as closely as possible to approximate a simple 1-dimensional transient line-source of heat in an infinite medium. The optimum design minimizes any corrections needed to account for the actual physical geometry of the cell and components. A typical device will have two hot wires of differing length operating in a differential mode to eliminate any axial conduction effects. The greatest contributor to axial heat leaks is due to the large diameter electric leads attached to the ends of each hot wire. Given that the measurement device adheres very closely to the model system of a transient line-source, the thermal conductivity can be found from the slope of the measured linear portion of the temperature versus time with a typical uncertainty of less than 1%. The thermal diffusivity can be determined from the intercept of the same linear temperature-time curve, with a typical uncertainty of less than 10%.

Typically corrections need to be made to the data to account for the fact that the actual measurement system is not a perfect line-source as modeled. The two largest corrections to the data to be considered are to account for the finite dimensions of the wire and the finite dimensions of the fluid medium surrounding the wire. The correction for the finite dimensions of the wire is largest at short elapsed times in the measurement of low-density gases. This correction can be minimized by using extremely small hot wires with diameters typically of the order of 4 microns. The correction for finite dimensions of the fluid medium is largest at long elapsed times in low-density (high thermal diffusivity) gas measurements. For low-density gas measurements, the Hot-Wire method can be performed in the steady-state mode to measure thermal conductivity with an uncertainty of about 2%.

An example of two different transient Hot-Wire devices for the measurement of the thermal conductivity and thermal diffusivity of fluids are the instruments developed by the Experimental Properties of Fluids Group at NIST.[161] The first device was a 316

stainless steel and copper pressure system designed to operate at low temperatures (30 to 340K) and pressures from vacuum to 700 bar. The second system was a 316 stainless steel and Hastelloy C pressure system designed to operate at high temperatures (260 to 750K) and pressures from vacuum to 700 bar. These hot-wire apparatus were reported to be able to accurately measure thermal transport properties in the liquid, vapor and supercritical fluid phases of pure fluids and mixtures. The hot-wire cells use 4 micron diameter tungsten, 12.7 micron diameter platinum, or 25 micron diameter anodized tantalum (electrically insulated) hot wires depending on the fluid of interest. The insulated hot wires were used (and necessary) for electrically conducting fluids.[162] For example for thermal properties have been collected for hydrogen, methane, ethane, and propane.[163]

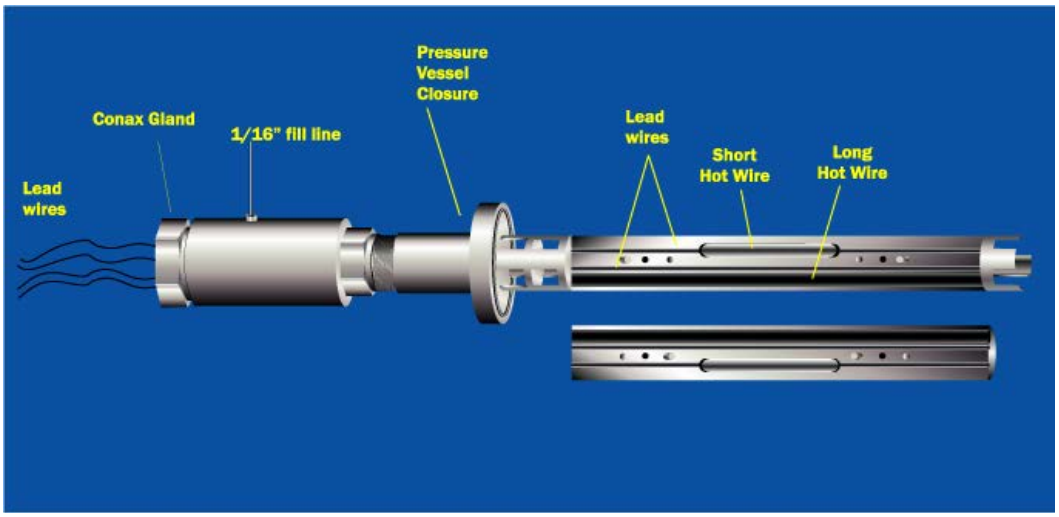

Figure 34. A schematic image of a two-wire Hot-Wire device for measuring thermal properties of fluids.[164]

5.13 Flash Method (ASTM 1461)

The flash method (ASTM E1461)[165], originally described by W.J. Parker[166], is a transient heat flow technique primarily used to measure the thermal diffusivity of materials. The method involves rapidly heating one surface of a small disk or slab of the material with a single pulse from a laser or other flash heating source, and monitoring the arrival and time response of the resulting temperature disturbance on the opposite surface using an infrared detector. A schematic diagram of such a measurement system is shown in Figure 35.

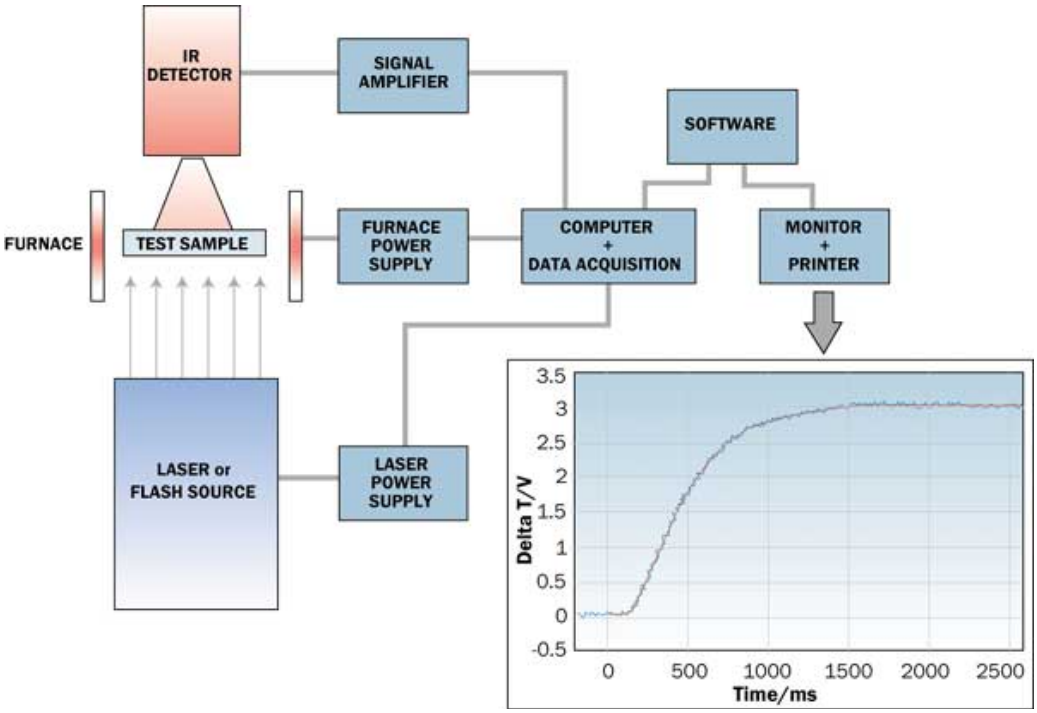

Figure 35. Schematic of flash diffusivity measurement and temperature rise curve.[167]

Typically, the sample geometry is a disk of 6 to 25 mm diameter, or squares of 6 to 25 mm on a side, with thickness ranging from 0.02 to 4 mm, depending on the thermal conductivity of the material and the equipment being used. A graphite film (~5 µm thick) is normally applied to the sample surfaces to increase the energy absorption efficiency of the front surface of the samples to the energy pulse and the radiative emittance of the back surface to the IR detector.

The fact that the temperature of the back surface of the sample is monitored with an infrared detector makes the measurement contactless. This and the optical flash heating can be a significant advantage for thin, low thermal resistance samples. This is because, unlike many other methods, there is no direct thermal contact of the heating source or temperature measurement device with the sample. Some of the uncertainties present in other methods that contribute to error in the measurements are due to:

- the contact resistance between heating/cooling plates or probes and the sample material, and
- the accurate measurement of surface temperatures using contact sensors.

In addition, for thin/thick film applications very thin samples and small thermal resistances can be accurately measured without stacking layers, allowing measurements at the application thickness.

An example of the components of a typical laser flash measurement system is presented in Figure 36. A thin parallel-plane cylindrical specimen is in thermal equilibrium (at a constant temperature) with the furnace environment. The laser-flash produces a short heating pulse on the bottom side of the sample. The increase of the temperature at the top surface of the sample is detected using an IR sensor.

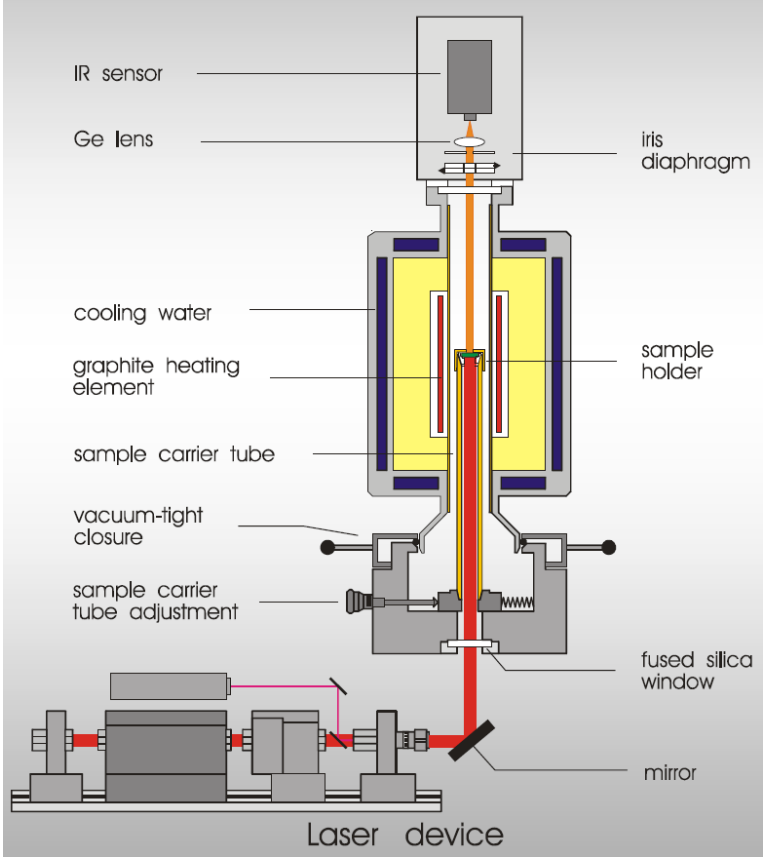

Figure 36. Diagram of a typical flash diffusivity measurement instrument.[168]

The flash method is used to measure the thermal diffusivity of materials. Thermal diffusivity is a measure of how quickly a temperature disturbance propagates through a material. From Equation 4, thermal diffusivity and thermal conductivity are related according to:

Equation 58 $$\alpha = k/\rho C_p$$

where α is the thermal diffusivity, k is the thermal conductivity, ρ is the density, C_p the specific heat, and ρC_p is the volumetric specific heat. Thus, the thermal conductivity of a material can be determined from measurements of the thermal diffusivity, bulk density and specific heat:

Equation 59 $$k = \alpha \rho C_p$$

Without going into detail, the temperature distribution after the flash pulse at any time t is given by

Equation 60 $$\Delta T(x,t) = \Delta T_\infty \cdot \left[1 + 2 \cdot \sum_{n=1}^{\infty} \cos\left(\frac{n \cdot \pi \cdot x}{h}\right) \cdot e^{\frac{-n^2 \cdot \pi^2 \cdot a \cdot t}{h^2}}\right]$$

where h is the thickness of the sample, x is the depth into the sample from the heated surface, ΔT_∞ is the increase of temperature after the flash pulse when a homogenous heat distribution over the entire sample has been reached. The finite width of the heating pulse can affect the measurement of thin and/or high diffusivity samples because the heating of the front surface can no longer be considered instantaneous relative to the time. To include this effect in the analysis, the thermal pulse width is included in the model. However, if there is no significant heat loss and the finite pulse can be ignored, then simplifications of Figure 37 lead to the following analytical solution (Parker expression[166]) for thermal diffusivity as a function of temperature:

Equation 61 $$\alpha(T) = -\frac{ln(1/4)}{\pi^2} \cdot \frac{h^2(T)}{t_{1/2}(T)}$$

Where $t_{1/2}$ is the time to reach $½\Delta T_\infty$. Therefore, in its most simple form, the thermal diffusivity can be determined by measuring the temperature change with time on the back side of the sample and inserting $t_{1/2}$ from the resulting data into Equation 61. An example of theoretical and experimental time profiles is shown in
Figure 37. The energy pulse is initiated at time zero, there is short lag as the pulse propagates through the sample thickness, and then a steep rise followed by a more gradual rise to a plateau where the heat from the laser pulse has become equally distributed in the sample. The red curve in
Figure 37 represents the theoretical temperature response given by Equation 61, after matching to the detector signal, which is displayed in blue. Assuming that ΔT_∞ is equal to ΔT_{max}, then $t_{1/2} = ½\Delta T_{max}$.

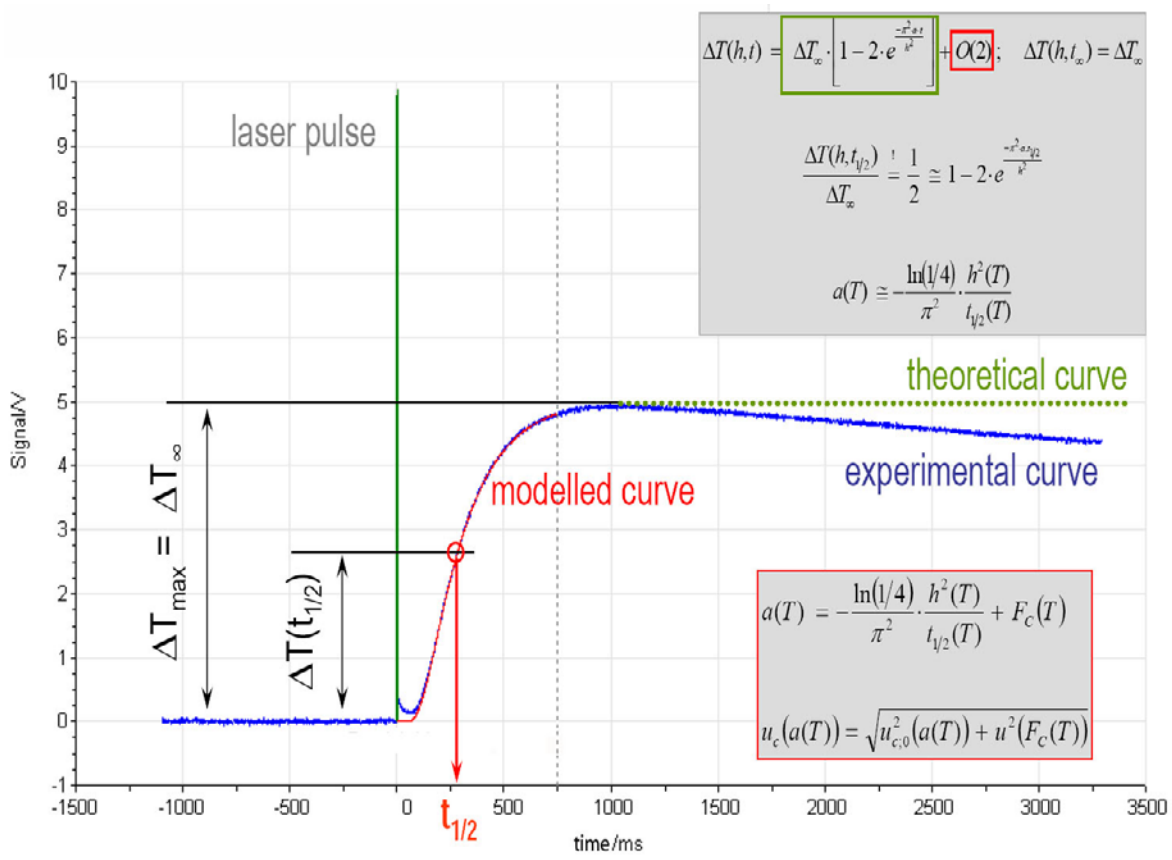

Figure 37. Example of theoretical and experimental flash diffusivity measurement data.[169]

To be able to calculate thermal conductivity from diffusivity one must know the specific heat of the sample material (Equation 59). The specific heat of the sample material is typically measured by differential scanning calorimetry, ASTM E1269.[170] This usually requires a separate, smaller diameter sample. For many single layer samples, the flash method itself can also be used to measure the specific heat of the sample.[166] This is done using a comparison technique that compares the magnitude of the increase in temperature of the sample due with a fixed energy pulse to that of a calibration standard of known specific heat, measured under exactly the same conditions. By first running the calibration measurement on a standard, the specific heat and thermal diffusivity of the test sample can be measured in a single run.

The specific heat of the sample is given by:

Equation 62

$$C_p = \frac{(mC_p\Delta T)_{cal}}{(m\Delta T)_{sample}}$$

Where m is the mass of the sample or calibration standard.

Multi-Layer

While the only single-layer materials have been discussed up to this point, thermal resistance and effective thermal conductivity of multi-layer samples can be measured in certain circumstances using flash diffusivity.[171]

Anisotropy

Anisotropy in thermal conductivity has been examined using flash methods. An example is some materials that are used in heat sinks, heat spreaders, or other areas of electronics package. In some composites, for example, the orientation of graphite or carbon fibers may result in a thermal diffusivity and thermal conductivity higher by a factor of two or more in the direction of the fibers compared to the direction across the fibers. In many cases, this property is desirable in order to move heat in a particular direction, or to reduce the maximum temperature at a "hot spot" by spreading heat laterally.[167] For hydrogen storage materials, anisotropy appears to be an important factor to be considered in storage system design, in particular, for compressed pellet materials.

Smith and Campbell employed a modification of the standard flash method to measure the in-plane, or radial, thermal diffusivity.[167] They were able to analyze materials that were isotropic in the plane, but have a different through-plane diffusivity. Their method employed a mask to collimate the laser beam and heat an approximately 5 mm diameter spot on the front face of a 25 mm diameter disk (Figure 38). This allowed heat to flow through the thickness of the sample and spread out in plane. Another mask is utilized on the opposite face to define an annulus of approximately 8 to 10 mm in diameter that is exposed to the IR detector.

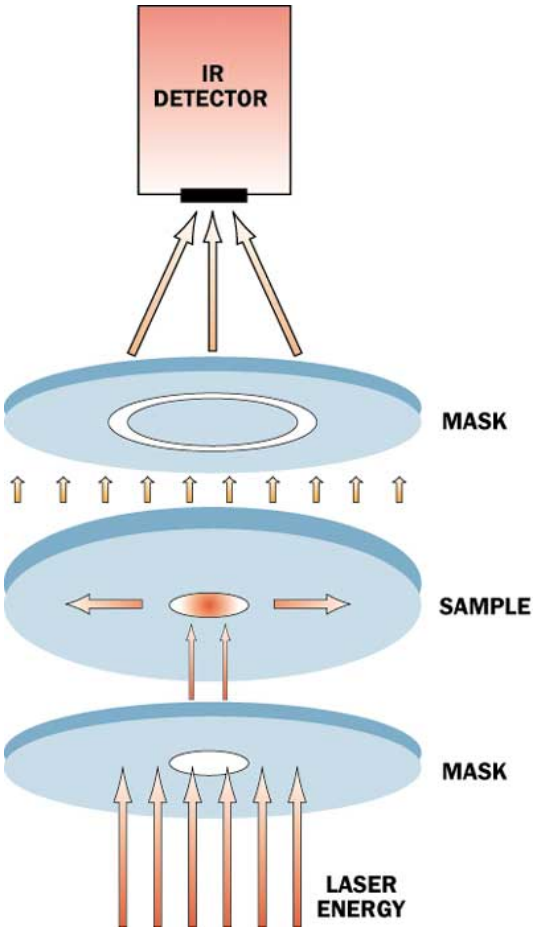

Figure 38. Schematic of radial or in-plane diffusivity measurement.[167]

The temperature rise measured of this annulus was then fit by a two-dimensional model with inputs of the through-plane thermal diffusivity, sample thickness and heating and viewing diameters to determine the in-plane thermal diffusivity.[172,173,174] This method requires a sample thickness of approximately 1 mm or less in order to maintain adequate sensitivity.

Finally, for materials that are significantly thicker than 1 mm or where it is not desirable to machine the thickness down to 1 mm, or for materials that are anisotropic in the plane, an alternate method is to measure the in-plane diffusivity. If the material thickness is not large enough to cut out a sample of a standard geometry in the direction of interest, a group of bars can be machined from the material, stacked up and held together to form a square sample (as shown in Figure 39). This is done such that the through-plane direction of the sample is the direction of interest. In this example, the diffusivity in the "x" in-plane direction of the material would be measured.

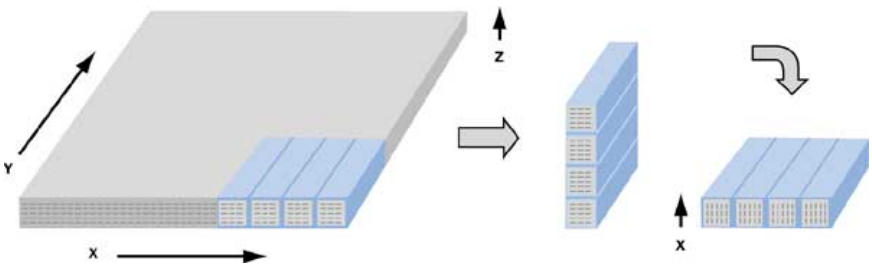

Figure 39. Preparation of an assembly of bars in the "x" direction for in-plane diffusivity measurement.[167]

The following are some specific requirements, characteristics of, and non-ideal limitations of the flash measurement method:

a) The sample must be homogeneous,

b) The sample must be flat and thin, with parallel surface,

c) Measurements are taken under isothermal conditions (constant furnace temperature) and temperature dependence is made by stepwise measurements,

d) The measurement involves relative temperature changes and, therefore, accurate absolute temperature measurements are not needed,

e) The heat capacity and density of the sample must have been independently measured for each sample to be able to determine the sample's thermal conductivity,

f) Local inhomogeneities occur in most materials,

g) Sometimes a simple interpretation of transient temperature curve is not possible,

h) Perfect adiabatic boundaries do not exist in real systems,

i) Advance software models now include non-adiabatic effects and finite pulse durations,

j) Infinitesimal initial heat doses cannot be achieved in real systems,

k) The first order solution to the model equation does not describe reality – but it can help in understanding fundamentals properties of the materials,

l) The above non-ideal behavior creates limitations in the use of the method – or example to high conductivity thin layers,

m) The above consideration may have a strong impact on the analysis of the data that cannot be solved by black-box routines.

n) Numeric models must be compatible with the material being measured.

6 Examples of Thermal Conductivity Measurements of Hydrogen Storage Materials and Storage System Design

6.1 On-board Reversible Hydride Storage Systems

The heat released or taken up in the interaction between gaseous hydrogen and the storage material will have a significant impact on how the storage system is designed. In physisorption the heat is generated on adsorption of molecular hydrogen to the surface of the storage material and range anywhere from -1.5 to -20 $kJ \cdot mol^{-1}$ H_2 depending on the material and hydrogen content. Hydride storage materials have a much wider range of enthalpies of reaction (from irreversible with positive enthalpies to very stable with formation enthalpies > 100 $kJ \cdot mol^{-1}$ H_2. For an ambient temperature reversible hydride with an equilibrium pressure of 3 bar will typically have an ideal enthalpy of reaction of about -43 $kJ \cdot mol^{-1}$ H_2. This is a significant amount of heat to be dealt with for most applications. For example, based on such a hydride, filling a hydrogen storage system with 5 kg of hydrogen in 5 minutes would produce > 350 kW of heat, or enough heat to boil approximately 11 gallons of water. Thus heat transfer is a very important part of the design of hydrogen storage systems. As a result, accurate thermal conductivity and heat capacity measurements of storage materials and components are critical to the development of viable storage products.

The following are a few examples that underscore the impact of reaction heat generation and the role of good data in being able to find effective heat transfer design solutions.

6.1.1 Introduction to Thermal Properties of Hydrides and Impact on Storage System Performance

The degree to which the thermal properties impact storage performance is a critical consideration in the design of metal-hydride storage hydrogen storage system. The thermal properties of metal hydrides can be dependent on many factors including hydrogen pressure, temperature, hydrogen concentration, particle size, and porosity. For this reason, knowledge about the influence of these factors on the thermal properties of metal hydrides is vital. Such knowledge will aid in the optimization of both materials and systems.

Classic metal hydrides provide a good starting point for the discussion of the impact of heat transfer on hydrogen storage systems design.[175] Metal-hydride powders typically have grain sizes on the order of 50–100 μm. The powder particles decrepitate into smaller particles with each hydriding/dehydriding cycle, eventually coming to a stable grain size of approximately 1 μm.[176] Due to poor particle to particle contact of the fine powders and poor thermal conductivity of metal-hydrides, these materials typically have very low effective thermal conductivities on the order of 0.1 $W \cdot m^{-1} \cdot K^{-1}$.[177] Heat transfer improvement methods generally take two forms: 1) the introduction of fins, foams, or meshes, and 2) binding metal hydrides into a solid matrix formed by high-conductivity materials such as graphite, copper, aluminum, or nickel.[175,178]

The effective thermal conductivity of a powder depends strongly on the thermal contact resistance between particles. Therefore, by compressing the powder particles together, the contact area and effective thermal conductivity can be increased. It has been demonstrated that powder beds under high internal stress have much higher thermal conductivities than those of loosely packed powders.[179,180] On-the-other-hand, too much compression of hydrogen storage powder materials can significantly reduce hydrogen storage capacity by making particles in-accessible to hydrogen or by reducing mass transfer in the case of complex hydrides. For example, highly compacted alanates exhibit 67% lower reversible hydrogen storage capacities than unconstrained samples.[181] Highly compacted hydrides also have an increased risk of rupturing the storage vessel on hydriding due to the large lattice volume expansion experience by most materials.[182]

With respect to modeling of metal-hydride beds, the materials themselves are usually modeled as porous media, and Darcy's law is used to calculate the gas velocity.[183] The following is a short synopsis of some prior work on the thermal modeling of hydride hydrogen-storage beds. Klein et al. calculated the effective thermal conductivity of a porous media based on a model assuming two half-spherical particles in contact and using a deformation factor to account for the change in shape under stress.[184] Several groups have proposed and used a homogenization method that is capable of considering microscopic behaviors, such as pulverization, changes of void fraction, and contact area, to calculate the effective thermal conductivities of metal-hydride beds.[185,186,180] Gadre et al. used a simple numerical model to predict the discharging behavior of a practical metal hydride bed and obtained relatively good agreement with experimental data.[187] Askri et al. examined the validity of ignoring radiation heat transfer for $LaNi_5$ and magnesium hydride systems and also examined hydrogen flow and heat transfer in a metal-hydride bed.[188] Guo et al. examined the importance of including both heat transfer by gas-phase convection and solid-phase conduction.[189] This aspect of hydrogen storage system development is still in its infancy and relatively little experimental measurements and modeling of heat transfer have been performed to date. There exists a significant need for combined modeling and experimental studies

of materials-based hydrogen storage systems. For accurate simulations and system development, it is vital that future work includes heat and mass transfer, stress analysis, and thermo-mechanical effects on thermal conductivities and mass transfer coefficients.[190]

A recent analysis of the influence on performance of thermal properties was done for one class of storage materials, namely high-pressure metal hydrides (HPMHs).[191] To achieve the targeted short hydrogen refueling time of less than 5 min the storage system design (heat exchanger) and material thermal properties (thermal conductivity) must provide adequate heat transfer to keep the bed cool during filling. Overall, it was found that the hydrogen fill time is most sensitive to the effective thermal conductivity of the HPMH and the coolant's temperature, followed by the contact resistance between the powder and cooling surface.[191] Much of the data for this analysis came from experimental measurements recently performed at the Purdue University Hydrogen Systems Laboratory (HSL).[154] Thermal property measurements were made in situ on the HPMH intermetallic alloy $Ti_{1.1}CrMn$ at pressures from 2.9 to 253 bar. Measurements were performed using the transient plane source (TPS) method, which is a variation of the hot wire technique. It directly measures thermal conductivity and diffusivity of hydride, and knowing the packing density, the heat capacity can be calculated. The contact resistance was also calculated using the measured temperature profile within the metal hydride powder. The effective thermal conductivity k_{eff} of the hydride of $Ti_{1.1}CrMn$ was measured to be around 1 $W \cdot m^{-1} \cdot K^{-1}$ depending on packing density (thus porosity) and particle size.

For this study thermal properties data was also taken from the literature. Suda et al. [15] measured the thermal conductivity of a similar alloy, $TiMn_{1.5}$, under steady state conditions.[192] For a particle size of 400 μm, they measured an effective thermal conductivity k_{eff} between 0.5 and 1.2 $W \cdot m^{-1} \cdot K^{-1}$ as the hydrogen pressure was increased from 0.5 to 40 bar.

In the HSL work the contact resistance, R_{tc} was calculated to vary between 400 and 1800 $mm^2K \cdot W^{-1}$ as a function of hydrogen pressure and number of hydriding cycles. There was a measured change in R_{tc} with cycling. This was attributed to Lattice expansion and contraction on hydrogen absorption and desorption caused the hydride material to pull away from the vessel walls, resulting in poor thermal contact. In another study, Dedrick et al. calculated the contact resistance for sodium alanate samples.[110] They found a contact resistance between the hydride particles and the measurement probe of about 3000 $mm^2K \cdot W^{-1}$, while between the hydride particles and the container wall they determined R_{tc} to be significantly higher (20,000 $mm^2K \cdot W^{-1}$), possibly due to the material being a loosely packed powder. Because of the dependence of R_{tc} on many factors such as particle size, shape, porosity, nature of contact surface, changes in morphology with cycling, and pressure, R_{tc} is a very difficult parameter to control or characterize.

Poor thermal properties of metal hydride powder render the design of an efficient HPMH heat exchanger quite challenging. The primary objective of the study by Visaria et al. was to understand the influences of various kinetic and thermal parameters on heat exchanger design, and to develop a scalable approach to designing a heat exchanger that is compact and yet, capable of filling a HPMH tank with hydrogen gas within 5 min. Using many of the above cited properties, they varied a variety of geometrical parameters like metal hydride thickness, and heat transfer parameters, like coolant temperature and heat transfer coefficient, in their model of a HPMH hydride hydrogen storage bed to analyze the effects on the hydriding process and ultimately for the purpose of uncovering a practical means for maximizing the reaction rate.[191] The results of their model analysis showed that many properties will affect the performance of an HPMH system to varying degrees. One example, shown in Figure 40, is a plot of the fill time as a function of the effective thermal conductivity of the metal hydride powder. The filling is very slow with low thermal conductivity, approaching 40 min for an effective thermal conductivity of 0.2 $W \cdot m^{-1} \cdot K^{-1}$ compared to 10 min for 1 $W \cdot m^{-1} \cdot K^{-1}$. Above 2 $W \cdot m^{-1} \cdot K^{-1}$, the thermal conductivity has only a weak effect. For example, increasing the conductivity from 5 to 10 $W \cdot m^{-1} \cdot K^{-1}$ decreases the fill time from 5.1 to only 4.5 min.

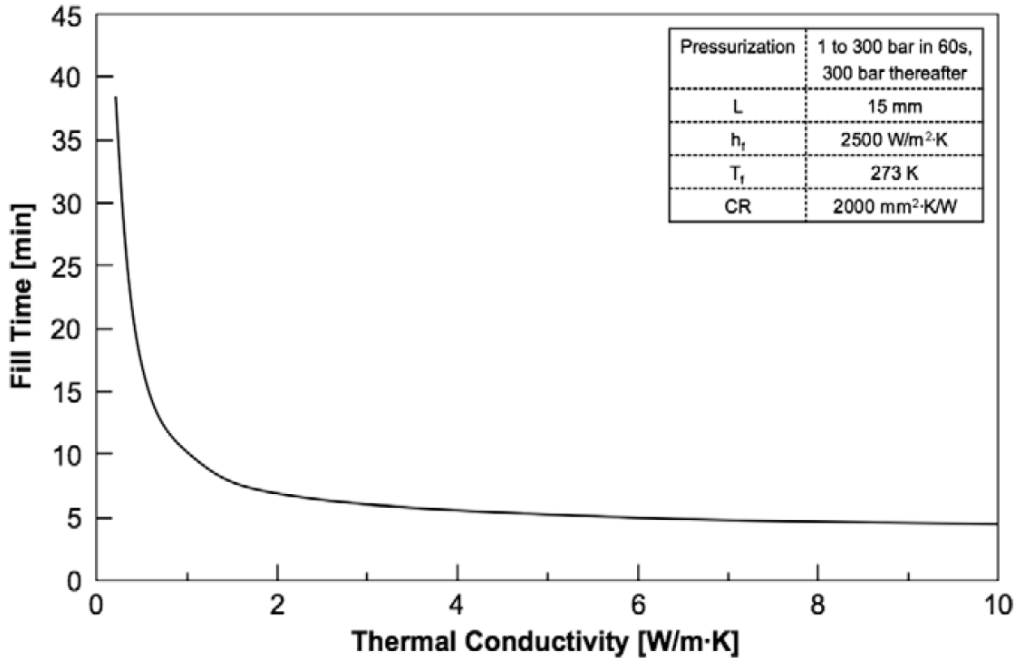

Figure 40. Effect of metal hydride thermal conductivity on H_2 fill time.[191]

As discussed earlier, high-pressure metal hydrides generally have low intrinsic thermal conductivity and other hydride-based hydrogen storage materials are essentially thermal insulators. The effective thermal conductivity of metal hydride powders can be improved with additives such as aluminum powder or carbon materials. Such additives by increasing the thermal performance of the system will improve kinetics and potentially the energy efficiency of the power system. On-the-other-hand, they also add inactive material mass and volume to the storage system. Because of this the trade-off between enhanced thermal performance and potentially reduced capacity must be carefully evaluated. At a system level, improving thermal performance through additives may reduce the requirements (and thus weight and volume) of the heat transfer hardware, possibly for a net gain in system capacity. For example, being able to increase thermal conductivity may allow higher coolant temperatures (Figure 41) for equivalent fill times, or a smaller heat exchanger.

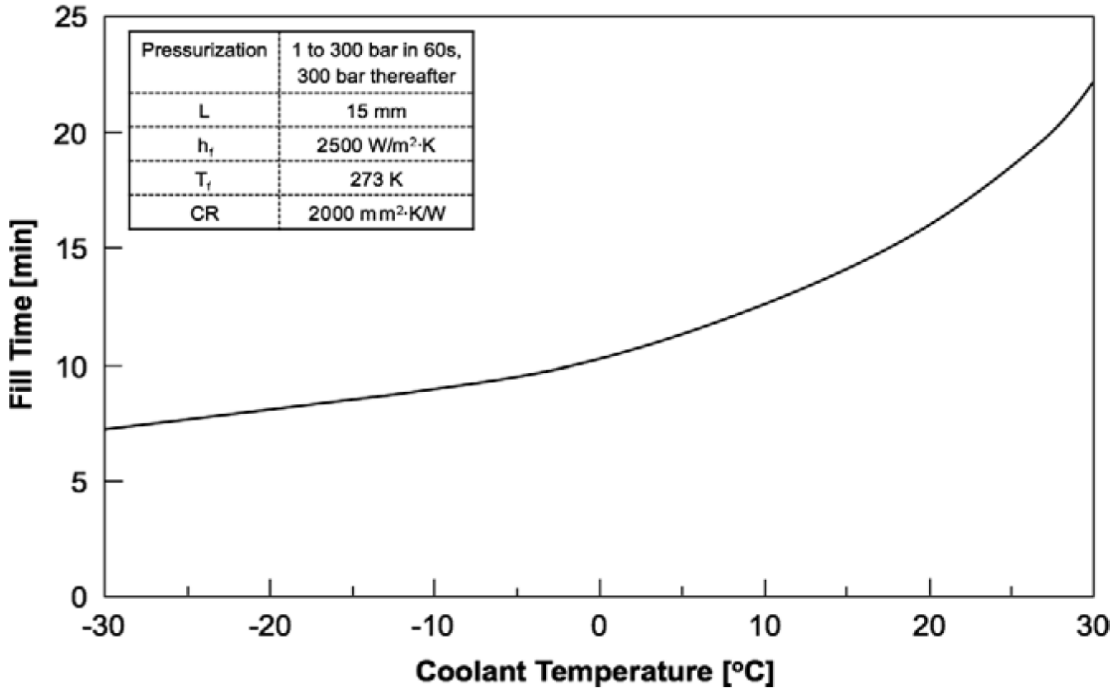

Figure 41. Effect of coolant temperature on H_2 fill time.[191]

Thus, the influence of materials engineering properties such as thermal conductivity on the overall system performance is important and complex. For this reason, being able to collect accurate values of these materials engineering properties under operational conditions is very critical for good system design.

An important part of the Visaria et al. study was a sensitivity analysis that was performed to evaluate the relative influence of key parameters and metal hydride properties on fill time. The fill time was calculated for each parameter by independently varying its magnitude within a practical range, while all other parameters were held constant at nominal values. As a base line, using the set of nominal values, it would take 10.6 min to complete 90% of the hydriding reaction for a 15-mm layer of metal hydride in the HPMH tank design used in their model. It may be noted that the bed thickness of 15mm was determined separately and then fixed for the sensitively study as it was considered the most important design parameter for the heat exchanger by Visaria et al. The results of this analysis are shown in Figure 42.

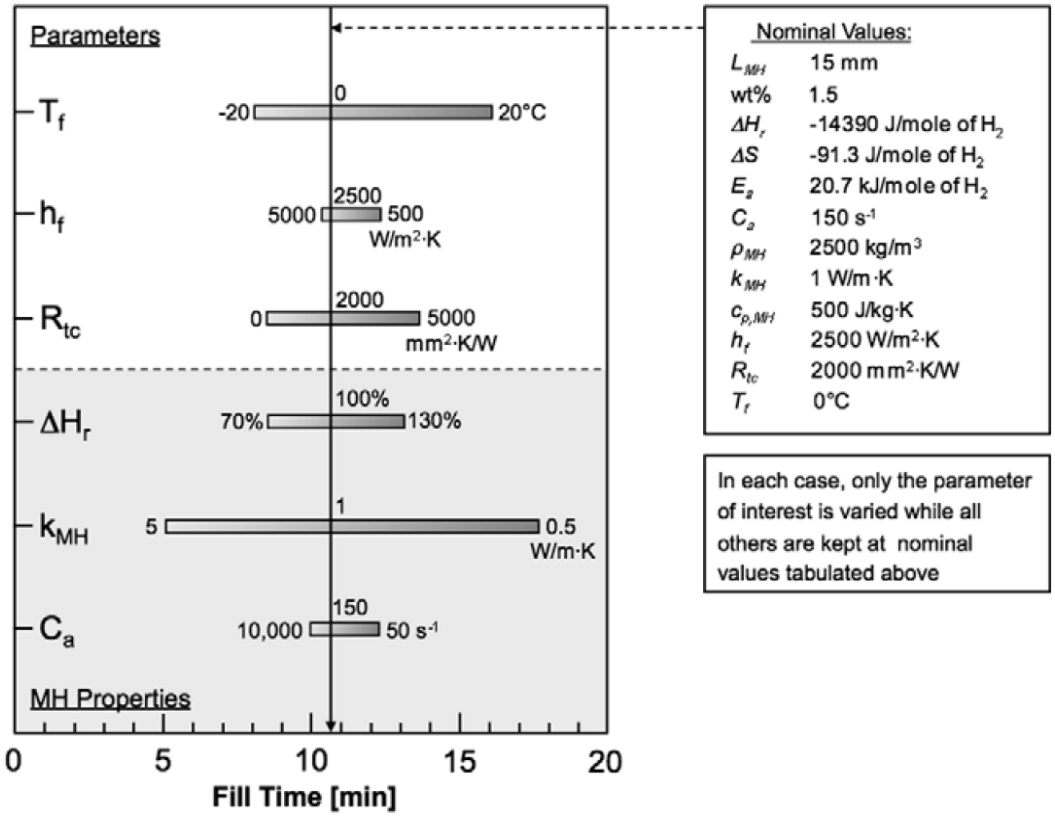

Figure 42. Sensitivity analysis of various parameters and properties influencing fill time.[191]

In the figure T_f is the temperature of the coolant fluid (°C), h_f is the convective heat transfer coefficient ($W \cdot m^{-2} \cdot K$), R_{tc} is the contact resistance ($mm^2 \cdot K \cdot W^{-1}$), ΔH_f is the enthalpy of formation ($kJ \cdot mol^{-1} H_2$), k_{MH} is the thermal conductivity of the metal hydride ($W \cdot m^{-1} \cdot K^{-1}$), and C_a is the hydriding constant or activation rate (s^{-1}). Notably, Figure 42 shows that the fill time is most sensitive to the effective thermal conductivity of the

metal hydride and, to a lesser extent, the coolant temperature. The thermal conductivity is also of greatest significance because it is not constant and will change during regular operation due to the transition from alloy to hydride. In addition the thermal conductivity also depends on properties such as the hydride particle size, shape, and packing density which may change with progressive system cycling. In the study, the k_{MH} was varied between 0.5 and 5 $W \cdot m^{-1} \cdot K^{-1}$. The lower range (0.5 to 1 $W \cdot m^{-1} \cdot K^{-1}$) corresponds to values measured for pure metal hydride powder.[193,154] The fill time was more sensitive to k_{MH} at lower k_{MH} values and a minimum value of about 1 $W \cdot m^{-1} \cdot K^{-1}$ is necessary for practical fill times.

The thermal contact resistance is the third parameter that was found to have an appreciable influence on fill time.[191] As mentioned, this parameter depends on a variety of factors and is difficult to control and characterize. R_{tc} may increase with time due to decrepitation, settling of powders and contraction of the material. Because of the sensitivity of the system performance to the thermal contact resistance, it will be important to perform good measurements and a thorough analysis of R_{tc} in prototype systems.

The influence of coolant flow rates, enthalpy of hydride formation, and activation rate of the hydride on fill times were also evaluated in this study. Overall, however, the results demonstrated that the most practical and effective means to reducing fill time are to: (1) enhance the thermal conductivity of the metal hydride, (2) reduce the coolant temperature, and (3) reduce the thermal contact resistance.

6.1.2 Example: Tests of System with Basic Heat Transfer:

An initial study on the scale up storage properties of an AB_5 metal hydride was performed by Challet et al.[194] This goal of that work was to evaluate a relatively small amount of material (150 g) to be used as a buffer tank to provide hydrogen when starting a fuel cell system. The material ($La_{0.55}Y_{0.45}Ni_5$) was selected as it would easily desorb hydrogen (about 2 grams) at low ambient temperatures with enough pressure to run a fuel cell until it reached an elevated operating temperature. It has an equilibrium pressure of 20 bar of hydrogen at 253K and can be used to fill a buffer tank in a fuel cell car and to deliver sufficient hydrogen for the cold start.

Tests were done by filling a 75 cm^3 stainless steel container with 150 grams of alloy powder. A thermocouple was introduced in the container in order to follow the temperature of the powder during hydrogenation reaction (Figure 43). To regulate the external temperature, the tank was immersed in a temperature controlled bath.

Figure 43. View of the buffer tank with the hydrogen connection (left) and thermocouple inlet (right).[194]

After activating the materials with four absorption/desorption cycles at 253K, absorption kinetic measurements were made at 253K, 268K and 298K using a quasi-static hydrogen pressure of 5 MPa. The reported absorption curves as a function of time are shown in Figure 44.

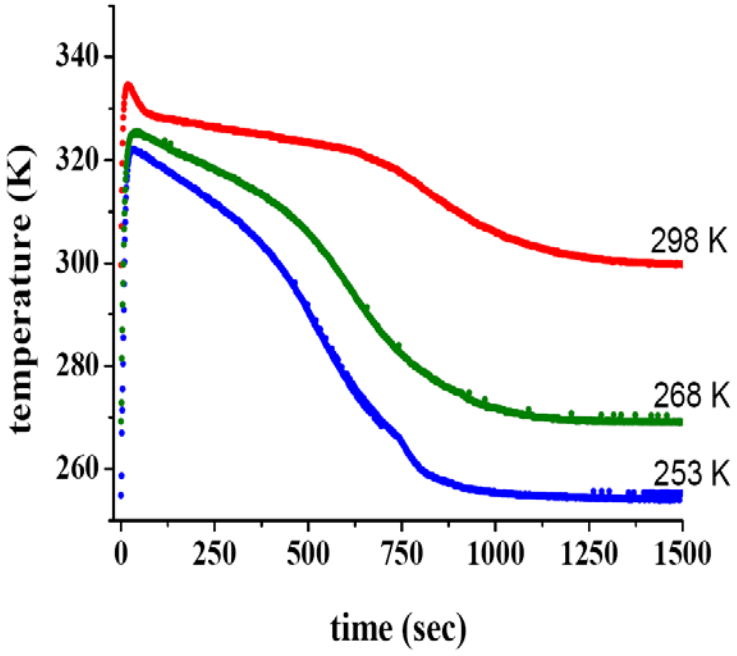

Figure 44. Evolution of the temperature as a function of time for the buffer tank.[194]

Measurements were also performed on a small sample (0.5 g) under similar conditions. From these curves, the time to reach 90% of conversion (t_{90}) was determined at each temperature and is reported in Table 4.

Temperature (K)	253	268	298
t_{90} (sec) small sample (0,5g)	234	76	149
t_{90} (sec) buffer tank (150g)	427	442	750

Table 4. Time to reach 90% of conversion (t_{90}) at quasi constant pressure (5 bar) as a function of temperature for a small sample (0.5 g) and a buffer tank (150 g) for the $La_{0.55}Y_{0.45}Ni_5$ compound.[194]

The intrinsic kinetics of the alloy for absorption is high as can be seen from the charging rates achieved on the small sample. However, for the larger quantity, the heat generated by the reaction leads to a large temperature increase in the test bed that slows down the reaction considerably. In going from 0.5 grams to 150 grams the reaction kinetics with the bed at room temperature is slower by a factor of about 5.

Because the hydriding thermodynamics of the alloy were known, the equilibrium pressure can be determined for any given materials temperature. This was done for the internal temperature of the material in the bed using the measured thermocouple temperature. A plot of the calculated equilibrium pressure versus actual pressure with the exterior bed temperature at 298K is shown in Figure 45.

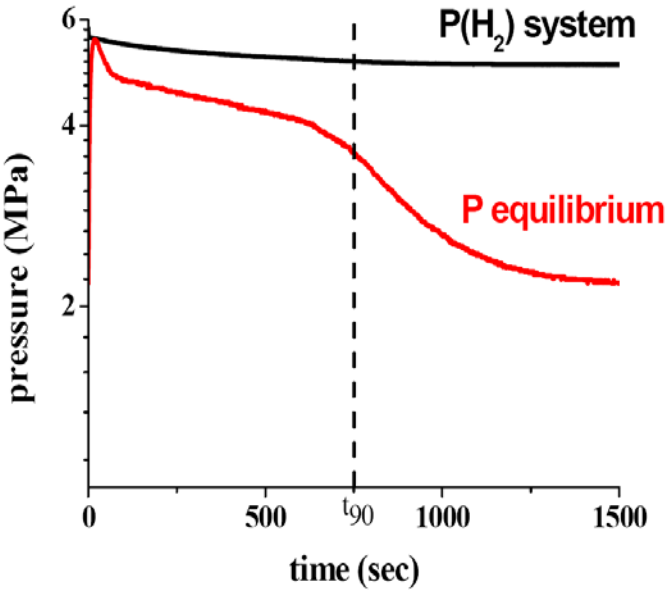

Figure 45. Evolution of the equilibrium pressure (calculated from the Van't Hoff law) and the system pressure (gas pressure) as a function of time for the buffer tank at 298K.[194]

In examining both Figure 44 and Figure 45, it can be seen that the temperature in the bed rises almost immediately to the equilibrium temperature of the applied pressure. Because the heat produced initially raises the temperature such that the equilibrium pressure is equal to the applied pressure the absorption reaction essentially shuts off. As the heat is slowly transferred to the exterior of the bed the temperature of the material drops as does the equilibrium pressure. The driving force for the reaction is the pressure differential (difference between applied pressure and equilibrium pressure). As the temperature and equilibrium pressure drop the rate of absorption increases. Likewise the rate of heat production increases.

Thus, the rate of hydrogen uptake is ultimately controlled by the rate of heat transfer from the material through the container walls into the surrounding bath. It is this heat transfer that controls the hydrogen uptake and release properties of the storage system. The study clearly demonstrated the need for the optimization of heat exchange in the design of hydrogen storage systems.

6.1.1 Example: Testing and Modeling of Advanced Heat Transfer System:

One example of the testing and modeling of a hydrogen storage bed that incorporates an advanced heat transfer design is the recent work by Botzung et al.[195] The goal of their investigation was to develop a metal-hydride hydrogen storage ballast tank to provide hydrogen for cold-starts and as a buffer for a combined heat and power (CHP) system. The system includes a hydrogen production unit using methane reforming, a 40 kW stationary proton exchange membrane fuel cell (PEMFC) and a hydrogen storage bed. A study was performed on a metal-hydride tank based on plate-fin technology. Data from those tests were used to validate a numerical model that was developed to be able to simulate the behavior of metal hydride tanks. The model was based on Fluent Software and took into account heat and mass transfers in porous media and the convective flow required to cool/heat the system during absorptions/desorptions. Measured thermal and mass properties of the hydrogen storage materials were integrated into the model. In this case, the metal-hydride storage material ($La_{0.90}Ce_{0.05}Nd_{0.04}Pr_{0.01}Ni_{4.63}Sn_{0.32}$) was chosen to match the particular operating temperatures and pressures of the application.

The metal-hydride tank used a rectangular integrated plate-fin type heat exchanger coupled with the use of aluminum foam design to decrease the hydrogen charging/discharging time but also allow easy of assembly and disassembly. The various components of the tank are shown in Figure 46.

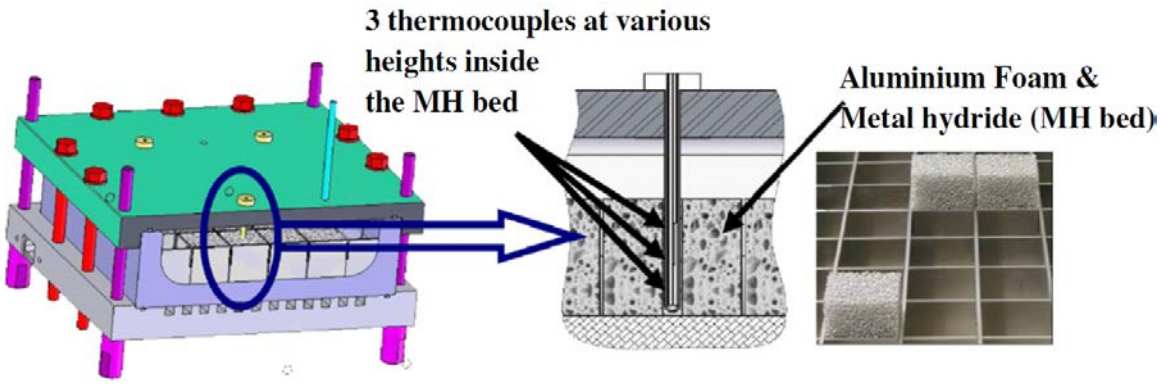

Figure 46. (left) plate and fin design of bed showing (center) placement of three thermocouples at different levels inside the bed, and (right) construction of combined metal-hydride and aluminum foam cells.[195]

The metal alloy powder was filled into aluminum foam inserted into cells in the bed constructed of with aluminum fins all to improve heat transfer. The heat exchanger and the vessel were made of aluminum for good thermal conductivity. The bed itself was cooled or heated with an oil-based heat transfer fluid through 12 square cooling channels in a heat exchanger at the base of the bed. A stainless steel filter plate was positioned above the metal-hydride material to avoid the transfer of powder particles into the hydrogen gas lines.

Absorption/desorption testing of a hydrogen storage bed can be carried out in a number of ways. However, the two most straight forward methods are charge (or discharge) at a constant hydrogen gas flow rate or at a constant hydrogen pressure. As an example the bed described above was charged with hydrogen at a fixed flow rate of 125 NL h^{-1} and the heat transfer fluid at 65°C. Some results of that measurement are shown in Figure 47. During absorption, the pressure increased from the equilibrium pressure (0.7 bar at 65°C) to the set point pressure (3.5 bar). The total hydrogen uptake is linear during 15.5 hours of charging.

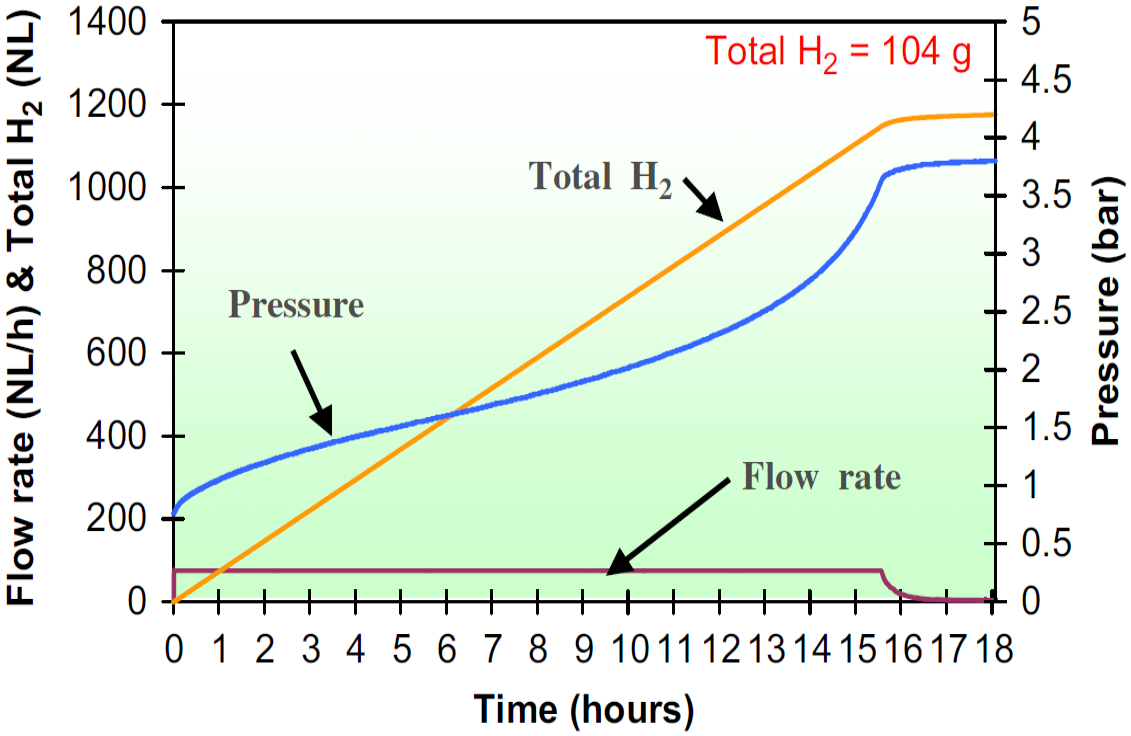

Figure 47. Pressure (blue) increase for an absorption cycle with a flow rate set to 125 NL·h^{-1} H_2 (purple) and heat transfer fluid set at 65°C. The conversion of flow rate to hydrogen uptake is shown (orange) with a final total H_2 uptake of 104 g.[195]

Modeling:

The study by Botzung et al. included three-dimensional modeling of the complete storage system taking into account boarder effects. In order to simulate the thermal and hydrogen flow rate behavior of the storage bed, the thermal and mass properties of the hydride were integrated in FLUENT modeling software using the PONS analytical model describing the Pressure-Concentration-Temperature (PCT) isotherms.[196] Figure 48 illustrates the accuracy of the fit of the PONS model to experimental PCT measurements at 25, 65, 75 and 85°C of this hydride.

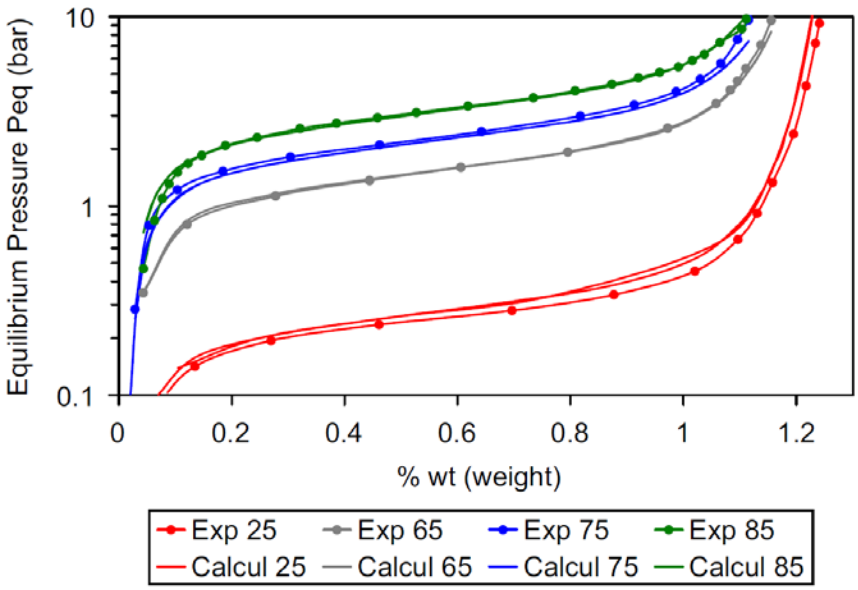

Figure 48. PCI curves of the hydride $MmNi_{5-x}Sn_x$ at 25, 65, 75 and 85°C.[195]

The computational setup and the boundary conditions are illustrated in Figure 49. The coolant was modeled by a heat exchange coefficient applied on each surfaces of the cooling channels. The hydride has two different computational domains, one being the metal-hydride powder / aluminum foam between the aluminum fins. The other domain is the metal-hydride powder in contact with the external adiabatic vessel walls. At the beginning of the absorption, the system is at 293K and the hydrogen is injected at the top of the system, then the hydride absorbs and the exothermic reaction raises the temperature as indicated in the calculated temperature contours at the right side of the figure.

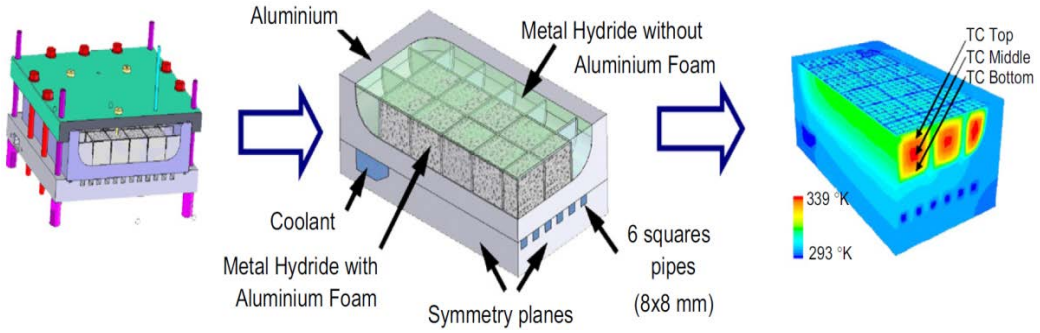

Figure 49. The bed (left), its modeled geometry (center), and calculated temperature contours of temperatures (right) during absorption.[195]

Simulation results for charging the bed are shown in Figure 50 and compared with measured data.

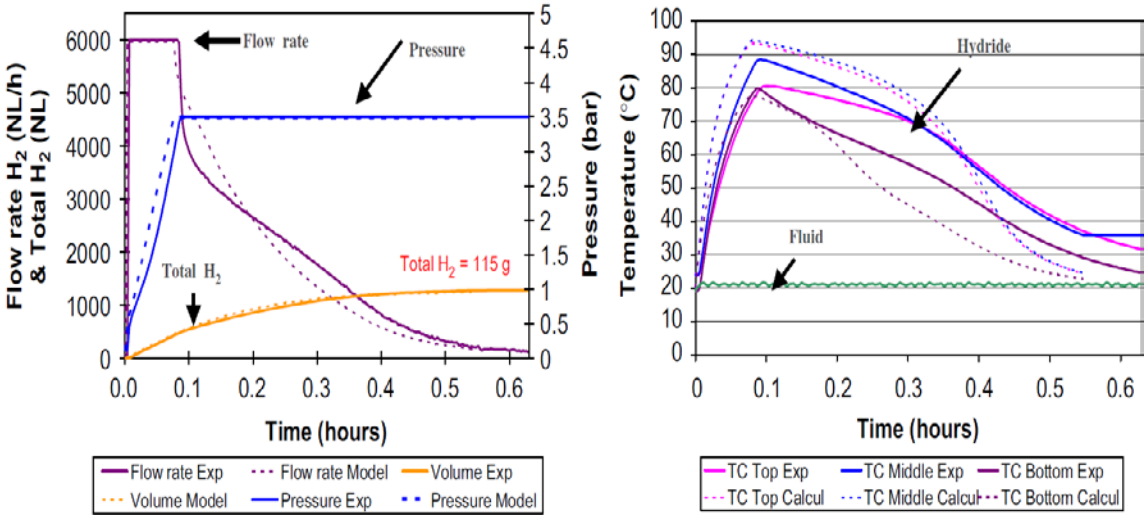

Figure 50. Experimental results vs. model results. The experimental results are plotted in continuous lines and the simulation results are plotted as dashed lines.[195]

The flow rate and hydrogen capacity (mass transfer) of the simulation are in relatively good agreement with the experimental results. During the first step of absorption (at a constant flow rate of 6000 $NL \cdot h^{-1}$), a strong increase of temperature is observed in the bed. Once the set point pressure has been reached (3.5 bar), the temperature starts to decrease down to the cooling fluid temperature. When the system reaches the set up pressure (3.5 bar), it absorbs hydrogen at a constant applied pressure and there is a decrease of the flow rate which reaches zero when the absorption is complete. The calculated temperatures during the absorption are in reasonably good agreement with the measured values.

The two examples presented above provide a valuable perspective on the importance of heat transfer in storage system design and more fundamentally the need for accurate determinations of the thermal conductivity of hydrogen storage materials.

6.1.1 Example: Thermal Conductivity Measurements of MgH_2

The thermal conductivity of MgH_2 powders and compressed composite of MgH_2 containing differing amounts of ENG (Expanded Natural Graphite) was examined by the group of Dr. De Rango.[197] The measurement method that was used axial heat flow method: A given power P is injected in the sample and the induced thermal gradient between 2 points of the sample is measured. This measurement is repeated for increasing powers, the curve is then linearized to deduce the conductivity. The measurement is also performed without sample in order to deduce the base line. Two different instruments were constructed, one for powder measurement in which hydrogen pressure can be applied (in situ) and one for compacted bars (typically 4x4x50 mm^3) under vacuum.

It was found that the thermal conductivity was strongly dependant from the applied hydrogen pressure Figure 51 and also the hydriding state (fully hydrogenated, partially hydrogenated or metallic). Moreover, the thermal conductivity evolved upon cycling due to microstructure evolution (decrepitation, grain growth, sintering, etc.).

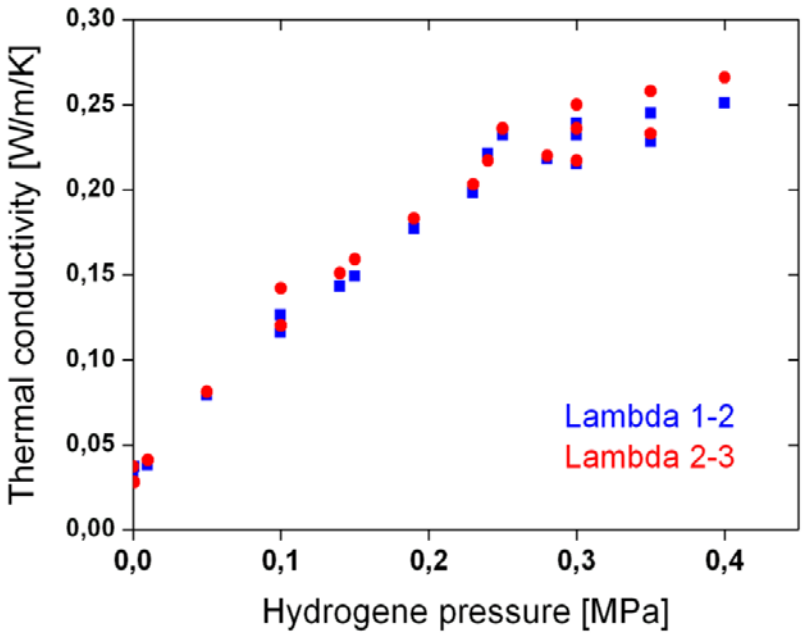

Figure 51. Thermal conductivity of two different ball-milled MgH_2 powder samples versus applied hydrogen pressure.[197]

An improvement in thermal conductivity was observed as a function of the addition of ENG into compressed powder compacts. In the particular case of MgH_2 (Figure 52), we clearly observe an improvement of the thermal conductivity with cycling. The radial thermal conductivity was found to be 2 times higher after about 10 cycles.

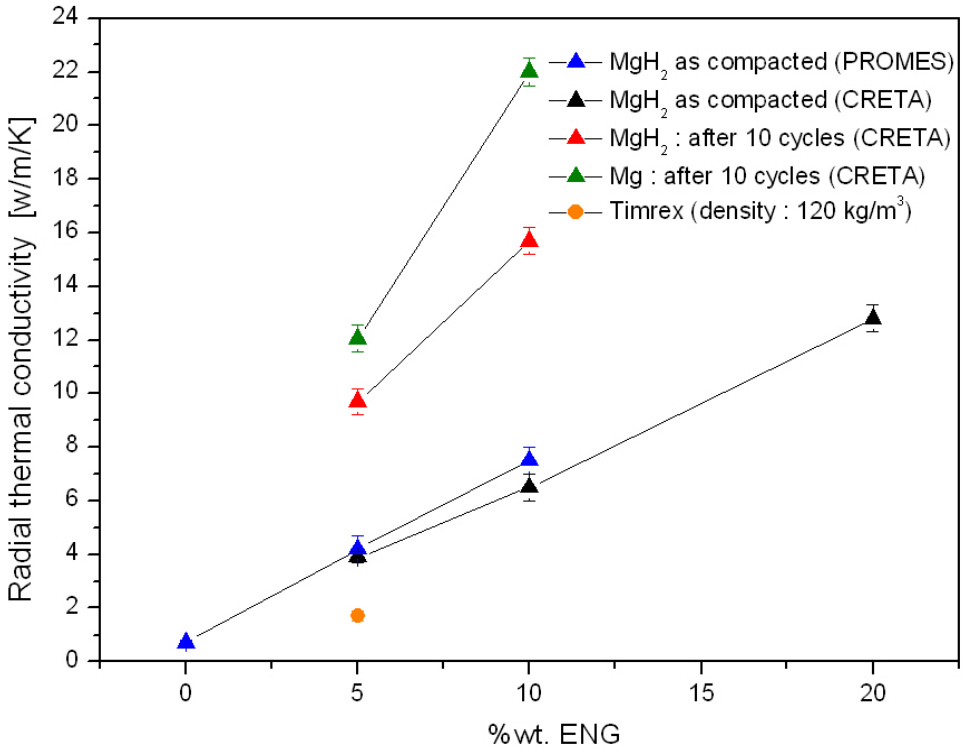

Figure 52. Radial thermal conductivity of MgH_2 composites as a function of ENG (Expanded Natural Graphite) content. Measurements were performed just after compaction (in the hydrogenated state) and after 10 hydrogen cycles (both in the metallic and hydriding state).[197]

It was, however, difficult to pursue measurement for a larger number of cycles because of the changes in the morphology and dimensions of the samples upon cycling. This was caused by irreversible deformations between absorption and desorption steps as show in the photo of Figure 53.

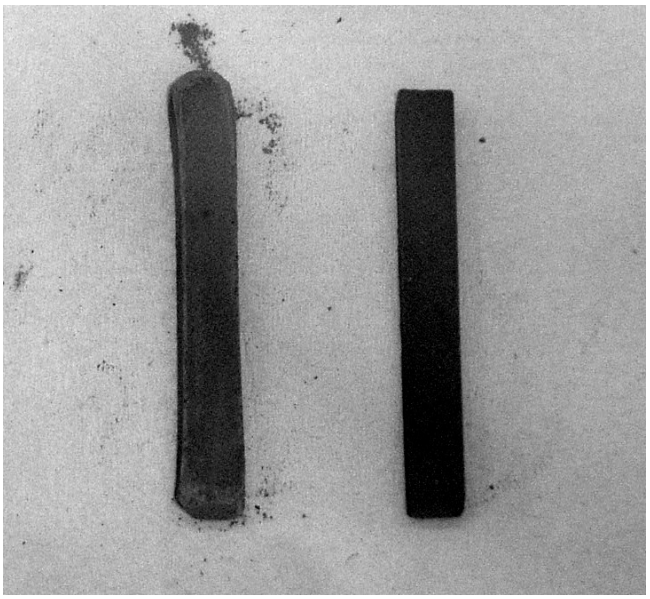

Figure 53. Aspects of the composites rods after 10 cycles (left) and before cycling (right).[197]

6.1.2 Example: In-Situ Thermal Probe Measurements of Alanates

Until 2005 the only engineering properties of the new generation of hydrogen storage materials based on complex hydrides was a value for the thermal conductivity of sodium alanate during absorption of hydrogen reported by Sandrock et al.[198] One of the first extensive engineering properties investigations of sodium alanates was performed by Dedrick et al.[110] In that work, the heat transfer properties of sodium alanate was studied as a function of cycle, phase, hydrogen gas pressure, and temperature using the Thermal Probe Method.

This study provides a good example of the challenges faced in making accurate measurements of the heat transfer characteristics of hydrogen storage materials. In particular, the characteristics of the sodium alanate and its decomposition /recombination imposed unique requirements on the measurements. The thermal properties measurement method and equipment had to be capable of accommodating significant sample morphology changes, absorption gas pressures up to 100 bar, and operating temperatures up to 180°C for measurements of materials with low thermal conductivity. Sodium alanates are highly air sensitive and, therefore, it was desirable to perform measurements in situ at different states of hydrogen absorption and desorption, adding another degree of complexity to the experimental measurements.

As a first step, the measurement apparatus itself had to be developed to meet all of the above requirements. For this reason a two-dimensional axisymmetric finite element model was created to design and optimize the geometry of the pressure vessel within which the thermal properties measurements were to be made. The model-based design enabled the (a) determination of the appropriate probe length required to minimize end effects on the measurement results, and (b) determination of the minimum amount of material required for the measurements. The apparatus was designed to measure apparent thermal conductivities up to 3 $W \cdot m^{-1} \cdot K^{-1}$ for measurement times between 100 and 1000 seconds with less than 10% error.

The final design consisted of a heated measurement pressure vessel, with a sample space 5.08 cm in diameter and 10.16 cm long, instrumented with 12 radially and axially distributed thermocouples. Measurements from the thermocouples were used to compare the measured temperature field with simulated results from the finite element thermal model. A solid model diagram of the resulting apparatus design is shown in Figure 54. The radial and axial thermocouples were later removed to measure higher conductivity samples and accurately measure the resistance between the alanate and the vessel wall.

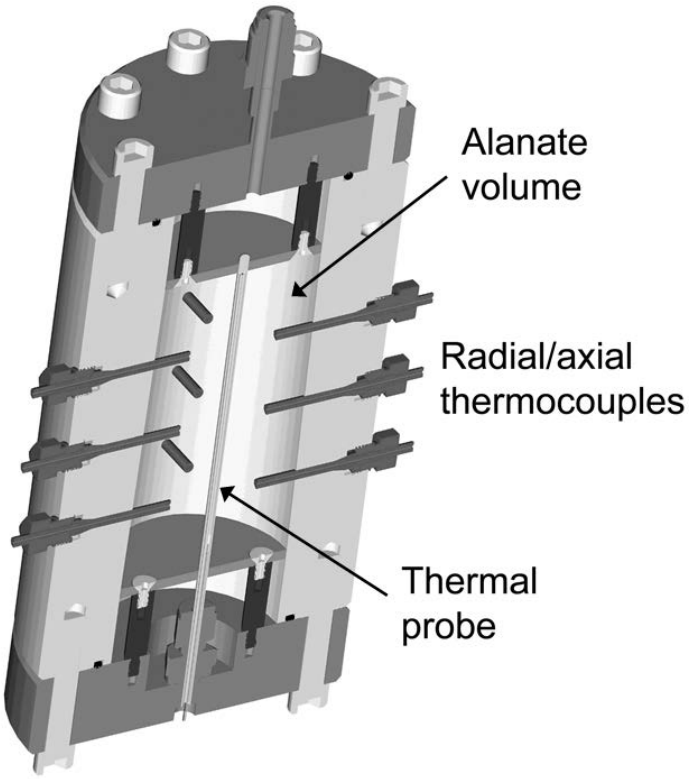

Figure 54. Solid model diagram of the sodium alanates thermal properties analysis chamber designed to meet the pressures and temperatures required for hydrogen absorption and desorption.[110]

The measurement chamber contained a thermal conductivity measurement probe running down the center of the vessel. The probe consisted of one nichome heating element, and one temperature measurement element encased in a stainless steel sheath. It was constructed to ASTM specifications with custom attributes to accommodate the alanate. A schematic diagram of the probe is shown in Figure 55.

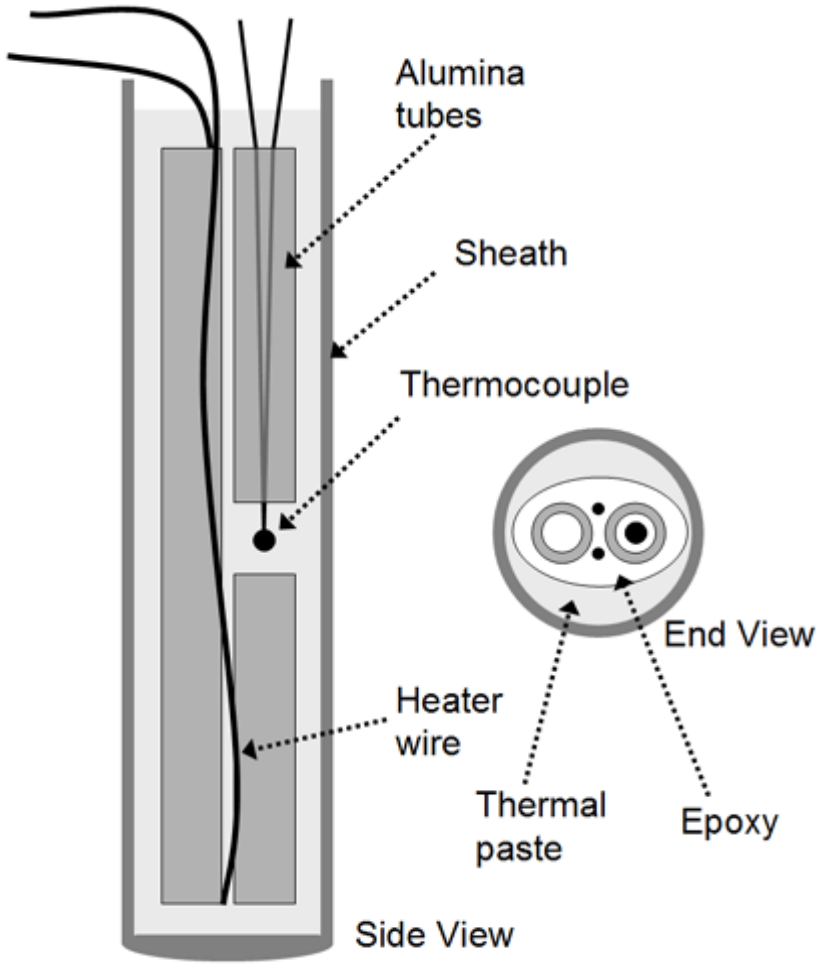

Figure 55. Schematic diagram of the transient thermal probe assembly consisting of a thermocouple and heating element encased in a stainless steel sheath.[110]

Prior to each measurement, the sample and instrument was allowed to come to complete thermally equilibrium. Measurements were conducted with the test chamber near room temperature to minimize the influence of absorption or desorption of

hydrogen during the thermal conductivity measurements. To analyze heat transport within the material, an appropriate constant current was applied to the probe heater to produce a constant power input to the bed. Then the probe temperature was measured as a function of time. Typically a probe temperature rise of 10°C within 1000 seconds was preferred for reasonable accuracies.

In this study,[110] the experimental probe temperature data was fit using the one-dimensional heat transfer solution described by Carslaw and Jaeger[199] and simplified by Blackwell[137] to give:

Equation 63

$$T(t) = A \cdot \ln(t) + B + C \cdot \frac{\ln(t)}{t} + D \cdot \frac{1}{t}$$

where thermal conductivity is defined as

Equation 64

$$K_{th} = \frac{r_P \cdot Q'}{2 \cdot A}$$

and wall resistance is defined by

Equation 65

$$H = \frac{1}{r_P} \cdot \left[\frac{2 \cdot K_{th}}{\frac{B}{A} - \ln(\frac{K_{th}}{\rho \cdot Cp}) + 2 \cdot \ln(r_p) - \ln(4) + 0.8141} \right]$$

where r_p is the probe radius, Q' is the power per unit length of probe, ρ is the packing density of the alanate, C_p is the heat capacity, and A, B, C, D are the fit coefficients. The fit coefficients C and D are influential during small time but their significance diminishes quickly with increase in measurement time. The application of Equation 63 is straightforward, with K_{th} being proportional to the inverse slope of linear region of the probe temperature vs. ln*(t)*.

A typical analytic fit to experimental data was shown in
Figure 56.[110] The quality of correlation between the data and the ideal analytic solution was characterized by Pearson's correlation which describes the degree of linear relationship between the data and analytic solution. Dedrick et al. obtained a Pearson's correlations greater than 0.9999 using this method.

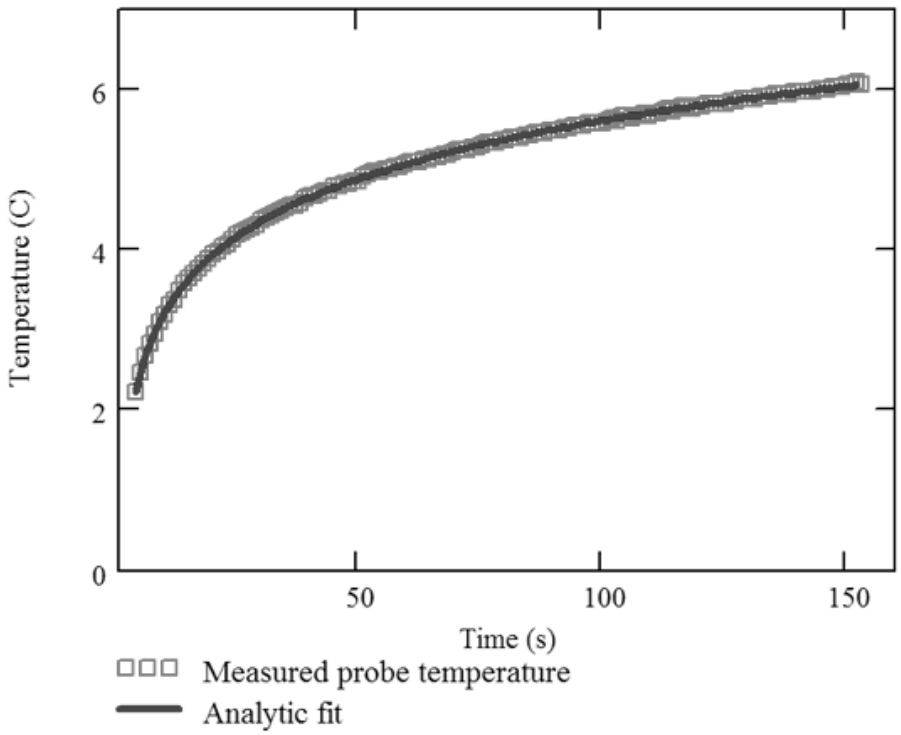

Figure 56. Example fit of analytic solution where influence of boundary is not observed. Pearson's correlations better than 0.9999 routinely achieved.[110]

It is important to note, however, that the analytic fit was only appropriate during a time period in which the boundaries and radial thermocouples do not affect the probe temperature. Unfortunately, the presence of the radial thermocouples limited the measurement range. The solution to this was addressed below.

In this example study[110] along with the work of others[200] found that C_p and H were unreliably sensitive to the short time analytic fit. This was due to the sensitivity of the short time solution to the construction of the probe, which was a non-ideal representation of the probe described by Blackwell.[137] Therefore, in the absence of experimental measurement, Derick et al. used specific heat values calculated from weighted mixtures of published values for each of the constituent components of the alanate compositions for each probe measurement taken.

It should be noted that these C_p values only described the solid phases and did not account for the presence of hydrogen gas. The effect of hydrogen gas was dependent on the free gas volume of the test chamber and the gas pressure. For example, in the experimental setup described in this example, 100 atm of hydrogen gas added between 10% and 14% to the total heat capacity of the bed depending on phase.

Three-dimensional numerical model

The determination of thermal conductivity by the analytical approach by Blackwell described above is valid for a medium that is effectively infinite.[137] In this example, it was found that the experimental apparatus described above, could only use this analytical approach accurately for materials with conductivity below ~0.7 $W \cdot m^{-1} \cdot K^{-1}$.[110] This limit was lower than initially predicted due to the influence of the radial thermocouple positioning tubes that were not described in the original design model. To overcome this limitation, and obtain accurate results at higher thermal conductivities, a three-dimensional finite element method was used to calculate the heat transfer between the heating probe and the sodium alanate bed.

The materials of the cell and alanates were assumed to have uniform effective densities, specific heats and thermal conductivities. A general-purpose heat transfer code,[201] was used to solve the standard heat conduction equation (Equation 66):

Equation 66

$$\rho C_p \frac{\partial T}{\partial t} = \nabla\left(k_{th} \nabla T\right)$$

where ρ, C_p, k_{th}, and T are the local values of the density, specific heat, conductivity and temperature. Contact resistance was accounted for using a heat transfer coefficient, H, as $q = H\Delta T$, where q was the heat flux and ΔT was the temperature difference between the surfaces in contact.

The authors used this model to determine the effective thermal conductivity and contact resistance through an iterative trial and error process to obtain agreement between the calculated and measured transient probe temperature profile. This approach has been used before to determine thermal physical properties of a small packed bed.[202] The modeling method was validated by comparing results with the analytical values from measurements of alanates at low k_{th} which were in good agreement. The model made it clear that the thermocouple positioning tubes had to be removed to increase the measurement range using the analytical fit approach to data analysis.[110]

Validation Testing

An important aspect of the work performed by Dedrick et al. was the validation of the experimental setup prior to measuring sodium alanate.[110] Their apparatus was tested using materials with well-known and consistent thermal conductivity values that were expected to be in the same range as the alanates (solid Teflon, closed pore polyurethane foam, and commercially available Ottawa sand). They found agreement between the measured results and the reported values of these materials that demonstrated a sufficient level of accuracy of the equipment (10% or better). They noted, however, that the measurements of the thermal conductivity of Ottawa sand

varied significantly with the presence, type and pressure of gas in the test cell. They also found that the surrounding gas increases the thermal conductivity of the sand to levels that are higher than either the sand or the gas alone. A low apparent thermal conductivity at vacuum was due to the domination of inter-particle contact resistance that provides a torturous and poor heat flow path. When a gas is present in the inter-particle space, enhanced heat flow paths are established through conduction/convection of the gas. Dedrick et al. postulated that that the thermal contact between particles was enhanced with the presence of the gas.

Discussion of error

An important aspect of the measurements performed by Dedrick et al., particularly with respect to Best Practices, was the inclusion of a discussion of the most significant errors.[110] It is the recommendation of this "Best Practices" document that instrumental error analysis, as well as testing of reputability and sources of error (using standard materials) as described below, be included in all reporting of materials engineering properties results.

Dedrick et al. performed repeatability tests on their experimental apparatus. Eleven consecutive measurements were made under identical conditions and presented below in Table 5. The largest variation from mean was determined to be 2.9%.

Consecutive Measurement	Measured k_{th} ($W \cdot m^{-1} \cdot K^{-1}$)	Variation from Mean (%)
1	0.84	1.7
2	0.82	-1.6
3	0.83	0.4
4	0.84	1.5
5	0.83	0.2
6	0.83	0.3
7	0.82	-1.4
8	0.83	-0.1
9	0.81	-2.9
10	0.84	0.9
11	0.84	1.0

Mean	0.83
Standard Deviation	0.01
Sample Variance	1.39E-04
Range	0.04

Table 5. Repeatability of 11 consecutive thermal conductivity measurements. Measurements completed in chamber without radial thermocouple tube inserts.[110]

The sources of experimental error included the measurement of temperature, pressure, and heater power measurement (usually much less than 1% contribution to error). The authors found that error caused by analytic fitting of the data was less than 10% for simulations of thermal conductivities up to 3 $W \cdot m^{-1} \cdot K^{-1}$ due mostly to boundary effects. However, they also discovered that the instruments' radial temperature probes (Figure 54) contributed to measurement error for higher conductivity measurements, and, therefore, were eventually removed for subsequent measurements. They also found that the power used for the experiment does not have a measurable effect on the results; however, the heater power was kept low to minimize the potential effect of heat transfer by thermal radiation.[141] Their conclusion was that measurements of an apparently infinite medium (where boundaries do not influence fit result), the error in their experimental measurements was estimated to be less than 10% with a repeatability variation of less than 2.9%.

As a very important note, that will apply to all such measurements, the authors found that it was important that full thermal equilibrium be attained (variation within the measurement noise, approximately ±0.01°C) before the measurement is conducted. Experiments demonstrated that failure to attain complete equilibrium can lead to measurement accuracy errors in excess of 10%.[110]

Thermal Conductivity of Alanates as a Function of Composition, Temperature and Pressure.

Using the experimental device described above the thermal properties of sodium alanate were studied by Dedrick et al. as a function of reaction composition, gas pressure (1 to 100 bar), and temperature (20 to 130°C).[110] These measurements were performed on material that was fully cycled (cycle 7).

Having removed the effect of the radial thermocouples to extend the measurement range and using the three-dimensional FE model to analyze data at higher gas pressures, five measurements were made on $NaAlH_4$ at temperatures ranging from 22°C to 130°C. The hydrogen gas pressure used (~ 60 bar) was above the equilibrium reaction pressure to ensure that decomposition would not occur. Under these conditions, the change in temperature showed less than 6% variation in thermal conductivity.

However, the study found that the thermal conductivity of the alanate system varied significantly with composition and gas pressure as shown in Figure 57.

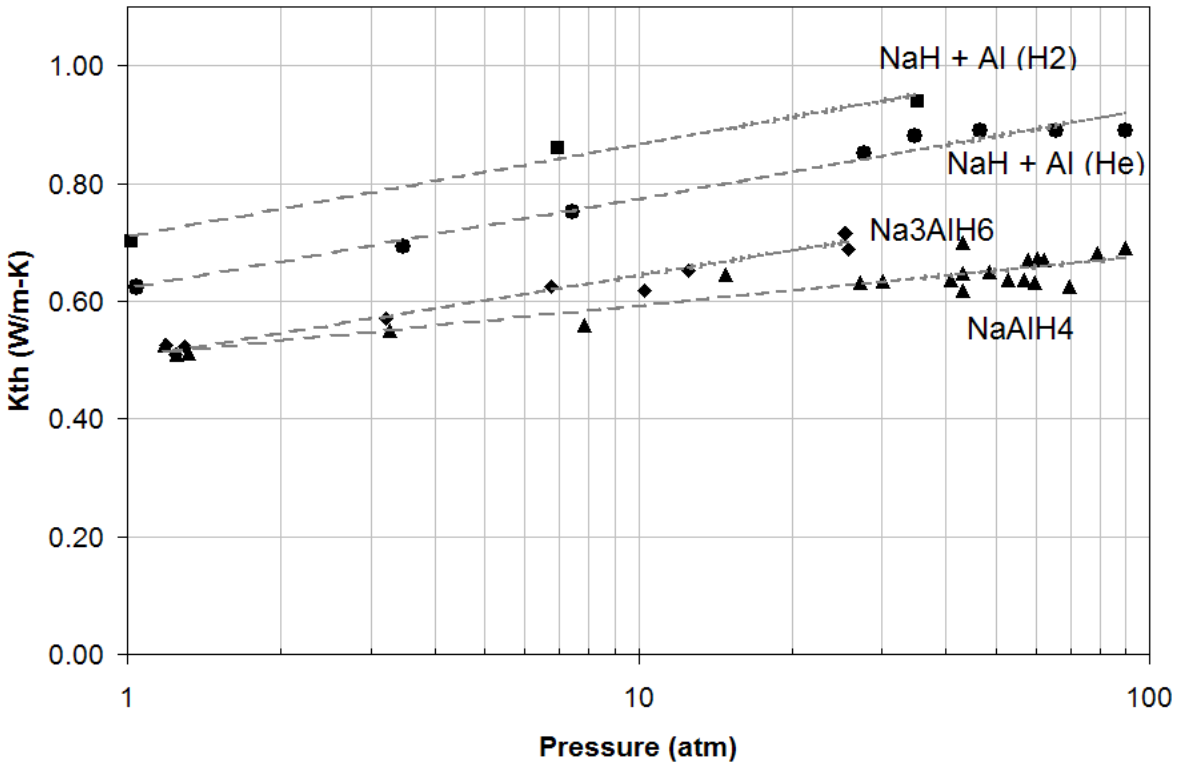

Figure 57. Gas pressure enhances the thermal conductivity of the sodium alanate bed. The enhancement is experienced with both hydrogen and helium as shown in the fully decomposed phase.[110]

Qualitatively, with respect to the material's composition, the thermal conductivity of the bed increased with the amount of free aluminum present (a function of the extent of decomposition).

The variation in thermal conductivity as a function of hydrogen gas pressure was found to correlate with log(P_{H2}) (Figure 57) and expressions were produced by fitting the data for each of three hydride states (desorbed, $NaAl_3H_6$, and $NaAlH_4$)

The linear dependence of thermal conductivity with ln(P_{H2}) mimics the thermal conductivity of a gas in a transition regime. It was hypothesized that this behavior could be due to the ratio of the hydrogen mean free path and an average critical dimension in the bed.[110] In a further set of experiments, also shown in Figure 57, similar measurements were made under a helium gas atmosphere giving a similar linear dependence on log gas pressure.

Contact Resistance Measurements

Contact resistance measurements were also made in this study.[110] The measurements were done with the material fully desorbed and fully hydride at various gas pressures. For each composition, two different measurements were performed; to measure the contact resistance between the outside wall and alanate, an external heat source was utilized; and to measure the contact resistance between the probe wall and alanate, the probe heater was used. In general, the contact between the alanate and vessel wall was poor and the resistance ranges from 300 to 560 $W \cdot m^{-2} \cdot K^{-1}$ at the probe, and 30 to 150 $W \cdot m^{2} \cdot K^{-1}$ at the external wall. The variation between the wall and the probe was explained by the observation that the material was found to be in tight contact with the probe surface while the alanate was partially separated from the vessel walls.

Thermal Conductivity as a Function of Cycling

An important aspect of hydrogen storage materials (particularly reversible hydrides) is that the thermal conductivity of bulk materials is very likely to change with cycling. Using the experimental setup described above, Dedrick et al. measured the thermal conductivity of the sodium alanate as a function of cycle both in the fully desorbed state under vacuum (NaH+Al), and in the fully hydrided state ($NaAlH_4$) under 1 bar of hydrogen (results shown in Figure 58).[110]

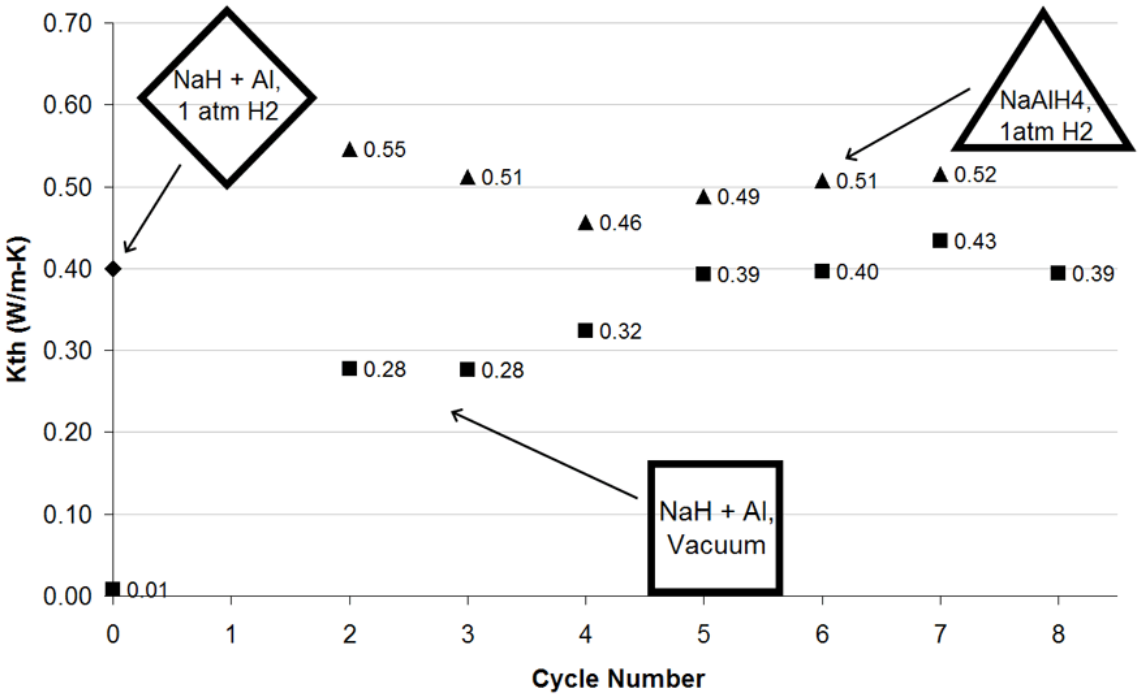

Figure 58. Thermal conductivity of sodium alanate as a function of cycle and phase. The variation with cycle stems from morphology changes experienced during decomposition/recombination.[110]

They found that, before cycling, the ball milled NaH+Al sample material had a *very* low thermal conductivity (<0.01 $W \cdot m^{-1} \cdot K^{-1}$) under vacuum. However, the effective thermal conductivity increased by 5000% with the introduction of hydrogen (similar to the gas effect measured on the Ottowa sand described above). The thermal conductivity of the Hydrided ($NaAlH_4$) material did not change significantly with cycling. On-the-other-hand, the thermal conductivity of the fully desorbed material under vacuum increased with cycling up leveling off after a half dozen cycles. This was attributed to the material experiencing significant morphology changes during "activation". The authors disassemble the test bed after nine cycles and found a significant density gradient in the sample material with the top 25% of the material having a packing density of 0.55 $g \cdot cc^{-1}$ while the bottom 25% was 0.74 $g \cdot cc^{-1}$. They concluded that the variation in packing density will certainly have some effect on the local thermal conductivity of the material. This is an important factor to be considered in how the measurements are made and ascribed to a hydrogen storage material.[110]

Variations in packing density may potentially have an important impact on (among other things) thermal conductivity in scaled-up hydrogen storage systems.

Particle Size

In the same study, the test bed was refilled with direct-synthesis sodium alanate made with 44 μm aluminum particle and cycled 5 times. This material produced using aluminum of much smaller particle size than the prior measurements. The effect of this was to significantly enhance the effective thermal conductivity of the bed.[110] Clearly, parameters such as particle size, compaction, cycling, composition, and additives (to mention a few) will all have some impact on the effective thermal conductivity of such hydrogen storage materials. Therefore, it is important to include a description of these properties along with reported results and it is also desirable to measure the effect on thermal conductivity with changes in these properties.

6.1.1 Example: In-Situ TPS Measurements of Hydrides

An example of in situ thermal properties measurements on hydrogen storage materials are the experiments on $Ti_{1.1}CrMn$ metal hydride performed by Flueckiger.[154] In that study, powders and pellets of $Ti_{1.1}CrMn$ from oxidized powders and activated form were tested as a function of hydrogen pressure. The effective thermal conductivity and thermal diffusivity of the alloy and hydride were made using an in situ transient plane source method. The Zehner-Bauer-Schlünder model was applied as an interpretive model for k_{eff} of the metal hydride powder. The Debye model was used as a comparison of C_p with experimental results. Experiments were performed on stainless steel samples for validation of the method.

Thermal properties (k_{eff} and α) of the metal hydride were measured with a commercial TPS setup.[154] The circular TPS sensor is shown in Figure 59.

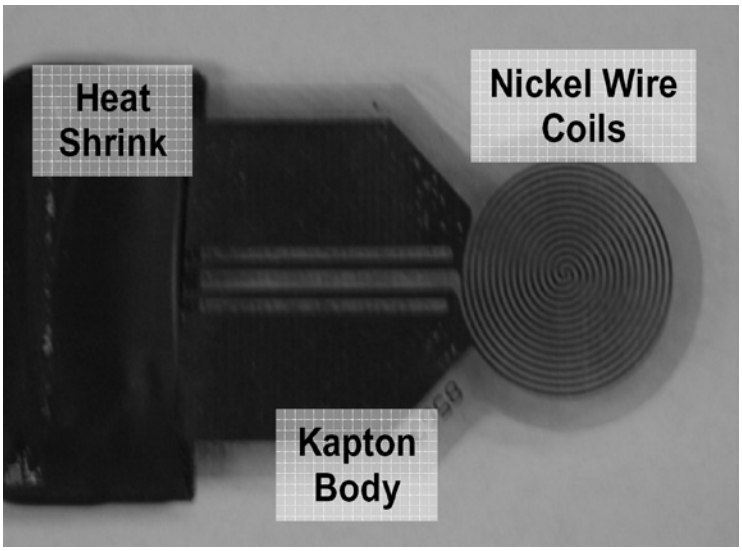

Figure 59. Commercial circular TPS sensor.[154]

In ex situ experiments, the sensor was inserted between two samples of test material and clamped together in the sample holder shown in Figure 60. The sample holder had a center screw to clamp the samples and the sensor together to obtain good thermal contact between them. The entire sample holder was surrounded by a thermal shield to prevent radiant or convective interference thermal effects from the surroundings.

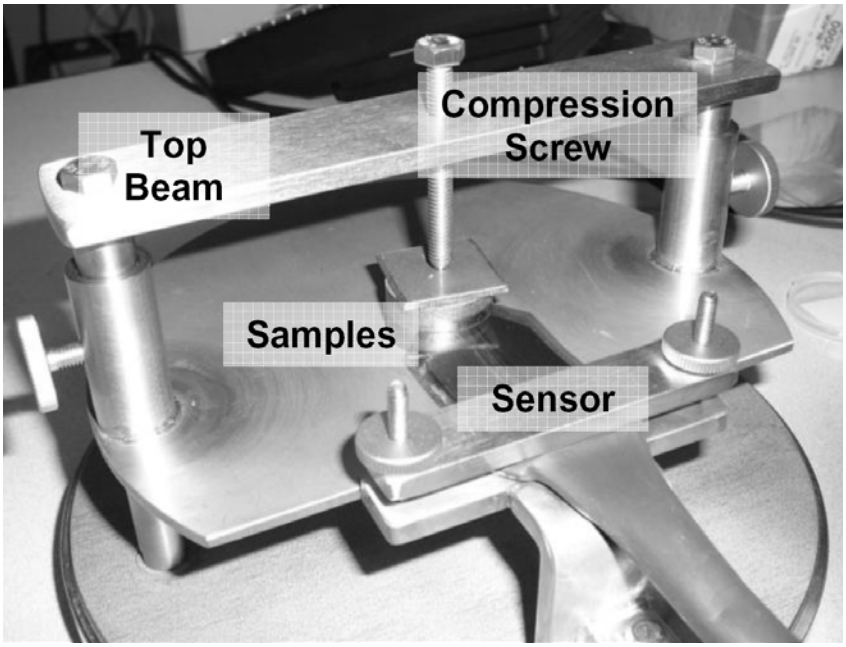

Figure 60. Ambient TPS instrumental setup.[154]

The alloy $Ti_{1.1}CrMn$ forms a hydride at high pressure, requiring up to 700 bar of hydrogen pressure to reach a fully reacted state. For in situ measurements, an integrated system was designed and constructed.[154] The three main components of the system were the transient plane source apparatus, a pressure vessel, and a hydrogen supply system. The pressure vessel was customized to allow thermal properties measurements during hydrogen absorption at high pressure (Figure 61).

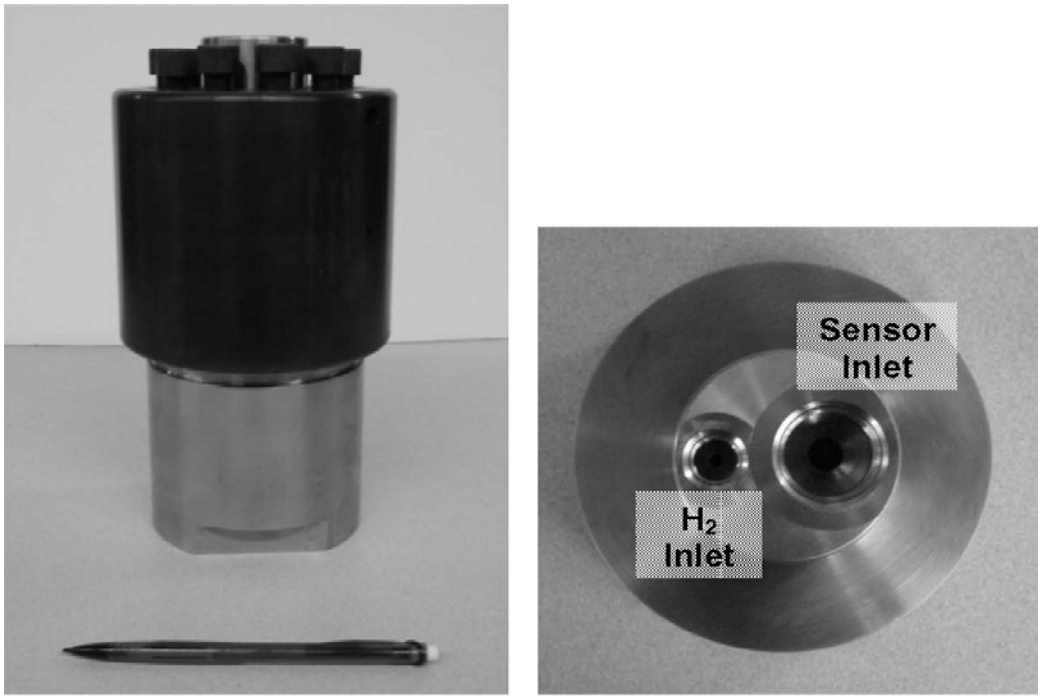

Figure 61. Customized high pressure vessel and cap.[154]

A custom sample holder TPS sample holder was designed for use in the pressure vessel (Figure 62). In an experiment, the sensor was placed in the center of the cavity in the sample holder and packed with metal hydride powder (Figure 63).

Figure 62. Custom in situ TPS sample holder.[154]

a)

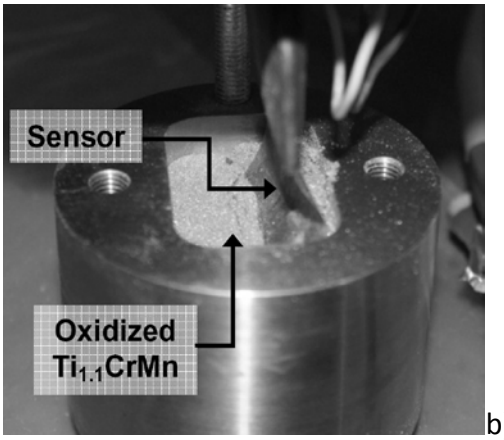

b)

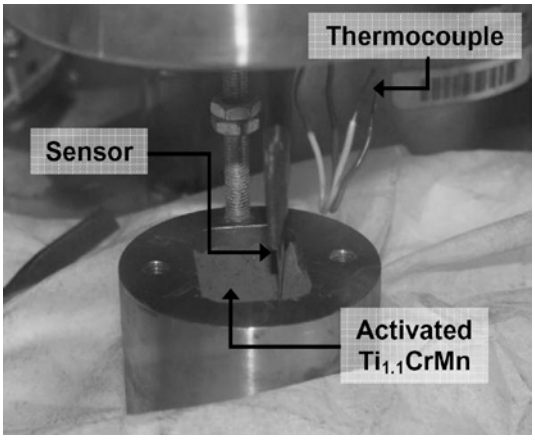

Figure 63. a) Oxidized and b) activated $Ti_{1.1}CrMn$ in custom sample holder.[154]

The pressure vessel was designed with seals that allowed the TPS sensor wires and two thermocouples to pass through the top of the vessel (Figure 64).

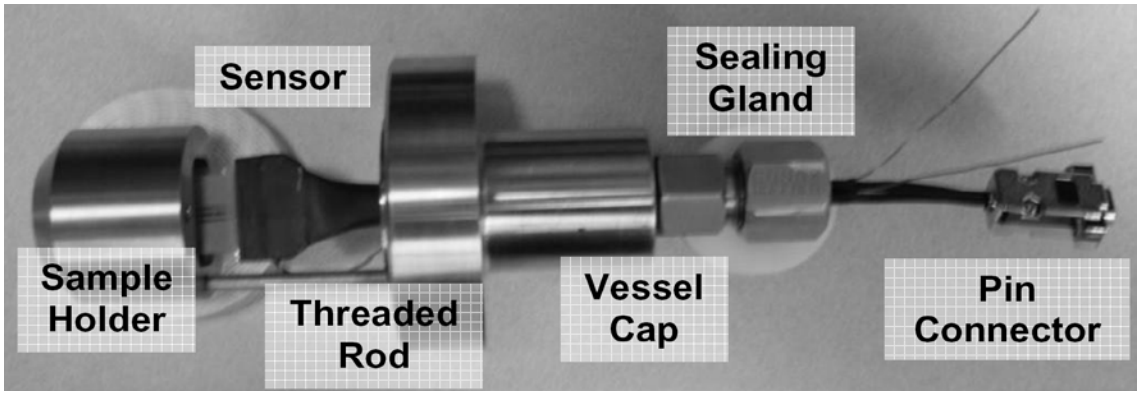

Figure 64. High pressure TPS sensor assembly.[154]

To make measurements on metal hydride using the TPS method pellets were made of the alloy and hydride. To ensure sufficient material volume for testing large diameter samples were die pressed from the powders.[154] Pellets made from pure starting powders were not mechanical stable enough for TPS testing as the experimental sensor was not in contact with a uniform surface. As a solution, polyvinylidene fluoride (PVDF) powder was used as a binding agent to overcome this problem and to compare with the previous laser flash data.

In addition to PVDF binder, oxidized pellets were also generated with aluminum powder as a binder. Aluminum powders of 3 to 5 µm diameter particles was initially added at 5 wt.% to oxidized $Ti_{1.1}CrMn$ powders. However, these were not sufficiently mechanically stable. As a result, the aluminum concentration was increased to 15 wt.% with the addition of 2 wt.% graphite powder for lubrication of the powder mixture. Despite the increase in binder, the surface quality of these pellets was still poor relative to the PVDF pellets.

The advantage of PVDF as a binder was chemical inertness, low material density of 1.78 $g \cdot cc^{-1}$, and low phase change temperature of 150°C. This temperature was important as the PVDF powder must be heated prior to compression. Above 150°C, the PVDF powder melted into the powder mixture and was then pressed and cooled to form a pellet. The thermal conductivity of PVDF is roughly 1 $W \cdot m^{-1} \cdot K^{-1}$. Thus the binder would also aid in maximizing the thermal performance of the resultant pellet. In addition, thermal enhancement powders such as graphite were added to increase the effective thermal conductivity of the mixture. Pellets of activated metal hydride prepared by compression of samples inside an inert gas glove box.[154]

Initial measurements were made on oxidized metal hydride pellet samples ex situ under and ambient air environment. These measurements would provide a baseline of thermal properties of un-hydrided material that was then compared with measurements of the same material in a hydrogen atmosphere and also during in situ hydrogen cycling.

To provide a comparison with previous laser flash data, pellets were composed of oxidized $Ti_{1.1}CrMn$, PVDF binder, and graphite thermal enhancement powders. Three metal hydride pellet sets were mixed and compacted with 5 wt.% PVDF and 9 wt.% graphite powder. Each set of pellets was analyzed five times with the TPS system to check the repeatability of the system and materials.

The averaged thermal properties and pellet porosity for each sample are listed in Table 6. The estimated uncertainty was similar to initial test measurements on stainless steel (about twice the standard deviation of the raw data). The pellet porosity was determined from the $Ti_{1.1}CrMn$ solid density of 6.2 $g \cdot cc^{-1}$. The laser flash data recorded for the same additive composition is included in the table for reference.[203]

Pellet Set	MH State	Method	k_{eff} ($W \cdot m^{-1} \cdot K^{-1}$)	α ($mm^2 \cdot s^{-1}$)	ε
1	Oxidized	TPS	6.94 ± 0.18	3.78 ± 0.47	0.09
2	Oxidized	TPS	6.29 ± 0.02	3.81 ± 0.12	0.10
3	Oxidized	TPS	6.72 ± 0.10	3.69 ± 0.20	0.08
Ref. 203	Non-activated	LFA	8.83	3.51	-

Table 6. Thermal properties of $Ti_{1.1}CrMn$ pellets (5 wt.% PVDF, 9 wt.% graphite).[154]

The TPS measurements in this work showed a good agreement between the three different pellet sets. A 10 % difference was observed between the smallest and largest k_{eff} values, and only a 3 % difference for α. However, there was a relatively large difference between the TPS and the laser flash results. While both test examined the same alloy ($Ti_{1.1}CrMn$), the physical state of the materials was different. The powder used for laser flash measurement was in a non-activated state from the supplier. In contrast, the powder used for TPS measurement had been activated and then oxidized back to an inert state.

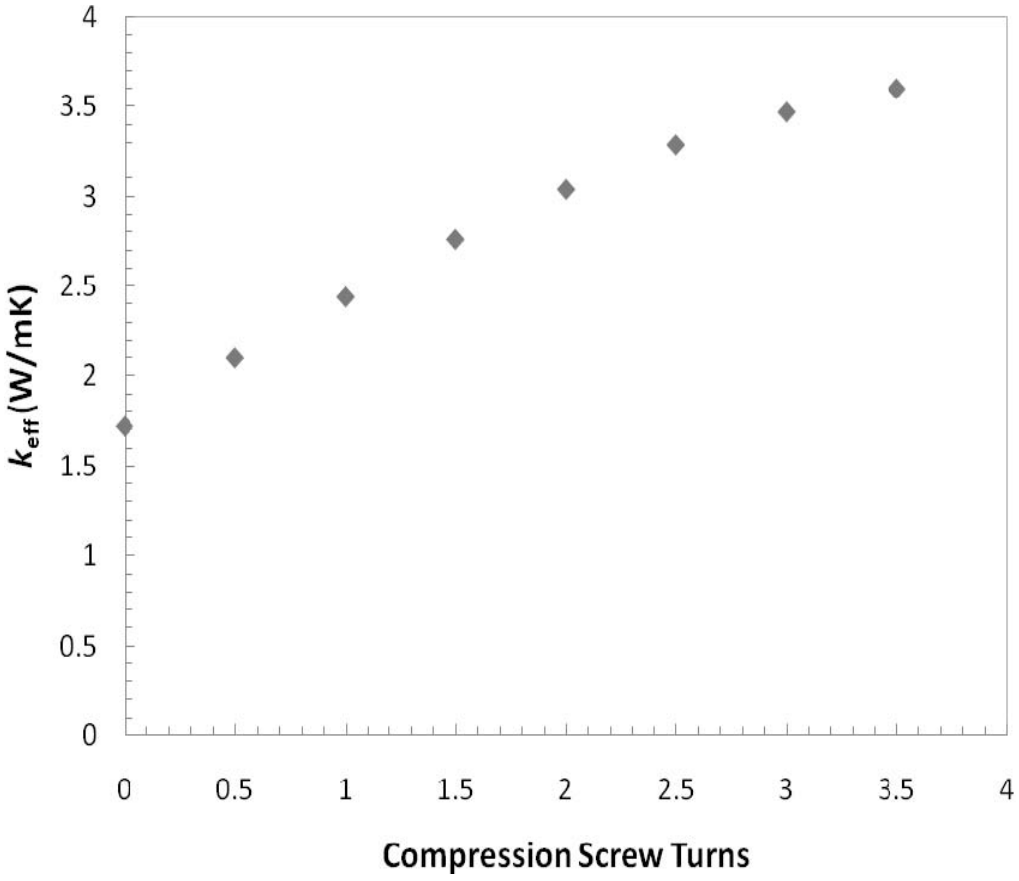

Figure 65. Effective thermal conductivity k_{eff} as a function of pellet compression.[154]

It should be noted that while the majority of the work in Flueckiger's study focused on samples prepared with the PVDF binder, some interesting observations were made for the materials compressed into pellets with aluminum powder. The TPS thermal property analysis revealed a strong dependency of k_{eff} on the compression force used in fabricating the pellets (Figure 65). As the TPS method mostly eliminates R_{tc} effects from the data analysis, this increase was probably due to structural alterations inside of the pellets with compression.

In this work, in situ measurements were first performed on oxidized $Ti_{1.1}CrMn$ powder under a hydrogen atmosphere.[154] The sample powder was packed in the custom sample holder with the TPS sensor. The applied hydrogen pressure during these experiments ranged from 0.17 to 275 bar and the sample temperature varied from 283 to 290K. At

each pressure, the uncertainty was estimated to be twice the standard deviation of the raw data. Each of these uncertainties was then averaged to yield a constant uncertainty for the entire data set. The k_{eff} data is shown in Figure 66. Also plotted is the associated ZBS model for k_{eff} with a variation in the flattening coefficient.

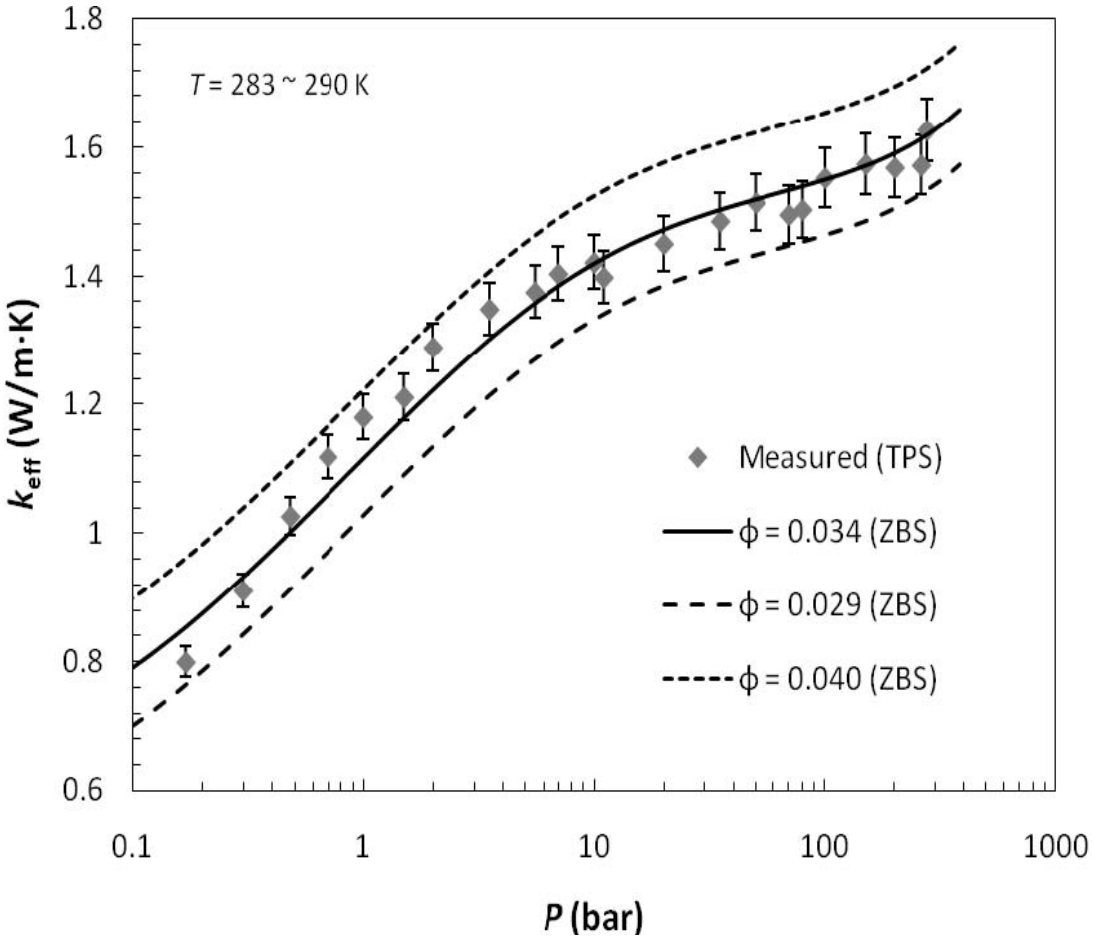

Figure 66. Effective thermal conductivity k_{eff} of oxidized $Ti_{1.1}CrMn$ as a function of hydrogen pressure.[154]

The k_{eff} of the oxidized powder varied from 0.8 to 1.6 $W \cdot m^{-1} \cdot K^{-1}$ as a function of the hydrogen gas pressure. As with the data in literature, the k_{eff} increased with gas pressure due to the increase in the thermal conductivity of hydrogen gas with pressure. The largest dependency on pressure occurred in the vacuum region below 1 bar, where the hydrogen molecules approached a rarified state in the powder mixture. After compiling experimental data, the ZBS model was fit to the k_{eff} values as a function of hydrogen pressure.

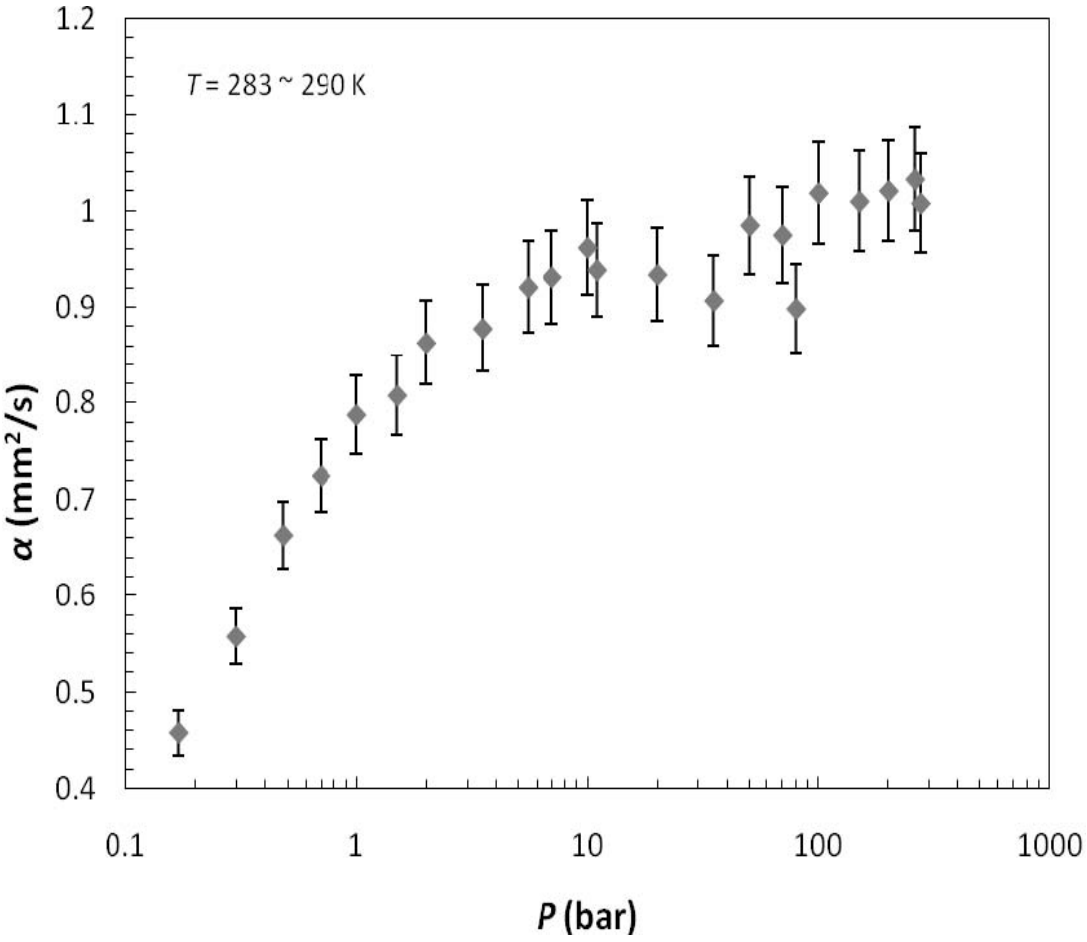

Figure 67. Thermal diffusivity α of oxidized $Ti_{1.1}CrMn$ as a function of hydrogen pressure.[154]

The experimental thermal diffusivity data for oxidized $Ti_{1.1}CrMn$ powder in a hydrogen atmosphere are given in Figure 67. As with k_{eff}, α data increased with hydrogen pressure. As diffusivity quantifies the ability of a material to conduct heat relative to the ability to store heat, the observed increase with hydrogen pressure was expected.

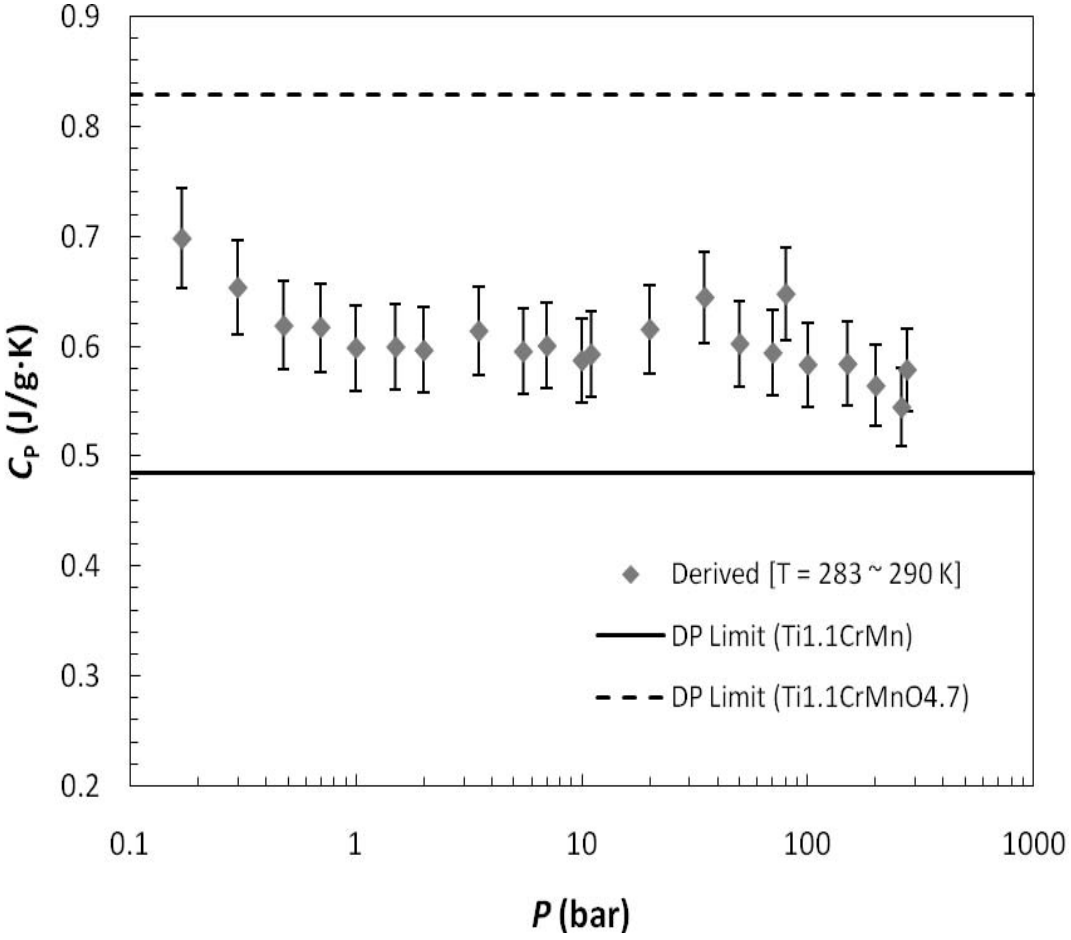

Figure 68. Heat capacity C_p of oxidized $Ti_{1.1}CrMn$ as a function of hydrogen pressure.[154]

C_p was derived with the isotropic thermal property relation from the direct measurement of k_{eff} and α of the oxidized $Ti_{1.1}CrMn$ powder (Figure 68).[154] To validate the C_p analysis, the Debye model was applied to the oxidized $Ti_{1.1}CrMn$ powder. According to the Debye model, the C_p of $Ti_{1.1}CrMn$ was 0.457 $J \cdot g^{-1} \cdot K^{-1}$ and the DP limit was 0.484 $J \cdot g^{-1} \cdot K^{-1}$. To assess the effect of oxidation on the predicted C_p, the Debye model and the DP limit were solved assuming each element had been converted to its most common oxidation state (TiO_2, Cr_2O_3, and MnO). This conversion added 4.7 mole of oxygen to every mole $Ti_{1.1}CrMn$. The model C_p increased to 0.792 $J \cdot g^{-1} \cdot K^{-1}$. The resultant DP limit increased to 0.829 $J \cdot g^{-1} \cdot K^{-1}$. The oxidized sample's C_p value falls between these two (un-oxidized and fully-oxidized) limits. If the true composition of oxidized $Ti_{1.1}CrMn$ were to be determined, the Debye model and DP limit could be further refined to more accurately predict the C_p of a given sample.

In a final series of experiment in the presented example, activated $Ti_{1.1}CrMn$ powders were examined.[154] The in situ sample holder was loaded with activated $Ti_{1.1}CrMn$ in an argon glove box and sealed. Initial TPS experiments were conducted under argon to validate the performance of the in situ equipment. After testing with argon gas, the pressure vessel was evacuated and refilled with hydrogen. TPS experiments were conducted from 2.9 to 253 bar over two separate pressurization cycles. The k_{eff} data for activated powder are shown in Figure 69 for both hydrogen cycles and the initial argon measurement. The previous oxidized sample results data were also included for comparison.

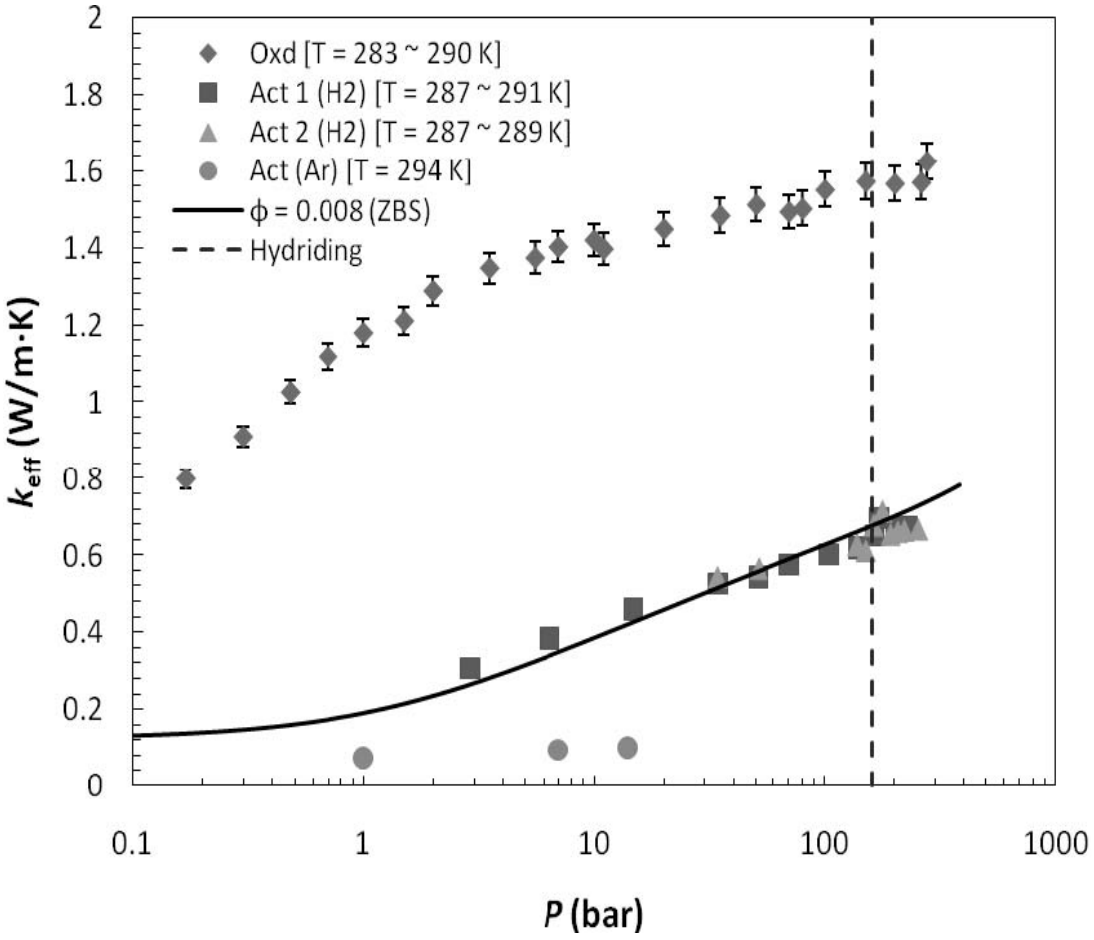

Figure 69. Effective thermal conductivity k_{eff} of activated $Ti_{1.1}CrMn$ as a function of hydrogen pressure.[154]

The k_{eff} data for the activated $Ti_{1.1}CrMn$ powder in argon was significantly less than the ex situ data, probably due to the smaller particle size and the poor thermal conductivity of argon relative to hydrogen. When the vessel was refilled with hydrogen, the k_{eff} data increased as a function of hydrogen pressure. This increase was due in part to the increase in the k value of hydrogen with pressure. However, the activated data was still less than the oxidized data; a disparity that was attributed to the smaller particle size (~2 μm) and increased bed porosity (0.7) of the activated sample.[154]

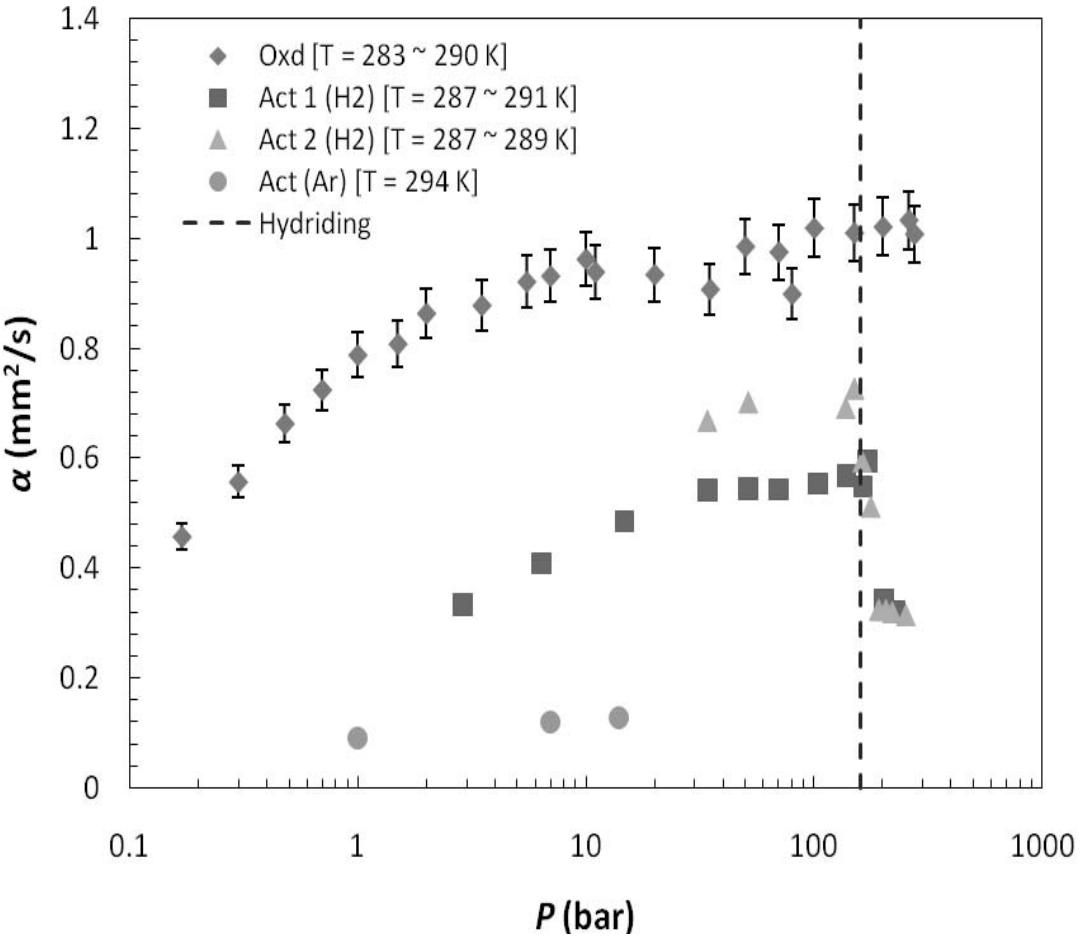

Figure 70. Thermal diffusivity α of activated $Ti_{1.1}CrMn$ as a function of hydrogen pressure.[154]

The measured α data for the activated $Ti_{1.1}CrMn$ powder is plotted in Figure 70 along with the oxidized sample data for comparison. In argon, α data for activated powder was 0.10 to 0.13 $mm^2 \cdot s^{-1}$, with a slight positive dependence on gas pressure. As with k_{eff}, these values were less than the oxidized case. Despite the disparity in α data between

activated and oxidized powder, there was a similar dependence on hydrogen pressure. Above 172 bar, α had a strong negative dependence on the hydrogen pressure, decreasing to 0.32 $mm^2 \cdot s^{-1}$ at 229 bar. This is the pressure region in which the hydride forms. At lower pressures there was also a relatively large difference in α between the first and second hydrogen cycle which was not seen in k_{eff}. This points to changes in the thermal properties of the materials with cycling, which is an important consideration for real applications that will involve hundreds of cycles.

As thermal diffusivity is a ratio of thermal conduction to thermal storage, this decrease during the absorption process implied a simultaneous increase in C_p as no absorption effects occurred in the k_{eff} results. The heat capacity C_p for activated $Ti_{1.1}CrMn$ material was derived from the k_{eff} and α data (Figure 71). Also plotted are the DP limits for $Ti_{1.1}CrMn$ and the β-phase hydride $Ti_{1.1}CrMnH_3$.

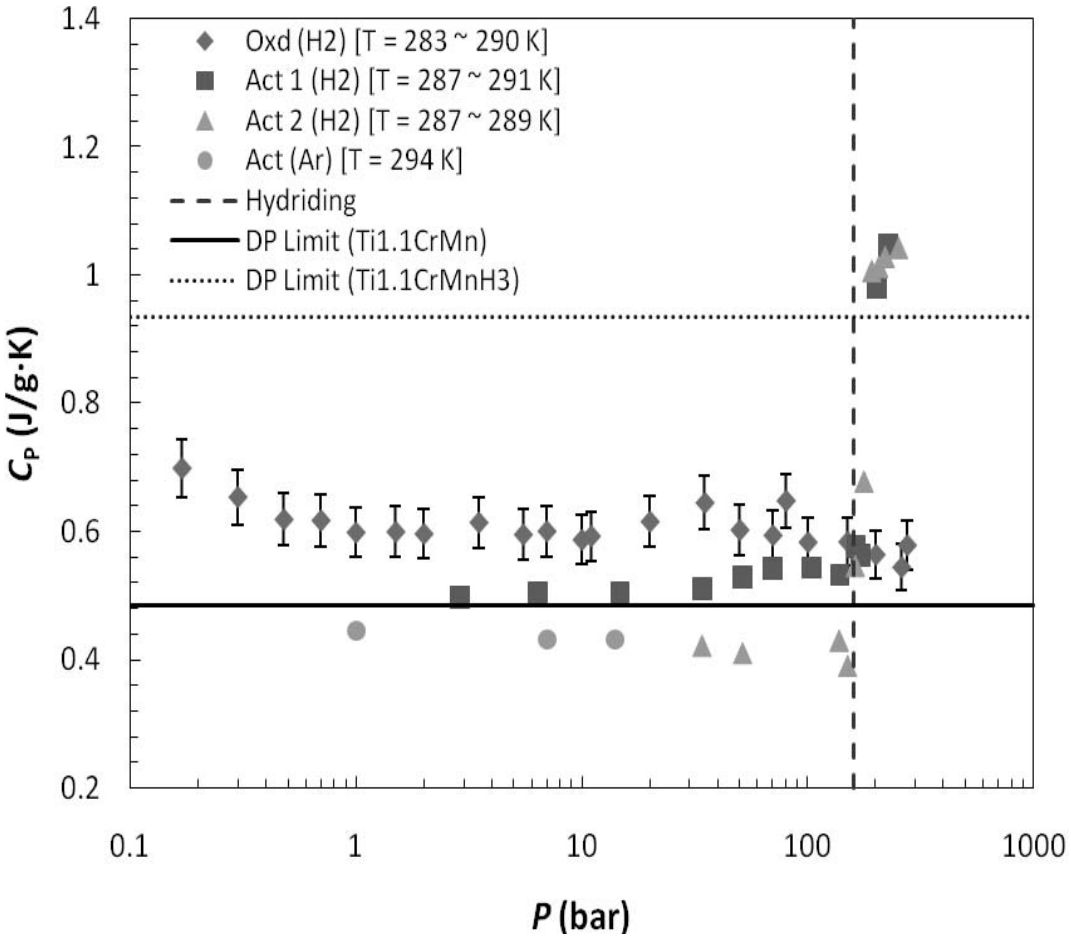

Figure 71. Heat capacity C_p of activated $Ti_{1.1}CrMn$ as a function of hydrogen pressure.[154]

Above 140 bar, the C_p increased strongly with hydrogen pressure up to 1.05 J·g^{-1}·K^{-1} at 229 bar. This was attributed to the hydrogen absorption process. The maximum C_p value was greater than that of both the Debye model (0.897 J·g^{-1}·K^{-1}) and the DP limit (0.935 J·g^{-1}·K^{-1}) for $Ti_{1.1}CrMnH_3$. This disparity implied the models were insufficient to be able to predict the C_p of $Ti_{1.1}CrMnH_3$.[154]

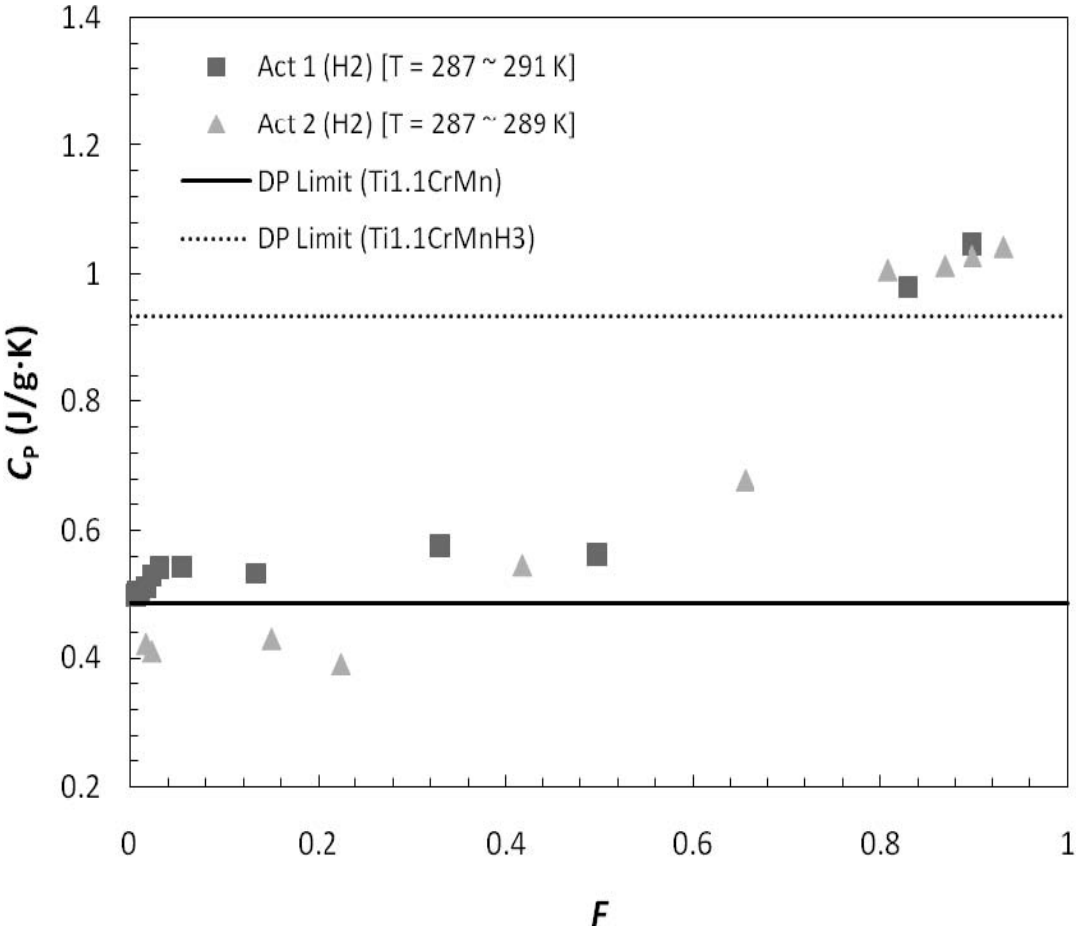

Figure 72. Heat capacity C_p of activated $Ti_{1.1}CrMn$ as a function of reacted fraction.[154]

In this work, it was observed that because C_p appeared to have a strong dependence on the absorption reaction, the experimental pressure and temperature data were converted to the reaction progress F (0=unhydrided, 1=fully hydrided). C_p data for the activated powder is plotted in Figure 72 as a function of reacted fraction along with the DP limits of both $Ti_{1.1}CrMn$ and $Ti_{1.1}CrMnH_3$. When plotted in this (phase diagram) fashion, it becomes more apparent that specific heat has a continuous transition from

the desorbed phase to the β-phase hydride. In a metal hydride hydrogen storage system, this C_p transition cannot be neglected in the design of the heat exchanger for the exothermic filling process. Clearly, for engineering analysis, more detailed in situ data on viable storage materials is needed to fully understand and accurately model such changes in thermal properties with hydrogen content, pressure, temperature, and cycling.

6.2 Thermal Conductivity of On-Board Rechargeable Physisorption Materials

With large pore sizes (e.g., >20 A° diameter) and high free volumes (e.g., > 90%)[204], the thermal conductivity of many microporous materials is low.[205,206,207,208] In fact, the atomic number density, which correlates with thermal conductivity, can be lower in MOFs (2.46 x 10^{28} atoms·m^{-3} for MOF-5) than in zeolites (5.13 x 10^{28} atoms·m^{-3} for sodalite)[209], indicates that MOFs may exhibit extremely low thermal conductivities, even compared to other microporous materials.[210,211]

This low conductivity can place limitations on the design of physisorption-based storage systems. Low thermal conductivity can have a great impact on the refueling time for adsorption processes which rely on a pressure or temperature-swing. Engineering solutions alone involve tradeoffs in efficiency or the density of stored hydrogen. For example, a heat-exchanger within the storage vessel adds volume and mass will lower the volumetric and gravimetric density of the system. Thus, the evaluation of the thermal conductivity of hydrogen physisorption storage materials and development of methods to improve thermal performance are of great importance.

Thus, many candidate hydrogen physisorption storage materials, such as MOF's and zeolites, have low thermal conductivities that are of the same order as insulating materials. For this reason, many of the techniques and issues found in experimental measurements of the thermal conductivity of insulation materials will apply as well to these hydrogen storage materials.

In addition, on-board physisorption materials will typically be operated in the range of temperatures from liquid nitrogen (77K) to room temperature (293K). The thermal conductivity of materials generally varies with temperature, particularly at cryogenic temperatures. For this reason, it is important that thermal properties measurements be made at a number of temperatures over this range.

With respect to thermal conductivity measurements of vacuum insulation materials, much effort and advances have already been achieved for measurements at low (cryogenic) temperatures. Measurements at cryogenic temperatures began in the 1950's when Fulk, Kropschot, and other researchers at the National Bureau of Standards (NBS) tested multi-layer insulation and evacuated powders.[212,213,114] Fulk et al. used

radial flow boil-off calorimeters to obtain their measurements. Most recently, J. E. Fesmire et al. have developed several measurement cryostats consisting of LN_2 boil-off calorimeters, which provide different insulation geometry and measurement methods.[214,215] Boil-off calorimetry has its limitations and does not appear to have been used for hydrogen storage materials to date. Some measurements are shown below for the thermal conductivity of Silica Aerogel powders and beads as a function of temperature (Figure 73). These measurements were done at low temperatures using cryogenic guarded hot plate, as well as, concentric cylinder methods.

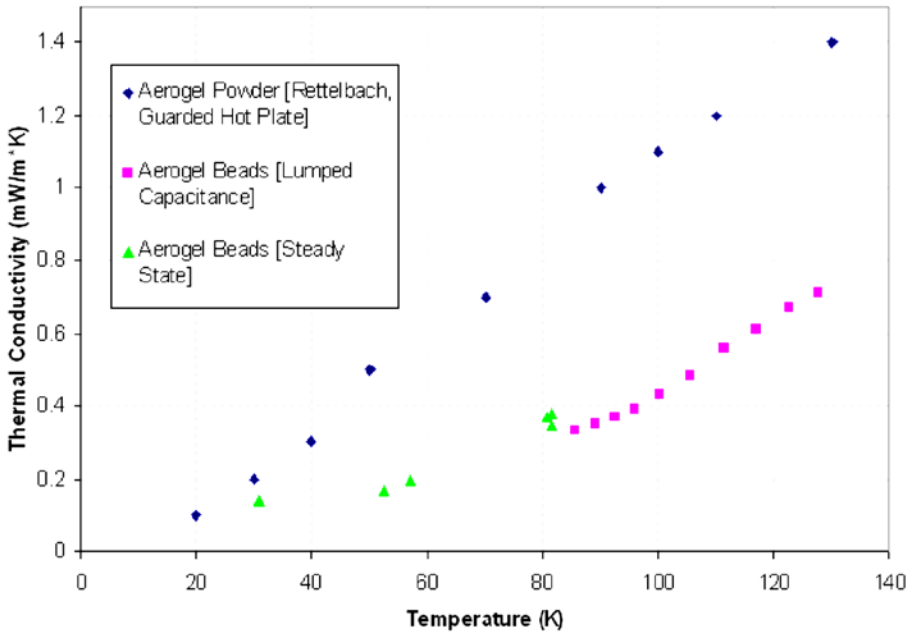

Figure 73. Effective thermal conductivity of aerogel.[216]119 Aerogel powder data from Rettelbach et al. using steady state guarded hot plate apparatus. Aerogel beads data from Barios using a concentric cylinder apparatus.

As mentioned, few thermal conductivity measurements have been conducted on materials specifically for hydrogen physisorption storage. One example of those measurements is the work by Huang et al. on MOF-5.[210] In that study, the thermal conductivity of MOF-5 single crystals was measured over a wide temperature range between 6K and 300K, using the longitudinal, steady-state heat flow method. Since MOF-5 has a cubic structure, its thermal conductivity is isotropic. Therefore, it was determined that it was only necessary to perform the measurements in one direction which is the basis of the method used. The apparatus used for the measurements and the thermal circuit diagram for the heat flow paths is shown in (
Figure 74).

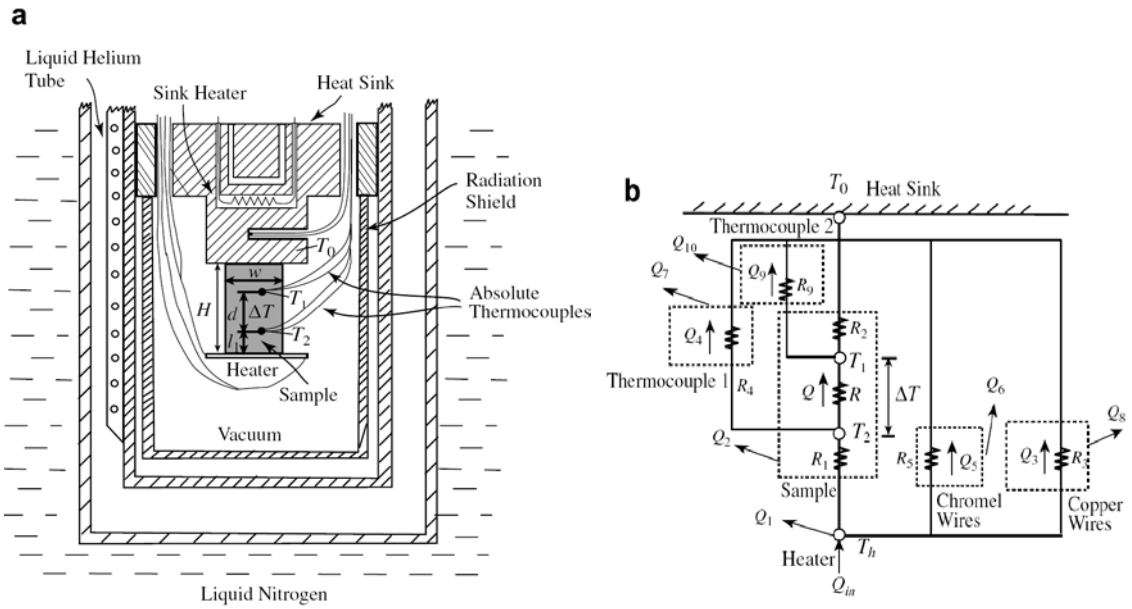

Figure 74. (a) The apparatus for the measurement of thermal conductivity. (b) The thermal circuit diagram for the heat flow path through the sample and various other paths.[210]

In preparing and making the measurements, the authors took into account the following important considerations:[210]

1) To avoid the formation of small cracks resulting from the adsorption of water vapor, the MOF-5 sample was prepared in a sealed airbag filled with a pre-purified nitrogen atmosphere.
2) As the cross-sectional area and length of the sample are critical for the determination of k, the dimensions of the sample were measured using a microscope.
3) Two fine copper-constantan thermocouples (the diameters of the copper and constantan wires are 30 lm and 10 lm, respectively) were attached to the surface of the sample, using SE4422, a fast-drying thermally conductive adhesive produced by Dow Corning. The distance d between the two thermocouple centers was also measured using a microscope.
4) The lengths of the heater and thermocouple wire leads were all 25 cm long enough to minimize the conduction loss.
5) The cryostat was then evacuated until the pressure was reduced to 10^{-7} torr to reduce heat loss to the environment.

6) The cryostat contained a radiation shield to reduce heat leak between the sample and the surrounding environment.
7) Liquid nitrogen was used to cool the sample from 300K to about 100K. Then liquid helium was used to cool the sample to 6K. It was noted that the cooling rate using liquid helium is fast and the resulting thermal stress may lead to the formation of defects within the sample, which may affect the low temperature results.
8) It was found that, at low temperatures below 100K, the liquid helium ran out before the time consuming heat loss measurement could be completed. The measurement is also challenging due to the potentially unstable outputs of thermocouples at low temperatures. The author's solution for low temperatures was to use a model to calculate the heat loss. The model also guided minimizing the error due to the heat loss.
9) The temperature readings were allowed to stabilize (5 – 10 min) at each temperature before current, voltage and temperature readings were made.

The measurements were made using a two-step process. In the first step a 1 mA DC current was input into the heater at each temperature measurement point with the sample and heater attached to the heat sink. The input current J_1, voltage $\Delta\phi_1$ and the temperature difference ΔT were recorded. In the second step, the sample together with the heater was detached from the heat sink to measure the heat loss term. The cryostat was evacuated and cooled again. Then, at the same temperature points, the input current of the heater was adjusted to raise the temperature of the sample to the same average ΔT measured in the first step and the corresponding current J_2, voltage $\Delta\varphi_2$ and the temperature difference were recorded. The thermal conductivity was calculated from:

Equation 67 $$k = (d / A \Delta T)(J_1 \Delta\phi_1 - J_2 \Delta\phi_2)$$

where A is the cross-section area perpendicular to the heat flow and d is the distance between the thermocouples mounted of the side of the sample.

The results of that study are shown in Figure 75. As the heat loss term (second term in Equation 67) could not be accurately measured below 100K, it was calculated according to a model presented in the cited publication.

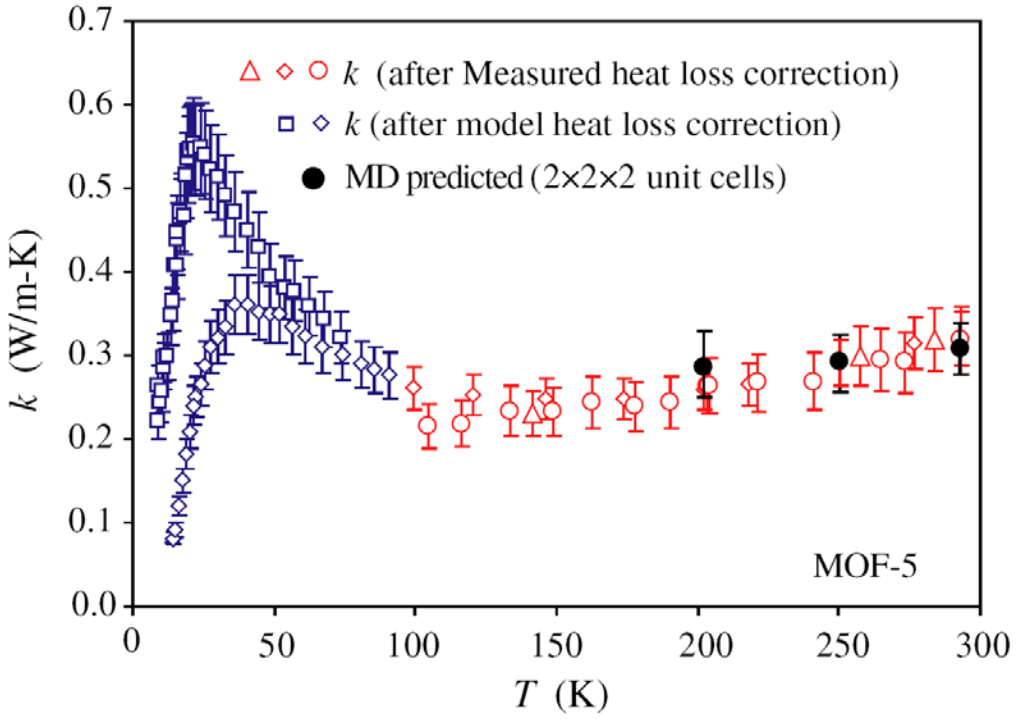

Figure 75. Variation of the MOF-5 thermal conductivity with respect to the temperature. Below 100K, the heat loss correction is made by the heat loss model. The MD predicted result of 2 x 2 x 2 unit-cell system, at 200K, 250K and 300K, are also shown.[217]

From these measurements, the authors of that study found that between 6K and 20K, the thermal conductivity increases with the increase in temperature and exhibits a peak near 20K. This peak results from the crossover between the decreasing mean free path and the increasing phonon specific heat with the increasing temperature. From 20K to 100K, the thermal conductivity decreases rapidly with increasing temperature. Above 100K, the thermal conductivity is nearly temperature independent, and its value at 300K is 0.32 $W \cdot m^{-1} \cdot K^{-1}$, a rather low value for crystals.

Besides these low temperature measurements other methods have been used to measure the thermal conductivity of physisorption hydrogen storage materials. Another example, in which measurements of density, thermal diffusivity, and heat capacity were used to calculate the heat capacity of MOF-5/ENG compacted composites is presented in section 9.2 which covers the possibility to improve thermal conductivity.

6.1 Thermal Conductivity of Off-board Regenerable Hydride Materials

6.1.1 Example: Ammonia borane

Many high-capacity compounds that contain only B, N, and H have been examined for off-board regenerable hydrogen storage. Examples include: amine boranes, boron hydride ammoniates, hydrazine-borane complexes, and ammonium octahydrotriborates or tetrahydroborates. Of these, amine boranes (and especially ammonia borane (AB: H_3BNH_3)) have been extensively investigated as hydrogen carriers.

Ammonia borane (AB) complex is a chemical hydride that is stable in air and water. It contains a large amount of hydrogen (19.6 wt.% and 2.74 $kWh \cdot L^{-1}$). AB in solid form, can readily release 13-15 wt.% hydrogen. However, because of the engineering issues surrounding the handling of solids onboard, recent research has focused on developing stable liquid fuels comprising AB in ionic liquids, or AB in liquid alkylamineboranes. The latter approach, while potentially realizing greater hydrogen capacity because of the contribution of the dehydrogenation of the liquid alkylamineborane, has run into difficulty because of catalyst deactivation. [218]

Release of hydrogen in the AB complex can occur by either thermolysis or hydrolysis. Thermolysis of AB generates, in addition to hydrogen, species such as borazine, monomeric aminoborane, and diborane. In the case of AB hydrolysis, ammonia is the secondary byproduct of the reaction.

Results have shown the liberation of 2 moles of hydrogen by thermolysis of AB complex with relatively minor expenditure of energy. Without downstream treatment, some quantities of borazine and poly-aminoborane are also generated.

Results for pyrolysis of the AB complex have shown it to be an overall exothermic process that requires induction energy to initiate AB decomposition until about 0.3 moles of H_2 is released. At this point, the reaction is self-sustaining and proceeds to completion with the additional release of 2 moles of hydrogen gas. Induction energy required to release 2 moles of H_2 is about 16.2 $kJ \cdot mol^{-1}$ of AB or 8.1 $kJ \cdot mol^{-1}$ of H_2, which corresponds to 3.35% of the chemical energy of hydrogen generated (on LHV basis). [219]

While one of the advantages of Ammonia Borane is that it is stable in air and water, a major problem for some types of measurements is that the neat material foams upon hydrogen release and also releases borazine and ammonia from side reactions. There are ways to reduce foaming and impurities by certain additives.

Because the material foams upon hydrogen release when heated, and simultaneously releases borazine and ammonia, thermal conductivity studies have generally not been made because of concerns over damaging or contaminating the measurement

instrument. In particular for thermal diffusivity, laser-flash, instrument which is considered sensitive to the above issues. For this type of equipment measurements are typically performed in air, but there is an option to flow through inert gas. The sample powder is pressed into a pellet which is sprayed with graphite and thereafter loaded into the sample holder, in air, limiting measurements to materials stable in air and not sensitive to moisture.

Thermal conductivity measurements of AB materials will be limited to equipment with a special sample cell that can accommodate for the foaming (volume expansion) and ideally trap the impurities from the side reactions to avoid instrument damage. Moreover, a sample cell that can be sealed in a glove box before transferred into the instrument would be necessary for air/moisture sensitive samples.

7 Experimental and Analysis Considerations

7.1 Form of Sample to be Measured

Note that, most thermal conductivity measurement techniques can only measure the thermal conductivity of homogeneous materials. They are not normally suitable for samples that have either discrete layers or inclusions. In the case of multi-component materials that have a homogeneous distribution of components (this could include, for instance, void spaces) the measured values will be the “effective” thermal conductivity of the whole of the sample.

Many of the above methods require solid and homogeneous samples and may not be appropriate for powder samples. This is because containing the powder within the apparatus is much more difficult than installing a solid specimen. Any mechanical supports used would create a heat leak and make material thermal conductivity much harder to calculate. Therefore, other configurations which may be more conducive to loose powders should be examined for most hydrogen storage materials (which typically consist of powders). An exception may be powders that have been pressed into compacts. However, one should consider whether the compacts in the as measured state will be representative of the hydrogen storage material after many cycles.

Another important consideration is that many of the methods and commercial instruments are designed to measure materials “ex-situ”. That is they are designed for measuring materials that are normally in an air environment, not under hydrogen. Ideally one would like to measure the thermal conductivity of hydrogen storage materials “In situ”, preferably, under different hydrogen pressures, temperatures, hydrogen contents, and after progressive cycling. This significantly narrows the field of methods that are applicable to such measurements.

7.1 Sensitivity of Samples to be Measured

Of particular concern is the reactivity of hydrogen storage materials with air and moisture. Many materials such as complex hydrides react strongly with air and moisture. Exposure to either may compromise a sample, machining any measurement results not representative of the materials as they will be used in hydrogen storage applications. This is especially true of high-surface area physisorption materials which generally take up significant amounts of water and may form some oxides on exposure to air. Even worse, exposure to air or contamination may cause some materials to become unstable and difficult or actually very dangerous to work with. For this reason, many hydrides (and sometimes physisorption materials) are typically prepared in an inert gas (Argon) atmosphere glovebox. At the same time, the measurement instruments must be capable of transferring the sample from the glove box to the instrument without air exposure before, during (and generally) after the measurements. Unfortunately, many commercial instruments are not equipped with the capabilities to handle air-less sample transfer and measurements with a high level of meticulousness or at all. In some cases (many physisorption materials), a bake-out of the sample on the measurements instrument is sufficient to remove most of the adsorbed impurities and this may be sufficient. At the other end of the spectrum, it may be necessary to install the measurement equipment in a glove box. This, however, can make the calibration, measurement, and servicing of the equipment quite cumbersome.

Note that a quick-sample transfer cannot be considered airless or reliable by any means.

7.2 Instrumentation Considerations

The various methods for precisely measuring thermal conductivity are much more complex than they may initially appear. For example, at first look the measurement of the thermal conductivity of a material by a simple hot-plate method could be made by placing a sample between two plates—one heated and the other cooled—and measuring the electrical power required to attain a steady-state temperature gradient across the sample. For such a simplified measurement device, large errors will arise due to the power that goes into the heater producing heat that does go exclusively into the sample but also into the surroundings. In addition, the sample will most likely not necessarily experience one-dimensional heat flow. This is especially true for very low conductivity samples, where insulation around the sample in the measurement instrument could have thermal conductivity comparable to that of the sample. Furthermore, the inhomogeneity and defects in the geometry and measurements of the

dimensions of the sample can also lead to significant errors. To tackle the foregoing issues of stray heat flow and heat flow direction, modern instruments have been developed with temperature-controlled "guards" to surround end plates and sample assembly to block the flow of heat in directions other than into the sample and to insure that the flow of heat through the sample is essentially one-dimensional. Even with considerable care, this "guarded hot plate" approach is still imperfect and requires theoretical, and often experimental, corrections for imperfections in design. This is especially true for measurements on low thermal conductivity insulators.

Measurement standards have been developed by ASTM, ISO, DIN and other societies to help ensure the most accurate measurements. As an example, the Guarded Hot-Plate methods can be used to further illustration some issues addressed by the standard in obtaining the most accurate thermal conductivity measurement results. There are two general types of guarded hot plate techniques. The first type, represented by ASTM C177-04[220] and ISO 8302:1991[221], is an absolute method where the apparatus is constructed in such a way that thermal conductivity may be directly obtained from measurement of electrical power, temperatures, and sample dimensions. The other type, represented by ASTM C518-04[222] and ISO 8301:1991[223], incorporates one or more heat flux meters in the stack of plates calibrated against standard samples whose conductivity was previously measured using the absolute approach.

These four standards have many features in common.[224] They all rely on a meter plate surrounded by a guard plate —both of which are electrically heated and set to the same temperature. Additionally, a gap separates the two plates. In two-sided designs, matched sample plates are placed on each side of the meter- and guard-plates. In the single-sided design, the sample is only placed against one side of the meter- and guard-plates. An insulating material and another heated guard are used in place of the second specimen. The size of the plates is envisioned to be 0.1 to 1 m diameter or square, with the smaller size being more appropriate for isotropic samples. A "similarly constructed" chill plate is placed on the far side of the sample or samples. The stack of heater-, sample-, and chilled plates may be oriented vertically or horizontally. The heated- and chilled-plates are preferably constructed from a high thermal conductivity metal, with electrical heaters arranged so as to insure that the plates are isothermal to within ± 0.1K. The temperatures of the plates may be measured using two or more thermocouples or other temperature sensors. The simplest approach uses fine thermocouples to measure the temperatures of the plates, which are assumed to be the temperatures on each side of the sample. However, this approach assumes that there is essentially zero contact resistance between the sample and the plates. The standards permit using compliant spacers between the sample and the plates to minimize contact resistance or, if the sample itself is compliant, a small amount of sample compression. For samples so compliant that they would crush under the load of the clamping force holding the stack together, spacers are allowed to prevent crushing. The standards call for treating the surface of the heated and cooled plates so as to give them high

emissivity. This would ensure that a fraction of the available heat flux is available as radiation, in addition to the heat transfer by conduction. The standards also call for cylindrical guards—with axial gradient preferably matching the gradient of the stack—surrounding the entire assembly. Because the entire apparatus must achieve near-perfect thermal equilibrium, the standards note that hours or even days may be required to achieve thermal equilibrium.

The standards stress three major points. First, great care must be taken to mathematically and experimentally correct for imperfections in design, including the effect of the gap between the meter plate and the guard plate and "edge heat flows at the periphery of the sample". Second, no one design is appropriate for every situation; every design must be considered on a case-by-case basis. Finally, the standards are not intended to be restrictive; research into new approaches is encouraged.

7.3 Temperature Measurements

Thermocouples are generally used to measure temperatures in analytical equipment for thermal conductivity and heat capacity measurements. There are important considerations in making accurate temperature measurements with thermocouples. These considerations concern both the thermocouples themselves and the electronic devices that convert voltages to temperature. With regard to the thermocouples it is generally advised to use isolated thermocouples. Typically, these are very thin thermocouples surrounded by an electrically insulating material encased in a thin protective sheath. This accomplishes two goals. The first is to avoid chemical interaction of the thermocouple sensor metals with the material being measured. The second is to avoid spurious voltage interactions from influencing the very small (millivolt) potential bringing produced and measured by the thermocouple. For Hydrogen storage materials measurements, sheaths made of 316L stainless steel are recommended for their inert behavior and resistance to hydrogen embrittlement degradation.

It is likewise important that the measurement equipment is well grounded to avoid potential noise and significant measurement error. Thermocouple leads can develop significant potential differences through charge build-up. This floating potential can come from the surrounding equipment or from the amplifier/multiplexer circuit itself. Part of the solution is to ground the negative thermocouple allowing static charge to discharge to ground. This preserves the common mode voltage at zero. This will typically be done in the analog measurement equipment used for converting thermocouple potential to temperature measurements. A second source of noise and error can come from ungrounded measurement and heating devices in the equipment. The solution is proper grounding of both the Amplifier/Multiplexer Circuit, as well as the sample, heater, and all components of the experimental equipment.

Heat transport by the thermocouple itself is a serious consideration. It is important that the thermocouple sheath is in good thermal contact with the sample or measurement device (either by soldering or a good pressure contact). However, Ideally thermocouple should not conduct heat away from the point of measurement. In reality this is not possible since some heat conduction invariably occurs in the thermocouple, thus wicking the heat away and cooling or heating the measurement site. This problem is compounded by low thermal conductivity (high resistivity) materials. For example, if a high conductivity 30 gauge thermocouple wire (type T) is used to measure plastic, the error can be as high as 40% of the difference between the ambient and the actual sample temperature. The following are some recommendations for reducing temperature measurement errors:

- Wire thermocouples should be no larger than 30 gauge, preferably, 36 gauge. Mineral insulated stainless steel sheathed thermocouples can typically be ordered with sheath diameters as small as 0.01 inches. Naturally, there is a trade-off between the reduced diameter and durability of the thermocouples. For applications where the thermocouple itself will be repetitively repositioned within or against the sample, it may be necessary to use more robust, larger diameter thermocouples. Insulated stainless steel thin shim style thermocouples may also be available.

- Type K offers the lowest wire-conductivity and thus the lowest conduction error and is applicable for most measurements near (-50°C) ambient and elevated temperatures (+500°C). However, type K thermocouple become significantly non-linear with a low potential to temperature ratio at cryogenic temperatures (specifically just above 77K). For cryogenic measurements, type N thermocouples are recommended. Note that most commercial thermocouples can be purchased in varying grades. Because of the sensitivity of these thermal measurements it is highly recommended that the most accurate grade of thermocouple be used for such analytical measurement applications.

- Laminated thin-foil type thermocouples are better for temperature measurements of surfaces of low conductivity materials and wire thermocouples should ideally be limited to measurement of metal and highly conductive surfaces. However, electrical and chemical isolation generally make the use of encased thin wire thermocouples the only practical option.

- Note that contrary to sample measurements; more massive thermocouples are desirable for measurement of bulk air gas temperatures where the averaging effect of the thermal mass can stabilize unwanted fluctuations.

- Infrared temperature sensors are used effectively in certain applications for measuring non-conductive surface temperatures. Such devices are particularly

useful when non-contact temperature measurements are required, such as in the Flash Diffusivity method. However, measurements are an average over the optical surface rather than a contact point measurement and the surface being measured must have a free optical path to the sensor.

7.1 Guarded Hot Plate - Sources of Potential Error

The Guarded Hot Plate method is an absolute method of measurement. It requires: the establishment of steady-state conditions, and the following measurements:

- measurement of the unidirectional heat flux in the metered region,
- measurement of the temperatures of the hot and cold surfaces,
- measurement of the thickness of the sample(s), and
- measurement of any other parameter which may affect the unidirectional heat flux through the metered area of the specimen.

We introduce here Figure 14 again to discuss potential sources of error in the guarded hot plate type instruments. Typically, in more advanced systems the heat metering section of the hot plate is surrounded on all lateral sides by a guard heater sections and possibly additional auxiliary heaters on the opposite side of each sample. In the single sided configuration, the heat flow is passing through a single sample and the back of the main heater acts as a guard plane creating an adiabatic environment. This can also be done by replacing the second sample in a double-sided instrument with a known insulating material. A diagram showing a single sided mode in an advanced double-sided Guarded Hot Plate configured with metered heating section is shown in Figure 76a.[116] Figure 76b illustrates heat flow at the gaps at the edge of the metered heating section. Figure 76c shows a diagram of an advanced system with a heater in the guard plate adjacent to the metering heater section, and Figure 76d provides the temperature profile for double- and single-sided mode of operation of the apparatus in c. The actual designs of guarded hot plates may differ markedly from the schematic design shown in the figure. This basic design was selected to illustrate the differences in temperature profiles that can arise when equipment designed for operation in a double-sided mode is used in a single-sided mode. Designs of actual guarded hot plates should be reviewed using this example as a guide to assess what problems they may have in either mode of operation.

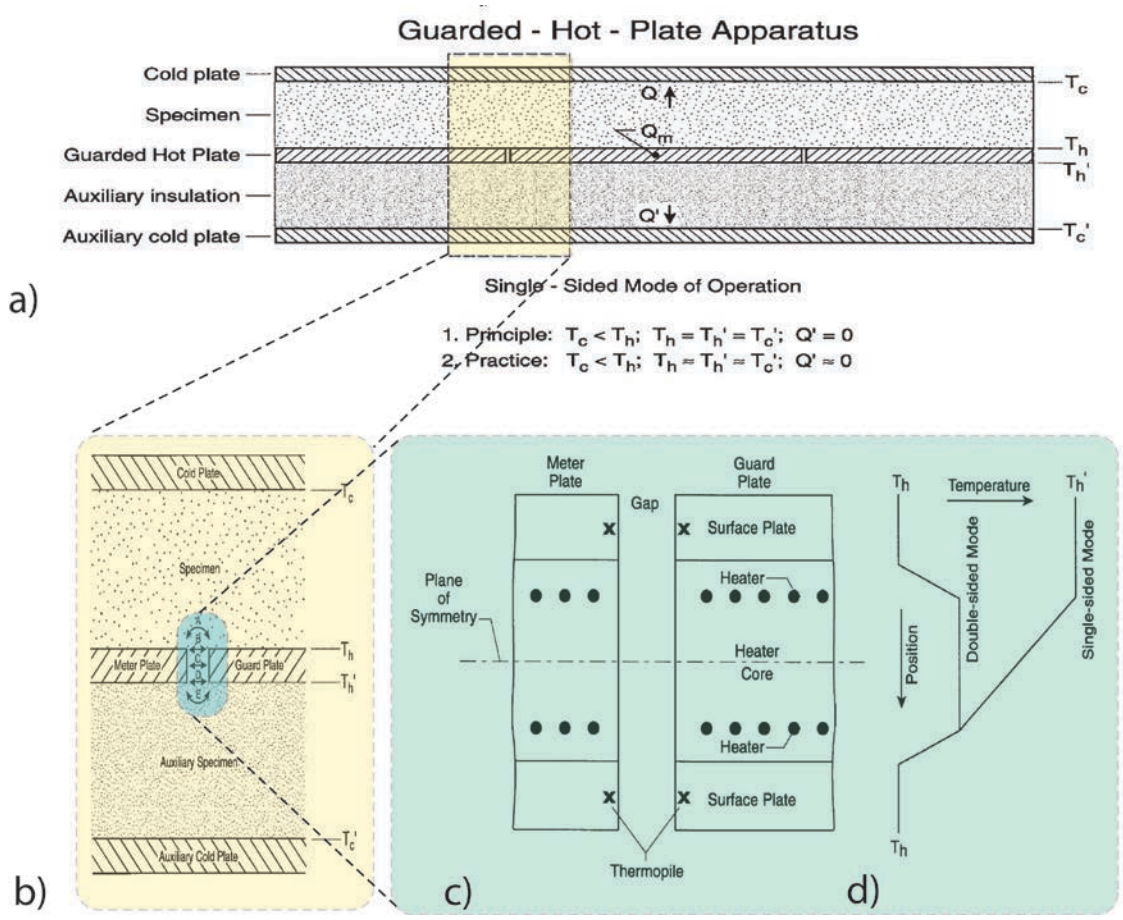

Figure 76. a) Schematic diagram of an advanced single-sided mode of operation Guarded-Hot-Plate apparatus, b) Diagram illustrating heat flows at gap region, c) Diagram of (hypothetical) Guarded-Hot-Plate with distributed heat source, and d) Corresponding temperature profile for double- and single-sided mode of operation.[116]

In the case of double-sided Guarded-Hot-Plate operated in single sided mode the samples effective thermal conductivity can be determined as follows, where

A = meter area of hot plate [m^2],
Q = heat flow through meter section of test sample [W],
C = thermal conductance of specimen [$W \cdot m^{-2} \cdot K^{-1}$],
R = thermal resistance of specimen [$m^2 \cdot K \cdot W^{-1}$],
k = thermal conductivity of specimen [$W \cdot m^{-1} \cdot K^{-1}$]
r = thermal resistivity of specimen [$m \cdot K \cdot W^{-1}$]
L = specimen thickness [m],
T_c = surface temperature of cold plate [K],

T_h = surface temperature of hot plate in contact with the sample [K], and the primes indicate values for the auxiliary insulation side of the measurement apparatus.

The heat flow through the specimen is given by

Equation 68 $$Q = Q_m - Q'$$

where Q is the heat flow through meter section of specimen, Q_m is the measured power input to meter plate and Q' is the heat flow through meter section of auxiliary insulation.

Q' is determined from the known thermal conductance C' of the auxiliary insulation material and the measured temperature gradient across the insulation according to

Equation 69 $$Q' = C' A (T'_h - T'_c)$$

where: C' is the know thermal conductance of the auxiliary insulation at a temperature corresponding to $(T'_h - T'_c)/2$. Both Q_m and Q' should be measured and determined in accordance with ASTM C 177.

Thus having determined Q, the thermal properties of the sample are given by

Equation 70 $$k = (LQ) / A (T_h - T_c)$$

Errors in the determination of Q (and thus k), can be introduced from several sources. These include:

- errors in measurement of the power input Q_m to the meter plate
- estimation of the heat flow, Q', through the auxiliary insulation,
- errors in measuring the thickness of the sample,
- errors in measuring the area of the metered hot plate, and
- for guarded hot plates, estimation of the heat flow across the gap between the meter and guard plates (gap error).

If possible, the terms, Q_m and Q' should be different by at least two orders of magnitude (the known conductance of the auxiliary insulation should be much smaller than that of the sample). This ensures that a large uncertainty in Q' will result in a small uncertainty in Q. For example, if the ratio Q_m/Q' is 100 and suppose that the error $\Delta Q'/Q'$ is 10%. The percentage uncertainty in Q due to $\Delta Q'$ would be 0.1 %.

Error may also occur due to undesired heat flows across the gap when a guarded-hot-plate apparatus designed for operation in a double-sided mode is used in a single-sided mode. Most guarded hot plates are constructed with a distributed heat source and surface plates of metal on either side of the heater core. When operated in a double-sided mode, the symmetrical construction will result in the surfaces on either side of the meter plate attaining nearly the same temperature. However, when operated in a single-sided mode, the temperature of the side of the meter plate that contacts the auxiliary insulation may be significantly hotter than the side that contacts the test specimen. Figure 76b illustrates heat flows in the region of the gap when temperature differences are present. Path A represents heat flow through the region of the test specimen that is in close proximity to the gap. Path E represents heat flow through the auxiliary specimen. Paths B, C, and D correspond to heat flows across portions of the gap on the test specimen side, in the center, and on the auxiliary specimen side, respectively. The critical requirement for eliminating heat flow across the gap is the proper design of the guarded hot plate and installation of the temperature sensors, such that the net heat flow between the meter and guard plates, integrated over all paths, be zero when the measured temperature difference is actually zero.

To illustrate, Figure 73c shows the cross section, near the gap, of a guarded hot plate designed for double-sided mode of operation. The meter and guard plates are identical in construction having a symmetrical heater core with (wire or ribbon) heaters electrically insulated from metal surface plates. The two heaters are assumed part of a single winding and cannot be operated separately. The thermopile used to control the temperature of the guard plate, relative to the temperature of the meter plate, has its junctions located in the surface plates.

The first temperature profile shown in Figure 76d is for the variation in spatially averaged temperature through the guarded hot plate when it is operated in the double-sided mode with identical heat fluxes on each side. The surface plates of metal have a high thermal conductivity and are presumed isothermal. The temperature gradient across the electrical insulating layer between each heater and the corresponding surface plate is due to the heat flow from that heater into the test sample in contact with the surface plate. The region between the heaters, on average, is isothermal since the net heat flow in or out of the region is zero. The temperature drop across each insulating layer, ideally, is proportional to the temperature drop across the test specimen times the ratio of the thermal conductance of the specimen to the insulating layer. If the insulating layer is thin and has a relatively high thermal conductivity, the temperature drop across each insulating layer will be a very small fraction of the temperature drop across the test specimen. If the heat flux to the guard heater is the same as that to the meter heater, that is, there are no significant heat losses from the outer edge of the guard plate, the temperature in the heater core region will be essentially the same for the guard plate as it is for the meter plate. In such a case, controlling the power input to

the guard plate so that the gap thermopile gives a null output, not only will result in the temperatures of the surface plates being identical but also will result in a temperature balance between the meter and guard plates reducing errors significantly.

When operated in a single-sided mode, half of the heat flow through the test specimen comes from the heater on the front side of the guarded hot plate, half from the backside heater. The second temperature profile in Figure 76d illustrates the variation in spatially averaged temperature through the guarded hot plate when operated in the single-sided mode with the same heat flux through the test specimen as above. The temperature drop across the insulating layer on the front side is the same as it was in the double-sided mode, since the total heat flow through that layer is the same in each case. However, the heat flow from the heater on the backside of the hot plate must pass through the heater core region, resulting in a significant temperature drop. In some guarded hot plate designs, the heater core is thick enough, and its thermal conductivity low enough, that the temperature drop across the guarded hot plate (T_h' - T_h) is a significant fraction of the temperature drop across the test sample. In such cases controlling the guard heater so that the thermopile produces a zero output may not ensure that there is a temperature balance between the meter and guard plates. If it does not, significant errors may occur in the determination of the heat flow through the test sample due to extraneous heat flows across the gap, across the portions of the test specimen, or the auxiliary specimen in the proximity of the gap.

The guarded hot plate method, although very effective for many practical tests on insulating materials, is difficult to apply to powders. This is because containing the powder within the apparatus is much more difficult than installing a solid specimen. Any mechanical supports used would create a heat leak and make material thermal conductivity much harder to calculate. Therefore, other configurations which may be more conducive to loose powders should be examined for most hydrogen storage materials (which typically consist of powders). An exception may be powders that have been pressed into compacts. However, one should consider whether the compacts in the as measured state will be representative of the hydrogen storage material after many cycles.

7.2 Flash Method - Sources of Potential Error

The basic principle of the Flash Diffusivity instrument is based on applying a heat source of energy to one side of the material and the instrument measures the speed of heat transfer through the material using a set of thermocouples. In a typical instrumental setup, a reference material is required for calibration which is measured concurrently to the test sample. Typically, the reference material is selected based on thermal properties which are presumed to be similar with the material being tested. The nature of the Flash Diffusivity measurement method may introduce some of the following errors.

1) First, the energy applied is a nearly instantaneous pulse of light that applies heat to the sample. This light needs to be applied perpendicularly through the sample. Therefore, it is important that the test sample has flat and parallel surfaces to ensure the heat path is evenly applied through the sample.
2) Second, the surface that receives the heat input should be prepared in a manner that allows for adsorption of the heat rather than a reflective surface.
3) Third, the method assumes the sample is in an ideal adiabatic condition.
4) Finally, the reference material selection is important to ensure the accuracy and resolution of the measurement.
5) Also, certain materials may change their properties based on air or humidity exposure. Therefore, the materials should be limited in their exposure to air by using inert measurement and transfer environments.
6) It is clear that the thermal properties will change based on the measurement temperatures. Therefore, thermal conditioning and stability is a critical parameter to these measurements.

Note that to derive thermal conductivity from diffusivity measurements one must also determine the bulk density and thermal conductivity of the sample. Each of these has their own sources of potential error. Those for the density measurements are outlined in the following section. The potential sources of error in making thermal conductivity measurements (based on DSC) are outlined in the subsequent section on Thermal Conductivity measurements.

7.1 Density Measurements - Sources of Potential Error

Note that in using diffusivity measurements to determine thermal conductivity, one must also measure the density and heat capacity of the material. The error associated with the density measurement mainly come from the measurement of the sample volume. The following are some important considerations for the density measurements:

1) Based on the structure and density of a hydrogen storage material, the handling and accuracy of the overall sample volume can be difficult.
2) It is important that the sample dimensions are taken without crushing or alternating the state of the sample since this will affect the density measurement.
3) The sample should be in the state in which the thermal conductivity analysis will be performed. In-other-words, in the completely hydrogen charged state,

desorbed state, or somewhere in between. This is because in the case of hydrides and to some extent certain physisorption materials (e.g. some MOFs) the volume of the material will increase when loaded with hydrogen. Some alloys have up to 40% lattice volume expansion on forming a hydride.

4) In the same vein, to accurately represent the materials in its "as used" state, it should probably be cycled with hydrogen many times until the material has reached a steady state storage performance and morphology. This will also be true of compacts that may experience mechanical degradation on cycling.

5) Again, the effects of air or humidity exposure on certain hydrogen storage material should be limited to avoid inaccuracy with the physical measurements which could change the density values.

7.2 Alternate Methods, Reproducibility, and Error Analysis

Differential scanning calorimetry has been used to determine both specific heats and effective thermal conductivities of metal hydride powders. Three intermetallics, $LaNi_{4.8}Sn_{0.2}$, $LmNi_{4.9}Sn_{0.1}$ and $MmNi_{4.7}Al_{0.3}$ for use in a thermal hydrogen compressor were examined in a study by Dehouche et al.[225] Knowledge of the thermal properties of metal hydride alloys are as important the design of metal hydrides hydrogen thermal compression systems as hydrogen storage systems. The specific heat c_p, determines how much the material temperature will increase (dT) with the introduction of a quantity of heat (dQ):

Equation 71 $$dQ = c_p\, dT$$

Thus, the specific heat of the metal hydride material has a significant impact on selecting the heating power needed to change the temperature of a porous bed. The effective thermal conductivity k controls heat transfer through the porous material. Low thermal conductivities cause slow hydrogen response times and less steady hydrogen flow rates for a given amount of power provided to the system. Obtaining high effective thermal conductivities is essential for effective control of hydride thermal compressors.

For specific heat measurements, Dehouche et al. used a differential scanning calorimeter (DSC). The analysis required three measurements: 1) a baseline run with no sample, 2) a reference run with a standard sample (e.g. sapphire), and 3) the sample run. A qualitative assessment of the final measurement can be made by observing that the only difference between the baseline run and the reference/sample runs should be the absence or presence of the reference/sample. An example of the data is shown in Figure 77.

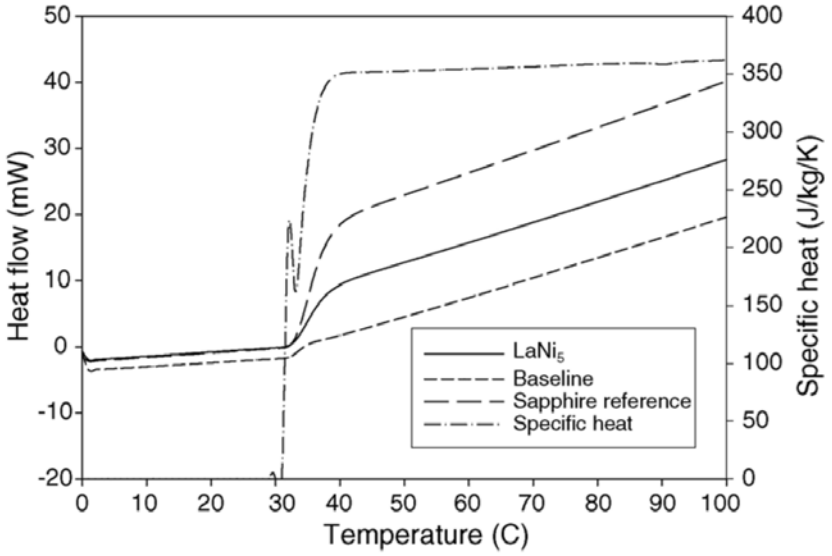

Figure 77. DSC plots of specific heat calculation.[225]

For metal hydrides of high density and specific heat, several hundred milligram samples may be needed. The specific heat of the sample is given by:

Equation 72 $$c_p = E\, P_X / m_X H_R$$

where m_X is the sample mass, H_R the heating rate, P_x the energy per unit time flowing into the sample, and E a unit-less calibration constant. P_x is found from the difference between the baseline curve and the sample curve. The calibration constant can be found by rearranging Equation 72 and inserting known values for the reference material:

Equation 73 $$E = c_p\, m_s H_R / P_S$$

where P_S is found using the difference between the reference curve and the baseline curve. These two equations can be simplified by the substitution of E such that:

Equation 74 $$c_{px} = c_{ps}\, (m_S P_X / m_X P_S)$$

An example of their measurement results is shown below for three different measurements of $LaNi_{4.8}Sn_{0.2}$. The three runs were made to ensure reproducibility, which is standard best practices. In this case the three measurements were within 2% of each other.

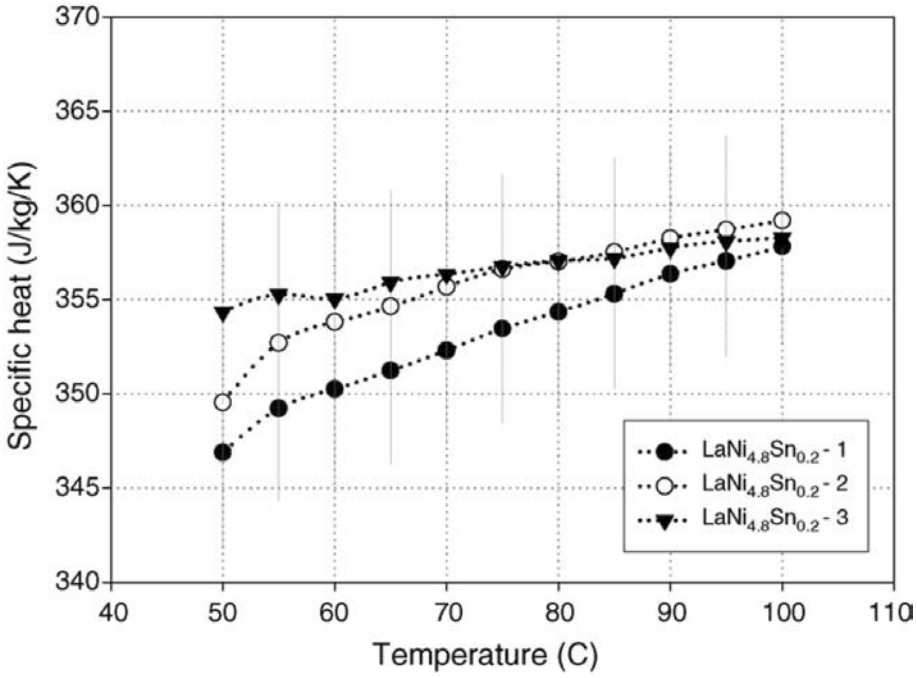

Figure 78. $LaNi_{4.8}Sn_{0.2}$ specific heat vs. temperature.[225]

While there were no other published values for these alloys, the results compared favorably to measurements of $LaNi_5$ of 355 $J \cdot kg^{-1} \cdot K^{-1}$ at 250K.[226]

In addition, an error analysis was performed using the method of total derivatives where for a function $F(x_1, x_2, x_3, ..., x_n)$ of n measured parameters $x_1, x_2, x_3, ..., x_n$, the error dF is given by:

Equation 75

$$dF = \sqrt{\sum_{i=1}^{n} \left(\frac{\partial F}{\partial x_i} dx_i \right)^2}$$

Thus, from Equation 74 the error in the specific heat measurement is:

Equation 76

$$dC_{P_x} = \sqrt{\left(\frac{m_s P_x}{m_x P_s} dC_{P_s} \right)^2 + \left(\frac{C_P P_x}{m_x P_s} dm_s \right)^2 + \left(C_P \frac{m_s P_x}{m_x P_s^2} dP_s \right)^2 + \left(C_P \frac{m_s P_x}{m_x^2 P_s} dm_x \right)^2 + \left(\frac{C_P m_s}{m_x P_s} dP_x \right)^2}$$

The authors of the study determined the average precision of specific heat measurements to be ±1.4%.

In the same study, the authors used a modification of DSC measurements to evaluate the thermal conductivities of the same materials as a function of powder compaction. Samples of activated powder were prepared either as compacted cylindrical pellets or

by completely filling the DSC pan. A standard with a sharp melting point was chosen (indium) and placed on top of the metal hydride sample such (Figure 79).

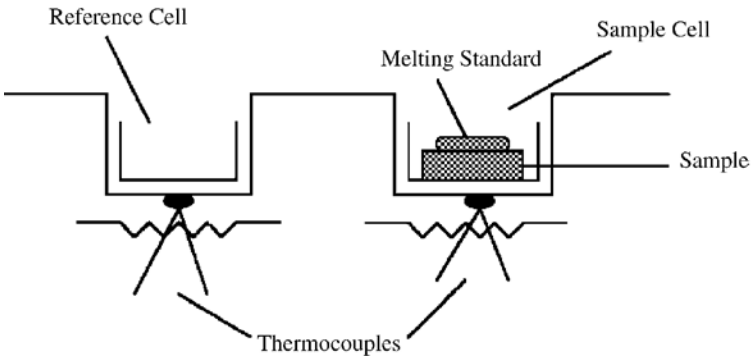

Figure 79. Sample arrangement for measuring thermal conductivity in a standard DSC unit.[225]

The DSC was heated at a constant rate to a temperature above the melting point of the standard. The measurement of the melting of the standard is influenced by the thermal conductivity of the sample such that the rate of melting of the standard is higher for samples of higher thermal conductivity. The result is that the slope of the melting curve is proportional to the thermal conductivity of the sample, as shown in Figure 80.

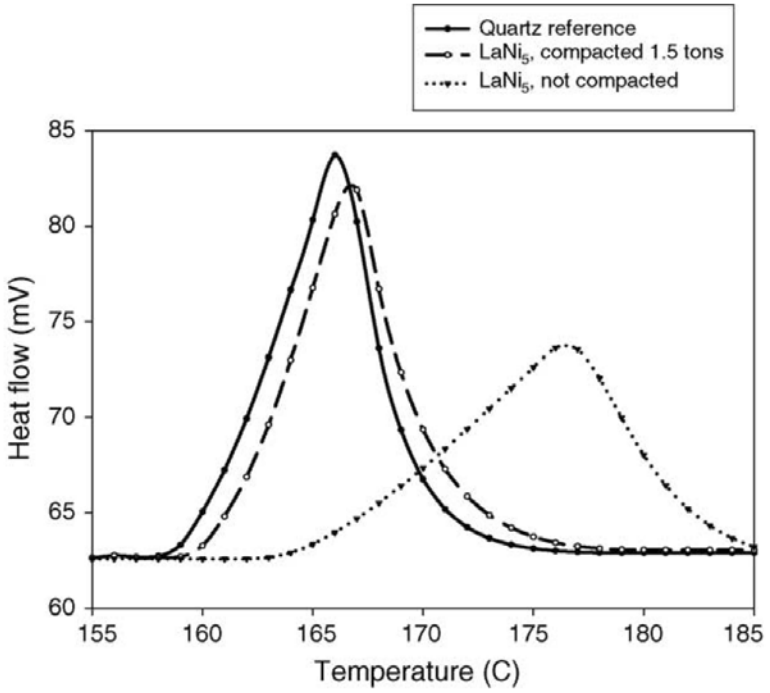

Figure 80. DSC melting curve slope variations with materials thermal conductivity.[225]

The thermal conductivity k is given for the sample x and a standard s (quartz), respectively, by

Equation 77 $$k_X = \bar{Q}_X D_X / A_X \Delta T_X \quad \text{and} \quad k_S = \bar{Q}_S D_S / A_S \Delta T_S$$

where A is the cross section area, $\bar{Q}$ is the energy input to the sample per unit time, D is the material thickness, and ΔT is the temperature difference between the thickness D. Knowing the values for the standard, this can be solved for the thermal conductivity of the sample:

Equation 78 $$k_X = k_S (\bar{Q}_X D_X A_S \Delta T_S \ / \ \bar{Q}_S D_S A_X \Delta T_X)$$

The heat flow per unit time through the material $\bar{Q}_X$ is equal to the heat of fusion of the melting standard ΔH_F divided by the time taken for the standard to completely melt

Equation 79 $$\bar{Q}_X = \Delta H_F / \Delta t$$

where Δt is the time between the onset of the melting peak and the maximum of the peak. Assuming that the same mass of standard is used in each case gives:

Equation 80 $$k_X = k_S (D_X A_S \Delta T_S \Delta t_S \ / \ D_S A_X \Delta T_X \Delta t_X)$$

Both Δt and ΔT are found to be inversely proportional to the slope of the first half of the melting peak giving:

Equation 81 $$k_X = k_S (D_X A_S / D_S A_X)(M_X / M_S)^2$$

where M is the slope of the first half of the melting peak.

It is important to note that quartz was chosen as the standard material because it has a low conductivity of the same order as the effective thermal conductivity of the metal hydride powders. Intimate contact between the melting point standard and the sample is essential to reduce thermal contact resistance, therefore, an initial scan was made to melt and solidify the indium. The thermal conductivity was measured at different

apparent densities for each activated metal hydride powder. Some of the results of the study are shown below.

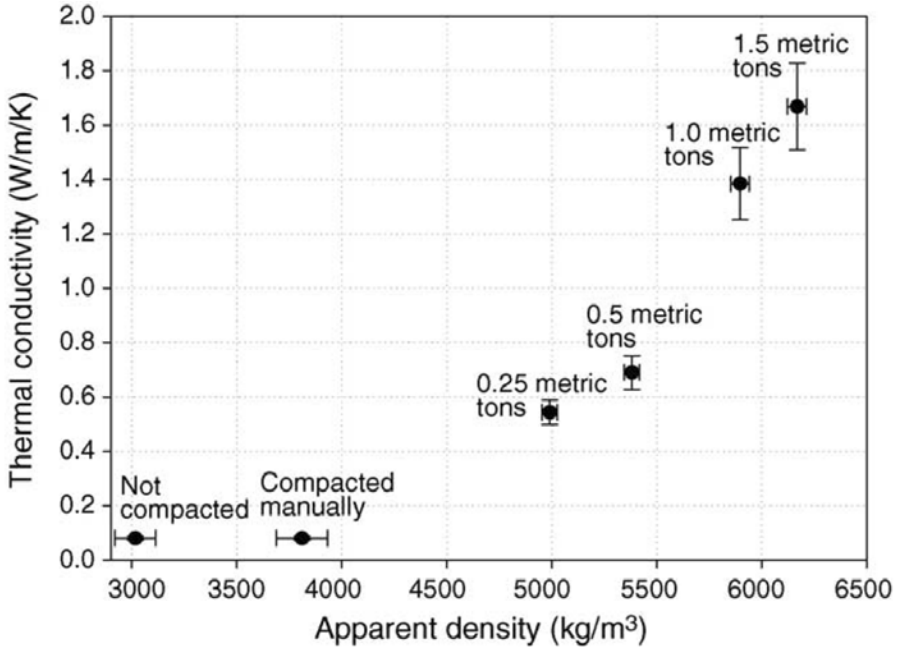

Figure 81. Thermal conductivity of $LaNi_{4.8}Sn_{0.2}$ vs. apparent density at 160°C.[225]

The study found that thermal conductivity is greatly influenced by the apparent density of the metal hydride. At low apparent densities, the thermal conductivity was nearly constant. After a certain point the k_{eff} follows an exponential growth curve. However, the effective thermal conductivity depended only minimally on the composition of the alloys.

Finally, the authors of that investigation also performed an error analysis on their thermal conductivity measurements, given by:

Equation 82

$$d\lambda_X = \sqrt{\left(\frac{D_X A_S}{D_S A_X}\left(\frac{M_X}{M_S}\right)^2 d\lambda_S\right)^2 + \left(\lambda_S \frac{D_X A_S}{D_S^2 A_X}\left(\frac{M_X}{M_S}\right)^2 dD_S\right)^2 + \left(\frac{D_X \lambda_S}{D_S A_X}\left(\frac{M_X}{M_S}\right)^2 dA_S\right)^2 + \left(2\lambda_S \frac{D_X A_S}{D_S A_X}\frac{M_X^2}{M_S^3} dM_S\right)^2 + \left(\frac{\lambda_S A_S}{D_S A_X}\left(\frac{M_X}{M_S}\right)^2 dD_X\right)^2 + \left(\lambda_S \frac{D_X A_S}{D_S A_X^2}\left(\frac{M_X}{M_S}\right)^2 dA_X\right)^2 + \left(2\lambda_S \frac{D_X A_S M_X}{D_S A_X M_S^2}\right)^2}$$

(where λ and k are used interchangeably for thermal conductivity). The found that the average error on measured thermal conductivities was approximately ±8.4% and that this was largely due to the precision of the temperature sensors of the DSC equipment (±0.1K). This error is larger than the differences observed between the different alloys.

7.3 Anisotropy in Thermal Conductivity

For practical hydrogen storage applications the issue of good heat transfer to and from the storage materials must be addressed. A couple common ways of doing this are:

A) to use fin and tube heat exchangers in which the metal hydride has been inter-dispersed between the thermal conducting (usually metal) fins, and
B) or to mix the hydrogen storage materials with other materials that enhance the thermal conductivity and then to compact the composite material to improve thermal conductivity and volumetric capacity.

While the second approach offers a simple, cost effective solution, the compaction of the composite material can cause anisotropy in the thermal conductivity due to the alignment of the thermal conductivity enhancing media in a preferred direction.[227]

A recent study by Fedchenia and van Hassel combined thermal conductivity measurements and modeling to investigate anisotropy in thermal conductivity of such composite hydrogen storage materials.[228] In this study, three materials, Ti-doped sodium aluminum hydride (SAH), an 8:3 mixture of Lithium Hydride and Magnesium Amide (LAMH), and a Metal Organic Framework (MOF-5) were mixed with expanded natural graphite 'worms', and uni-axially pressed in a square die to compact the material into cube shaped samples. A Hot Disk Thermal Constants Analyzer (Figure 82) was used to measure thermal conductivity. The analyzer supplies a constant power to an initially isothermal sample via a sensor located in the middle between two cube shaped samples and follows, during a limited heating period, the resulting temperature increase using the same sensor also as a resistance thermometer.

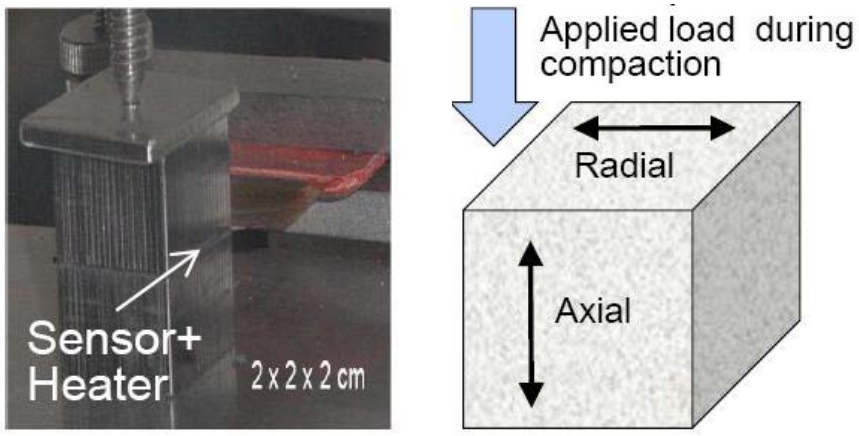

Figure 82. a) Thermal measurement system and b) Material compaction process.[228]

Thermal conductivity measurements were conducted in the axial direction of the sample (direction from which the compaction load was applied) and perpendicular to the axial direction by simply turning the cube shaped sample sideways and repeating the measurement. These two sets of data consisted of measured time traces of the change in temperature. These were recorded and analyzed using the COMSOL model developed in the study in order to quantify anisotropy in the thermal conductivity.[228]

The COMSOL model poses a classical Inverse thermal problem that is very demanding computationally and prone to non-unique solution.[229] Previously the common approach was the reduction of number of identified thermal parameters and usage of reduced and/or simplified physical models.[230,231]

In similar hot disc heating experiments, the inverse problem of thermal parameter identification had been solved using an analytical solution for the hot disc in infinite media.[230] This approach becomes prohibitive for material exhibiting anisotropic properties. It also does not allow inclusion of the heat transfer coefficient for the boundary between the sensor and the material. The latter becomes important for the materials modified by the applied stress as it results in different contact surface properties. Not accounting for this will lead to the wrong relation between the heat applied from the hot disc and the heat transfer properties of the material. Another shortcoming of this approach is that only thermal diffusivity can be estimated from the analytical model.[231] The heat capacity must be measured in a separate experiment. Therefore, here, reasonable detailed physical model has been used for material parameters identification.

In the work by Fedchenia and van Hassel the Inverse Thermal Problem was solved using COMSOL as a forward solver for a realistic 3D transient thermal model of the experiment, Figure 83, running under Matlab optimizer *patternsearch* that implements a derivative free direct search algorithm.[231]

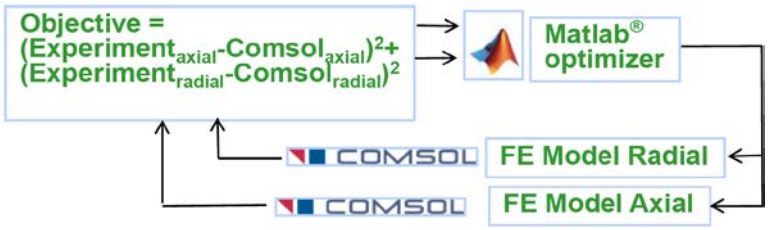

Figure 83. Schematics of interaction between Matlab optimizer and solving the backward problem and Comsol solving the forward problem.[228]

The *patternsearch* technique is very robust, quickly converges to the vicinity of the minimum, does not require calculation of derivatives and allows work with different norms. However, it was pointed out by Fedchenia and van Hassel that the major problem of this approach is that it is very slow for certain type of objective function landscapes such as long narrow valleys once the vicinity of the minimum has been reached. Unfortunately, this is the case for the thermal problem that attempts to evaluate many parameters at once when variation of some of them results in opposite trends that compensate each other. The study noted that it would be highly desirable to find some acceleration strategy of the derivative free direct search algorithms. The authors implemented an acceleration strategy through an amendment of existing algorithm.

Finally, it should be noted that in the experimental and computational analysis the following important assumptions and conditions were made:

- The outside material surface is kept under the constant ambient temperature.
- Zero heat flux conditions have been imposed on the surfaces of symmetry.
- The sensor properties stay the same for all measurement.

The accuracy of the method was evaluated in the study. Figure 84 shows the difference between the Comsol model and the measurements. Most of the error is in the initial period of the heating process implying that the hot disc sensor model is too crude for that short time interval.

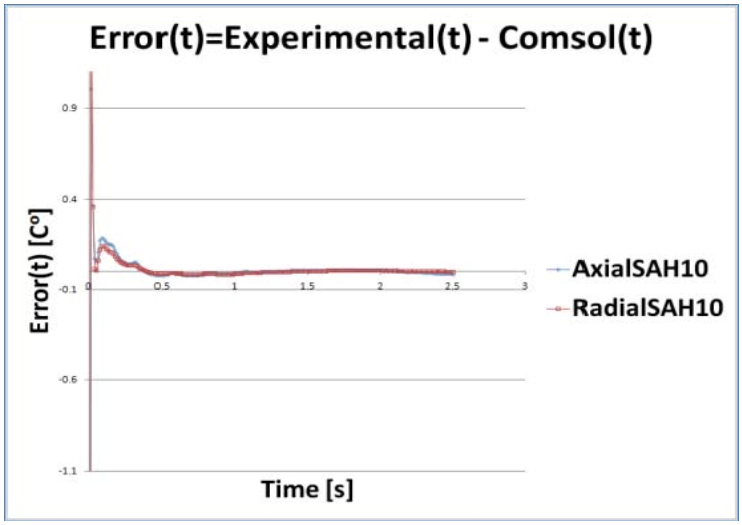

Figure 84. The difference between Comsol model and experimental measurements.[228]

Figure 85 demonstrates that considerable improvement could be achieved in solution of inverse thermal problem by increasing the number of experimental run data used in the calculation from 2 to 3 directions (i.e.. taken in all 3 perpendicular directions).

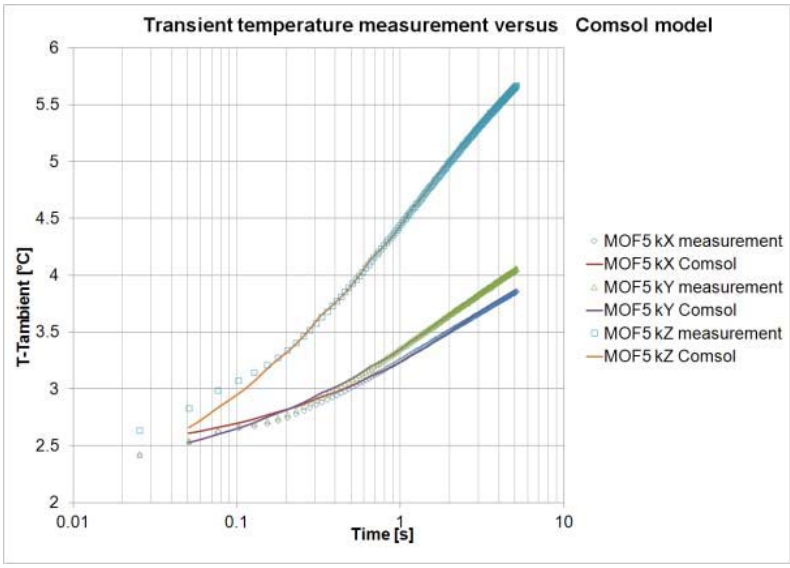

Figure 85. Experimental measurements versus Comsol inverse problem solution for MOF5 compound when three time traces of measurements in all perpendicular directions have been used in objective function.[228]

Some results of the study are show in Figure 85. There clearly is anisotropy in the thermal conductivity of these compressed mixture materials.

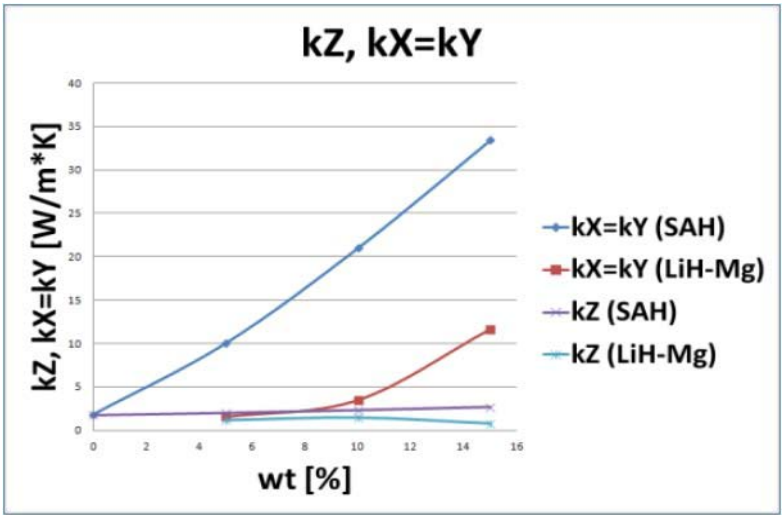

Figure 86. Thermal Conductivities in different axial directions of two different hydrogen storage materials mixed with expanded natural graphite 'worms' that have been uni-axially compressed in a square die.[228]

Important question remains about the impact of uncertainties in the experimental setup on the accuracy of the inverse problem solution. It has been determined that a small variation of starting time delay as well as dissipated power might decrease the error.

The above experimental method and analysis was applied by the same authors to compare the effectiveness of two different thermal conductivity enhancers. The results of that work are presented in Figure 87.[232]

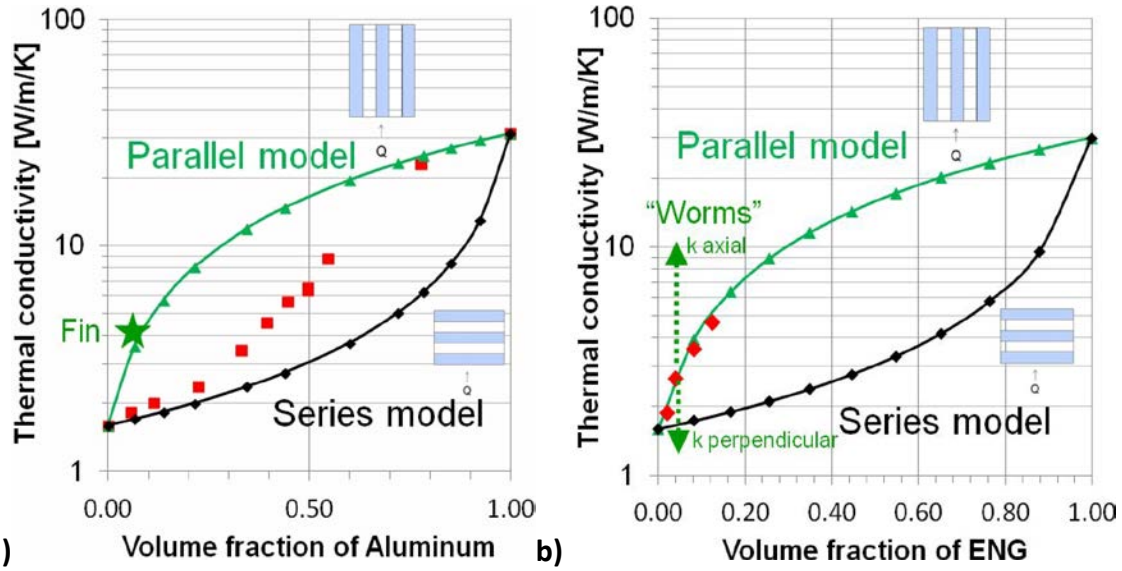

Figure 87. Thermal Conductivities in different axial directions of sodium Aluminum Hydride (SAH) mixed with a) aluminum powder and b) expanded natural graphite 'worms' that have been uni-axially compressed in a square die (Experimental data: green star and red points).[228]

From these and prior results the authors made the following conclusions:

- Fast refueling time with SAH requires an effective bed thermal conductivity of 4-8 $W \cdot m^{-1} \cdot K^{-1}$,
- Compaction of SAH without additives is not sufficient (AMR 2010)
- Aluminum powder is not effective in improving thermal conductivity, one would have to use aluminum fins rather than powder.
- Expanded Natural Graphite can be effective when used in form of 'worms' which will result in anisotropic thermal conductivity.

Similar anisotropic effects were found by Pohlmann et al. in several studies on the introduction of Expanded Natural Graphite (ENG) into amides, alanates, as well as Mg and Mg-alloys for hydrogen storage.[233,234,235] For example, measurements of MgH_2-ENG mixtures are shown in Figure 88 below.

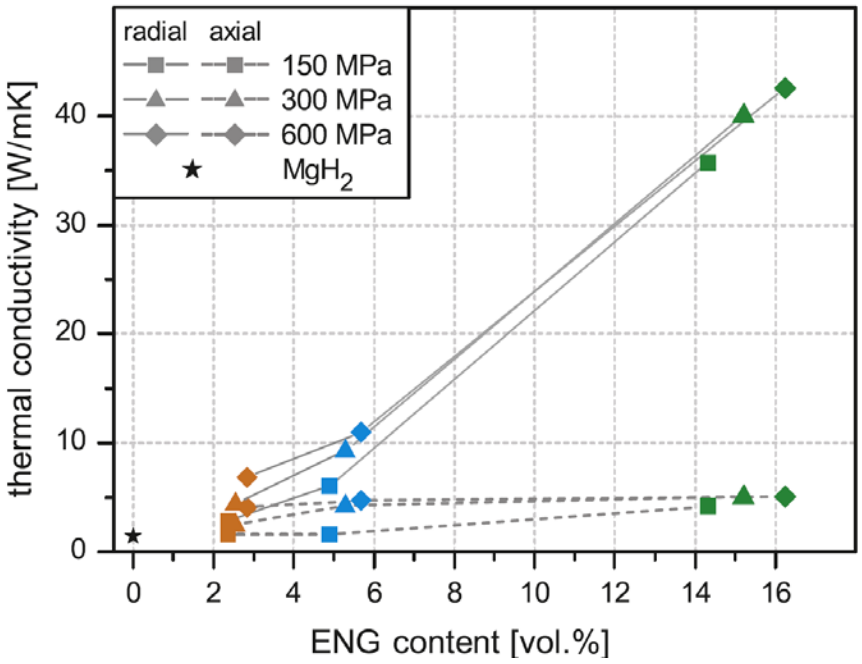

Figure 88. Thermal conductivities of the MgH_2-ENG specimens in radial (solid lines) and axial (dashed lines) direction for different compaction pressures vs. ENG content (5 wt.% orange, 10 wt.% blue, 25.5 wt.% green).[235]

In their work on Mg-Ni alloys, Melt-spun alloy flakes were mixed with different amounts of up to 25.5 wt.% ENG. These mixtures were compacted to cylindrical pellets using compaction pressures up to 600 MPa. It was found that the heat transfer characteristics could be tailored in a wide range, e.g. the thermal conductivity of magnesium alloy-ENG compacts were tuned from 1 up to 47 $W \cdot m^{-1} \cdot K^{-1}$.[234]

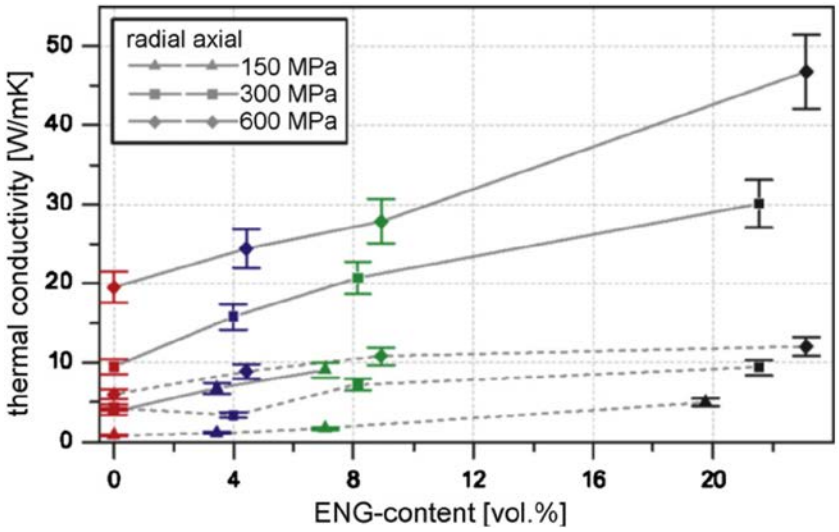

Figure 89. Radial (solid line) and axial (dashed line) thermal conductivities of the $Mg_{90}Ni_{10}$–ENG compacts at compaction pressures of 150, 300 and 600 MPa vs. ENG content (0 wt.% red, 5 wt.% blue, 10 wt.% green, 25.5 wt.% black).[234]

In order to measure the thermal conductivity of the compressed pellets, they were cut into 2 mm thin slices in axial as well as radial direction (Figure 90). The slices were then examined using the flash method of measurement to determine the thermal diffusivity.

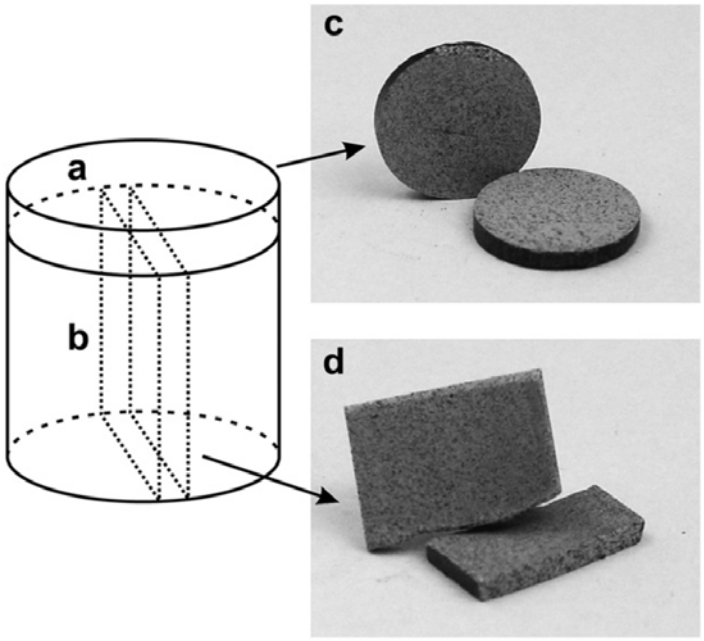

Figure 90. (a, c) Radial and (b, d) axial cross-sections of the consolidated pellets used for temperature diffusivity measurements).[235]

Thermal conductivity was calculated by multiplying temperature diffusivity, density and specific heat capacity as described above. The specific heat capacity was determined using the DSC method. The authors determined that the total measurement error resulted in an uncertainty of less than 10% for the thermal conductivities.[235]

7.4 Sample Size Effects

Experimental measurement of thermal conductivity consists of accurately determining the time dependent temperature rise at a specific point on a conducting pattern (the measurement and heating sensor which consists of a resistive coil which is generally a spiral, circular or square) and using it to solve the heat equation. For a simple case when the conducting pattern is in contact with a semi-infinite medium along the axial direction, the heat generated by the conducting pattern flows along the axial direction and the heat equation can be represented approximately by a 1-dimensional equation. This approximation requires minimizing the heat loss or gain along the radial direction. This renders constrains on the geometric configuration and the sample size. Geometric configuration and the minimum size of the sample are typically influenced by the magnitude of thermal conductivity of the material itself. When the material's thermal conductivity is high as in the case of metals, the sample needs to be longer, because the heat flux is generally higher and heat loss from the lateral surface is relative smaller. A longer sample in the axial direction helps to establish a reasonably large temperature gradient which can be accurately measured. When the thermal conductivity is low (as is the case for powder materials), the heat flux is low, and only a relatively small thickness is required to generate accurately measurable gradient. Instrumentation suppliers typically provide the lower limit of the sample size that can be analyzed accurately.

7.5 Influence of Sample Homogeneity

Accuracy of thermal conductivity measurements depends on the homogeneity of the samples. When a sample is inhomogeneous, it possesses non-uniform bulk density. Since, both the thermal conductivity and thermal diffusivity of the sample depends on the density of the material, the non-uniform density leads to non-uniform heat flow along the sample's bulk. This results in erroneous calculation of thermal conductivity.

However, the *effective* thermal conductivity of homogeneously mixed multi-component materials can be measured as long as the mixture is homogeneous. An example is the influence of thermal conductivity on the packing in polymeric composite materials as was investigated by Mamunya et al.[236] They observed that the thermal conductivity of polymeric composites with metal powder filler is a linear function of the packing

fraction of the metal powder (Figure 91). The explanation of this behavior is that particles are closer to each other with higher metal filler volume content, which assists efficient heat flow through the composite.

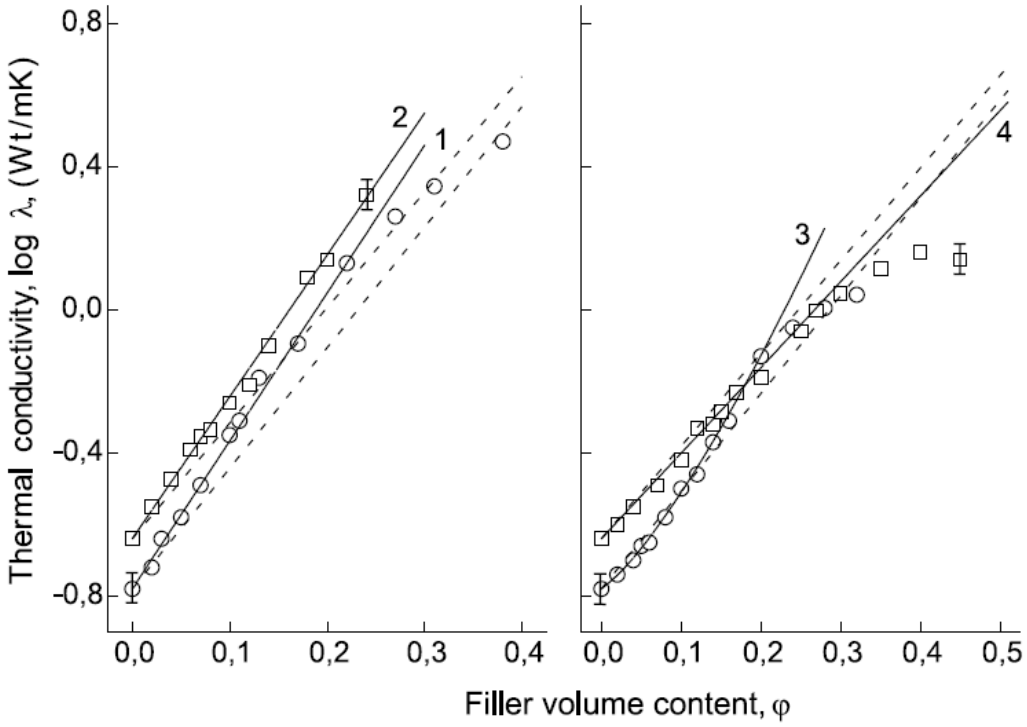

Figure 91. Linear dependence of thermal conductivity of polymeric composite materials with the metal filler volume content.[236]

7.6 Challenges of Thermal Conductivity Measurements at Cryogenic Temperatures

Measurement of thermal conductivity at cryogenic temperatures poses several challenges:

1. For subzero temperature measurements, it is important that experiments are performed under vacuum, inert gas, or dry air to avoid any water condensation on the sample or measurement system.

2. For cryogenic temperatures, the system should be purged with helium and then evacuated to avoid any condensation of residual oxygen or nitrogen.

3. Thermal conductivity measurement of certain materials requires using a contact agent, such as water, glycol or glycerin to improve their thermal contact with the measurement system. At cryogenic temperatures, the properties of the contact materials change significantly which render them less useful under such conditions.

7.7 Thermal Conductivity and Cycling

Thermal conductivity of hydrogen storage material with given phase composition does not vary significantly with the cycling. For porous materials where the hydrogen is stored via physisorption, the effect of cycling on the thermal conductivity is expected to be a minimum but this has yet to be shown. For storage materials, such as chemical hydrides, variation in the thermal conductivity may be observed. This is particularly true of materials that segregate or change within the first few cycles (activation). Dedrick et al. investigated the effective thermal conductivity of SAH system as function of cycling (Figure 92).[110] They found that for this system, the effective thermal conductivity of the adsorbed state with 1 bar of hydrogen does not change significantly with the cycling after the first couple of cycles. However, long term cycling (100+ cycle) thermal conductivity measurement on these, physisorption and other hydrogen storage materials are yet to be performed.

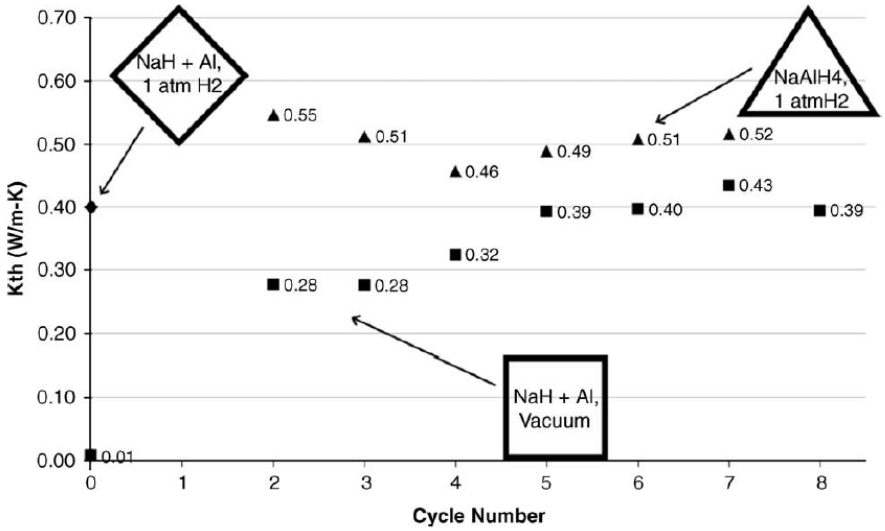

Figure 92. Variation of thermal conductivity of SAH (sodium aluminum hydride) system with different sorption cycles.[110]

7.8 Other Limitations, Caveats, Precautions, Issues

1. Handling of samples transfers heat to the specimen and causes so-called thermal contamination in thermal conductivity measurements. Effect of this can be minimized by wearing gloves while handling samples and starting the measurement only after thermal equilibrium is reached. In Figure 93, a temperature rise from around 18.0°C to 18.6°C is caused by heat transferred during sample handling.
2. It is advisable to perform experiments in closed thermal chamber or in a glove box. This avoids contamination of samples which are highly sensitive to air or moisture. Air movement around the measurement system causes variation in the temperature and long thermal equilibration times, seen as the scattered temperature data near 18.0°C in Figure 93. Performing measurements inside a controlled chamber avoids this.

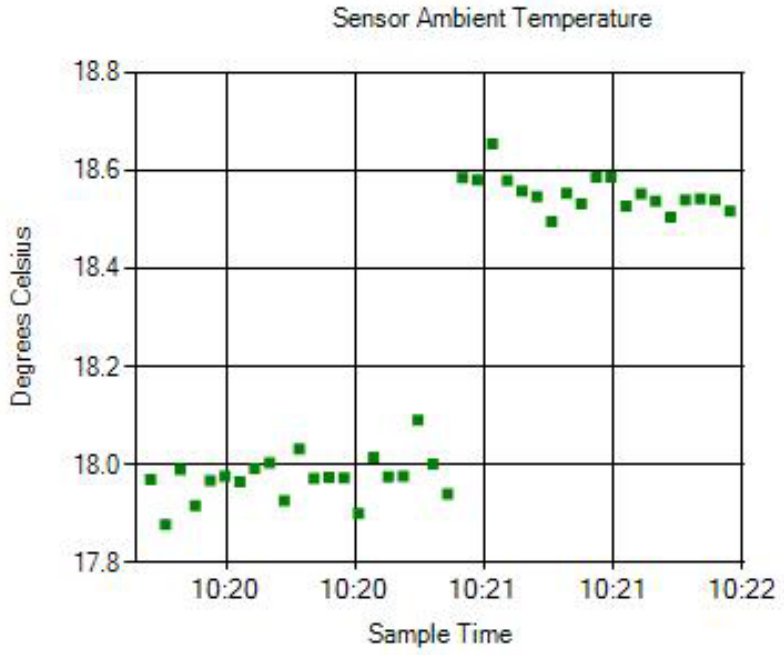

Figure 93. Temperature of the sensor increases from 18.0 to 18.6°C due to the heat transferred during the sample handling. The wider scatter of the temperature data around 18.0°C is the influence of the air movement in the vicinity of the measurement system. [237]

8 Modeling the Need for Experimental Data

8.1 Overview

An extensive study of metal hydride and adsorbent based hydrogen system designs is currently being conducted by the DOE Hydrogen Storage Engineering Center of Excellence (HSECoE). The goal of the HSECoE is to design and test semi-scale prototype hydrogen storage systems having the potential to meet the DOE technical targets for light duty vehicles.[238] At the time this section was written, the HSECoE was at the initial stages of designing the prototypes.

It is difficult and expensive to design and conduct experiments that fully measure the complex processes occurring during the loading and discharge of hydrogen from a storage media, let alone perform sensitivity studies for a complete system. Any such experiments would be limited to a particular hydride and system design. Without a great deal of experience it is very difficult to know, a priori, the type and location of necessary measurements required to characterize the performance of the system. A much more efficient approach is to evaluate proposed designs for hydrogen storage systems through the use of numerical models that couple heat, mass and momentum transport with reaction kinetics (for metal hydrides) or sorption thermodynamics (for adsorbents). By systematically combining scoping models that quickly evaluate whether a storage system and its associated media has the potential to meet performance targets with more sophisticated models that provide detailed predictions of operational performance, the most promising designs can be efficiently identified. An example of a scoping model for metal hydrides is the acceptability envelope.[239]

In addition to evaluation of specific designs, the detailed models provide insight into system behavior that was used to improve designs that passed the screening tests.[240,241] With regards to prototype development and testing, the detailed models will used to: design the prototype storage systems, determine the test matrix and the requirements for the test station, and determine the location and types of measurements to be made. Data obtained from the tests will be used to refine the models, which, in turn, will be used to predict the performance of full-scale storage systems.

8.2 On-Board Reversible Hydride Storage Systems

In metal hydride systems the rate of hydrogen uptake, or discharge, is dictated by the chemical kinetics of the material. Thus, for a given temperature and pressure the

kinetics determines the ultimate limit to the rate at which a metal hydride based system can store or release hydrogen. Although the temperature and pressure may be adjusted to maximize the reaction rate, no design improvements can enhance rates of hydrogen uptake or discharge beyond this limit. Maintaining the system at the optimal temperature requires that the system has sufficient heat transfer capability to remove the heat of reaction released during the charging process and to transfer heat uniformly throughout the hydride bed during the discharge phase. Heat transfer rates are governed by the thermal conductivity of the hydride bed and the distance from heat transfer surfaces (the characteristic thermal transport length). Metal hydrides typically have very low thermal conductivities, necessitating relatively close spacing of heat transfer surfaces, the addition of thermal conductivity enhancing amendments to the hydride, and/or the structuring of hydride into geometric shapes that enhance heat transfer.

Any meaningful consideration of thermal conductivity must also take into account the required rate of heat removal along with the other parameters that control the transfer and generation of heat. Properties that must be simultaneously considered are:

$\Delta H_{overall}$ = The overall heat of reaction [J·mol^{-1} of H_2[

$\rho_{Hydride}$ = Bulk hydride density (in reference form) [kg·m^{-3}]

M_{Hyd_Eff} = Mass of hydride (in reference form) required to load the target amount of H_2 in the specified time (relates to kinetics) [kg]

ΔT = Temperature range for acceptable kinetics (to give charge/discharge rate of $\Delta m_{H2} / \Delta T$) [K]

$\Delta m_{H2} / \Delta t$ = Required rate of charging/discharging [mol·s^{-1}]

k = The bed thermal conductivity [W·m^{-1}·K^{-1}]

L = Characteristic distance between heat transfer surfaces [m]

The acceptability envelope, described in Corgnale, Hardy, et al., develops a relation between these parameters that permits charging/discharging targets to be satisfied.[239] As most heat exchange designs are either rectangular, as for fins, or cylindrical, as for tube arrays, a relation applicable to either configuration was derived. Boundary conditions and the specific form for the parameter L are discussed in Corgnale, Hardy, et al.[239] The relation, or parameter grouping, is

Equation 83

$$\left(\frac{1}{L^2}\right)\left(\frac{k\ M_{Hyd\_eff}\ \Delta T}{-\Delta H_{overall}\ \rho_{Hydride}}\right) = \frac{1}{mM_{H2}}\frac{\Delta m_{H2}}{\Delta t}$$

Where: m = 8 for rectangular coordinates or 4 for cylindrical coordinates

The parameter grouping defines an envelope, or range, of coupled media and system properties necessary for the storage system to meet the technical specifications. Figure 94 shows the coupling between charging time, heat transfer surface spacing and thermal conductivity for the charging of $NaAlH_4$ with a base case (BC) range of thermal conductivities and thermal conductivities enhanced by graphite addition (GA).

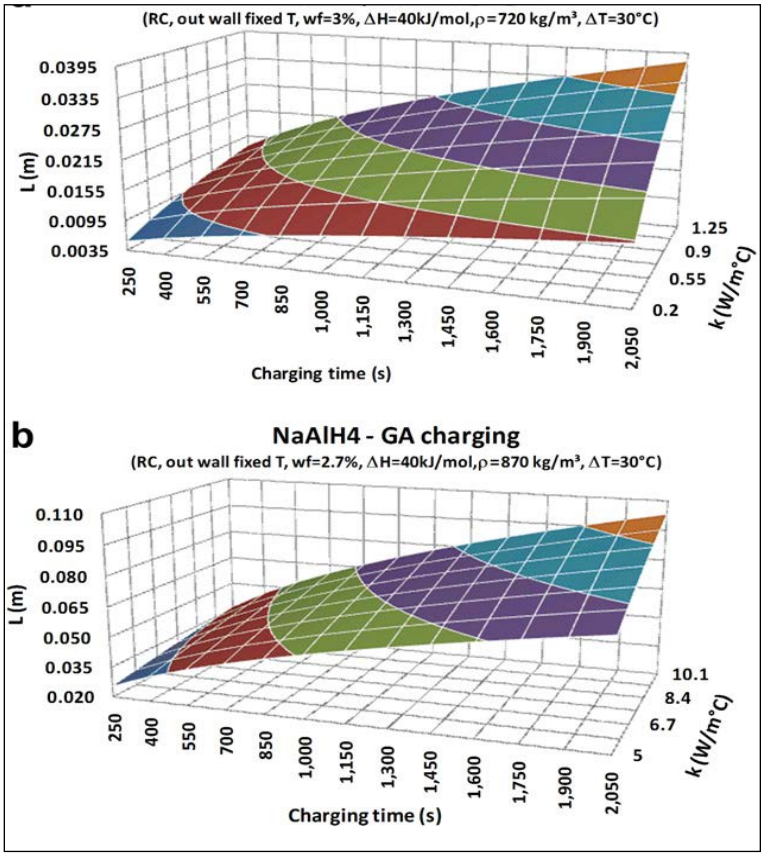

Figure 94. $NaAlH_4$ bed size profile vs. charging time and thermal conductivity for rectangular coordinates (RC) and wall fixed temperatures considering the nominal, or baseline material (a) and the graphite added material (b). L represents the distance between the two heat transfer surfaces.[242]

During hydrogen uptake metal hydrides experience a significant increase in volume. The amount of volume increase depends on the particular hydride and can exceed 40% of the volume of the depleted material. The volume reversibly decreases as hydrogen is extracted from the hydride. For some hydrides the expanded material can be compressed, while for others the expansion is rigid and can apply high stresses to adjacent surfaces, such as vessel walls or fins. The change in volume complicates the design of heat transfer components, making it difficult to maintain good thermal contact

throughout the charging and discharging process. It is also expected that the thermal properties of the metal hydride will change with the morphology of the material. Hence, characterization of volumetric and its influence on material properties are necessary for the design of metal hydride based storage systems.

Beyond simple charging and discharging scenarios, chemical kinetics and heat transfer capabilities determine the performance of the storage system for a variety of initial conditions. For example, when the discharge process is stopped the bed will transition to a stable temperature, pressure and composition. These conditions would be initial conditions when the discharge process was re-started or when a partially discharged storage vessel is recharged.

As a specific example, the detailed 2 and 3-dimensional finite element models were applied to a storage system utilizing $TiCl_3$ catalyzed sodium alanate ($NaAlH_4$).[240] The storage system had the configuration of a cylindrical shell, tube and fin heat exchanger. The bed was divided by an array of fins that are normal to the axis and extend in the radial direction. The fins were press-fit to coolant tubes that are parallel to the axis. The left illustration in Figure 95 shows a storage system developed and tested by the United Technologies Research Center™ (UTRC™), see Mosher, et al.[242], which has a similar geometric configuration.

Specifically, the detailed models were applied to a storage system having 9 coolant tubes and 8 tubes used to inject hydrogen into the hydride bed, see the right illustration in Figure 95. The areal average velocity of the heat transfer fluid in the coolant tube was 13 $m \cdot s^{-1}$ and its temperature was assumed constant at 373K. Separate calculations indicated that that for a 1m long tube, the temperature of the heat-transfer fluid would increase by only 2.42K. The initial bed temperature was 373K. Initially the hydrogen pressure in the tubes and the bed was 1 bar. The bed was initially pure NaH, with the stoichiometric quantity of Al required to complete the reaction to $NaAlH_4$. To effect charging of the media, the hydrogen pressure in the injection tubes was exponentially increased to 50 bar, reaching 99% of the final value in 10 seconds. As the gas pressure increased, the resulting pressure gradient caused the gas to flow from the tube and into the bed, according to the Blake-Kozeny equations. The hydrogen temperature in the injection tubes was fixed at 373K.

The model focused on a layer of hydride material located at sufficient distance from the axial ends of the bed that the axial boundary conditions are periodic from the axial mid-plane of one fin to the axial mid-plane of the adjacent fin. Therefore, symmetry conditions could be applied to the axial mid-plane of the hydride layer and the axial mid-plane of the fin. Further, there are planes of azimuthal symmetry, as shown in the right illustration in Figure 95. The geometry used for the 3-dimensional model, along with the mesh, is shown in Figure 96. The model simultaneously solved the mass and energy

conservation equations. The velocity of hydrogen in the bed was determined from the Blake-Kozeny equation.[243]

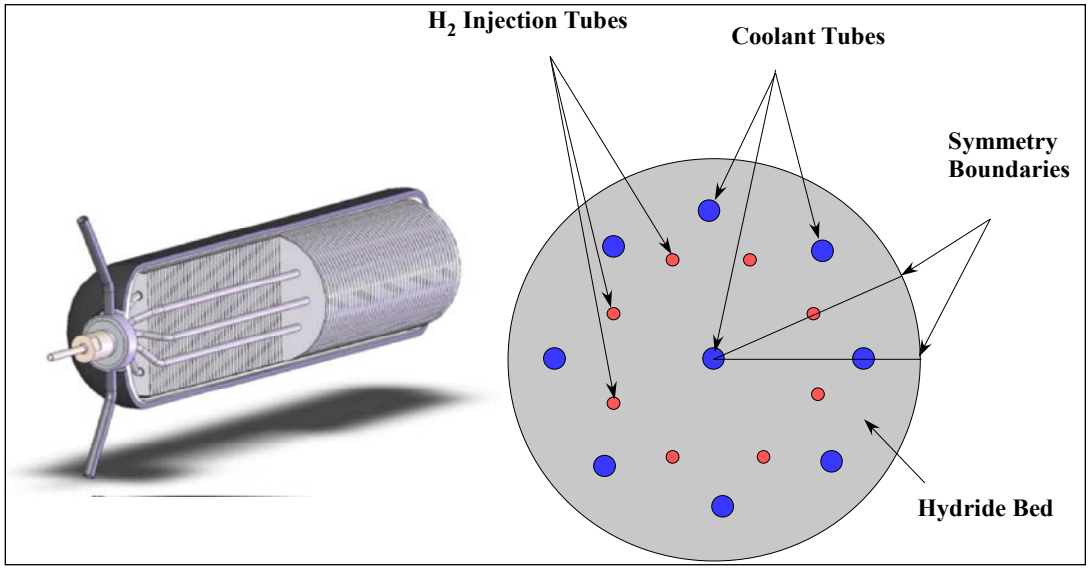

Figure 95. The illustration to the left is a shell, tube and fin hydride bed configuration.[242] The illustration to the right is a cross-section of the hydride bed used in the detailed model.[240]

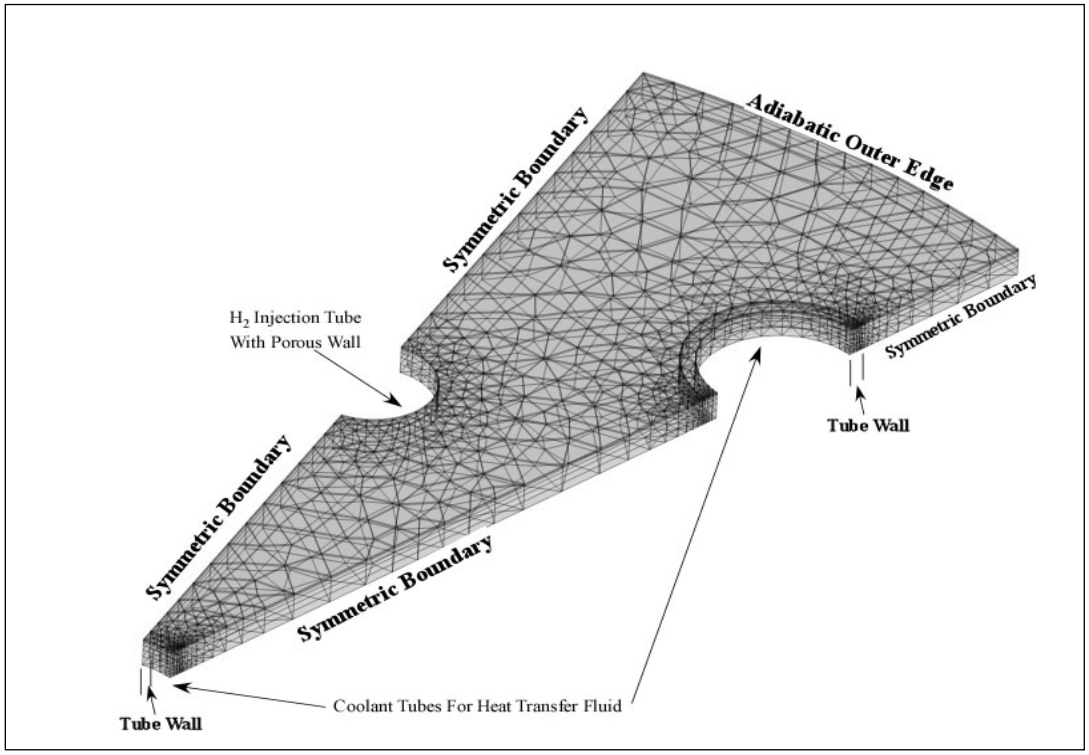

Figure 96. Geometry used for computations in the 3-dimensional model. The geometry for the 2-dimensional model is the planar form of that in the figure.[240]

The governing equations used in the model are the mechanism for introducing physically measured property data into the numerical prediction of storage system performance. The mass conservation equation for the hydride bed is:

Equation 84

$$\frac{\partial C_{nd}}{\partial t} + \nabla \cdot \left(C_{nd} \vec{v} \right) = \frac{1}{C_{ref}} \left(\frac{S_{H_2}}{\varepsilon} \right)$$

Energy conservation within the hydride bed is given by:

Equation 85

$$\rho_{bed} C_{p\ bed} \frac{\partial T_{nd}}{\partial t} - \nabla \cdot k \nabla T_{nd} = -\varepsilon \rho_{H_2} C_{p\ H_2} \left(\frac{\partial T_{nd}}{\partial t} + \vec{v} \cdot \nabla T_{nd} \right) + \frac{1}{T_{ref}} \left(\frac{\partial P}{\partial t} + \varepsilon \vec{v} \cdot \nabla P \right) + \frac{1}{T_{ref}} \text{Source}$$

Where: C_{nd} = The non-dimensionalized concentration of H_2 = $\frac{C}{C_{ref}}$

C = Concentration of H_2 in the bed void space [mole $H_2 \cdot m^{-3}$]

C_{ref} = Reference H_2 concentration in the bed void space [mole$\cdot m^{-3}$]

$C_{p\ bed}$ = Specific heat of hydride bed [J$\cdot$ $kg^{-1} \cdot K^{-1}$)]

$\vec{v}$ = Mean interstitial H_2 velocity [m$\cdot s^{-1}$]

S_{H_2} = Rate of H_2 generation per volume of bed from all chemical reactions [mol $H_2 \cdot m^{-3} \cdot s^{-1}$]

T_{nd} = $\frac{T}{T_{ref}}$ = Non-dimensional temperature

T_{ref} = Reference temperature [K]

ε = Void fraction (porosity) of particle bed

ρ_{bed} = Bulk mass density of bed [kg$\cdot m^{-3}$] = $(1-\varepsilon)\rho_{bed\_particle}$ = $\frac{\text{Mass of solid}}{\text{Total volume}}$

ρ_{H_2} = H_2 density [kg$\cdot m^{-3}$]

k = Bed thermal conductivity [W$\cdot m^{-1} \cdot K^{-1}$]

$C_{p\ H_2}$ = Specific heat of H_2 [J$\cdot kg^{-1}$]

P = Pressure [Pa]

Source = Enthalpy change due to chemical reactions [W·m^{-3}] =

$$-\left(\sum_i\left[\frac{1}{M_i}\frac{\partial \rho_i}{\partial t}\Delta H_i\right]\right)$$

M_i = Molecular weight of species i per mole [kg·g^{-1}·mole^{-1}]

ρ_i = Bulk mass density of species i [kg·m^{-3}]

ΔH_i = Enthalpy of reaction on a molar basis of species i [J· (mole of i)$^{-1}$]

Sodium alanate undergoes the 2 step reaction given by Equation 86. Parameters governing the forward and reverse rates for the individual stages of this reaction were obtained from data.

Equation 86
$$\underbrace{NaAlH_4}_{Species\,1} \underbrace{\leftrightarrow}_{Reaction\,1} \underbrace{\frac{1}{3}Na_3AlH_6}_{Species\,2} + \frac{2}{3}Al + H_2 \underbrace{\leftrightarrow}_{Reaction\,2} \underbrace{NaH}_{Species\,3} + Al + \frac{3}{2}H_2$$

A comparison of loading rates for the 0-dimensional kinetics scoping model, and the 2 and 3-dimensional finite element models, in terms of the weight fraction of stored hydrogen, is shown in Figure 97. For the 0-dimensional kinetics scoping model, the weight fraction of stored hydrogen had no spatial dependence. However, for the 2 and 3-dimensional finite element models, the weight fraction of stored hydrogen was a function of position and time. Therefore, for the 2 and 3-dimensional models, the weight fraction of stored hydrogen was expressed as an area or volume average, respectively. To demonstrate capability, the 2 and 3-dimensional finite element models were run for initial NaH concentrations of approximately 331 and 13,333 mole·m^{-3}. Increasing the initial NaH concentration resulted in increased transient temperatures, which impacted the rate of hydrogen uptake. The kinetics scoping model determined charging rate by solving the kinetics equations for a fixed temperature of 373K and a fixed hydrogen pressure of 50 bar.

Loading rates predicted by 3-dimensional finite element models, which allowed for axial heat transfer to the fins, were essentially identical to those for the 0-dimensional kinetics model. The higher loading rates for the 2-dimensional (radial and azimuthal) finite element model, with an initial NaH concentration of 331 mole·m^{-3}, resulted from higher bed temperatures due to the absence of fins. However, for the larger initial NaH concentration of 13,333 mole·m^{-3}, temperatures in the 2-dimensional model were sufficiently high to reduce, and in some locations reverse, reaction 1 of the hydriding reactions, see Equation 86. This led to the reduced loading rate shown in Figure 97.

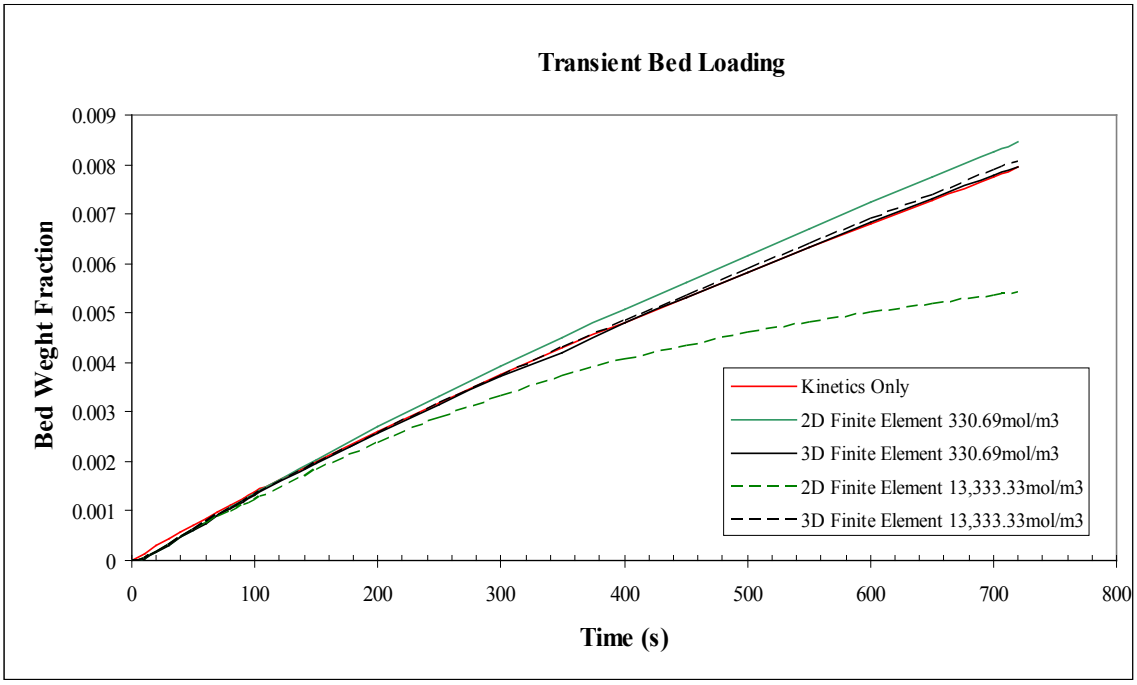

Figure 97. Comparison of the weight fraction of stored hydrogen for the kinetics scoping model and the 2 and 3-dimensional finite element bed models.[240]

Unless it is removed, heat generated during the loading of the bed could result in a temperature transient that impacts the reaction rates. However, the low thermal conductivity of the alanate necessitated design features that maintained a relatively short length scale for heat transfer within the bed. The models in this document were developed for shell and tube (the 2-dimensional finite element model) and shell, tube and fin (the 3-dimensional finite element model) configurations.

Figure 98 shows plan and isometric views of the temperature profile in the 3-dimensional model at 40 seconds into the charging transient. The image on the left shows the reduction in temperature from the mid-plane of the hydride layer to the mid-plane of the fin. The plan view, on the right, shows the temperature profile over the mid-plane of the hydride layer.

Figure 99 compares the transient temperature profile for the 2-dimensional model, which does not have fins, to the temperature profile at the mid-plane of the hydride layer for the 3-dimensional model at 120 seconds. As expected, these figures show that heat transfer to the fins resulted in a more uniform temperature profile.

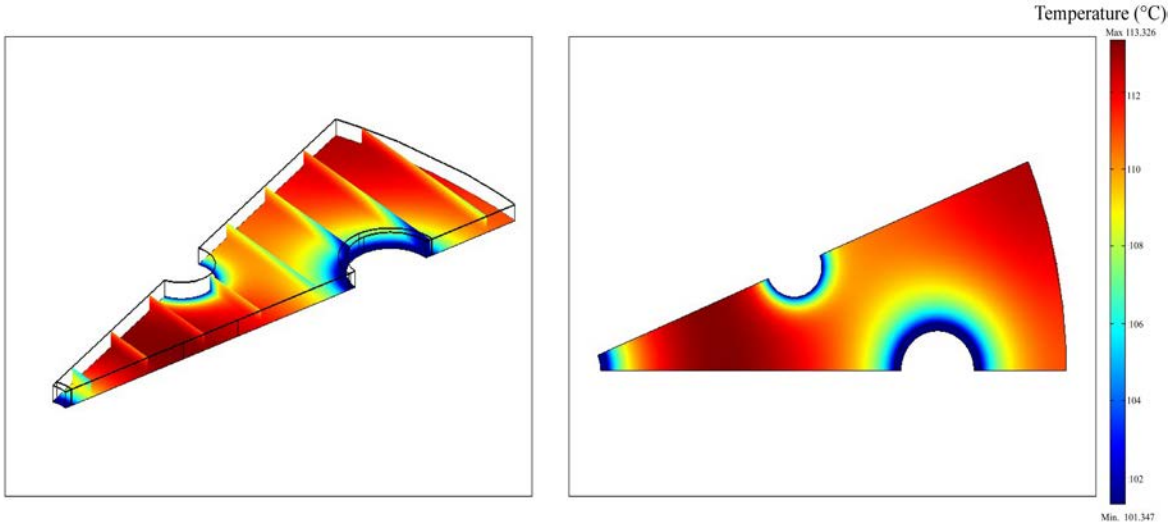

Figure 98. Isometric and plan views of temperature profile for 3-dimensional model at 40 seconds. Base of isometric figure is at bed mid-plane (center of the hydride bed layer between fins).[240]

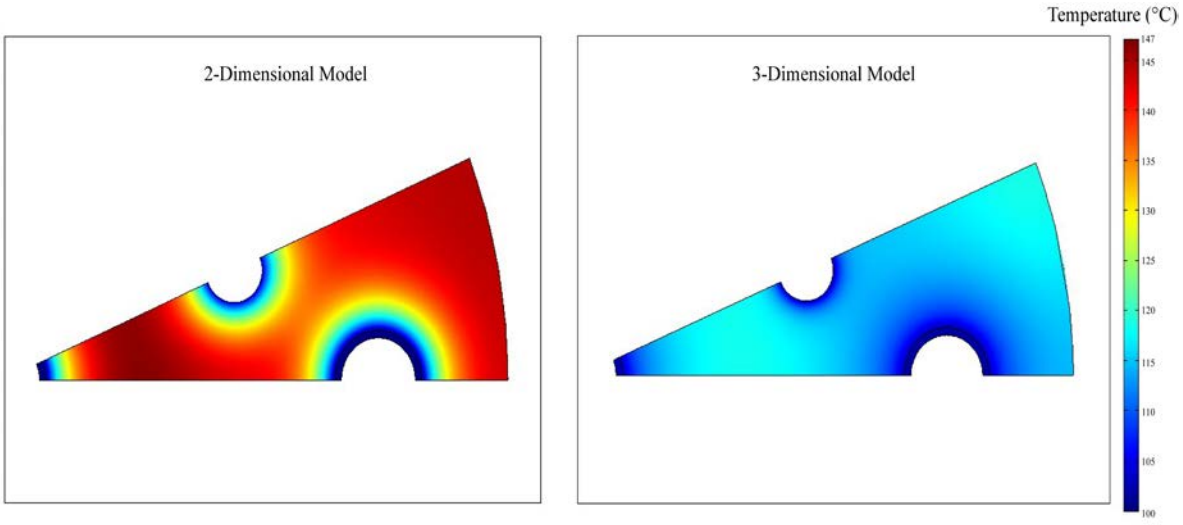

Figure 99. Comparison between 2-dimensional and 3-dimensional bed mid-plane temperature profiles at 120 seconds.[240]

Conversion of NaH to Na_3AlH_6 and then to $NaAlH_4$ occurred as the bed was loaded with hydrogen. However, the formation of hexa and tetra-hydrides was most rapid in locations that had temperatures and pressures conducive to higher reaction rates. To use the bed efficiently, the concentration of tetra-hydride must be relatively uniform at the termination of the loading phase. Optimizing hydrogen loading rates and achieving

full utilization of the bed requires design features that ensure proper heat transfer and flow.

Figure 100 shows the transient concentrations of Na_3AlH_6 and $NaAlH_4$ for the 2-dimensional model and at the mid-plane of the hydride for the 3-dimensional model after 120 seconds of charging.

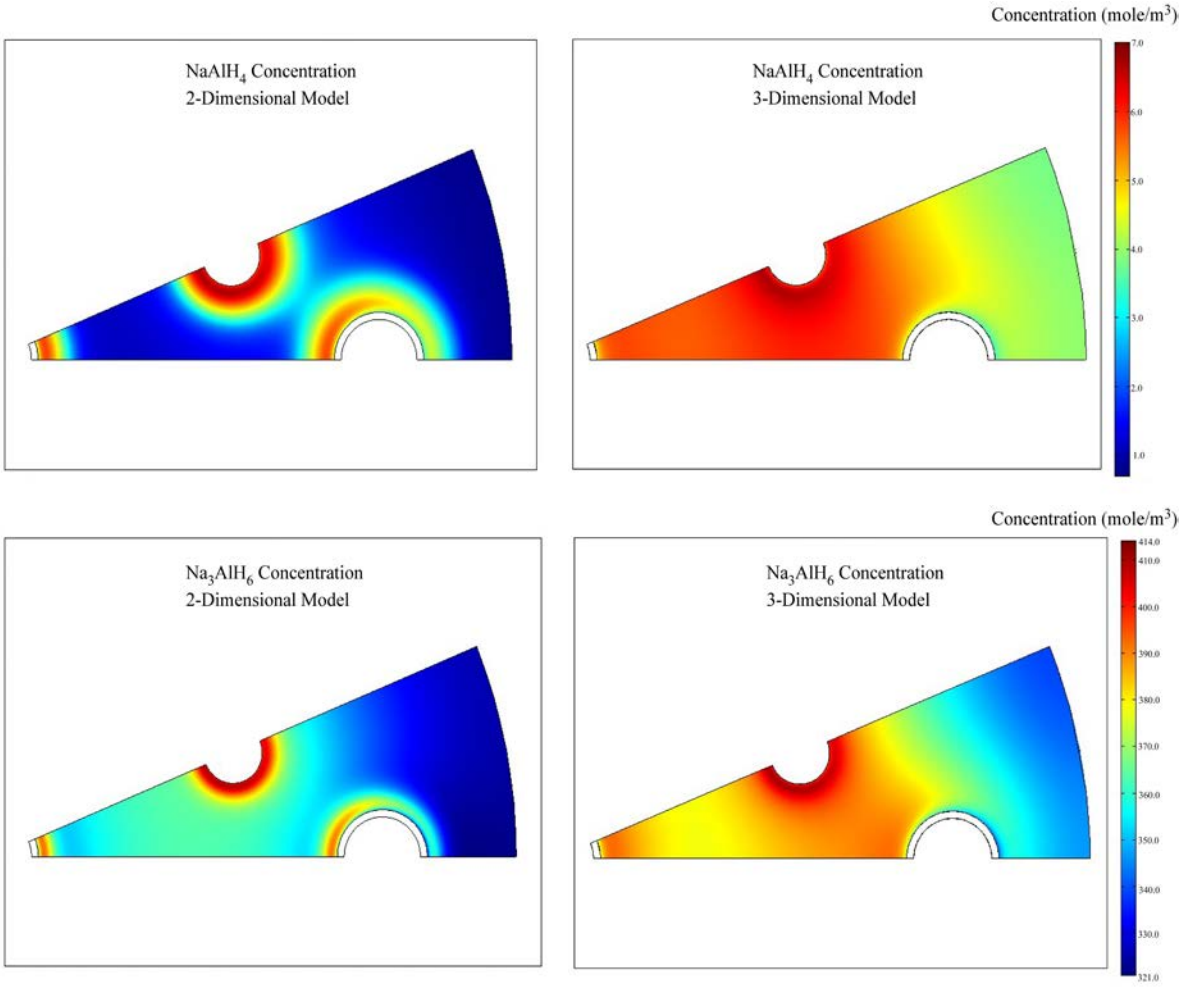

Figure 100. Comparison of 2-dimensional and 3-dimensional bed mid-plane hydride concentrations at 120 seconds.[240]

As an alternative to transverse fins, other heat transfer designs, such as metallic honeycombs, were considered.[244] Figure 101 shows the temperature distributions for this design. The initial and charging conditions were the same as for the transverse fin calculations discussed previously.

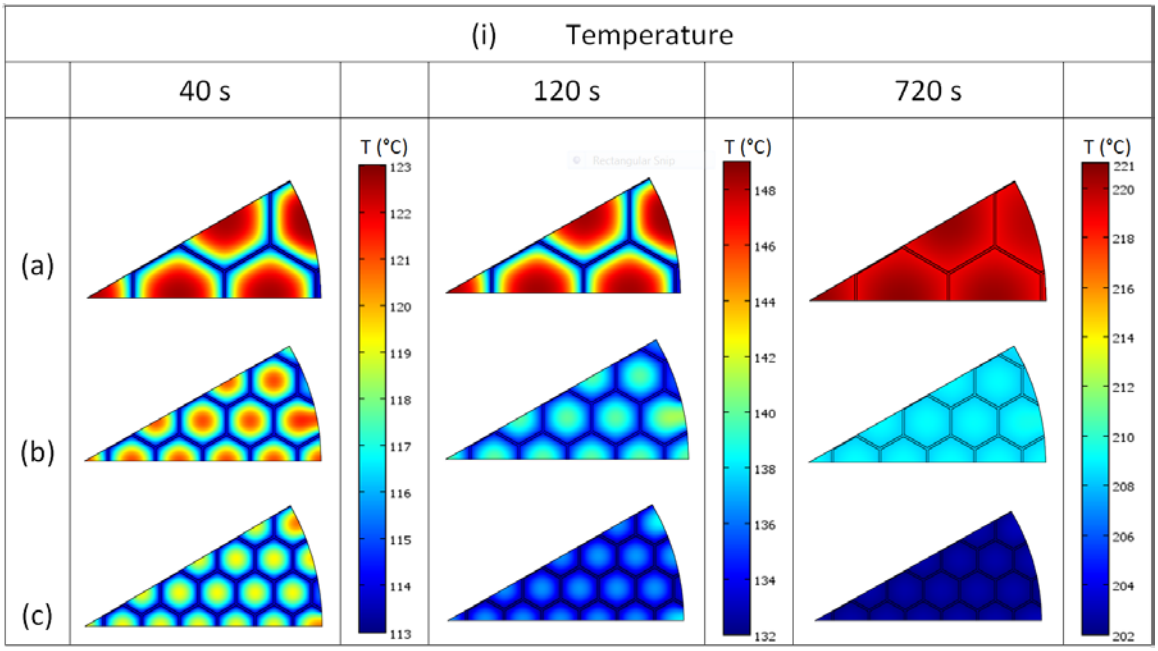

Figure 101. Temperature profiles for an embedded metallic honeycomb heat exchange surface.[244]

Studies performed within the HSECoE showed that for metal hydrides available as of 2011, the most limiting characteristics for the viability of on-board recharging are either the chemical kinetics or the density. Metal hydrides with rapid kinetics, such as $LaNi_5$, have densities that preclude meeting the target gravimetric capacity. Conversely, those metal hydrides with more suitable gravimetric capacities had reaction rates that were too slow to meet the target recharging times.

8.3 On-Board Rechargeable Physisorption Storage Systems

Adsorbents show promise for meeting the DOE technical targets for storage vessel performance, but currently require temperatures ranging from ~80-160K to store sufficient hydrogen for practical application. To facilitate adsorbent based storage system design, the HSECoE employed both numerical modeling and experiments to understand and predict adsorbent based storage system behavior. Although the general numerical model developed by the HSECoE was applicable to a range of

adsorbents, MaxSorb MSC-30™ (equivalent to AX-21™) and MOF-5™ (Basolite Z100-H) were specifically investigated. The model simultaneously solved the conservation equations for heat, mass and momentum together with equations representing adsorbent thermodynamics. Thermodynamic expressions for the quantity of hydrogen adsorbed and the internal energy of the adsorbed phase were based on the work of Richard, Bénard and Chahine.[245,246] Compressibility factor and property data for real (non-ideal) hydrogen were obtained from the NIST REFPROP 23 database.[247] Model validation was performed against data from experiments with MaxSorb™ performed at the Université du Québec à Trois-Rivières (UQTR), Richard, et. al.[248] The model was applied to conceptual storage system configurations and a comparison between MaxSorb™ and MOF-5™ performance was made.

As for the metal hydride models, the governing equations for the adsorbent model connect physically measured parameters to numerical predictions. Mass conservation equation in the adsorbent bed was given by:

Equation 87

$$\varepsilon \frac{\partial \rho}{\partial t} + \nabla \cdot \left(\rho \vec{v}_s \right) = -M_{H2} \rho_{Ads} \frac{\partial n_a}{\partial t}$$

where:
ρ = Mass density of hydrogen (kg·m^{-3})
$\vec{v}_s$ = $\varepsilon \vec{v}$ = Superficial gas velocity (m·s^{-1})
n_a = Absolute adsorption (mol of H_2·kg^{-1} adsorbent)
ε = Effective porosity, volume available for flow = $\rho_{Ads}(V_v - V_a)$
ρ_{Ads} = Bulk mass density of adsorbent (kg·m^{-3})
M_{H2} = Molecular weight of hydrogen (0.002016 kg·g^{-1}·mol^{-1})

The momentum conservation equation for the adsorbent bed was:

Equation 88

$$\frac{\rho}{\varepsilon}\frac{\partial \vec{v}_s}{\partial t} + \left(\frac{\mu}{\kappa} + \frac{S_0}{\varepsilon^2} \right) \vec{v}_s = -\nabla P + \nabla \cdot \left[\frac{\mu}{\varepsilon} \left(\nabla \vec{v}_s + \nabla \vec{v}_s{}^T \right) \right] - \nabla \cdot \left[\left(\frac{2\mu}{3} - \eta_d \right) \left(\frac{1}{\varepsilon} \right) \left(\nabla \cdot \vec{v}_s \right) \underline{\underline{I}} \right]$$

where:
μ = Dynamic viscosity of hydrogen (Pa·s)
S_0 = Mass source of hydrogen per unit of total volume (kg·m^{-3}·s^{-1})
P = Pressure (Pa)

η_d = Dilatational viscosity of hydrogen (Pa·s)

$\underline{\underline{I}}$ = 2nd order identity tensor = δ_{ij}

In the adsorbent bed the permeability, κ, was represented by the Ergun equation,[243] as:

Equation 89

$$\frac{1}{\kappa} = \underbrace{150\frac{(1-\varepsilon)^2}{D_p{}^2\varepsilon^3}}_{\text{Contribution of viscous effects}} + \underbrace{1.75\frac{\rho}{\mu D_p}\frac{(1-\varepsilon)}{\varepsilon^3}|\vec{v}_s|}_{\text{Contribution of inertial effects}}$$

inverse of Ergun permeability

Energy conservation in the adsorbent bed was given by:

Equation 90

$$\varepsilon c\frac{\partial h}{\partial T}\frac{\partial T}{\partial t} - \nabla\cdot k\nabla T$$

$$= -c\frac{\partial h}{\partial T}\vec{v}_s\cdot\nabla T \underbrace{-\frac{T}{c}\frac{\partial c}{\partial T}\left(\varepsilon\frac{\partial P}{\partial t} + \vec{v}_s\cdot\nabla P\right)}_{\text{Pressure work}} + \underbrace{\frac{\mu}{\varepsilon}\left[\left(\nabla\vec{v}_s + \nabla^T\vec{v}_s\right) - \left(\frac{2}{3} - \frac{\eta_d}{\mu}\right)\nabla\cdot\vec{v}_s\underline{\underline{I}}\right]:\nabla\vec{v}_s}_{\text{Viscous dissipation}}$$

$$\underbrace{-\frac{hS_0}{M_{H2}} - \rho_{Ads}\left(\underbrace{\frac{\partial\Delta U_a}{\partial t} + \frac{\partial(u_0 n_a)}{\partial t}}_{\substack{\text{Change in Internal Energy of Sorbed}\\ \text{Phase (per mass of adsorbent)}}}\right)}_{\text{Sorption Energy}} - \rho_{Ads}C_{P\,Ads}\frac{\partial T}{\partial t}$$

where: ΔU_a = Internal energy per mass of adsorbent of the condensed phase of the gas at a temperature T and pressure P relative to free gas at a temperature T and a pressure of 1 atm (J·kg^{-1})

c = Molar concentration of H_2 (mol·m^{-3})

h = Molar enthalpy of the gas (J·mol^{-1})

T = Temperature (K)

u_0 = Molar internal energy of free gas at the system temperature T and a pressure of 1 atm (J·mol^{-1})

$C_{p\,Ads}$ = Specific heat of adsorbent (J·kg^{-1}·K^{-1})

The model was validated against experiments performed at UQTR in which MaxSorb™ was charged with hydrogen. However, the apparatus used in these experiments was originally designed to evaluate the global thermal behavior of the adsorbent system during the charging process. For this reason the measurements made in the tests were not ideal for the detailed model and it was necessary to apply approximate boundary conditions to properly account for parasitic and other forms of heat transfer.

The reference by Richard, Cossement, et al., gives a detailed description of the apparatus used for the UQTR experiments, which is shown schematically in Figure 102.[248] As shown in the figure, the storage vessel was contained in a Dewar. The total internal volume of the storage vessel was 2.5 L; the mass of MaxSorb™ contained in the vessel was 0.671 kg. During the charging tests the Dewar was filled with liquid nitrogen; temperatures and pressures within the storage vessel, along with the inlet gas flowrate, were measured during the charging process. In the model, the storage vessel alone was considered and assumed to be axisymmetric. Boundary conditions at the vessel surface were based on liquid nitrogen conditions within the Dewar. Materials comprising the vessel, its contents, the thermocouple support and the thermocouple locations, along with applied boundary conditions, are shown in Figure 102.

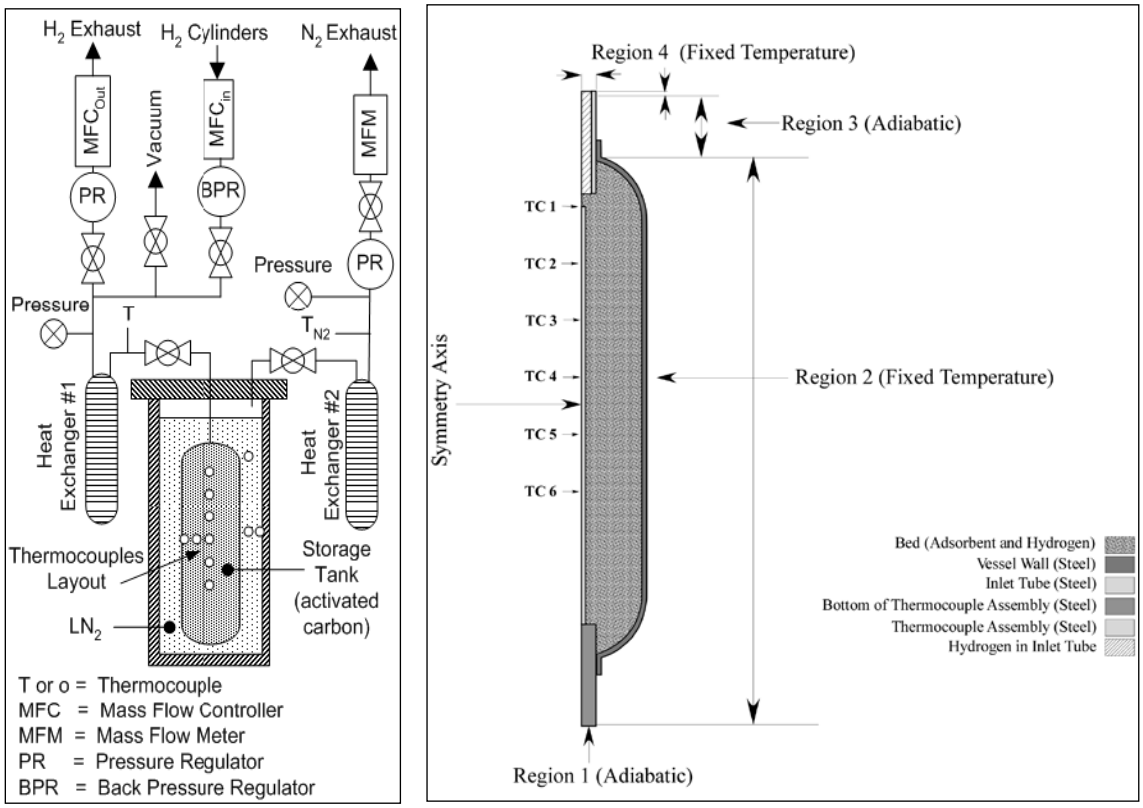

Figure 102. A schematic of the UQTR experimental apparatus is shown at left. The system represented in the model, including composition and boundary conditions is shown on the right.[241]

The initial vessel pressure was 1.82 bar and the initial bed and vessel temperatures were approximately 79K. Hydrogen was fed to the vessel at approximately 16 SLPM at a temperature ranging from 290 to 296K, over the approximately 1600 s duration of the charging transient. The measured liquid nitrogen temperature of approximately 80K was the boundary condition for Region 1 in Figure 102, while an adiabatic boundary condition was applied for Region 2.

Figure 103 shows the measured and predicted temperatures for the axial thermocouples, TC1, TC2, TC3 and TC6. Because the temperatures for thermocouples TC4, TC5 and TC6 were very close, the temperature profiles for thermocouples TC4 and TC5 were omitted to clarify the graph. The greatest difference between predicted and measured temperatures occurred for TC2. Differences between predicted and measured temperatures tended to decrease for TC3 through TC6. Overall differences between temperatures from the model and data are similar to those in Paggario, et al.[249] which also compared a model and data for cryogenic hydrogen adsorption on activated carbon.

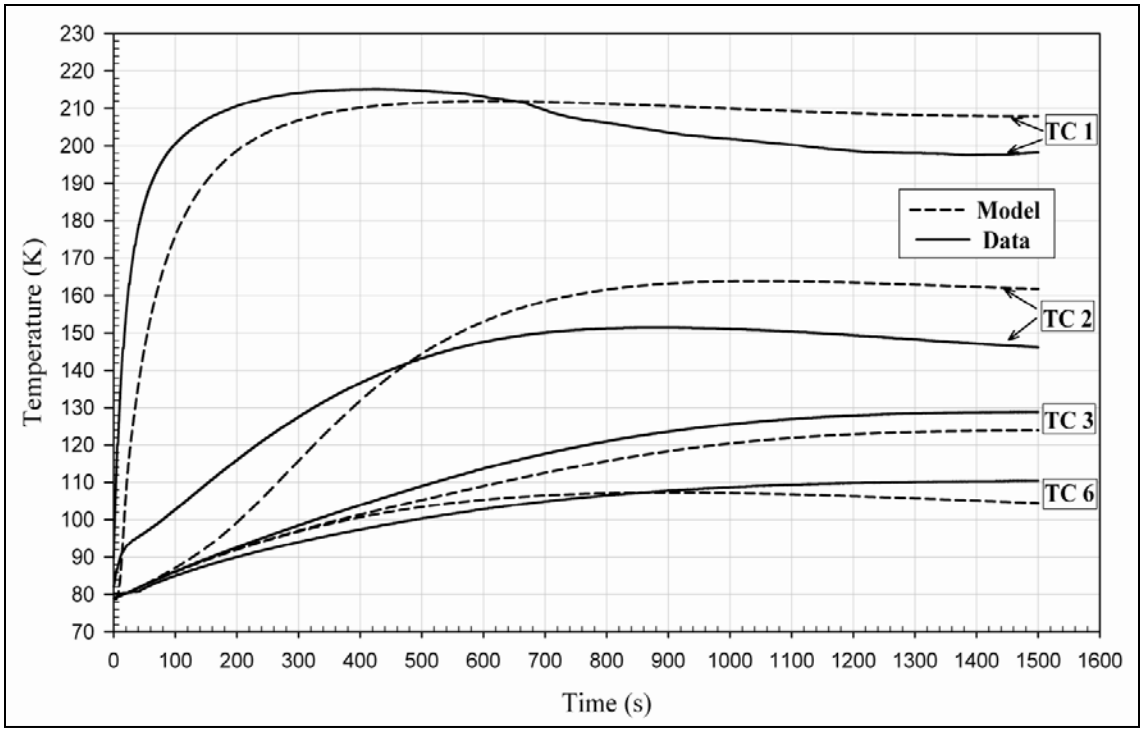

Figure 103. Validation of model against low temperature data.[241]

Major contributors to the observed differences included:

1. **Boundary conditions on the vessel.**
    a. The model was found to be very sensitive to boundary conditions applied to the wall of the tank that contained the adsorbent.
    b. In the experiments, nitrogen was added to the Dewar before charging and boiled off without replacement during the charging process. Therefore, the location of the interface between gaseous and liquid nitrogen changed during the charging transient, moving downward along the wall of the storage vessel. The moving interface, together with boiling heat transfer and convection resulted in a very complex thermal boundary condition at the surface of the storage vessel. Convection heat transfer from the storage vessel to the liquid and gas phase nitrogen occupying the Dewar was extremely difficult to characterize. Further, correlations for this type of convection heat transfer are not available.

2. **Variation in the bulk bed density.**

   The density of the MaxSorb™ likely varied within the vessel. This would affect local heat generation rates, specific heat capacity (ρC_p), thermal contact resistance and bed thermal conductivity. Also, if the bed density were reduced above and along the thermocouple assembly, it would enhance the transport of hot gas fed to the vessel; especially along the upper part of the thermocouple. If this occurred, it would explain the rapid initial temperature rise observed for TC1 and TC2; indeed, scoping calculations showed that this could occur.

3. **Parasitic heat transfer through the metal thermocouple support.**

   It was known (see the reference by Richard et al.[248]) that heat leaks to the ambient existed. While the amount of heat leakage was established in the reference, sufficed for a global energy balance, more precise information is required for the detailed model.

4. **Scoping calculations**

   Scoping calculations have shown that, as expected, the model was quite sensitive to changes in the adsorbent thermal conductivity. In the validation models, the thermal conductivity of the adsorbent was given an approximate fixed value of 0.2 $\mathrm{W \cdot m^{-1} \cdot K^{-1}}$. It is known, however, that the adsorbent thermal conductivity decreases with decreasing temperature – but specific values were unavailable at the time this comparison was performed. Temperature gradients within the bed will therefore yield non-uniform bed thermal conductivities, which would impact heat transfer.

Total hydrogen concentrations calculated by the model are shown in Figure 104. The model had the ability to compute spatial pressure gradients within the vessel and indicated that the pressure was nearly uniform during the charging process. At 100s, the model predicted that the hydrogen concentration was lowest at the top of the adsorbent bed. This was due to the influx of gas at a temperature of approximately 290K, which reduced the amount of adsorbed hydrogen at that location. As the transient progressed, the amount of stored hydrogen increased. However, the heat released during the charging process resulted in elevated temperatures, and relatively lower amounts of stored hydrogen, in the interior of the bed. Higher hydrogen concentrations were predicted along the cold surfaces in the vessel, which includes the tank wall and the central thermocouple support. Lower temperatures occurred at the surface of the steel thermocouple support because it provided a path for heat transfer to the liquid nitrogen within the Dewar.

In summary, although the hydrogen adsorption model compared reasonably well with data, there were discrepancies attributed to experimental measurements and material property data. In the comparisons between the model and data, no attempt was made to "tune" input parameters to obtain a better fit. In the future, refinements to the experimental rig will be made to better control inlet hydrogen temperature and the surface temperature of the pressure vessel that contains the adsorbent. Specifically, the volume of the Dewar will be increased to ensure that the pressure vessel is always completely surrounded by liquid nitrogen, thermocouples will be used to more completely monitor vessel surface temperatures, and the inlet hydrogen temperature will be better measured and controlled. Further, the thermal conductivity of the adsorbent bed will be carefully characterized and implemented in a future data-model comparison.

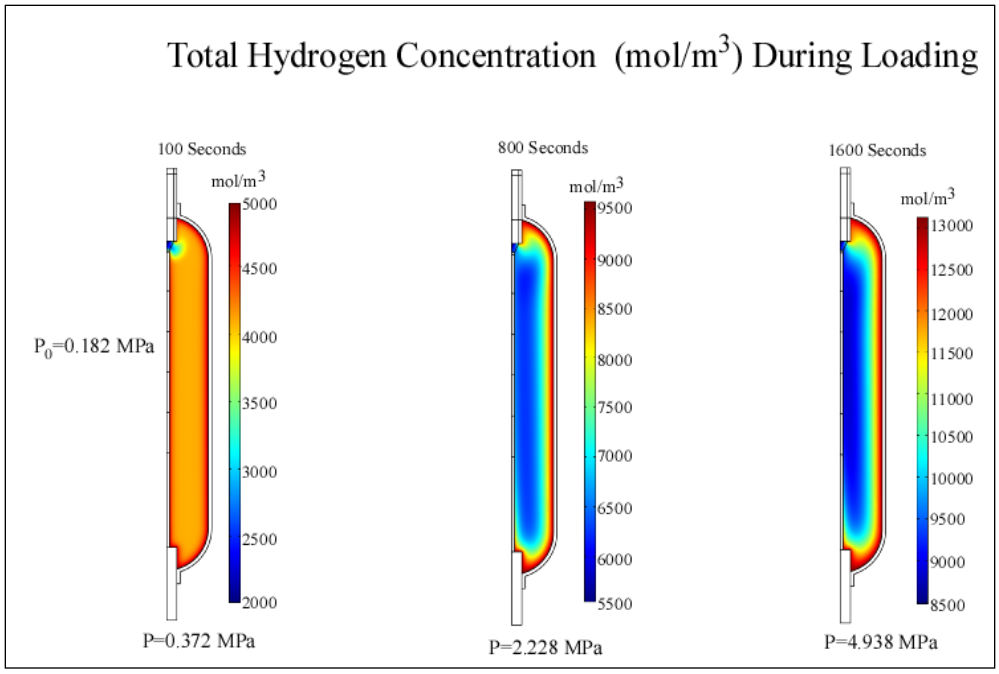

Figure 104. Hydrogen concentration profiles during the charging process. In this figure P_0 is the initial pressure and the initial temperature was 80K.[241]

The low thermal conductivity of MaxSorb™ and MOF-5™ in their nominal forms makes it difficult to use heat conduction alone to remove thermal energy released during the charging process. To make heat conduction a viable mechanism the adsorbent would require amendments such as expanded natural graphite to increase its thermal conductivity or closely spaced heat transfer surfaces would need to be incorporated into the vessel design to reduce the conduction transport length. Either way, the gravimetric and volumetric capacities of the system would be compromised by the addition of non-adsorbing material. An alternative method for heat removal is passing cold hydrogen through the bed to transfer heat by convection.[250,251] For this process, some hydrogen would be adsorbed and the remainder would be cycled through the bed and recovered, (see Figure 102-Figure 104). Because adequate hydrogen superficial velocity is required for the viability of flow-through cooling, the bed permeability must be high enough that the required flow can be attained for reasonable pressure gradients.

According to the 2015 DOE Technical Targets, a storage vessel must be charged with sufficient hydrogen to supply 5.6 kg of hydrogen to a vehicle's fuel cell in addition to hydrogen required to power support systems, such as pumps, heaters, etc. An integrated system model was used to estimate the total amount of required hydrogen which, with the vessel operating requirements, dictated the volume of the storage vessel, shown in Figure 105-Figure 107. The total amount of hydrogen available is that

recovered by transitioning the storage vessel from its initial state at full charge to its limiting final state. Both adsorbed and compressed gas phase hydrogen stored in the pores of the adsorbent are included in the total. The adsorbents, MaxSorb™ and MOF-5™, were assumed to be in nominal powder form and occupied a volume of 0.164 m^3. Prior to charging the storage vessel was assumed to be at 180K and 5 bar, which reflects its limiting state (highest allowed temperature and lowest allowed pressure) upon arrival at the fueling station. To enforce rapid charging of hydrogen the vessel pressure was raised from 4 to 200 bar in 20 seconds and the temperature of hydrogen entering the vessel was fixed at 80K. The average velocity of hydrogen exiting the vessel, for the purpose of cooling, was allowed to increase from 0 to 9 $m \cdot s^{-1}$ over a 2 second time interval, starting at 3 seconds after initiation of the charging transient. The vessel dimensions and geometry are shown in Figure 105-Figure 107, which also show the charging rate of total hydrogen, which includes the adsorbed hydrogen and compressed hydrogen in the void spaces of the adsorbent.

Figure 105 and Figure 106 show hydrogen charging rates for a vessel cooled by passing hydrogen axially through the adsorbent bed. Because the vessel wall participates in the transient by way of its thermal energy stored at the initial state, the effect of the heat capacity (ρC_p) was investigated. Figure 105 shows the effect of the heat capacity the vessel wall on the charging of a MaxSorb™ based vessel. Reducing the wall heat capacity can be seen to markedly affect the rate of hydrogen storage by reducing the initially stored amount of thermal energy that must be removed by convection.

Figure 106 shows the difference in the rate of hydrogen storage for MaxSorb™ and MOF-5™ based vessels, which are otherwise identical and are charged under the same conditions. From the plot, it can be seen that MOF-5™ charges more rapidly than MaxSorb™. The reason for the difference is that the lower heat capacity (ρC_p) of MOF-5™, due to its lower bulk density, results in a lower amount of stored thermal energy and, thus, a more rapid reduction in temperature. Because the temperature of the MOF-5™ bed is reduced more quickly, the hydrogen loading rate is increased.

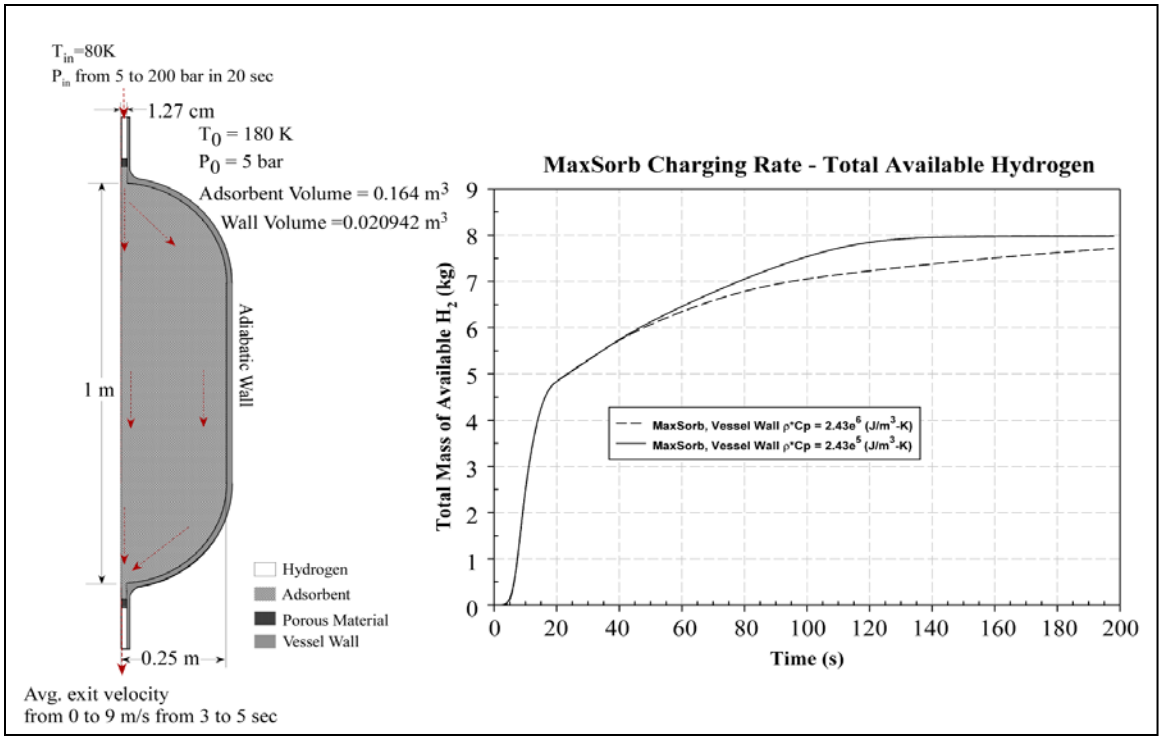

Figure 105. The effect of vessel wall heat capacity on charging rates for axial flow-through cooling of MaxSorb. The term 'available hydrogen' refers to the amount of hydrogen released upon return to the initial state.[241]

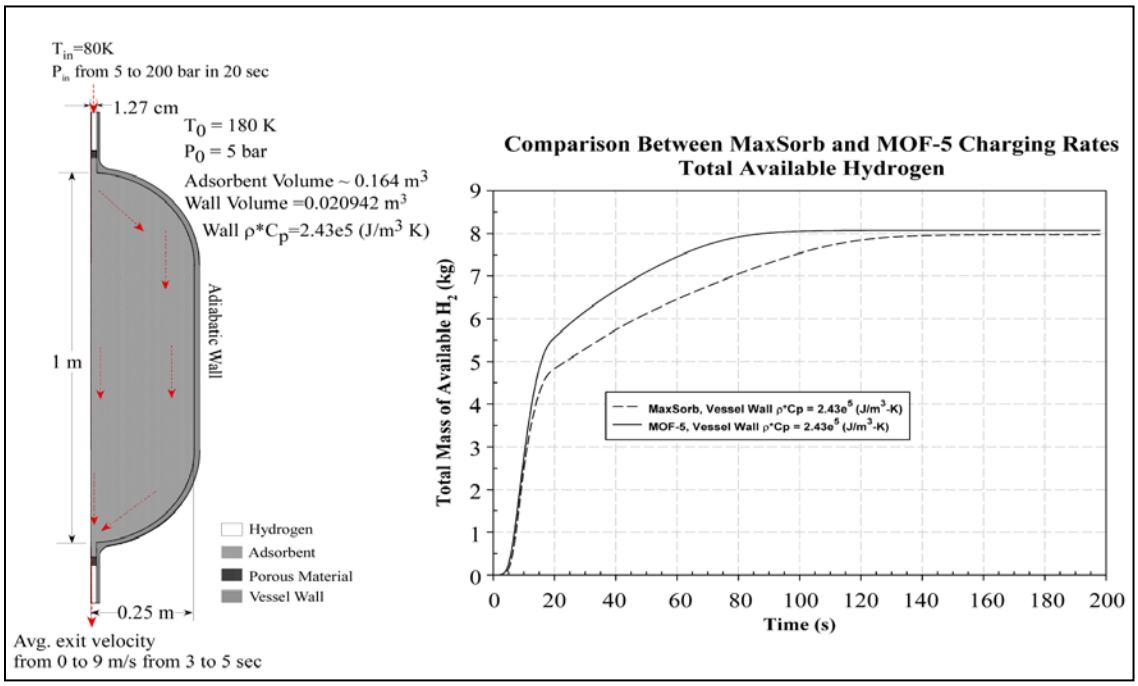

Figure 106. Comparison of charging rates for axial flow-through cooling of MaxSorb and MOF-5.[241]

Figure 107 compares MaxSorb™ charging rates for the axial and for radial passage of cooling hydrogen through the adsorbent bed. The assumed radial flow configuration is depicted in the schematic in Figure 107. Here, radial hydrogen flow was achieved by passing hydrogen through a porous rod, having a higher permeability than the bed, along the centerline of the vessel and out through a porous liner, composed of the same material, along the wall of the vessel. For this radial cooling configuration, charging was not quite as rapid as that obtained for axial flow.

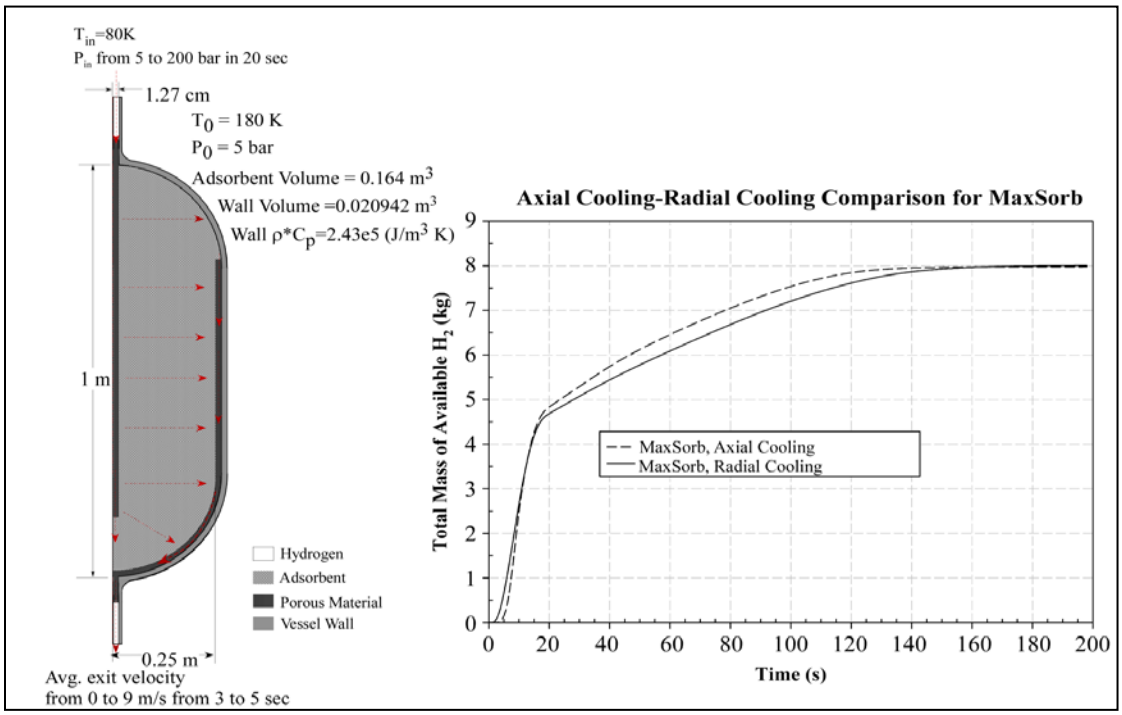

Figure 107. Comparison of charging rates for radial and axial flow-through cooling of MaxSorb.[241]

It has been noted that pressure work can make significant contribution to the heat released during charging.[252,253] The rate of heat generation by pressure work is:

Equation 91

$$-\varepsilon \frac{T}{c}\frac{\partial c}{\partial T}\frac{\partial P}{\partial t}$$

The rate of heat generation due to adsorption is:

Equation 92

$$-\rho_{Ads}\left[\frac{\partial}{\partial t}\left(\Delta U_a + n_a u_0\right) - h\frac{\partial n_a}{\partial t}\right]$$

Figure 108 shows the relative contributions of heat generation by pressure work and heat due to adsorption for MOF-5™ and MaxSorb™, in the axial flow-through system shown in Figure 106. The curves in Figure 108 show that the contribution of pressure work to the total heat generation can be significant. The relative significance of pressure work depends on: the ratio of gas stored in the adsorbed phase to that in the gas phase, the adsorbent thermodynamics and the change in pressure. During a transient, the rate of heat transfer will control the local temperature, which, in turn will make the ratio of pressure work to adsorption heat a function of time.

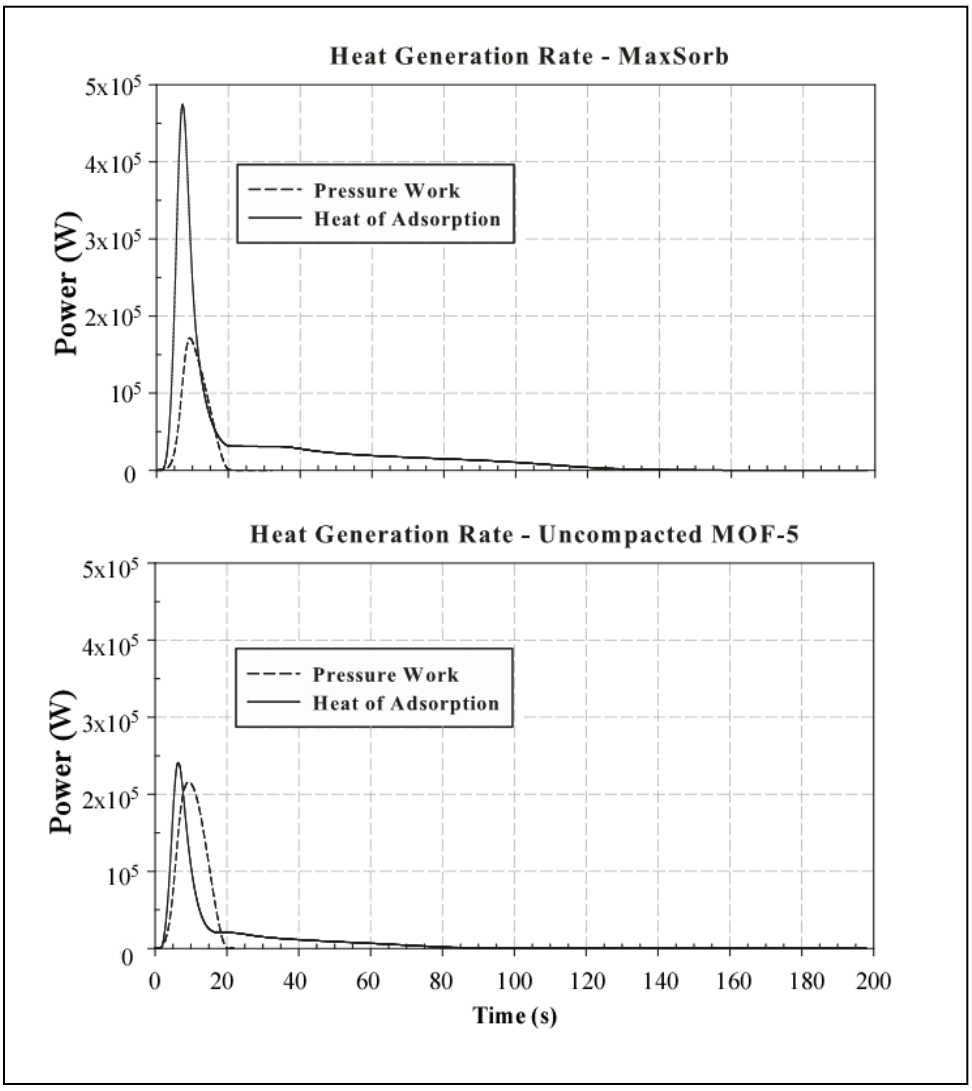

Figure 108. Relative contribution of pressure work and heat of adsorption for MaxSorb™ and MOF-5™. System configuration and operating conditions are those of Figure 106.[241]

Table 7 gives the total (integral) contribution of pressure work and heat due to adsorption for the MOF-5™ and MaxSorb™ systems over the charging transient. The operating condtiones (inlet and exit boundary conditions, internal flow geometry, initial conditions, and the mass of the vessel wall) are the same as for the calculation that generated Figure 105. All these factors affect heat dissipation within the vessel. Also shown in Table 7 are the quantities of available hydrogen stored in the adsorbed volume, V_a, and the gas phase volume.

	Total Pressure Work (MJ)	Total Adsorption Heat (MJ)	Total Available H_2 in Adsorbed Volume (kg)	Total Available H_2 in Gas Volume (kg)
MaxSorb™	1.39	4.81	4.57	3.15
MOF-5™	2.03	2.14	3.40	4.91

Table 7. Contribution of Pressure Work and Adsorption to Heat Generation.[241]

The mass of hydrogen exhaust from the vessel and its average temperature for the charging process assumed above, are shown in Table 8. The total mass of available hydrogen for each case in Table 8 is shown in Figure 105-Figure 107. To improve the efficiency of the flow-through cooling process it is desirable to minimize both the mass and average temperature of the exhaust gas, or more precisely to minimize its total enthalpy. Lower total enthalpy better facilitates mixing the exhaust hydrogen with cold hydrogen and using the mixture to initiate cooling and charging of another discharged vessel, which would be at an elevated temperature upon arrival at the fueling station.

	Charge Time (s)	Mass of Exhaust H_2 (kg)	Average Exhaust H_2 Temperature (K)
MaxSorb Low Wall ρC_p	140	17.9	133.67
MaxSorb Nominal Wall ρC_p	198*	27.51	120.06
MOF-5 Low Wall ρC_p	95	11.61	132.42
MaxSorb Low Wall ρC_p Radial Cooling	155	19.58	137.49

* Had not reached full capacity

Table 8. Exhaust Hydrogen Characteristics.[241]

As noted in the reference by Richard et al., the mass of hydrogen stored on a volumetric basis by an adsorbent exceeds that stored by compression alone up to a particular pressure.[248] Above this pressure, which depends on temperature, more hydrogen is stored by compression and the advantage of using an adsorbent is lost. The pressure at which storage by pure compression equals that by adsorption is called the breakeven pressure. In hydrogen storage applications the breakeven pressure is a design parameter used to determine whether it is advantageous to use an adsorbent rather than compression alone to store hydrogen.

For the flow-through cooling concept, the model was used to evaluate:

1. Concept viability,
2. Effect of vessel heat capacity and type of adsorbent,
3. Effect of radial or axial flow designs,
4. Relative importance of pressure work and heat release due to adsorption, and
5. State of exhaust hydrogen, which is a factor in the efficiency of the charging process.

Calculations for the flow-through system demonstrated the need to control the thermal contact between the adsorbent bed and the vessel wall and/or the heat capacity of the wall. It was found that, under certain conditions, pressure work could be a significant contributor to the total energy released, see Figure 108 and Table 7. At higher temperatures less gas is stored by adsorption. Therefore, during the charging process, the fraction of the total energy released due to pressure work increases with increasing temperature.

Figure 109 shows the total mass of stored hydrogen on a volumetric basis for MaxSorb™, MOF-5™ and compression for pressures up to 35MPa and temperatures of 70, 80, 90 and 100K. For the adsorbents, the concentration includes adsorbed hydrogen plus compressed hydrogen in the void volume. The compressibility factor from the NIST REFPROP database[247] is used in all calculations for this figure and the adsorbent storage is based on the Dubnin-Astakhov parameters for each of the adsorbents. At temperatures above 70K, the breakeven pressures for MOF-5™ exceed those for MaxSorb™. On a volumetric basis, MaxSorb™ stores more hydrogen than MOF-5™ until the MaxSorb™ breakeven pressure is approached. However, since the bulk density of MOF-5™ is half that of MaxSorb™ the capacity of MOF-5™ is greater on a mass basis. Recent unpublished work suggests that MOF-5™ can be compacted without significant loss of hydrogen storage capacity. If so, it may be possible for its volumetric capacity to be improved.

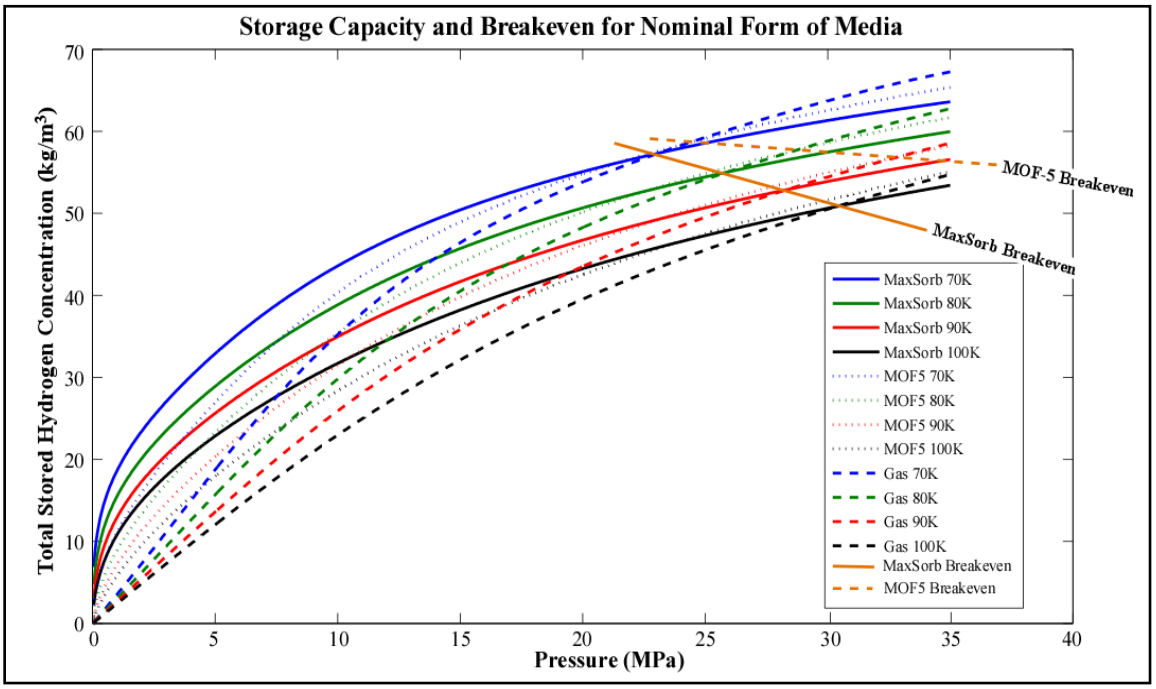

Figure 109. Storage capacity and breakeven curves for MOF-5 and MaxSorb.[241]

9 Options for Improving Thermal Conductivity

From Equation 5 (shown again below), it can be seen that thermal conductivity k is a function of a material's thermal diffusivity α, density ρ and heat capacity C_p.

Equation 93 $$k = \alpha \rho C_p$$

The diffusivity and heat capacity are intrinsic properties of the material. This leaves two options for improving thermal conductivity of hydrogen storage materials. The first is to increase the material's density. This is often done by compressing the storage materials (typically powders) into denser compacts. While this can be quite helpful in improving heat transfer, at some point compression is likely to decrease hydrogen storage capacity and/or kinetics. It is also possible that the material will not remain as a densified compact for long with repetitive hydrogen uptake and release cycling.

The second method is simply to add another material with higher thermal diffusivity or heat capacity to the hydrogen storage material. The problem with this approach is that the conductivity enhancing material generally does not contribute to hydrogen storage and so improves heat transfer at the expense of increased mass (lower gravimetric and volumetric storage capacities). This is typically done by adding a highly conductive light weight material such as expanded natural graphite (ENG) worms (i.e., natural graphite soaked in sulfuric acid and heated to high temperatures) [211, 254, 255, 256, 257, 258] or aluminum foams. Figure 110 shows a schematic diagram of a metal-hydride aluminum foam tank designed, built and tests by SRNL.[187,259,260,261,262]

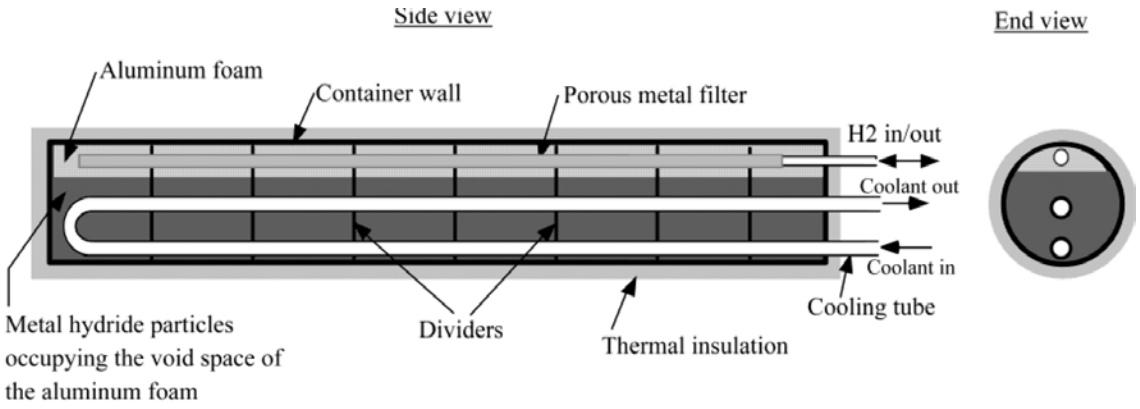

Figure 110. Schematic of the SRTC metal hydride hydrogen storage vessel.[255-262]

The following are some recent examples of materials and methods that have been used to improve and measure the thermal conductivity of different types of hydrogen storage materials.

9.1 Thermodynamic Improvements of On-board Reversible Hydride Materials

9.1.1 Introduction

The thermal conductivity of storage materials can have a strong impact on the design of materials-based hydrogen storage systems. This property of the material combined with the heat-transfer design of the system control the flow of heat and by consequence the rates of hydrogen release and uptake (in reversible systems). The heat of sorption will likely have a large impact on the heat load of the system, in particular for charging filling hydrogen in reversible systems. It has been reported that for the ideal reversible hydride system of an automobile the rapid fill requirements would require nearly 0.7 MW of cooling.[39]

Various methods have been employed to improve the thermal conductivity of hydrogen storage materials. These include:[39]

1) ***Coatings:*** Coating metal hydride pellets with high-conductivity ductile metals such as copper. [263,264,265,266] Conductivities as high as 9 $W \cdot m^{-1} \cdot K^{-1}$ have been reported for $LaNi_5$ coated with 25 wt.% copper.[264] However, the impact on capacity at high loadings as well as reduction hydrogen permeation and degradation on decrepitation are all challenges to the successful implementation of this method.

2) ***Sintering:*** The introduction of conductivity metals by sintering or alloying with hydride forming intermetallics has shown improvements in the over-all thermal conductivity of these materials. $LaNi_5$ sintered together with aluminum at up to 20 wt.% additions resulted in effective thermal conductivities of 10-33 $W \cdot m^{-1} \cdot K^{-1}$.[267,268,269,270] Again the same issues as those found for coatings apply to the applicability of this method.

3) ***Structures:*** The use of thermally conductive structures such as copper wire matrices[271], periodic plates[272], nickel foams[266], and to a large extent, aluminum foams[273] have been examined over the years. An example is presented below. One of the major difficulties of the foam structures has been the incorporation of powders into the foam matrix. This could be less of an issue for hydrides that can be deposited in the pores in vapor or liquid form. There is currently a lot of interest in incorporating hydrides into nano-porous materials with the hope of changing kinetics and also possibly thermodynamics. It would seem that, if successful, there would be an added advantage of improve heat transfer in systems where the matrix is a good thermal conductor.

4) ***Additives:*** The addition of thermal conductivity enhancers into powdered hydrogen storage materials has been receiving a lot of attentions. In particular, the addition of Expanded Natural Graphite (ENG) fibers has been the focus of several recent publications. ENG fibers are produce by exposing natural graphite to sulfuric acid and heating to high temperatures. These materials possess the advantages of high thermal conductivity, porosity, dispersibility and low cost, but have highly anisotropic, in-plane thermal conductivities (> 500 $W \cdot m^{-1} \cdot K^{-1}$ vs. through-plane of < 5 $W \cdot m^{-1} \cdot K^{-1}$). An example is presented in section 9.1.3 .

As we are mostly concerned with thermal conductivity measurements in this document, the focus has been on improving and testing the thermal conductivity of the storage materials. However this is only one aspect of achieving adequate heat transfer in the storage system. Many options exist for improved thermal conductivity in the materials, however, overall success of one method or another will depend on many factors including, compatibility of the storage, conduction and structural materials, impact on total storage capacity, impact on kinetics, flow rates, and reaction rates, the ability of combined materials to maintain enhanced properties over many cycles, etc.

9.1.2 Example: Hydrides in Aluminum Foam Matrix

An example of the possibility to improve thermal conductivity and hence recharging performance in a hydride bed is given in the modeling work by Couturier et al. [274] in that study a heat and mass transfer model was proposed for a 1 kg hydrogen tank based on $LaNi_5$ in an aluminum foam matrix. They found that it was heat transfer considerably more than gas transport or reaction kinetics that limited the hydrogen charging time.

In their study, the heat transfer inside the metal hydride bed was evaluated first as a function of the effective thermal conductivity of the metal hydride bed. The thermal conductivity k_{eff} was varied between 1.32 and 80 $W \cdot m^{-1} \cdot K^{-1}$ and the overall heat transfer coefficient from the bed to the cooling fluid between 10 and 100000 $Wm^{-2}K^{-1}$. The calculated amount of hydrogen absorbed after 5 minutes is displayed in Figure 111.

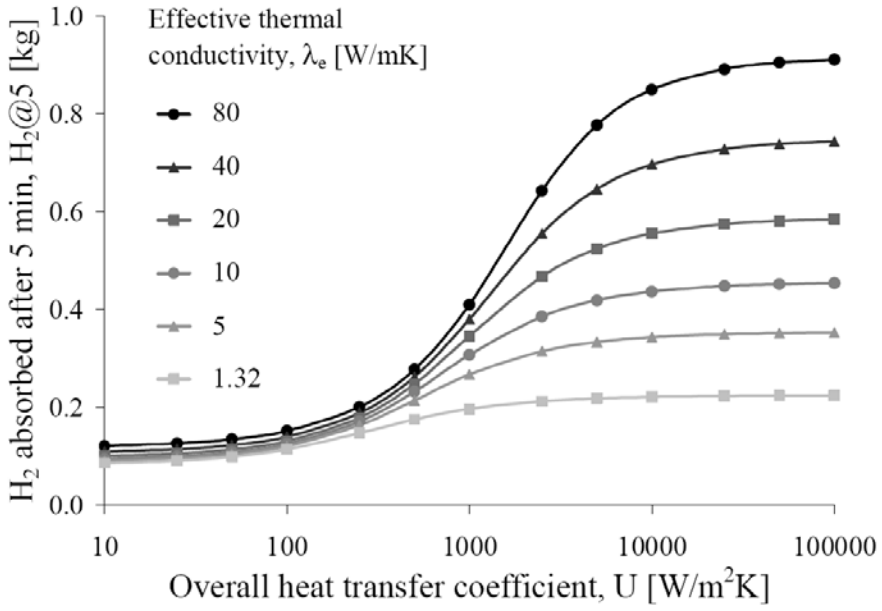

Figure 111. Influence of heat transfer.[274]

A base-line case was run for a reference storage tank, simulation is performed for an effective thermal conductivity of 1.32 $W \cdot m^{-1} \cdot K^{-1}$ and an overall heat transfer coefficient of 2500 $Wm^{-2}K^{-1}$. This led to an amount of 212 g hydrogen being absorbed in the tank after 5 minutes. They found that for this typical low value of the effective thermal conductivity within the bed, an improved overall heat transfer coefficient had little effect on the charging rate. At the other extreme of thermal conductivity and heat transfer coefficient, the model gave a charge of more than 900 g of hydrogen within the 5 minutes (the 2010 DOE target). They concluded that both the effective thermal

conductivity inside the metal hydride bed and internal heat transfer have to be maximized in order to decrease refueling to a reasonable time frame.

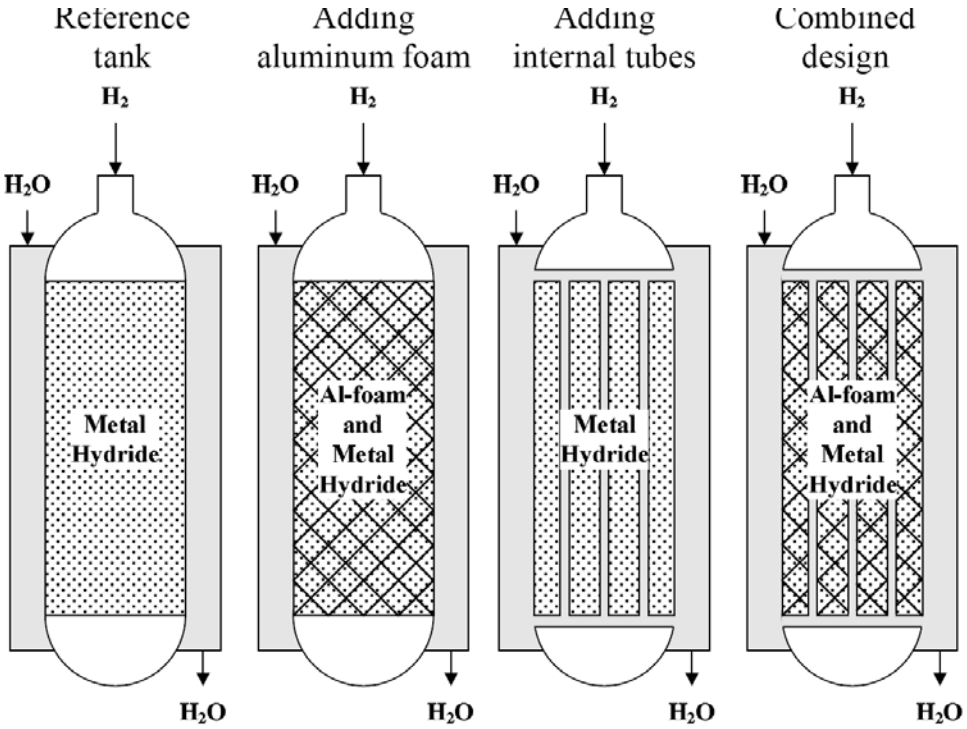

Figure 112. Design solutions to increase the heat transfer.[274]

Based on the need to increase both thermal conductivity within the material and heat transfer out of the tank, the authors of this example modeled hydride beds containing hydrides in an aluminum foam matrix, a fluid heat transfer system, and a combination of both as shown in Figure 112. The simulations were done using aluminum foam (bulk density 2700 kgm^{-3}) with high conductivity (237 $W \cdot m^{-1} \cdot K^{-1}$) and the addition of heat exchanger tubes inside the tank. The amount of hydrogen absorbed within 5 minutes was calculated with their model for the two separate solutions plus the combination of both.

The addition of aluminum foam in the metal hydride bed increases the effective thermal conductivity of the bed. Additionally, adding a chemically inert material reduces the heat produced per unit of volume, which is also beneficial for better hydrogen charging dynamics. However, higher tank volumes result in longer heat transfer paths, which can inhibit the hydrogen refueling process. Simulations were performed for volumetric fractions of aluminum $\boldsymbol{a}$, varying between 0.1 and 0.9. The volume V of the tank was:

Equation 94 $$V = \varepsilon V + (1-\varepsilon)(1-\alpha)V + (1-\varepsilon)\alpha V$$

where εV is the gas phase, $(1-\varepsilon)(1-\alpha)V$ is the $LaNi_5$ alloy, and $(1-\varepsilon)\alpha V$ is the aluminum. The effective thermal conductivity k_{eff} and effective volumetric heat capacity (ρC_p), of the bed were calculated based on Equation 94. Their analysis results are shown in Figure 113.

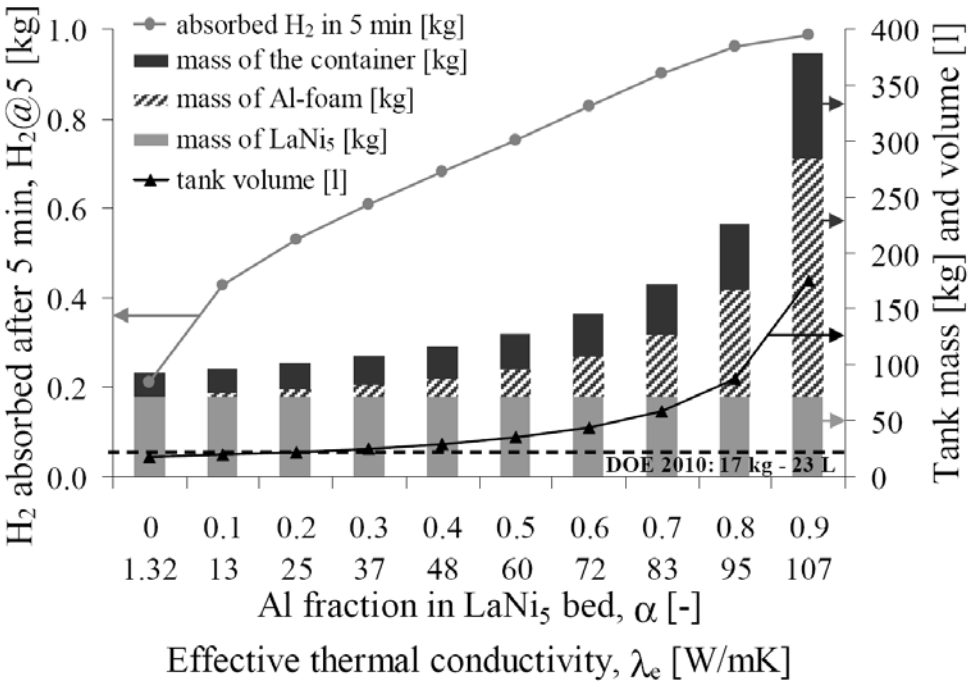

Figure 113. Influence of aluminum foam.[274]

It was found that the amount of hydrogen being absorbed within 5 minutes was strongly influenced by the amount of added aluminum foam. Comparing this with the change in thermal conductivity shown in Figure 113, it seems that the addition of aluminum foam resulted in a better performance. On-the-other-hand, the authors found a dramatic increase in the total mass of the tank with increasing aluminum addition over 0.6 (60% of the hydride mass). In this particular example the maximum DOE volumetric target at that time (23 liters) was reached at an aluminum volume fraction of 0.24.

9.1.3 Example: Alanates Mixed With Expanded Natural Graphite

In another example, an extensive work on complex hydrides with thermal conductivity enhancers was performed and a prototype hydrogen storage system developed by Sandia National Laboratories working together with General Motors using the complex metal hydride sodium alanate. Initial studies were performed on the thermal properties of sodium alanates to produce the data to carry out heat transfer analyses that was needed for designing the demonstration system.[275] The two most important thermal properties needed were the heat capacity and thermal conductivity of the sodium alanates in various states of hydrogen loading. The heat capacity value was estimated based on the constituents of sodium alanate, thermal conductivity, on-the-other-hand was determined experimentally.

In that work the thermal conductivity of sodium alanate was measured using the Thermal Probe Method based on ASTM D 5334.[110, 276] However, the thermal conductivity of sodium alanate was too low, even with excess aluminum, to perform adequately in the demonstration system design. Therefore, other methods for enhancing the thermal conductivity of the material were investigated as a part of that work.

Prior work on metal hydrides had shown that the addition of expanded natural graphite (ENG) fibers had increased thermal conductivities to as high as 10 $W \cdot m^{-1} \cdot K^{-1}$ with ENG mass fractions as low as 5%.[277] Therefore, in the Sandia/GM work, experiments were carried out to understand the mass fraction of ENG fibers required to give the required thermal conductivity when mixed with sodium alanate. To characterize the effective thermal conductivity of sodium alanates/ENG fiber mixtures, the group developed a new experimental apparatus along with modeling capabilities.

Figure 114 shows the results of their work.[275] The plot in the figure presents the effective thermal conductivity of sodium alanates mixed with ENG fibers at 5% and 10% mass loading compared to sodium alanates alone. The authors noted that the sodium alanates used contained excess aluminum. The relatively high baseline thermal conductivity values were ascribed to the presence of this additional aluminum. The measurements were conducted at different hydrogen content of the sample (x-axis). Thus, the thermal conductivity measurements covered the alanates in three states of decomposition, from the desorbed state of sodium hydride and aluminum, to the hexahydride and aluminum state, and finally to the tetrahydride with some excess aluminum. It can be seen that the thermal conductivity increases significantly on desorption (higher aluminum content) and that it is more than doubled by the addition of up to 10wt.% ENG.

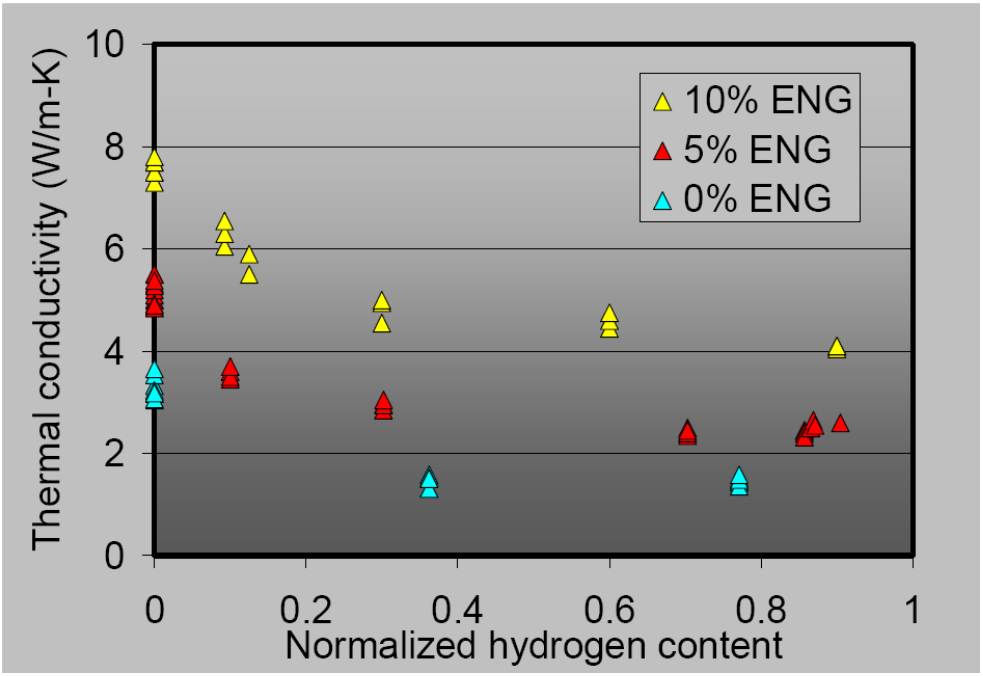

Figure 114. Effective thermal conductivity of sodium alanate/ENG mixtures.[275]

The data in Figure 114 were curve fit to a polynomial which was subsequently used in heat transfer model as part of the design of the demonstration system. The mathematical expression for this curve fit was represented by the following polynomial in the units of 10^{-2} $Wcm^{-1}K^{-1}$,

Equation 95 $$k(\psi, E) = 11.7\psi^4 - 32.5\psi^3 + 33.2\psi^2 - 14.8\psi + 40E + 3.4$$

where Ψ is the fractional hydrogen content (0-1, relative to 4.4 wt.%) and E is the weight fraction of ENG.

9.2 Thermodynamic Improvements of Physisorption Materials

Recently, a study was undertaken by Liu et al. to investigate MOF-5 composite materials with enhanced thermal conductivity.[211] In this work the authors synthesized MOF-5-based composites containing 1-10 wt.% of expanded natural graphite (ENG) worms (natural graphite soaked in sulfuric acid and heated to high temperatures) that were pressed into cylindrical pellets with densities of 0.3, 0.5, and 0.7 $g{\cdot}cm^{-3}$. They found that pellets of 0.5 $g{\cdot}cm^{-3}$ density 10 wt.% ENG had a factor of five improvement in thermal conductivity relative to neat MOF-5, increasing from 0.10 to 0.56 $W{\cdot}m^{-1}{\cdot}K^{-1}$ at room temperature.

In this study the thermal conductivities compressed pellets were determined at 26, 35, 45, 55 and 65°C by measuring the thermal diffusivity (α), the bulk pellet density (ρ), and the specific heat capacity (c_p) and using the equation

Equation 96 $$k = \alpha \rho c_p$$

The specific heat capacity measurements were performed on 6.35 mm diameter compressed pellets using a commercial differential scanning calorimeter (DSC) which was calibrated with a sapphire standard. The following important conditions were implemented in the measurements:

- MOF-5/ ENG mixtures were prepared by ball milling.
- Specimens were compressed in cylindrical punches and dies under the following conditions: A) 6.35 mm diameter for specific heat capacity and surface area measurements using a press which was housed inside a glovebox and B) 12 mm diameter for thermal diffusivity and XRD measurements outside of the glovebox with dry nitrogen gas was blown across the die set during pressing.
- Bulk densities were calculated from the mass and physical dimensions of each pellet.
- Pellets were placed inside an alumina crucible inside an airless glovebox and then transferred to the DSC external to the glovebox.
- Data was collected using a heating rate of 5°C·min^{-1} and a He carrier gas flow of 20 ml·s^{-1}.

Thermal diffusivity measurements were performed using a commercial xenon thermal flash diffusivity instrument. The following important conditions were implemented in the measurements:

- N_2 was used in the instrument as protective gas.
- Samples were made from pellets 12mm in diameter and 2mm average thickness.
- The instrument was calibrated using an iron standard.
- A thin layer of silver paint was applied to the top surfaces to prevent the pellets from fracturing during measurement.
- The lower surfaces of the pellets were coated with graphite to improve light absorption.

- Before the measurements, the pellets were degased by evacuating them at room temperature for at least 2 h and then heated at 130°C under vacuum for at least 3 h.

It was found that the presence of ENG may "protect" the MOF during compression. However, this protective effect appeared to cease with higher compacting pressures (density $\geq$ 0.7 g·cm^{-3}). At this density the pellets having higher ENG content exhibit lower surface areas relative to the neat MOF-5 pellet. At moderate densities (up to 0.5 g·cm^{-3}) and concentrations (up to 5 wt.%) ENG additions to MOF-5 do not significantly degrade hydrogen storage properties that are correlated with surface area (Table 9).

Hydrogen adsorption at 77 K by the MOF-5/ENG pellets with 0 wt.% and 10 wt.% ENG.

Description	Density (g/cm^3)	Max H_2 adsorption at 77 K (wt.%)
Powder MOF-5	0.13	5.64
0 wt.% ENG	0.31	5.76
	0.51	4.72
	0.603	4.17
10 wt.% ENG	0.324	4.75
	0.479	4.21
	0.716	3.49

Table 9. The maximum hydrogen excess adsorption at 77K by the MOF-5/ENG pellets with 0 wt.% and 10 wt.% ENG.[211]

The heat capacity of pellets of neat MOF-5 and MOF-5/ENG composites pellets were measured at temperatures of 26, 35, 35, 55 and 65°C and are plotted in Figure 115. The specific heat capacity at 26°C for MOF-5 with density of 0.3 g·cm^{-3} is 0.73 J·g^{-1}·°C^{-1}, and is comparable to that of graphite (0.71 J·g^{-1}·°C^{-1}). For a fixed density, the specific heat capacity was found to increase with increasing ENG concentration. The specific heat capacity of neat ENG is comparable to that of neat MOF-5, suggesting that the C_p of the MOF-5/ENG blends should not be altered relative to the neat MOF-5 compacts. A possible explanation given in this study for the observed increase in heat capacity with increasing ENG additions may be traced to ENG's ability to preserve the crystallinity of MOF-5 during the compaction process.[211]

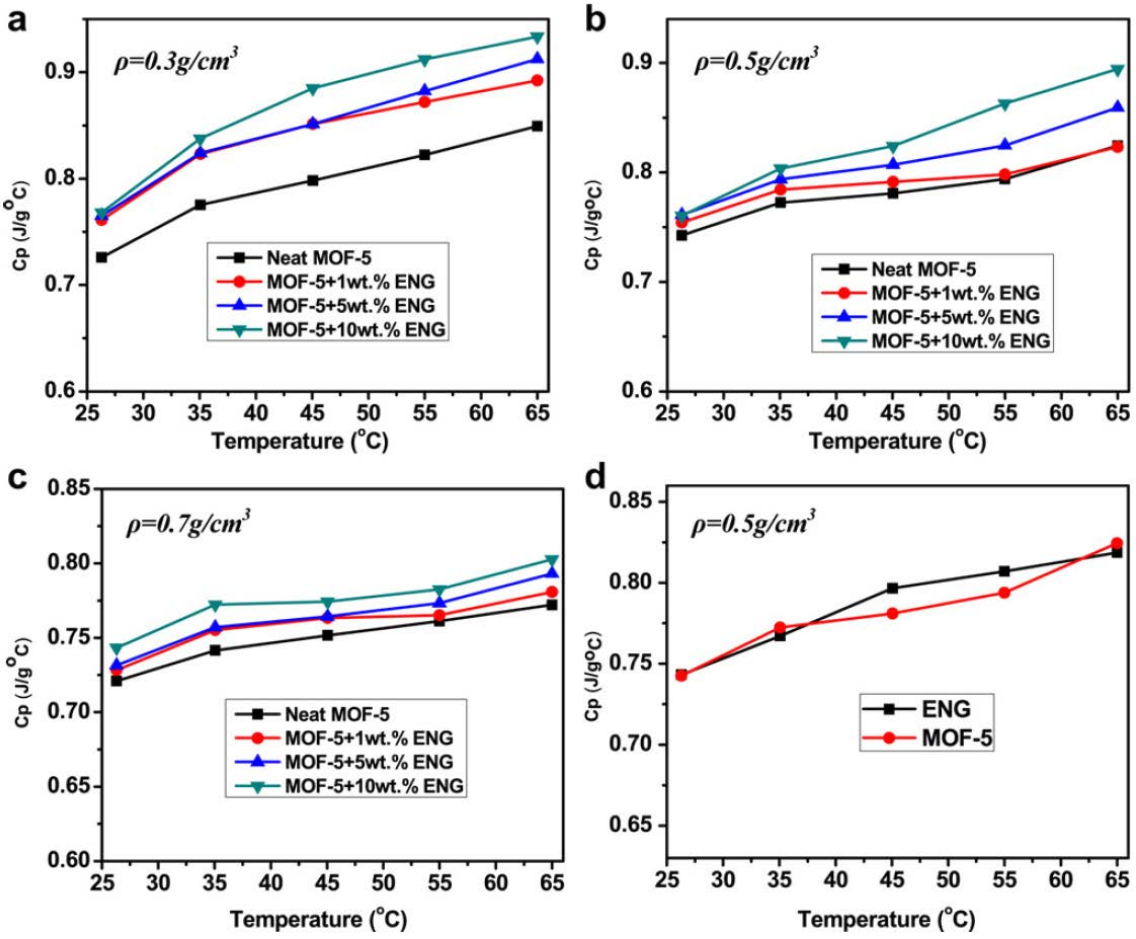

Figure 115. Specific heat capacity of pellets of neat MOF-5 and MOF-5/ENG composites as a function of density, ENG content, and temperature. (a)-(c) Pellets with densities of 0.3, 0.5, and, 0.7 g·cm^{-3}, respectively; (d) comparison of neat MOF-5 pellets with neat ENG pellets, both with density of 0.5 g·cm^{-3}.[211]

The thermal conductivity for compacts of MOF-5 and MOF-5/ENG composites were calculated based on Equation 96, and as a function of pellet density. These are shown in Figure 116. The neat MOF-5 pellets exhibit very low thermal conductivities independent of density. This study found that the ENG content to 5 or 10 wt.% resulted in a significant enhancement in thermal conductivity. The thermal conductivity at 26°C for the 0.5 g·cm^{-3} compact increases by factors of five upon addition of 10 wt.% ENG (0.56 W·m^{-1}·K^{-1}) a value that nearly doubles that obtained for single crystal MOF-5.[210,217] The thermal conductivities of the composite pellets showed only a weak temperature dependence over the narrow temperature range examined. Increasing pellet density also resulted in an increase in the thermal conductivity. An enhancement of more than 2.5 times was achieved (from 0.35 to 0.90 W·m^{-1}·K^{-1}) for composite pellets containing 10 wt.% ENG.

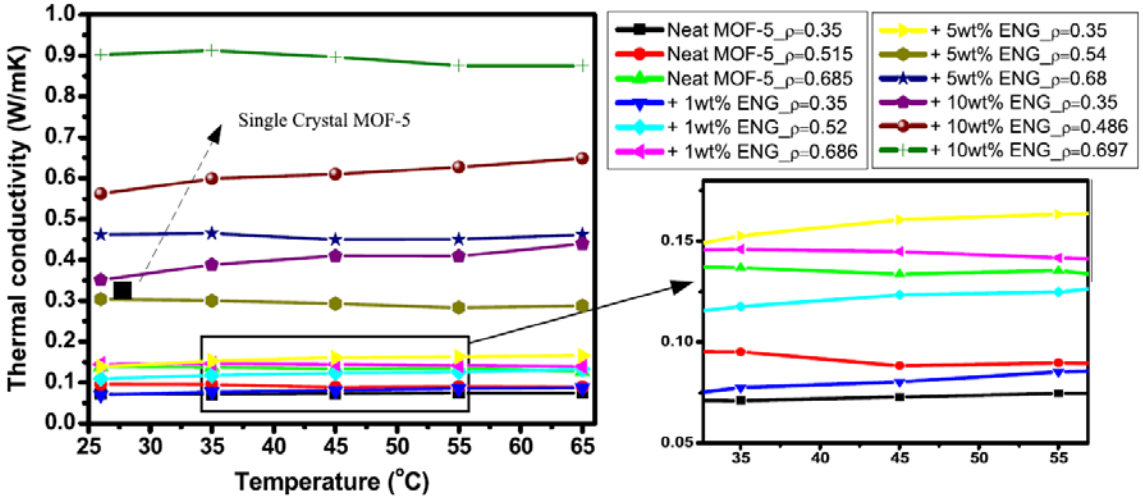

Figure 116. Thermal conductivity of pellets of neat MOF-5 and MOF-5/ENG composites as a function of density, ENG content, and temperature (T: 26-65°C).[211]

All of the combined results of the study indicated that, for densities up to 0.5 g·cm^{-3}, the addition of up to 10 wt.% ENG helps to preserve the crystallinity and surface area of MOF-5-based composites while significantly improving the thermal conductivity.

Heat Capacity

1 Introduction and Definitions

The heat capacity of a material is the property that quantifies the amount of heat required to change a substance's temperature by a specific amount. It is measurable physical quantity denoted by a capital C which is expressed in the International System of Units (SI) in units of joules (J) per degree kelvin (K). Heat Capacity itself is an extensive (scales with the size of system) property of a material. In many cases it is more convenient to report heat capacity as an intensive property (an intrinsic characteristic) of a particular substance. This is done by defining the related quantities: For pure homogeneous chemical compounds with established molecular or molar mass heat capacity as *Molar heat capacity*, which is the heat capacity per mole of a pure substance, and the *specific heat capacity* or *specific heat*, which is the heat capacity per unit mass of a substance (usually denoted with a small c). In some situations it is useful to specify the volume-specific heat capacity, commonly called volumetric heat capacity, which is the heat capacity per unit volume. This almost exclusively used for liquids and solids. With gases, the volumetric heat capacity may be confused with specific heat capacity at constant volume. Heat capacities of materials generally correlate to the number of atoms or particles in a sample and, therefore, when expressed in terms of a quantity related to the number of particles (i.e. Molar or Specific), the values tend to vary within a narrow range. Specifically:

1.1 Per Mole of Molecules

When the specific heat capacity, c, of a material is measured, different values arise because different substances have different molar masses. "Molar" heat capacity per mole of molecules, for solids, liquids and gases, produce values that are arbitrarily large because molecules can be arbitrarily large. Thus, specific heat capacities on a per mole of molecules-basis are thus not intensive quantities, and increase without limit as the mass of the molecule increases.

1.2 Per Mole of Atoms

On a per atom-basis, the heat capacity molecular substances rest within the range of 0 to $3R$ (where R is the gas constant). This is because heat is stored independently by each atom in a substance, not primarily by the bulk motion of molecules.

It is very important to specify whether measured values are on a mole-of-molecules basis or a mole-of-atoms basis. This is particularly true when comparing measured values with literature values.

1.3 Heat Capacity General Considerations

The heat capacity of most systems is not a constant. Instead, it depends on the state variables of the system under study. In particular, heat capacity is dependent on temperature itself, as well as on the pressure and the volume of the system.

When energy is transferred to a system as heat the temperature of the system generally increases. The relation between the amount of heat transferred and the temperature is of practical importance and it depends on the size, composition and mass of the system. For an infinitesimal transfer, the change in temperature is proportional to the heat transferred. The value of the ratio is the heat capacity and is defined by Equation 97.

Equation 97

$$\boldsymbol{C = \frac{\delta Q}{dT}}$$

Since δQ is not exact, C will depend on the path of transformation. Most transformations take place at either constant pressure or constant volume. When this distinction is important, a subscript p or V is added to indicate whether the heat capacity of a constant pressure or constant volume process is used, respectively. The heat required to bring a change of temperature dT is therefore $C_p\,dT$ or $C_V\,dT$ according to the constraints imposed on the system.

Heat capacity can be measured under various conditions. Typically measurements are made either under constant pressure (C_p) or in a constant volume (C_V). Gases and liquids are usually measured at constant volume. Note that, measurements that are made under constant pressure produce larger values than those at constant volume because the constant pressure values also include heat energy to do work to expand the substance against a constant pressure as its temperature increases. This difference is particularly important in measurements on gases where C_p values under constant pressure can be as much as 60% greater than those at constant volume.

The following are some important characteristics of the heat capacity of materials.

- Heat Capacity of any substance is positive.

- Heat Capacity is discontinuous at phase transitions.

- For solids and liquids, the Heat Capacity at constant Volume (C_V) and constant pressure (C_p) for any given substance are nearly equal. This means that for a liquid or a solid, the heat capacity doesn't depend on how you perform the heating.

• For a gas, the Heat capacity depends on how one does the heating. For an ideal gas, C_p is always greater than C_V by a constant value. For one mole of gas, the difference between C_p and C_V is the constant R (the universal gas constant) and represents the capacity of the gas to perform expansion work at constant applied pressure.

• The molar heat capacities of most metals around room temperature are all around 25 $J \cdot K^{-1} \cdot g^{-1}$. This is because the capacity to accommodate energy depends on the number of metal atoms.

• Specific heats of substances are sensitive to changes in temperature. However, the effect of temperature is negligibly small for the specific heats of monoatomic gases. Therefore, for monoatomic gases, such as argon, helium, etc., c_v = 12.5 $kJ \cdot kmol^{-1} \cdot K^{-1}$ and c_p = 20.8 $kJ \cdot kmol^{-1} \cdot K^{-1}$ may be used independent of temperature.

• Specific heats change slowly with temperature for diatomic gases, such as O_2, H_2, and N_2. Conversely, specific heats vary significantly with temperature for polyatomic gases, such as CO_2, CH_4, C_2H_6, etc.

Because specific heat capacities of substances comprising molecules are not fixed constants and vary somewhat depending on temperature, it is important that the temperature at which the measurement is specified. The following are examples for liquid water of common ways to cite the specific heat of a substance:

- Specific heat capacity (mass basis): c_p = 4.1855 [$J \cdot g^{-1} \cdot K^{-1}$] (15°C, 101.325 kPa)
- Molar specific heat capacity: $c_{v,m}$ = 74.539 [$J \cdot mol^{-1} \cdot K^{-1}$](25°C)

For liquids and gases the pressure at which the heat-capacity data was measured should be referenced. Most published data are for standard pressure, which has different definitions depending on the reference organization. The International Union of Pure and Applied Chemistry (IUPAC) updated its recommendation from one atmosphere to the round value 100 kPa (≈750.062 Torr).[278]

Measurement of the heat capacity at constant volume can be unreasonably difficult for liquids and solids due to the very large pressures required to maintain a constant volume. For this reason heat capacities of solids and liquids are usually measured at a constant pressure allowing the sample to change volume freely. This explains why experimental values of C_p are more accessible than C_V in spite of the fact that it is easier to predict theoretical values of C_V rather than those of C_p. This distinction can typically be ignored for simple analyses of solid hydrogen storage materials (excluding the gas phase).

1.4 Theory

The internal energy U of a closed system changes either by adding or removing heat Q from the system, or by the system performing work *W* or having work done on it. This is described by the first law of thermodynamics:

Equation 98 $$dU = dQ - dW$$

If work is performed as a result of compression or expansion of the system volume this expression becomes:

Equation 99 $$dU = dQ - PdV$$

Where P is pressure and V is volume. By definition, the *heat capacity* C of an object is the ration of heat introduced into a system to the change in temperature it causes:

Equation 100 $$C \equiv \frac{Q}{\Delta T}$$

However, because

Equation 101 $$Q = \Delta U - W$$

the heat capacity can be described for a number of physical conditions of an object or system including: constant V, constant P, constant P & V, ….

By definition the two most common heat capacities, at constant volume C_V and at constant pressure C_p are:

Equation 102 $$C_V \equiv \left(\frac{\partial U}{\partial T}\right)_V$$

Equation 103 $$C_P \equiv \left(\frac{\partial H}{\partial T}\right)_P$$

where H is the enthalpy of the process.

For example, if a process is performed at with the system held at a constant volume then *dV=0* and by Equation 99

Equation 104 $$C_V = \left(\frac{\Delta U - W}{\Delta T}\right)_V = \left(\frac{\Delta U}{\Delta T}\right)_V \equiv \left(\frac{\partial U}{\partial T}\right)_V$$

For a process with no change in kinetic or potential energy, in which work involves only a change in volume at constant pressure, H is given by:

Equation 105 $$H = U + PV$$

The change in enthalpy dH of the process given by:

Equation 106 $$dH = dU + d(PV) = dQ + VdP = dQ$$

since *dP=0*. Thus, from Equation 100:

Equation 107 $$C_P = \left(\frac{\partial Q}{\partial T}\right)_P \equiv \left(\frac{\partial H}{\partial T}\right)_P$$

Or, equivalently, from Equation 106 the heat capacity at constant pressure C_p is:

Equation 108 $$C_P = \left(\frac{\Delta U - W}{\Delta T}\right)_P = \left(\frac{\Delta U - \left(-P\Delta V\right)}{\Delta T}\right)_P \Rightarrow \left(\frac{\partial U}{\partial T}\right)_P + P\left(\frac{\partial V}{\partial T}\right)_P$$

The difference in these two heat capacities can be determined in terms of state variables P, V, and T.[279] Subtracting Equation 104 and Equation 108

Equation 109 $$C_P - C_V = \left(\frac{\partial U}{\partial T}\right)_{P,N} + P\left(\frac{\partial V}{\partial T}\right)_{P,N} - \left(\frac{\partial U}{\partial T}\right)_{V,N}$$

The fundamental thermodynamic relation expresses an infinitesimal change in internal energy U in terms of infinitesimal changes in entropy S, volume V, and pressure P for a closed system in thermal equilibrium is given by:

Equation 110

$$dU = TdS - PdV$$

Using Equation 109 and Equation 110 the difference in C_p and C_V becomes:

Equation 111

$$C_P - C_V = T\left(\frac{\partial P}{\partial T}\right)_{V,N}\left(\frac{\partial V}{\partial T}\right)_{P,N}$$

where the partial derivatives are taken at constant volume and constant number of particles, and constant pressure and constant number of particles, respectively.

This relationship can also be expressed in terms of the following materials properties:

The thermal expansion coefficient, α defined by:

Equation 112

$$\alpha = \frac{1}{V}\left(\frac{\partial V}{\partial T}\right)_{P,N}$$

The isothermal compressibility β_T defined by:

Equation 113

$$\beta_T = -\frac{1}{V}\left(\frac{\partial V}{\partial P}\right)_{T,N}$$

And the isentropic compressibility β_S defined by:

Equation 114

$$\beta_S = -\frac{1}{V}\left(\frac{\partial V}{\partial P}\right)_{S,N}$$

Such that:

Equation 115

$$C_P - C_V = VT\frac{\alpha^2}{\beta_T}$$

or

Equation 116

$$C_P - C_V = \frac{T}{\rho}\frac{\alpha^2}{\beta_T}$$

where ρ is the density of the substance under the applicable conditions.

The corresponding expression on a mass or mole basis (specific heat capacities, intensive properties) at constant volume and constant pressure remains the same since the thermodynamic system size-dependent quantities, whether on a per mass or per mole basis, cancel out in the ratio because specific heat capacities are intensive properties:

Equation 117

$$c_P - c_V = \frac{T}{\rho}\frac{\alpha^2}{\beta_T}$$

The heat capacity for solids at constant volume is not easily measured. The difference relation Equation 116 enables C_V to be determined from C_p which is much more readily measured.

The heat capacity ratio or adiabatic index is the ratio of the heat capacity at constant pressure to heat capacity at constant volume. It is sometimes also known as the isentropic expansion factor and is denoted as γ or sometimes as k.

Equation 118

$$\gamma = \frac{C_P}{C_V} = \frac{\beta_T}{\beta_S}$$

The ratio of heat capacities in Equation 118 allows one to express the isentropic compressibility in terms of the heat capacity ratio.

1.4.1 Heat Capacity of Ideal Gases

An ideal gas satisfies the following equation of state:

Equation 119

$$PV = nRT$$

where n is number of moles of gas in the thermodynamic system under consideration, and R is the universal gas constant. In addition, the internal energy is a function of temperature only. Therefore:

Equation 120

$$\left(\frac{\partial U}{\partial P}\right)_T = \left(\frac{\partial U}{\partial V}\right)_T = 0$$

Because U is only a function of T, from the first law (Equation 99) and the definition of C_V (Equation 102) one finds that:

Equation 121

$$C_V = \left(\frac{\partial U}{\partial V}\right)_T = \frac{\partial U}{\partial V}$$

and therefore:

Equation 122

$$dQ = C_V dT + PdV$$

From the ideal gas law, and considering a quasi-static process

Equation 123

$$PdV + VdP = nRdT$$

Reducing Equation 122 to:

Equation 124

$$dQ = (C_V + nR)dT - VdP$$

or

Equation 125

$$\frac{dQ}{dT} = C_V + nR - V\frac{dP}{dT}$$

At constant pressure this reduces to:

Equation 126

$$\left(\frac{dQ}{dT}\right)_P = C_V + nR$$

or by definition (Equation 107):

Equation 127

$$C_P = C_V + nR$$

or

Equation 128

$$C_P - C_V = nR$$

From the results for any material the difference in molar heat capacity at constant pressure and constant volume is (Equation 117);

Equation 129

$$c_P - c_V = \frac{T}{\rho}\frac{\alpha^2}{\beta_T}$$

Therefore, for an ideal gas;

Equation 130

$$R = \frac{T}{\rho}\frac{\alpha^2}{\beta_T}$$

Combining Equation 118 and Equation 128, one can determine heat capacities in terms of the heat capacity ratio γ.

Equation 131

$$C_V = \frac{R}{\gamma - 1} \quad \text{and} \quad C_P = \frac{\gamma R}{\gamma - 1}$$

The heat capacity ratio γ for an ideal gas can be related to the degrees of freedom *f* of a molecule by:

Equation 132

$$\gamma = 1 + \frac{2}{f} \quad \text{or} \quad f = \frac{2}{\gamma - 1}$$

Therefore for a monatomic ideal gas, with three degrees of freedom:

Equation 133

$$\gamma = \frac{5}{3} \approx 1.67$$

For a diatomic gas with five degrees of freedom (at room temperature: three translational and two rotational degrees of freedom; the vibrational degree of freedom does not contribute except at high temperatures):

Equation 134

$$\gamma = \frac{7}{5} = 1.4$$

This allows for the theoretical determination of heat capacities of ideal monatomic and diatomic gases.

1.4.2 Factors that affect specific heat capacity

The heat capacity of a system is directly proportional to the amount of substance it contains. Doubling the amount of substance in a system doubles its heat capacity. On a mass or mole basis the specific heat capacity of a system is a function of the structure of the substance.

Recalling that

Equation 135

$$C = \frac{Q}{\Delta T}$$

One can see that heat capacity of a material will be larger for a material that can store more heat for a given change in temperature. Another way to say this is that any kind of thermal energy that can be stored that does not contribute to temperature change will increase a material's heat capacity.

Heat can be stored as kinetic energy of atoms as they move and molecules as they rotate. But thermal energy may also be stored as potential energy associated with higher-energy modes of vibration of the particles in a substance. On-the-other-hand, it is only the average kinetic energy of particles in the substance that contributes to temperature change. Considering this, then it is a substance's ability to store thermal energy as potential energy that will raise the heat capacity of a substance the most.

The different modes of motion by which a substance can absorb thermal energy are known as its degrees of freedom. These include kinetic energy of translation and rotation, as well as, both the kinetic and potential energy of vibration of atoms. It is these degrees of freedom of motion which classically contribute to the heat capacity of atomic matter (loosely-bound electrons occasionally also participate). Only three translational degrees of freedom (corresponding to the three independent directions in space) are available for any individual atom, whether it is free, as a monatomic molecule, or bound into a polyatomic molecule. Molecules store potential energy in vibrational modes. Potential energy stored in these internal degrees of freedom contributes to a substance's energy content, but not to its temperature. The more internal degrees of freedom a substance has, the more the substance's specific heat capacity will increase, as long as temperatures are high enough to overcome quantum effects.

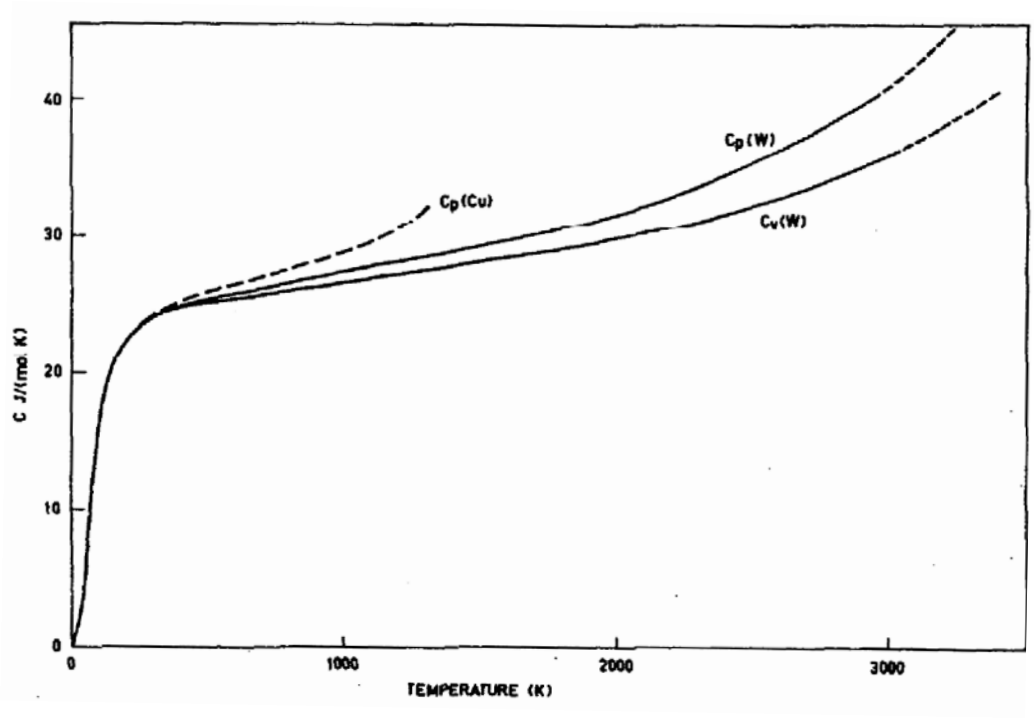

Figure 117. Measured heat capacity of standard reference materials: Copper at constant pressure and Tungsten at constant pressure and constant volume as a function of temperature. [280]

Dulong and Petit predicted in 1818 that the product of solid substance density and specific heat capacity (ρC_p) would be constant for all solids. This amounted to a prediction that volumetric heat capacity in solids would be constant. In fact, their experimental work showed that what was constant was the heat capacity of solids adjusted by the presumed weight of the atoms of the substance. This is known as the Dulong–Petit law. It shows that it is the heat capacity per atom (not per unit of volume) which is closest to being a constant in solids. Since that time, it has become clear that heat capacities per particle for all substances in all states are the same, to within a factor of two, so long as temperatures are not in the cryogenic range. For very cold temperatures, heat capacities fall dramatically and eventually approach zero as temperature approaches zero.

In a system (substance) composed of microscopic particle thermal energy is absorbed through the degrees of freedom accessible to each particle. At elevated temperatures, these degrees of freedom produce a specific heat capacity that classically approaches a value given by the Dulong-Petit law of about 24.9 joules per kelvin for each mole of atoms. In modern terms the Dulong-Petit law provides that, regardless of the nature of

the substance or crystal, the specific heat capacity of a solid substance equals $3R \cdot M^{-1}$, where R is the gas constant (measured in joule per kelvin per mole) and M is the molar mass (measured in kilogram per mole). While there are exceptions, the heat capacity per mole of many solids including most metals and simple crystalline solids is close to $3R$.

Specific heat capacities tend to fall at lower temperatures where thermal energy storage begins to be limited by quantum effects. Because of this, heat capacity drops towards zero as the temperature approaches absolute zero due to loss of available degrees of freedom.

1.4.3 Heat Capacity of Solids

As mentioned above, in 1819 Dulong and Petit discovered that many solids had a heat capacity of approximately 2.49×10^4 J·kilomole^{-1}·K^{-1} at room temperature. This phenomena was explained by considering every atom inside the solid as an oscillator with six degrees of freedom. The total thermal energy of a sample of matter or a thermodynamic system is consequently the average sum of the kinetic energies of all particles in the system. For a system of *N* particles each with *f* degrees of freedom its thermal energy is

Equation 136

$$U_{Thermal} = Nf(\tfrac{1}{2}k_B T)$$

where T is the temperature and k_B is the Boltzmann constant. The Boltzmann constant (k_B) is the gas constant *R* divided by the Avogadro constant N_A:

Equation 137

$$R = \frac{k_B}{N_A}$$

It has the same dimension (energy divided by temperature) as entropy.
Thus, for *f* = 6 of a solid, Petit-Dulong's results reduce to:

Equation 138

$$c_v = 3R$$

This limit of $3R$ per mole atom specific heat capacity is approached at room temperature for most solids. However, there are significant deviations for some solids composed of the lightest atoms which are bound very strongly, such as beryllium (where the value is only of 66% of $3R$), or diamond (where it is only 24% of $3R$).[281]

1.4.3.1 The Einstein Model of Heat Capacity of Solids

The Petit-Dulong relation breaks down as heat capacity decreases as temperature approached absolute zero. A model was initially developed by Einstein to explain this deviation in the heat capacity measurements at low temperature. Einstein made three assumptions in his model of the heat capacity of solids. These were that:

1) solids are composed of a lattice structure consisting of N atoms. Each atom moves independently in three dimensions within the lattice (3 degrees of freedom). Thus, the entire lattice's vibrational motion can be described by a total of $3N$ motions, or degrees of freedom.
2) the atoms inside the solid lattice do not interact with each other, and
3) all of the atoms inside the solid vibrated at the same frequency.

In Einstein's model the total energy for a system of N three-dimensional oscillators is:

Equation 139

$$U = 3NkT^2 \frac{\partial}{\partial T} \ln Z = N\left(\frac{1}{2}h\upsilon + \frac{h\upsilon}{e^{\frac{h\upsilon}{kT}} - 1}\right)$$

From which the heat capacity is derived to be:

Equation 140

$$C_V = \frac{\partial U}{\partial T} = 3N\frac{\partial}{\partial T}\left(\frac{h\upsilon}{e^{\frac{h\upsilon}{kT}} - 1}\right) = 3N\frac{1}{k}\left(\frac{h\upsilon}{T}\right)^2 \frac{e^{\frac{h\upsilon}{kT}}}{\left(e^{\frac{h\upsilon}{kT}} - 1\right)^2} = 3Nk\left(\frac{h\upsilon}{kT}\right)^2 \frac{e^{\frac{h\upsilon}{kT}}}{\left(e^{\frac{h\upsilon}{kT}} - 1\right)^2}$$

Where h is Planck's constant, k_B is Boltzmann's constant, and v is the oscillator frequency of the atoms inside the solid. [282] The term $h\upsilon/k = \theta_E$ is the Einstein temperature. The Einstein temperature indicates the probability that a molecule has in its degrees of freedom to store energy in its atomic oscillators (or bonds). In-other-words, the Einstein temperature points to the likelihood of a particle absorbing energy from a collision and converting that energy into stored heat or heat capacity. As the Einstein temperature increases, the greater the probability of a particle being excited to the next vibrational state and, therefore, the higher the specific heat. When the temperature is very large compared to the Einstein temperature the specific heat approaches $3R$ *(3Nk)*.

Equation 141

$$c_v \approx 3k = 3R$$

This is shown below Figure 118 in the calculated heat capacity of a solid using the Einstein model.

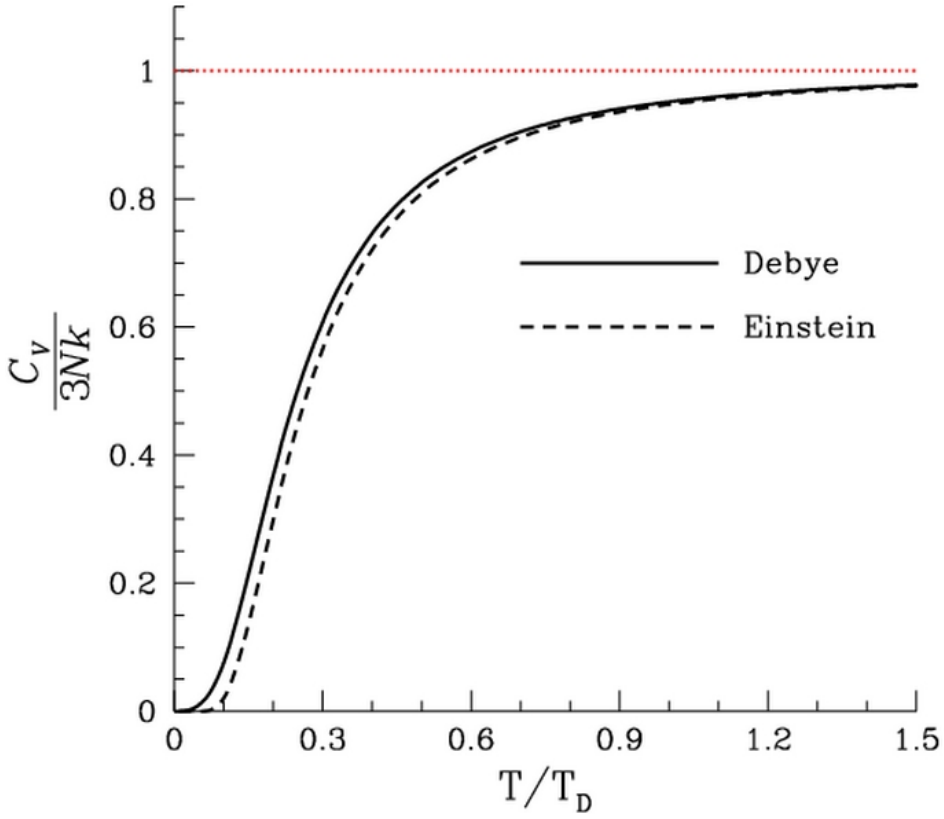

Figure 118. The dimensionless heat capacity divided by three, as a function of temperature as predicted by the Debye model and by Einstein's earlier model. The horizontal axis is the temperature divided by the Debye temperature (T_D or Θ_D). Note that, as expected, the dimensionless heat capacity is zero at absolute zero, and rises to a value of three as the temperature becomes much larger than the Debye temperature. The red line corresponds to the classical limit of the Dulong-Petit law.[281]

Thus, Einstein's model and the Petit-Dulong model approach each other at high temperatures accurately. However, the Einstein model allows for the heat capacity equation and the vibrational frequencies in the solid to change as the temperature changes which is not taken into account in the Petit-Dulong model.

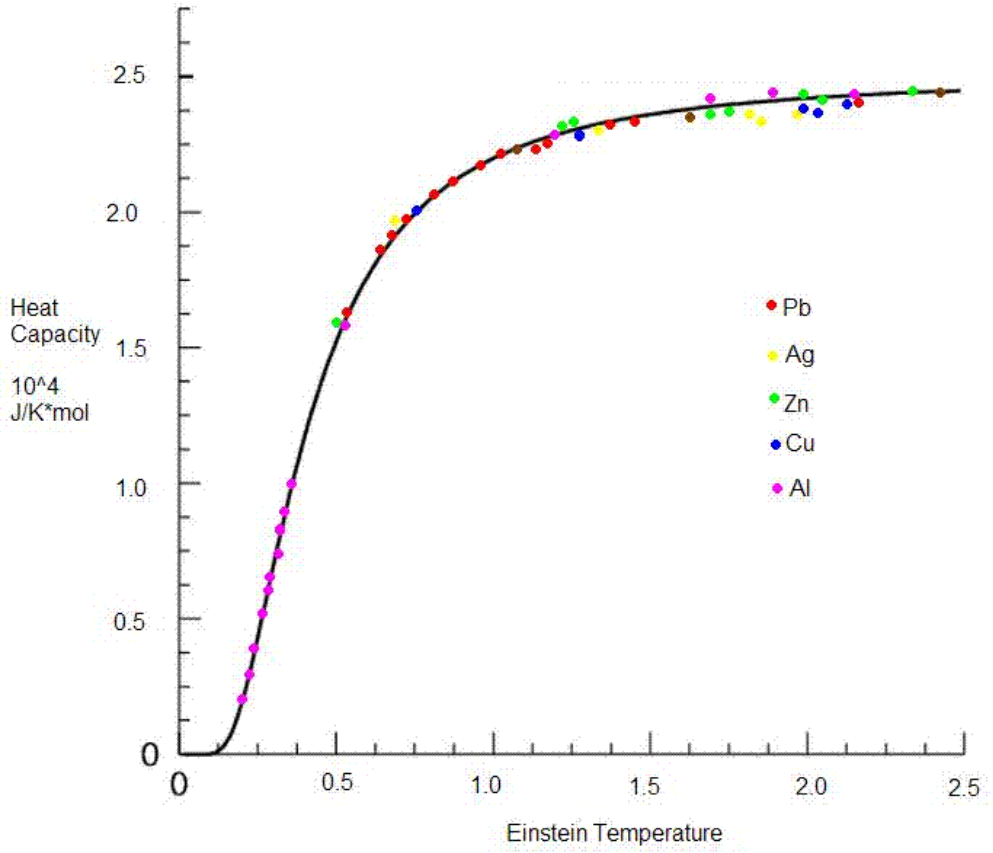

Figure 119. Graph of the heat capacity of several solid metals as a function of the Einstein Temperature $\theta_E = hv/k$.[282]

While Einstein's model is close to predicting low temperature heat capacities, it is not completely accurate. Below approximately 15K, Einstein's model deviates from experimental values. This can be seen in the plot of the specific heat of Pb at low temperature (Figure 119).

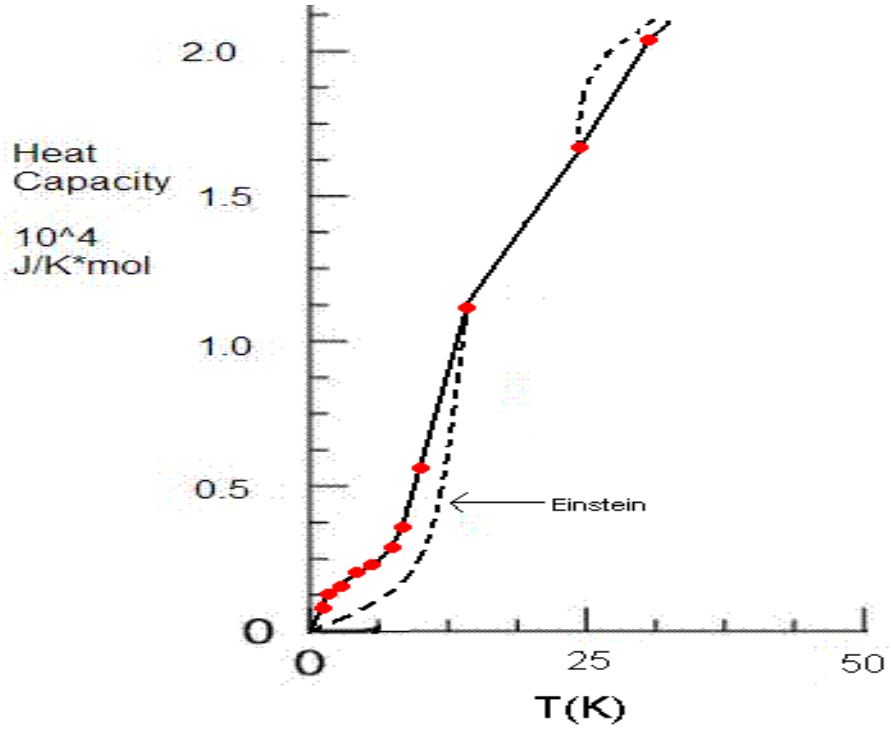

Figure 120. Graph of the heat capacity of lead compared to the expected values calculated from Einstein's model.[282]

The inaccuracies lie in the assumptions of the model. Einstein's first assumption has been shown to be accurate; however his second assumption is not. If atoms inside a solid do not interact sound could not propagate through it. Also if atoms in a solid do not interact, then heat could not propagate through solids.

1.4.3.1 The Debye Model of Heat Capacity of Solids

In fact, particles in a lattice do not vibrate independently. There exist collective modes of vibration. This can be evaluated as elastic waves propagating in the solid where the energy of the elastic wave of frequency ω is quantized. These quanta of elastic vibrations are called *phonons*. The Debye model was developed by Peter Debye in 1912 for estimating the phonon contribution to the specific heat (heat capacity) of solids. There is an upper limit of the frequency that can exist in the crystal. This *cut-off frequency* ω_D is known as the *Debye frequency*. The upper limit of the frequency exists because the wave-length in the lattice cannot be shorter than the shortest inter-atomic spacing. An equivalent reason is (as described above) the maximum possible number of vibrational modes in the crystal is equal to the number of atoms in the crystal N, times

3. Based on the propagation of energy as a wave in a crystal, with $\omega = v_s q$ and given the frequency limit, the heat capacity becomes:

Equation 142

$$C_v = \left(\frac{\partial U}{\partial T}\right)_V = \frac{3V}{2\pi^2 v_s^3}\frac{\hbar^2}{kT^2}\int_0^{\omega_D}\frac{\omega^4 e^{\hbar\omega/kT}}{\left(e^{\hbar\omega/kT}-1\right)^2}d\omega$$

or

Equation 143

$$C_v = 9R\left(\frac{T}{\Theta_D}\right)^3\int_0^{\omega_D}\left(\frac{\hbar\omega}{kT}\right)^4\frac{e^{\hbar\omega/kT}}{\left(e^{\hbar\omega/kT}-1\right)^2}d\omega$$

where, $\Theta_D = \hbar\omega_D/k$, is defined as the *Debye temperature*. This is the Debye model for the heat capacity of solids. It is shown for comparison with the Einstein model in Figure 118. The heat capacity is often plotted versus *reduced temperature* , $T^* = T/\Theta_D$. The Debye temperature contains the information about the particular crystal substance. The C_V curve is identical for all substances when plotted versus reduced temperature as in Figure 118.

The accuracy of the model can be evaluated by looking at the high and low temperature limits.

For $T >> \Theta_D,\ C_v = \left(\frac{\partial U}{\partial T}\right)_V \rightarrow \frac{1}{3}\left(\frac{\Theta_D}{T}\right)^3 = 3R$.

For $T << \Theta_D,\ \omega_D \rightarrow \infty,\ \text{and}\ C_v = \left(\frac{\partial U}{\partial T}\right)_V \rightarrow \frac{4\pi^4}{15} = \frac{12\pi^4}{5}R\left(\frac{T}{\Theta_D}\right)^3 \propto T^3$.

The Debye model does a good job of representing the experimental temperature dependence of the specific heat at high temperatures and also at low temperatures where the Einstein and Petit-Dulong models do not.

1.4.4 Heat Capacity of Liquids

The heat capacity of liquids is only rarely covered in statistical physics textbooks as well as books dedicated to liquids.[283,284,285,286,287,288,289] Among the three basic states of matter (solid, liquid, gas), liquids are least understood from a theoretical point of view. The interatomic, or intermolecular, interactions in a liquid are strong, and therefore strongly affect the thermal energy of liquids leading to large variations in specific heat.

However, the interactions are substance-specific which means that explicit knowledge of the interactions must be known to be able to calculate system energies. For this reason, it is argued that, in contrast to gases and solids there is no general expression for the energy of liquids.[289]

Solids and gases both have at least one thermal energy term that is small compared to others allowing for simplifications or corrections that enable accurate modeling of specific heats. The small atomic displacements in a solid make it possible to expand the energy in terms of phonons and obtain general expressions for heat capacity. Small interactions between molecules in gases make it possible to treat interactions as a perturbation and obtain general expressions for the corrections to the energy. Unfortunately, neither of these situations exists globally for liquids. Unlike solids, liquids possess large atomic displacements. And liquids with strong interactions and solid like densities cannot be modeled in the same way as gases.

Some experimental observations of the heat capacity of liquids is noteworthy.[290] For many simple liquids, the heat capacity per atom decreases from approximately $3k$ per atom at the melting point to about $2k$ at high temperatures.[291,292] Similar behavior has also been observed for complex liquids.[293]

From the theoretical viewpoint, liquids have been viewed to occupy an intermediate state between gases and solids.[290] Liquids are a fluid as are gases, intuitively appearing closer to gases in terms of their properties. However, except for close to the critical point, liquids have solid like densities and, like solids, can support shear waves at high frequencies.

Whether to treat real dense liquids from the gas or solid state theory has been a question with a long history.[283] Liquids have mostly been approached using kinetic gas theory with the addition of liquid interaction energy.[283,284,289] However, this approach relies on the knowledge of interatomic interactions as well as correlation functions which are generally not available.[294,295] Even when simple model systems are available they do not provide an adequate explanation of the experimentally observed decrease of heat capacity from $3k$ to $2k$ at high temperature.[290]

An alternative approach is to address liquids from the perspective of the thermal behavior of solids.[283] In this approach the liquid structure remains is unchanged, like a solid, during a short time τ. τ is a relaxation time that is defined as the average time between two consecutive local structural rearrangements in a liquid at one point in space. An important advantage of this approach is that strong particle interactions are included in the consideration from the outset. With a τ greater than the experimental time scale, a liquid becomes a solid for practical purposes.

Bolmatov and Trachenko have proposed that as far as energy and heat capacity are concerned, liquids can be understood on the basis of their solid like properties, consistent with Frenkel's general concept.[290] They have found good agreement between theoretical and experimental data of the heat capacity of liquids by relating liquid energy to τ. In addition, the original theory was harmonic. However, anharmonic effects are known to be particularly large in liquids, where the coefficients of thermal expansion considerably exceed those in solids.[296] Therefore, anharmonic effects were included in the approach to liquids from the solid state and compared with experimental data for five commonly discussed liquids by Bolmatov and Trachenko. They found good agreement between theoretical predictions and experimental data with no free fitting parameters.[290] Some results of that work are presented below in Figure 121.

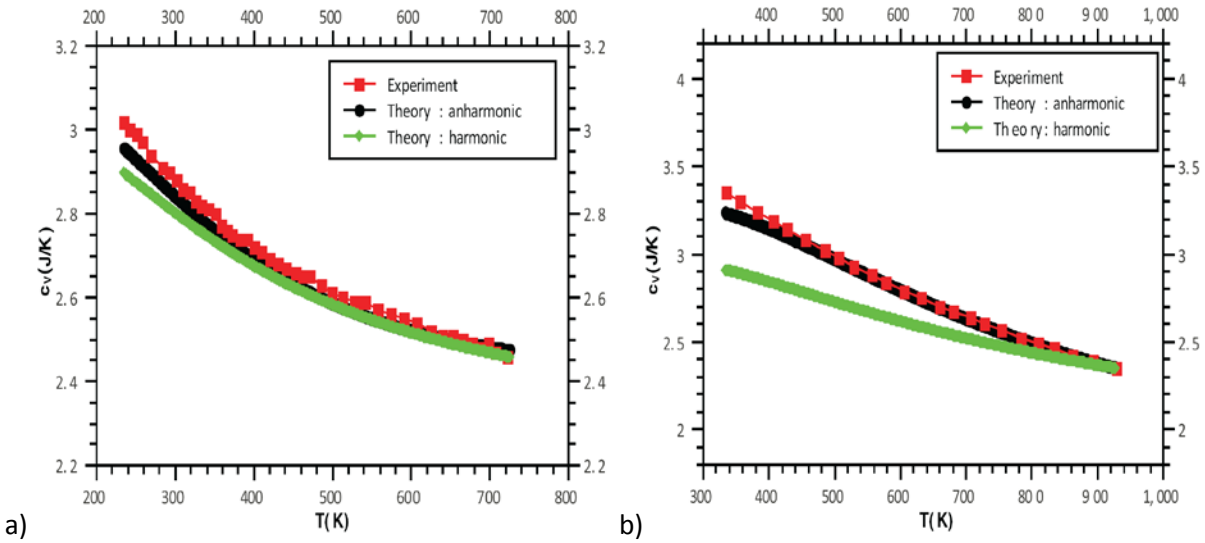

Figure 121. Experimental and theoretical c_v for liquid a) Hg and b) Rb. Experimental c_v is shown in red square symbols. Calculated harmonic and anharmonic c_v are shown in the green and black curves, respectively.[290]

1.4.5 Heat Capacity of Gases

Thermal energy in monatomic gases like Argon and Helium exists only as translational motion consisting of whole-body movements in 3D space where particles move around and exchange energy through collisions. This limited motion results in three translational degrees of freedom. The three translational degrees of freedom apply to all individual atoms, whether they are free monatomic molecules, or bound in a polyatomic molecule.

The energy of rotation of an individual atom (free or bound) about itself is proportional to the moment of inertia of the atom. This number is extremely small compared to moments of inertia of collections of atoms. Similarly, in diatomic gases the energy of axial rotation of the molecule can also be neglected as they occur around an axis with a moment of inertia too small to be able to store significant heat energy. On-the-other-hand, quantum energy levels for a rotating object is inversely proportional to its moment of inertia, and becomes very large for objects with very small moments of inertia. Thus, in monatomic gases essentially no thermal energy is stored through the rotation of atoms on their axes because the energy spacing of quantum levels is too large given the small moments of inertia. For polyatomic molecules, however, rotations around other axis may be available for storing thermal energy at ambient temperatures. Other internal vibrational degrees of freedom may also occur at higher temperatures.

On a per-atom or per-mole basis, the heat capacity of molecules can only exceed the heat capacity of monatomic gases through vibrational modes. For this reason, nearly two-times as much energy can be stored in a solid as compared to a monatomic gas for a given increase of temperature, due to the additional vibrational modes of atoms in the solid. As discussed earlier, the heat capacity in solids has a quantitative limit of about $3R$ (24.9 J·mole^{-1}·K^{-1}) per mole of atoms, where six degrees of freedom (three kinetic and three potential) are available to each atom. In-other-words, each of these six degree of freedom can contribute up to $½R$ per mole of atoms to the specific heat capacity. For gases, on-the-other-hand, the heat capacity never falls below the minimum of $^{3}⁄_{2}R$ per mole of atoms, because the kinetic energy of gas molecules is always available to store at least this much thermal energy.

As the temperature approaches absolute zero, quantum effects heavily influence the ability to store thermal energy and heat capacity falls toward zero due to loss of available degrees of freedom. Quantum theory can be used to quantitatively predict specific heat capacities in simple systems.

Note, as discussed in the introductory section, it is very important to specify whether - measured specific heats are presented on a per-mole-molecule or per-mole-atom basis. For example, ideal gases have the same numbers of molecules per volume, so increasing molecular complexity will add heat capacity on a per-volume and per-mole-of-molecules basis, but on a per-atom basis, the specific heat may increase or decrease depending on whether the temperature is sufficient to store energy through atomic vibrational modes.

1.4.5.1 Monatomic Gases

For a monatomic gas, assuming no electronic or nuclear quantum excitations occur, each atom in the gas has only 3 degrees of freedom (translational motion). In a monatomic gas system with N atoms, each with $3N$ total degrees of freedom the heat capacity at constant volume is given by:

Equation 144

$$C_V = \left(\frac{\partial U}{\partial T}\right)_V = \frac{3}{2}Nk = \frac{3}{2}nR$$

Or on a molar basis:

Equation 145

$$c_V = \frac{C_V}{n} = \frac{3}{2}R$$

Thus, for monatomic gases, the specific heat is this minimum value of half of 3R ($^3/_2$R) per mole atoms due to loss of all potential energy degrees of freedom. The table below presents measured molar constant volume heat capacity for some monatomic gases.

Monatomic gas	$C_{V,\mathrm{m}}$ (J·mol^{-1}·K^{-1})	$C_{V,\mathrm{m}}/R$
He	12.5	1.50
Ne	12.5	1.50
Ar	12.5	1.50
Kr	12.5	1.50
Xe	12.5	1.50

Table 10. Experimental molar constant volume heat capacity measurements taken for each noble monatomic gas (at 1 atm and 25°C).[281]

Thus, the experimental heat capacities of the monatomic noble gases agrees well with this simple statistical mechanics-based explanation.

From Equation 128, the constant pressure specific heat capacity of a monatomic gas is given by:

Equation 146

$$c_P = c_V + R = \frac{5}{2}R$$

1.4.5.1 Polyatomic Gases

Small polyatomic gas molecules approach the $^3/_2R$ lower limit of monatomic gases. Most other polyatomic gases have heat capacities that are intermediate between $^3/_2R$ and the upper limit of $3R$ per mole of atoms of solids. Complex molecules exhibit higher values of heat capacity values. This is particularly true at higher temperatures for which all vibrational modes are available. In the limit, very large and complex gas molecules approaches the stored energy behavior of solids.

Diatomic Gas

For an ideal gas consisting of diatomic molecules are rotational and vibrational degrees of freedom in addition to the three translational degrees of freedom. As mentioned above, while there are three rotational degrees of freedom, only two have any significant contribution to heat capacity because the moment of inertia about the inter-nuclear axis is very small with respect to other moments of inertia in the molecule. Thus, there are three translational degrees of freedom, two rotational degrees of freedom, and one vibrational degree of freedom. Each rotational and translational degree of freedom contributes $½R$ to the molar heat capacity of the gas. Each vibrational mode will contribute $½R$ of kinetic energy and $½R$ of potential energy for a total contribution of R to the molar heat capacity. The combined degrees of freedom contribute the following to the molar constant-volume heat capacity for each diatomic molecule:

Equation 147

$$c_V = \frac{3}{2}R + R + R = \frac{7}{2}R$$

The table below presents measured molar constant volume heat capacity for some diatomic gases.

Monatomic gas	$C_{V,m}$ (J·mol^{-1}·K^{-1})	$C_{V,m}/R$
H_2	20.18	2.427
CO	20.2	2.43
N_2	19.9	2.39
Cl_2	24.1	3.06

Br_2 (vapor)	28.2	3.39

Table 11. Experimental molar constant volume heat capacity measurements taken for diatomic gases (at 1 atm and 25°C).[281]

From these measured values, it can be seen that a simple evaluation of heat capacity based on degrees of freedom does not necessarily explain the specific heats of these diatomic gases. One reason for this is that the stored energy in vibrational and to some degree in rotational modes are subject to quantum states. Assuming that molecules stay at the lowest (zero) quantum state for vibrational modes, the total molar constant volume heat capacity reduces to:

Equation 148

$$c_V = \frac{3}{2}R + R + 0 = \frac{5}{2}R$$

In general then the lighter diatomic molecules have c_v approximated by $^5/_2R$ and heavier diatomic gas molecules approach $^7/_2R$. As the temperatures rises and the quantum vibrational energy level spacing's become finer, allowing the 2 additional vibrational states to become active, all diatomic gases approach this $^7/_2R$ value.[297] Note that, on a mole-of-atoms basis, this is seven-sixths of the specific heat capacity of a monatomic gas. Thus, the additional vibrational modes of pairs of atoms allow a higher heat capacity per atom in a diatomic gas than can be achieved by a monatomic gas.

It is important to note that even though higher heat capacities per atom are achieved by gases as the temperature is increased, the values are still considerably lower than those found in solids (i.e. for a diatomic gas vs. solid: $^7/_2R$ compared to $2 \cdot 3R$). In general, solids are most efficient, on an atomic basis, at storing thermal energy.

1.4.1 The Heat Capacity of Selected Materials

The specific and molar heat capacity of selected materials is presented below in Table 12. The table demonstrates the variation the in the heat capacity of various solids and gases to provide an appreciation for the differences one may find in a hydrogen storage system.

Table of specific heat capacities at 25°C (298K) unless otherwise noted Substance	**Phase**	**(mass) specific heat capacity c_p or c_m J·g^{-1}·K^{-1}**	**Const. pressure molar heat capacity $C_{p,m}$ J·mol^{-1}·K^{-1}**	**Const. volume molar heat capacity $C_{v,m}$ J·mol^{-1}·K^{-1}**	**Volumetric heat capacity C_V J·cm^{-3}·K^{-1}**	**Cons. vol. atom-molar heat capacity in units of R $C_{v,m(atom)}$ atom-mol^{-1}**
Air (Sea level, dry, 0°C (273.15K))	gas	1.0035	29.07	20.7643	0.001297	~ 1.25 R
Air (typical room conditions[A])	gas	1.012	29.19	20.85	0.00121	~ 1.25 R
Aluminum	solid	0.897	24.2		2.422	2.91 R
Ammonia	liquid	4.700	80.08		3.263	3.21 R
Argon	gas	0.5203	20.7862	12.4717		1.50 R
Beryllium	solid	1.82	16.4		3.367	1.97 R
Chromium	solid	0.449	23.35			2.81 R
Copper	solid	0.385	24.47		3.45	2.94 R
Gold	solid	0.129	25.42		2.492	3.05 R
Graphite	solid	0.710	8.53		1.534	1.03 R
Helium	gas	5.1932	20.7862	12.4717		1.50 R
Hydrogen	gas	**14.30**	28.82			1.23 R
Iron	solid	0.450	25.1		3.537	3.02 R
Lithium	solid	3.58	24.8		1.912	2.98 R
Lithium at 181°C	liquid	**4.379**	30.33		2.242	3.65 R
Magnesium	solid	1.02	24.9		1.773	2.99 R
Methane at 2°C	gas	2.191	35.69			0.66 R
Nitrogen	gas	1.040	29.12	20.8		1.25 R
Oxygen	gas	0.918	29.38	21.0		1.26 R
Silica (fused)	solid	0.703	42.2		1.547	1.69 R
Silver	solid	0.233	24.9		2.44	2.99 R
Sodium	solid	1.230	28.23			3.39 R
Tin	solid	0.227	27.112			3.26 R
Titanium	solid	0.523	26.060			3.13 R
Tungsten	solid	0.134	24.8		2.58	2.98 R

Notable minima and maxima are shown in Bold. [A] Assuming an altitude of 194 meters above mean sea level (the world–wide median altitude of human habitation), an indoor temperature of 23°C, a dew point of 9°C (40.85% relative humidity), and 760 mm–Hg sea level–corrected barometric pressure (molar water vapor content = 1.16%).

Table 12. Heat Capacities of selected materials.[281]

Note that on a moles of *molecules* basis, high specific heats are obtained for high **molar** value materials such as paraffin, gasoline, water and ammonia. If, on-the-other-hand, specific heat is expressed per mole of *atoms* for these substances, none of the C_V values greatly exceed the theoretical Dulong-Petit limit of $3R$ = 25 J·mol^{-1}·K^{-1} per mole of atoms. Some solids at standard temperatures show large deviations from the Dulong-Petit law value of $3R$ (last column). These departures are usually due to low atomic weight plus high bond strength (as in diamond) causing some vibration modes to have too much energy to be available to store thermal energy at the measured temperature. For gases, the deviation from $3R$ per mole of atoms is generally due to one or both of two factors: (1) the inability of the higher quantum energy vibration modes in molecules to be excited at room temperature, and (2) the loss of potential energy degrees of freedom in small gas molecules because most atoms in the molecule are not bonded maximally in space to other atoms.

1.4.2 The Heat Capacity of Hydrogen

The behavior of the specific heat of hydrogen as a function of increasing temperature was extremely puzzling early in the 20th century (Figure 122). The molar heat capacity of molecular hydrogen not $^{7}/_{2}R$ at all temperatures as classical theory predicts. In fact it is about $^{5}/_{2}R$ at room temperature, as if it were a rigid molecule that does not vibrate. And it decreases to $^{3}/_{2}R$ at 60K, as if it can no longer rotate. At higher temperatures the molar heat capacity does increase, though it never quite reaches $^{7}/_{2}R$ before the molecule dissociates.

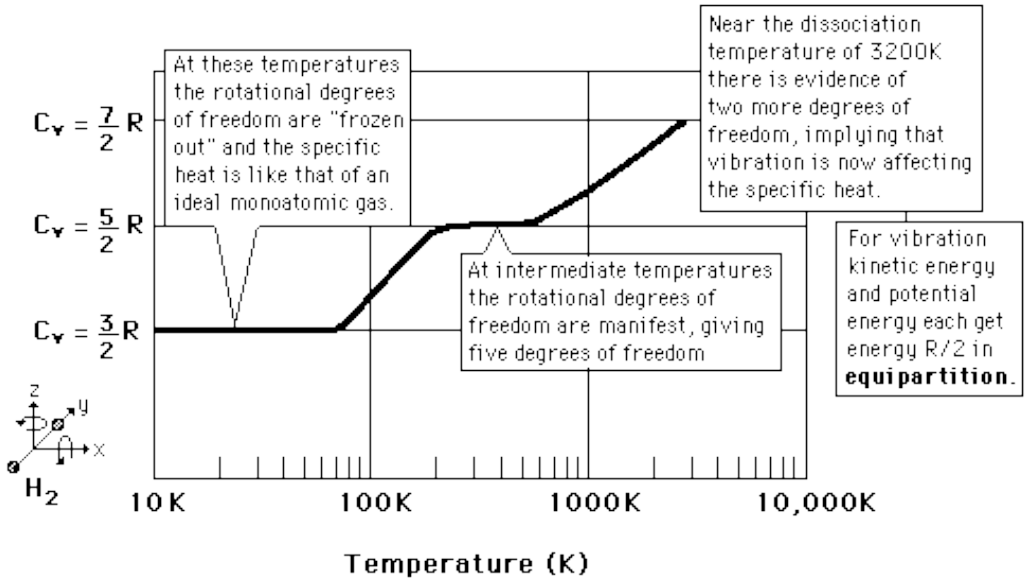

Figure 122. The specific heat capacity at constant volume of hydrogen as a function of temperature.[298]

Essentially, at low temperatures the specific heat behaves like a monoatomic gas, but at higher temperatures it has a value similar to other diatomic molecules. It took the development of the quantum theory to show that diatomic hydrogen, because of its small rotational inertia, required a large amount of energy to excite the first molecular rotation quantum state. At low temperatures this quantum state is not achievable and thus hydrogen acts like a monoatomic gas.

An example of measured values of the heat capacity at constant pressure for hydrogen as a function of temperature is shown in the figure below. Curve *A* represents the molecular heat capacity if the quantized rotational- vibrational levels above the minimum dissociation energy arc included as molecular levels, curve B represents the molecular heat capacity if the molecular levels are regarded as extending only up to the minimum dissociation energy, and curve C represents the model results of Davis and Johnston.[299]

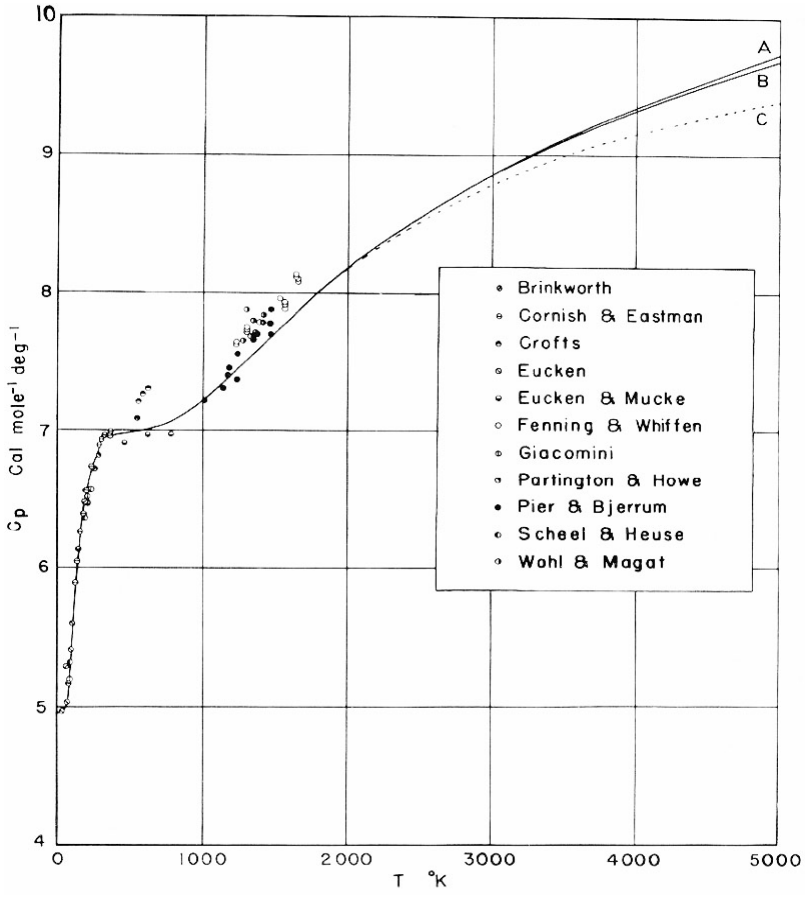

Figure 123. Graph of measured heat capacity at constant pressure (1 bar) of hydrogen as a function of temperature.[300]

The specific heats, c_s, at constant density of liquid and solid hydrogen and deuterium along the saturated vapor lines at low temperature are given shown in Figure 124.

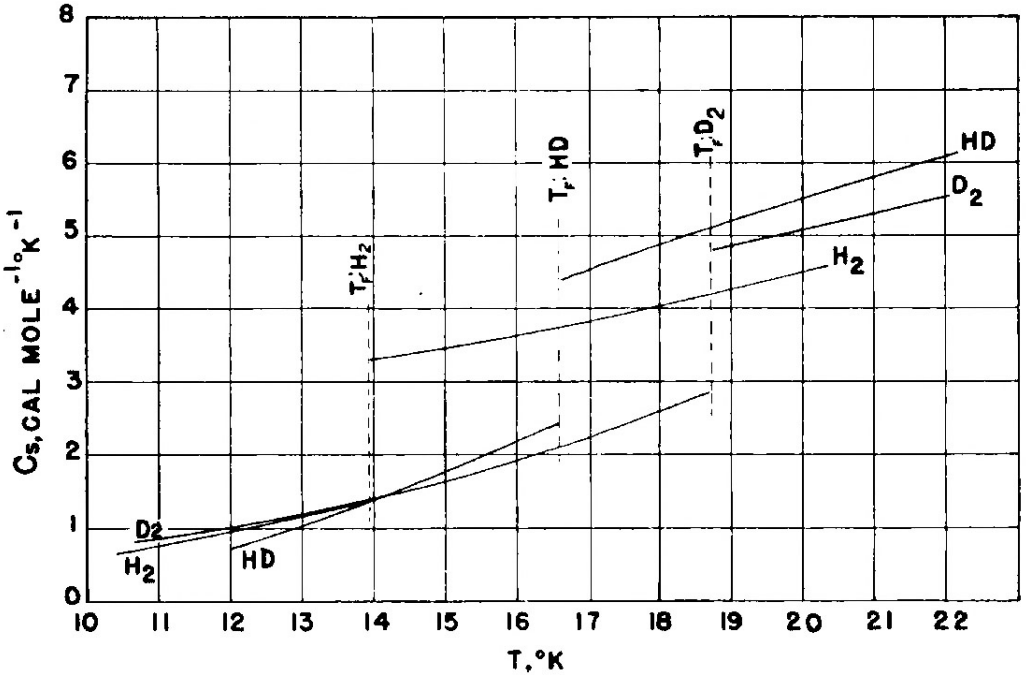

Figure 124. Specific heat, c_s of solid and liquid H_2, HD, and D_2.[300]

These plots are given for c_s the molar specific heat along a saturation curve rather than c_v, the molar specific heat at constant volume. The difference between c_s and c_v for hydrogen is large when compared with the differences for other substances having higher boiling temperatures. In general, (c_s – c_v) is large for low-boiling point substances because of their larger expansivity. The Debye temperature θ in the Debye specific heat function that fits the c_v data on solid H_2 is 105K, as compared with 91K for C_s.

Experimental data (dotted curves) and theoretical data for the specific heat, c_p of compressed liquid and gaseous hydrogen at low temperatures is presented in Figure 125. The full line curves apply only to the vapor and were obtained by calculation from the PVT correlations and specific heats in the ideal gas state. The heavy curve shows c_p for saturated vapor.

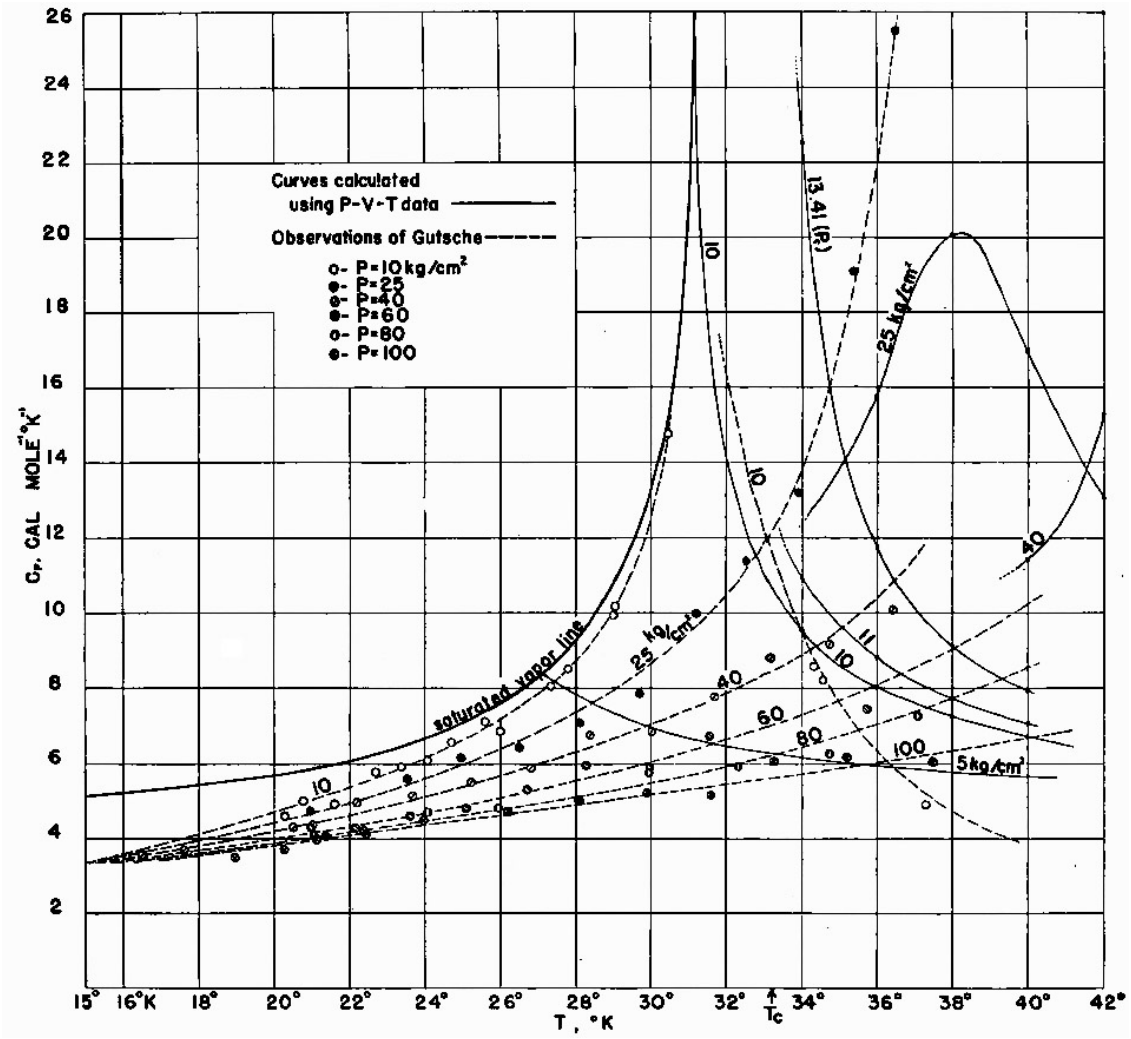

Figure 125. Specific heat, c_p of compressed liquid and gaseous H_2 at low temperatures.[300]

Calculated specific heat values c_v and c_p for hydrogen (normal) as a function of temperature and pressure are shown in Figure 126 and Figure 127 in respectively for reference. These were calculated using the NIST Reference Fluid Thermodynamic and Transport Properties Database software (REFPROP): Version 9.0.[301] These values can be compared with experimental data collected over a similar temperature and pressure range.[302] These figures demonstrate that c_v and c_p remain relatively constant with pressure above about 40K but can vary significantly on approaching the liquification temperature of hydrogen. Note also that c_v experiences much larger changes as a function of temperature than c_p. This is important as the system volume rather than pressure is constrained in hydrogen storage applications.

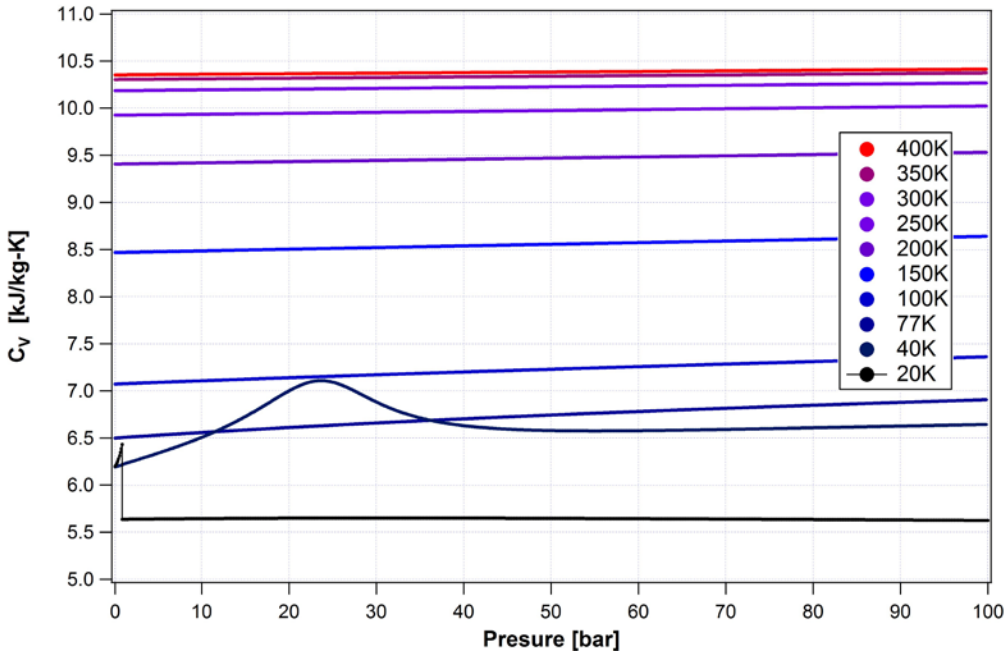

Figure 126. Calculated specific heat mass basis at constant volume, c_v of normal H_2 as a function of pressure and temperature.[303]

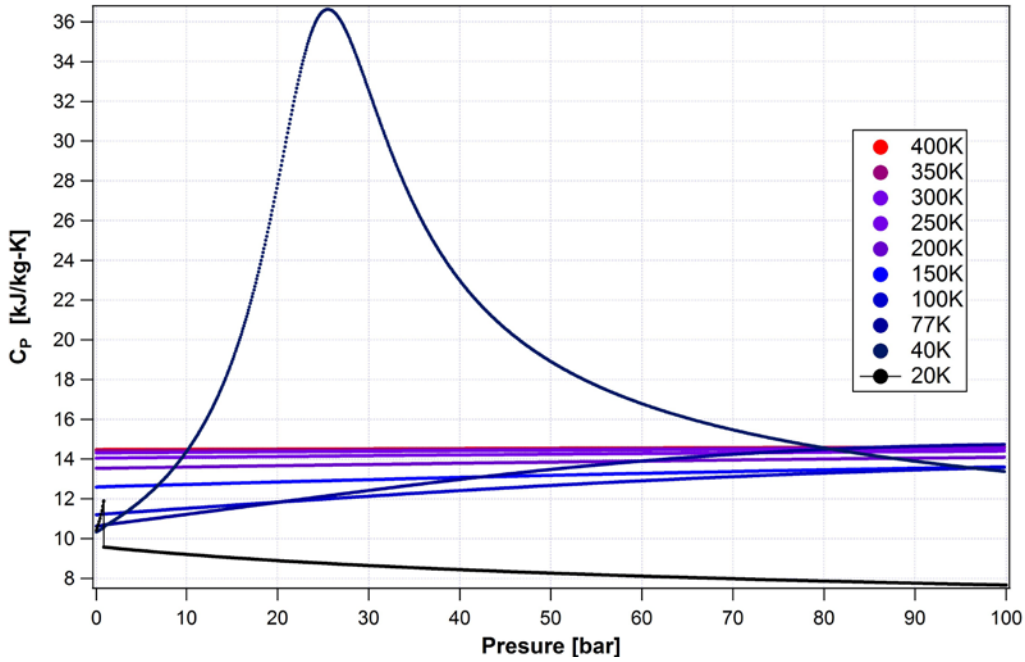

Figure 127. Calculated specific heat mass basis at constant pressure, c_p of normal H_2 as a function of pressure and temperature.[303]

1.5 Impact of Heat Capacity on Storage System Design

1.5.1 Heat Capacity of Hydrogen Gas on Filling

A temperature change will occur on filling a tank with compressed hydrogen gas alone, regardless of what storage material it may contain. This is also an important consideration in the engineering design of the storage system. Especially since the filling of a vehicular storage system is assumed to take place in a very short period of time (5 minutes or less). Neglecting heat transfer, in the most basic approach, the temperature change due to filling can be evaluated through the thermodynamics of an ideal gas.[304] When filling of an pressure vessel at an initial temperature (T_i) and pressure (P_2) from a constant temperature (T_1) and pressure (P_2) gas reservoir, the final temperature (T_2) is given by:

Equation 149

$$T_2 = T_1 \left\{ \frac{\left(\frac{P_2}{P_1}\right)}{1+\left(\left(\frac{P_2}{P_1}\right)-1\right)\left(\frac{T_1}{\gamma T_i}\right)} \right\}$$

Where γ is the ratio of constant pressure c_p and constant volume c_v specific heats. An interesting aspect of this formulation is that, for the case where ($T_i = T_1$), as the gas pressure difference increases without limit, the gas temperature rise approaches a fixed value given by the ratio:

Equation 150

$$T_2 = \gamma T_1$$

Thus, for example for hydrogen, the ratio of specific heats is 1.4, so the final temperature of the gas would be 150°C (1.4 x 300K) in filling an evacuated tank with high-pressure hydrogen at 27°C. Such a temperature increase may present serious system integrity issues. Equation 149 also leads to one inlet temperature (214K) being needed to maintain a constant gas temperature in the tank for all pressure ratios. These results do not take into account the real gas behavior or any heat transfer to the walls of the tank.

An iterative model was developed by James et al. which included real gas effects such as variable specific heats and compressibility, as well as transient heat transfer from the gas to the pressure vessel and from the pressure vessel to the surroundings through convection and radiation.[305] In that work, it was found that, although transfer from the tank to the surroundings was very small, the heat transfer from the hydrogen to the pressure vessel was quite large.

This is shown in Figure 128 where only a few degrees of temperature lag separate the vessel temperature from the gas temperature. However, this temperature rise may present a variety of problems:

1) it would require a higher peak pressure (464 bar) to assure complete filling of the tank when it cools back to a nominal (345 bar) pressure level,
2) advanced liner materials or the epoxy matrix material may degrade at these elevated temperatures
3) hydrogen storage materials may not react or behave as desired at these elevated temperatures.

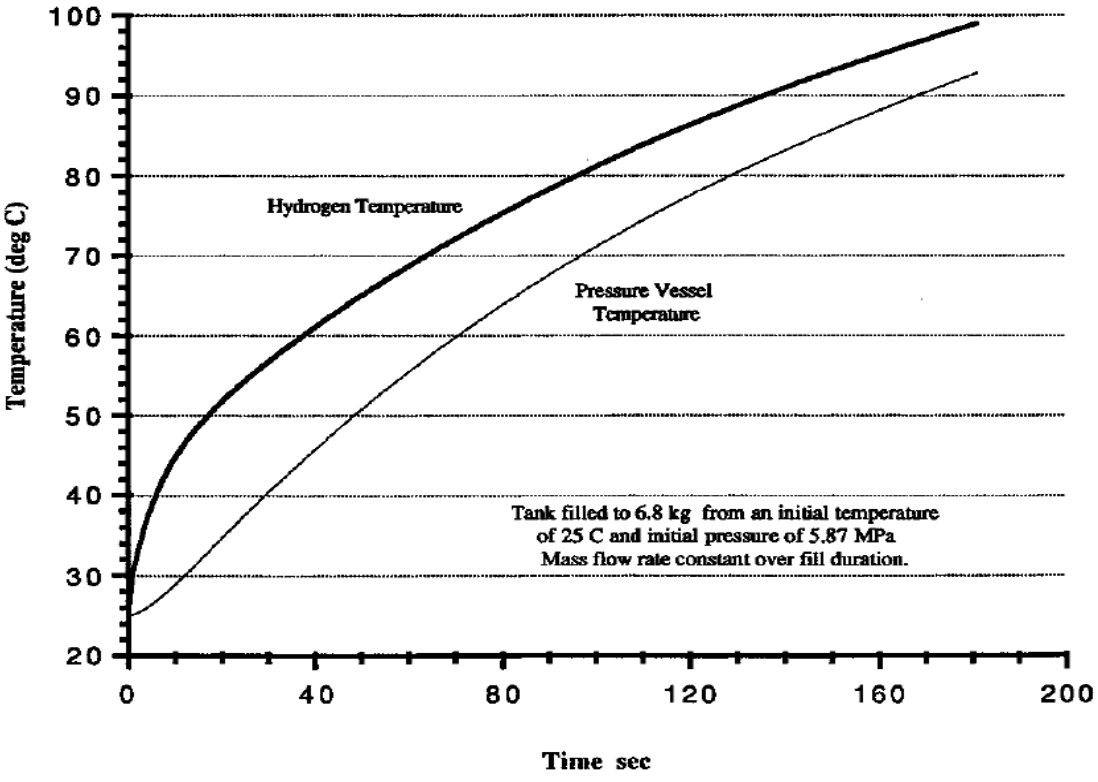

Figure 128. Calculated temperature rise of hydrogen in a tank and the tank temperature over time when filled with H_2 at 5.87 MPa.[305]

2 Heat Capacity Measurement Methods

2.1 Standards

The following are a list of pertinent ASTM standards for the test methods commonly used for measuring the heat capacity of materials.

2.1.1 Measurement Method Practice Standards

- **ASTM E1269 – 11: Standard Test Method for Determining Specific Heat Capacity by Differential Scanning Calorimetry.**[306]

  Differential scanning calorimetric measurements provide a rapid, simple method for determining specific heat capacities of materials.

Scope

1) This test method covers the determination of specific heat capacity by differential scanning calorimetry.
2) This test method is generally applicable to thermally stable solids and liquids.
3) The normal operating range of the test is from − 100 to 600°C. The temperature range can be extended, depending upon the instrumentation and specimen holders used.
4) The values stated in SI units are to be regarded as the standard.
5) Computer or electronic-based instrumentation, techniques, or data treatment equivalent to this test method may be used.
6) Note 1—Users of this test method are expressly advised that all such instruments or techniques may not be equivalent. It is the responsibility of the user of this test method to determine equivalency prior to use.
7) This method is similar to ISO 11357–4, but contains additional methodology not found in that method. Additionally, ISO 11357–4 contains practices not found in this standard. This method is similar to Japanese Industrial Standard K 7123, but contains additional methodology not found in that method.
8) This standard does not purport to address all of the safety concerns, if any, associated with its use. It is the responsibility of the user of this standard to establish appropriate safety and health practices and determine the applicability of regulatory limitations prior to use. Specific precautionary statements are given in Section 9.

- **ASTM E967 - 08 Standard Practice for Temperature Calibration of Differential Scanning Calorimeters and Differential Thermal Analyzers.**[307]

  Differential scanning calorimeters and differential thermal analyzers are used to determine the transition temperatures of materials. For this information to be meaningful in an absolute sense, temperature calibration of the apparatus or comparison of the resulting data to that of known standard materials is required. This test method is useful in calibrating the temperature axis of differential scanning calorimeters and differential thermal analyzers.

Scope

1) This test method describes the temperature calibration of differential thermal analyzers and differential scanning calorimeters over the temperature range from 40 to +2500 C.
2) This test method is similar to ISO standard 11357-1.
3) This standard does not purport to address all of the safety concerns, if any, associated with its use. It is the responsibility of the user of this standard to establish appropriate safety and health practices and determine the applicability of regulatory limitations prior to use.
4) Specific precautionary statements are given in Section ASTM E968.

- **ASTM E968 - 02(2008) Standard Practice for Heat Flow Calibration of Differential Scanning Calorimeters.**

  Differential scanning calorimetry is used to determine the heat or enthalpy of transition. For this information to be meaningful in an absolute sense, heat flow calibration of the apparatus or comparison of the resulting data to that of a known standard is required. This practice is useful in calibrating the heat flow axis of differential scanning calorimeters or quantitative differential thermal analyzers for subsequent use in the measurement of transition energies and specific heat capacities of unknowns.

Scope

1) This practice covers the heat flow calibration of differential scanning calorimeters over the temperature range from − 130°C to + 800°C.
2) Values given in SI units are to be regarded as the standard.
3) Computer or electronic based instruments, techniques or data manipulation equivalent to this practice may also be used.

4) This standard does not purport to address all of the safety concerns, if any, associated with its use. It is the responsibility of whoever uses this standard to consult and establish appropriate safety and health practices and determine the applicability of regulatory limitations prior to use.

2.1.2 Recommended Standard Reference Materials

A set of recommended values for the heat capacity, thermal expansion, and transport properties of key solids has been prepared for use as standards.[308,309] For example, for metals of comparable thermal properties, heat capacity reference materials data was collected by CSIRO for Copper and Tungsten.

Table 13 below presents a list of common standards for the temperature calibration of DSC instrument.

Standard	Melting point (°C)	Heat of fusion (J/g)
Indium	156.6	28.42
Tin	231.9	
Lead	327.5	
Zinc	419.5	108.26
K_2SO_4	585.0	
$K_2Cr_2O_7$	670.5	
Substance	**Transition**	**Transition temperature (°C)**
Cyclopentane	Crystal	−151.16
Cyclopentane	Crystal	−135.06
Cyclohexane	Crystal	−87.06
Cyclohexane	Melt	6.54
n-Heptane	Melt	−90.56
n-Octane	Melt	−56.76
n-Decane	Melt	−29.66
n-Dodecane	Melt	−9.65
n-Octadecane	Melt	28.24

Table 13. Commonly used standards and reference materials.[26]

2.1 Differential Scanning Calorimetry

The main technique used for making Heat Capacity or Specific Heat measurements is Differential Scanning Calorimetry (DSC). A helpful and readily available introduction to DSC measurements is the online book chapter: "A Practical Introduction to Differential Scanning Calorimetry", by Paul Gabbott, in the book "Principles and Applications of Thermal Analysis"[26]

In this section of this document, the pertinent aspects of DSC Heat Capacity measurements of hydrogen storage materials are reviewed.

DSC is used, among other things, for the quantitative determination of the specific heat (heat capacity, C) of a material. Since the measurements are typically done at constant pressure it is C_p values that are measured. DSC heat capacity measurements can be performed by either using a single temperature ramp or using modulated temperature techniques. The single temperature ramp is the more commonly applied method. This standard method provides a fairly rapid method for determination of C_p.

This method consists of controlling the temperature of the measurement to produce an isothermal period, a controlled temperature ramp and final isotherm. To determine the heat capacity of a sample three identical successive measurements are performed with the following samples:

1. a baseline with un-crimped empty pans placed in the furnace.
2. a reference (typically sapphire) to the sample pan.
3. the sample material of interest.

This produces three heat flow curves as shown in the example of Figure 129.

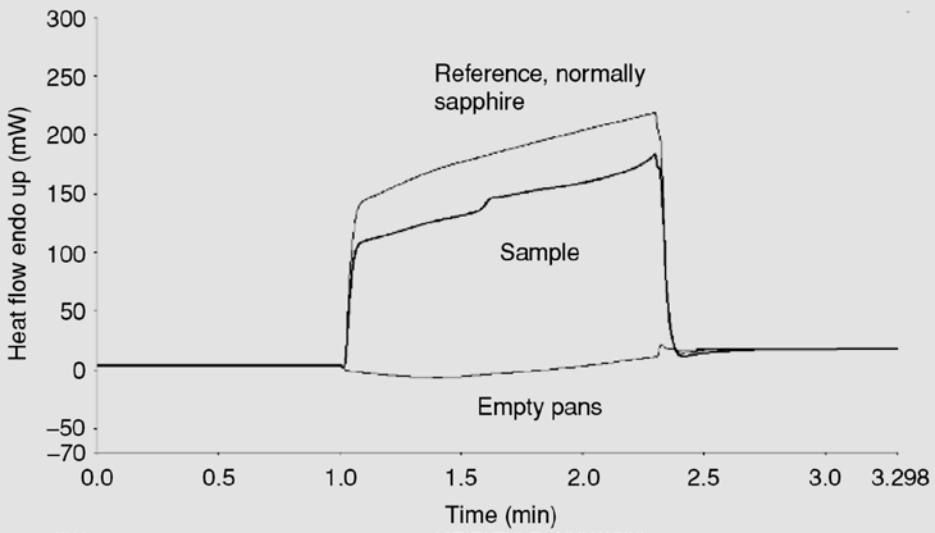

Figure 129. Heat capacity of PET obtained using fast scanning techniques showing the three traces required for subtraction. The height of the sample compared to the empty pan is divided by the scan rate and the mass of sample to obtain a value for C_p. This is referenced against a known standard such as sapphire for accuracy. If small heating steps of, for example 1°C, are used the area under the curve can be used to calculate C_p. This calculation is employed as an option in stepwise heating methods.[26]

The C_p of the sample material is determined by subtracting a baseline from the heat flow curves as follows. The three curves are plotted such that the isothermal sections are matched. The data is corrected for the mass of the pans and samples. Then the baseline data (empty pans) is subtracted from the other measurements and finally the sample data referenced against the standard.

The following are some important considerations to be followed when making these measurements:

1) The DSC instrument must be very stable. It is not recommended to use an instrument at the extremes of its temperature range where stability may be compromised.
2) For a very stable DSC instrument the baseline and reference runs that have been initially made may be used for subsequent samples, but only if the weight and heat capacity of different sample pans are taken into account.
3) The method is based on the subtraction of data from measurements made at different times. Thus, any drift in the instrument will cause error in the results.

4) The most commonly used reference standard is sapphire. This is probably appropriate for many hydrogen storage materials, however, it is best if the reference standard has C_p values similar to that of the samples being measured.
5) It is important that the mass of the reference standard is similar to the sample. The sample should not be a lot larger that the reference in order to avoid increased error.
6) There may be a number of factors which dictate the chosen scan rate, for example the possibility of hydrogen release from the sample if measured in the hydrided state. However, it should be noted that faster scan rates result in increased values of heat flow giving increased accuracy of measurement. This also reduces the measurement time and, thus, any drift in the instrument. It has been reported that fast scan rates can produce extremely accurate data.[310]
7) The accuracy that can be obtained depends upon the instrument and method.

The stepwise heating methods employ heating steps in which the temperature may be raised by only a fraction of a degree between a series of isotherms. The analysis of C_p is performed in essentially the same manner as described above. The stepwise or modulated methods are reported to give a very accurate value for C_p because of the series of short temperature intervals.

2.2 Heat Capacity Measurement of Liquids by DSC

Differential scanning calorimetry (DSC) is often used for measuring the heat capacity of liquids and is typically run to provide isobaric heat capacity, C_p. One significant difficulty in the measurement of liquids stems from the potential volatility of the liquid, especially if measurements are to be made near the boiling point of the liquid. Not all calorimeters are well suited to the measurement of C_p in liquids. For example, adiabatic calorimeters that typically make measurements at a single temperature cause the collection of the temperature dependence of the heat capacity $C_p(T)$ to be a long and arduous task. While DSC is not a standard technique for determining liquid heat capacities, it is the most suitable choice for measurements over a range of temperatures. The limitation is that most DSCs lack the resolution needed for the precise determination of C_p of liquids.

As an example, Cerdeirina et al. described measurements using a technique for measuring C_p of liquids based on the scanning method.[311] Their publication describes the method in detail, including an evaluation of the Scanning versus Isothermal Step methods, and focused on calibration of the instrument using liquids of known heat capacities following the recommendations of the GEFTA working group `Calibration of Scanning Calorimeters'.[312,313,314,315] Typically, DSCs are calibrated based on the Joule effect.

Detailed descriptions of DSC instruments can be found in the literature.[316,317,318,319,320] Cerdeirina et al. provided the following short description of their experimental equipment.[311] The commercial instrument had two differential measurement vessels (reference and measuring) assembled in a calorimetric block immersed in a thermostating liquid with a Peltier temperature controller. This design ensures a highly uniform temperature and very low thermal inertia. Temperature was measured in the block close to the vessels with a repeatability of within 0.01K. The measurement assembly was placed in an inert atmosphere of dry nitrogen. Their instrument's calorimetric measurement was based on Calvet's principle (differential heat flow rate measured by a thermopile around each vessel). This provided the power of differential scanning calorimetry and the precision of Calvet calorimetry, making it suitable for the precise determination of heat capacities over a wide range of temperatures. The primary technique employed was the Isothermal Step method which was the recommended and most widely used choice with DSC calorimeters on account of its precision.

2.2.1 Experimental Considerations

The presence of the vapor phase in the measurement zone causes C_p measurement errors that must be avoided or compensated for. Conventional calorimeter sample vessels will have a vapor phase present and, therefore, require corrections to the data to account for this. Specially designed liquid heat capacity vessels can circumvent this issue by avoiding the presence of the vapor phase over the liquid in the detection zone. Thus, no vapor phase correction is needed.

Another important consideration is that the experimental configuration and stability of the instrument is constant over the period of time that the calibrations and measurements are performed.

The calorimetric signal is proportional to the heat capacity per unit volume. Therefore, precise determination of C_p on a mass basis requires the accurate determination of the density of the liquid under the measurement conditions. The authors in the present example used a vibrating tube density meter.[311]

The use of liquids of known heat capacity is a suitable choice for calibration in both the isothermal step and the scanning method. The following calibration and measurement protocol was used in the experiments by Cerdeirina et al.[311] (I - calibration) both vessels were filled with heptane (reference liquid), (II - calibration) heptane was replaced with a reference material in the measuring vessel, and (III - measurement) the reference material was replaced by the sample in the measuring vessel. The reference vessel held

the same liquid in the three experiments. Experiments I and II were performed in triplicate under identical conditions. Experiment I determines the asymmetry of the measuring system. This is usually performed with two empty vessels, however, the authors chose to fill both with heptane in order to determine the asymmetry in both the vessels and the effect of the volume difference between them. The reference material used in experiment II was butan-1-ol. This was chosen because of its well-known heat capacity and of the fact that $C_p V^{-1}$ for most liquids is between those of heptane and butan-1-ol.[311]

Measurement rates should be chosen where quasi-stationary conditions are valid. In this case a time greater than 10 times the calorimeter's time constant was used. Ideally the isothermal starting and ending lines coincided in all experiments. This allows the heat flow calculation to always be referenced to the same baseline.

In the present example, the accuracy of the Scanning method of measurement was tested against the result of the Isothermal Step method.[311]

2.2.2 Isothermal Step Method

The Isothermal Step method of measurement was performed at temperature increment of 1K by stepping up (and then down) in temperature at a constant rate of 0.2K min^{-1} to a maximum of 1K difference from the central measurement value. The positive and a negative temperature stepping increments were programmed in each experiment in order to minimize the effect of convection currents due to the liquid phase outside the thermostated zone. The heat capacity of the sample was computed from the peak areas obtained in each experiment I, II, and III. The peaks were integrated with respect to a linear baseline joining the isothermal starting and ending lines. The isobaric molar heat capacity $C_{p,\mathrm{m}}$ of the sample was calculated from the following equation

Equation 151
$$(C_{\mathrm{p,m}})_{\mathrm{S}} = M_{\mathrm{S}} \left[\frac{\rho_{\mathrm{RM}}((C_{\mathrm{p,m}})_{\mathrm{RM}}/M_{\mathrm{RM}}) - \rho_{\mathrm{R}}((C_{\mathrm{p,m}})_{\mathrm{R}}/M_{\mathrm{R}})}{\rho_{\mathrm{S}}} \times \frac{S_{\mathrm{S,R}} - S_{\mathrm{R,R}}}{S_{\mathrm{RM,R}} - S_{\mathrm{R,R}}} + \frac{\rho_{\mathrm{R}}(C_{\mathrm{p,m}})_{\mathrm{R}}}{\rho_{\mathrm{S}} M_{\mathrm{R}}} \right]$$

where ρ denotes the density; M molecular weight; and subscripts S, RM, and R properties of the sample, reference material and reference sample, respectively.

2.2.3 Scanning Method

In the Scanning method, the temperature was changed at a constant rate over the entire measurement range. This was done for both heating and cooling in order to minimize the effect of convection currents. $C_{p,m}$ at temperature T was calculated from

Equation 152

$$(C_{\mathrm{p,m}})_{\mathrm{S}} = M_{\mathrm{S}}\left[\frac{\rho_{\mathrm{RM}}((C_{\mathrm{p,m}})_{\mathrm{RM}}/M_{\mathrm{RM}}) - \rho_{\mathrm{R}}((C_{\mathrm{p,m}})_{\mathrm{R}}/M_{\mathrm{R}})}{\rho_{\mathrm{S}}} \times \frac{((\mathrm{d}H/\mathrm{d}t)_{\mathrm{S,R}}/\beta_{\mathrm{S,R}}) - ((\mathrm{d}H/\mathrm{d}t)_{\mathrm{R,R}}/\beta_{\mathrm{R,R}})}{((\mathrm{d}H/\mathrm{d}t)_{\mathrm{RM,R}}/\beta_{\mathrm{RM,R}}) - ((\mathrm{d}H/\mathrm{d}t)_{\mathrm{R,R}}/\beta_{\mathrm{R,R}})} \times + \frac{\rho_{\mathrm{R}}}{\rho_{\mathrm{S}}}\frac{(C_{\mathrm{p,m}})_{\mathrm{R}}}{M_{\mathrm{R}}}\right]$$

where $\beta = dT/dt$ is the scanning rate.

The determination of the scanning rate β used in this calculation may impact the results. Sarge et al. found calculating β from pairs of consecutive T and t values to be a more accurate than was using the preset rate.[314,315] Figure 130 shows the variation of the measured temperature rate versus the set rate over the course of an experiment.

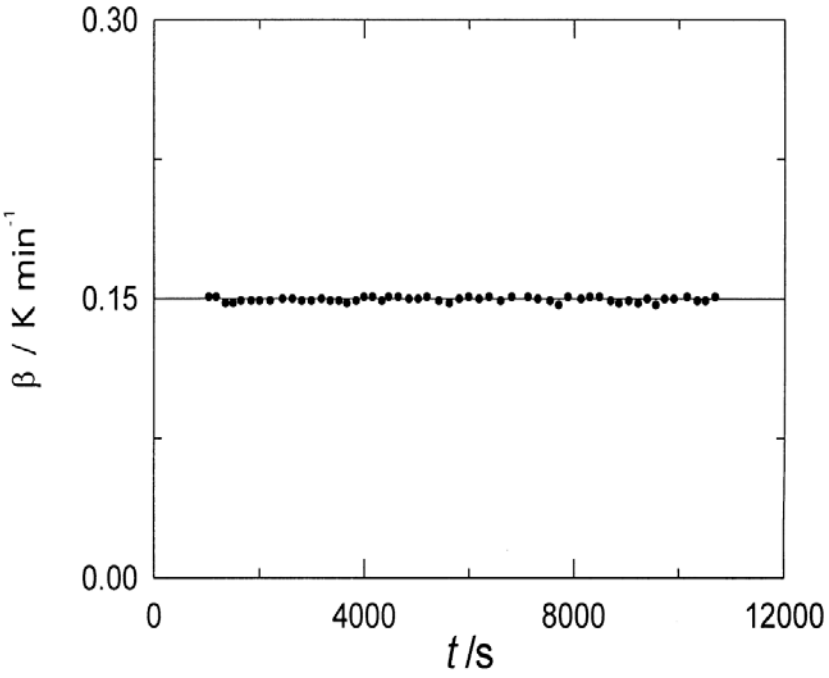

Figure 130. Scanning rate β against time t (•) measured values and (—) preset Value.[311]

In this case, the calculated and preset values were quite similar allowing the set value to be used with confidence in the calculations. The scanning rate was chosen to not be too low avoiding unduly long experiments or too high in order to avoid an excessive thermal lag between the recorded and real temperatures. Cerdeirina et al. observed no significant differences using scanning rates over the range (0.05±0.80) $Kmin^{-1}$. They chose an operating scanning rate β = 0.15 $Kmin^{-1}$, where the thermal lag was about 0.5K. They reported that, although this resulted in no appreciable error in $C_{p,m}$ for pure liquids, the temperature used was incorporated an appropriate correction.[311]

2.2.1 Results

Cerdeirina et al. tested 7 different liquids and 3 different binary mixtures and came to the conclusion that Micro DSC calorimeters are suitable for the precise determination of liquid heat capacities by providing convenient operation over wide range temperatures. They also determined that the precision of the scanning method is identical to that of the isothermal step method, which is much more time-consuming.[311] One example of their comparative results are shown below in Figure 131.

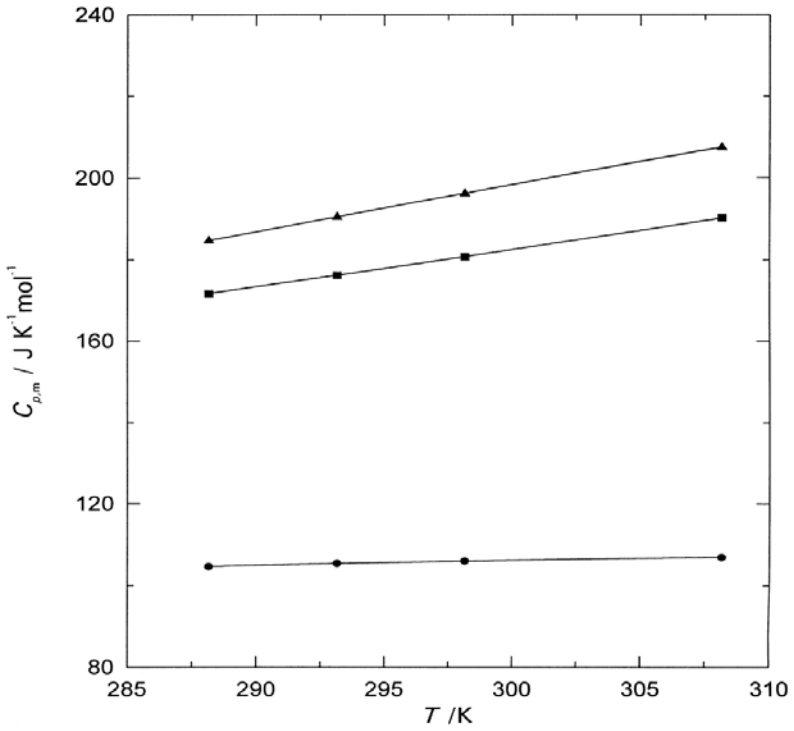

Figure 131. Isobaric molar heat capacities $C_{p,m}$ against temperature T. Isothermal step method: (l) nitromethane, (s) butan-2-ol, (n) 2-methyl propan-1-ol, and the (—) Scanning method.[311]

3 Experimental and Analysis Considerations

3.1 Differential Scanning Calorimetry Measurement Considerations

3.1.1 Overview - Sources of Potential Error

Differential scanning calorimeter (DSC) is used to measure the heat capacity for the calculation of thermal conductivity as well as the evaluation of heat capacity. The DSC method evaluates the difference in heat flow between the sample and a reference material as a function of temperature in a controlled atmosphere. In a common setup there is a resistance heater and a temperature sensor either below or surrounding each of the test and reference samples. Electrical currents are applied to the two heaters to increase the temperature at a selected rate. The difference in the power, necessary to maintain the materials at the same temperature, is used to calculate the heat capacity. The nature of the DSC measurement method may introduce some of the following errors.

1) A flow of nitrogen or He purge gas is maintained over the samples to create a reproducible and dry atmosphere. The nitrogen or He also reduces oxygen and moisture contamination or interaction with the samples at high temperatures. The flow of nitrogen or He is an important factor in the measurement process. If the purge gas is too low, moisture accumulates in the test unit which effects to the accuracy of the results. If the purge gas is too high, temperature equilibrium is hard to reach; the results include noise that results in poor measurement values.
2) During the testing, the materials are typically sealed into small holders. The shape, sample alignment (either horizontal or vertical), and material used for the holders are important to generate the appropriate accuracy and resolution in the measurement process.
3) In a similar manner, the heating rate is another factor that needs to be set correctly to balance between the resolution at lower rates and sensitivity at higher rates.
4) The selection of the reference material should have similar heat capacity to the test sample to improve the accuracy because the DSC measures the difference in heat flow between the sample and reference.
5) During the initial experimental set-up temperatures in the instrument need to reach a stable level before performing the measurements.

Accurate DSC measurements of heat capacity require good experimental practices. The following information and advice is adapted from the chapter, "A Practical Introduction to Differential Scanning Calorimetry", by Paul Gabbott, in the book "Principles and Applications of Thermal Analysis" which provide sound advice on important considerations for making accurate DSC measurements.[26]

3.1.2 Encapsulation

The sample pan encapsulates the sample Encapsulation preventing contamination of the analyzer and ensuring good thermal contact of the sample with the furnace. Errors due to poor sample encapsulation is one of the most important considerations in obtaining good data.

Air-less sample preparation and transfer

Hydrogen storage materials are particularly susceptible to reaction with (hydrides) or uptake of impurities from air (e.g. hygroscopic properties of adsorption materials). Thus, it is very important that samples be prepared in an air-free environment. For example, ball-milling of hydrides in an inert atmosphere and bake-out of high-surface area adsorbents. Like-wise, it is critical that samples be loaded into DSC sample pans and tested without air exposure. In the majority of cases, an inert gas glove box will be required for most preparation, loading, and transfer operations. Sample pans are available that can be sealed (inside of a glove box) to ensure that the sample will not be exposed to air. However, one should evaluate, in advance, whether the sample will decompose, react, degas, or expand in the sealed sample pan during a measurement. These issues risk injury to persons and equipment, or, even small sample transformation leading to error in the measured results and must be avoided. In addition, it is advisable to weigh the pan containing the sample before and after the DSC measurements to ensure that no leakage or air contamination has occurred during the experiments. If, after the measurement, the sample pan weighs less, then the sample or inert gas leaked out of the pan or the sample degased. If it weighs more, then it is likely that air entered the pan and contaminated the sample. In either case the data has been compromised.

Temperature range

The sample pan must be designed for the measurement temperature range (should not melt).

Pressure build-up and pan deformation

It is important to determine in advance if whether the sample needs to be run in a hermetically sealed pan or not. Considerations are whether the sample will evolve a gas or volatiles during heating that will lead to pressure buildup in a sealed pan. The hydrided or adsorbed state of many hydrogen storage materials are very likely to degas

during a DSC run. Hermetically sealed pans such as those made of aluminum cannot withstand high internal pressure and will deform resulting in potential artifacts that may be misinterpreted. Sample leaking and bursting can occur. One option is to use crimped pans that do not seal, or use lids with multiple holes. Disposable high-pressure capsules which avoid the need for cleaning may be appropriate. However, potential decomposition pressures should in the pan should be assessed in advance.

Reactions with the pan

Samples that react with a pan can cause serious damage to an analyzer since they may also react with the furnace beneath. Hydrides may react with pan materials including aluminum. If in doubt a separate analysis of materials should be performed before any DSC measurement.

Pan cleanliness

As received pans may be slightly contaminated, possibly with a trace of machine oils used in pan manufacture and should be cleaned prior to use. Spilled sample or contaminants should be removed from the outside surface of the pan.

Pans with very small holes

Pan and lid systems with very small holes (typically about 50 μ) have been developed that can be used to relieve internal pressure, as long as the hole does not block. Again, however, mass loss by hydrogen release or degasing of contaminates may cause errors in measuring heat capacity.

Liquid samples

Sealable pans that can withstand any internal pressure build-up should be used with liquid samples. Instrument damage and measurement errors can be caused by overfilling the pan or contaminate the sealing surfaces.

Sample contact

It is important that samples maintain good thermal contact with the pan. Liquids and powders (pressed into the pan) give good thermal contact. Bulk samples may need to be cut with a flat surface that will contact the base of the pan. Note that grinding samples specifically for such measurement may induce changes their properties. If thin films are being measured, multiple layers may be needed to have enough mass. These should be pressed well together to avoid layer effects. Samples with low-density typically have poor heat transfer, and so should be compressed, if it is possible to do so without changing the material's properties.

3.1.3 Temperature range

Heat capacity measurements should be done at temperatures phase transitions and typically in the range of the operating temperatures of the storage application. Temperatures should certainly be below the decomposition temperature of the material which would lead to a very noisy drifting response and melting or volatiles that can contaminate the system. It is good practice to establish the decomposition temperature first using a TGA analyzer.

3.1.4 Scan rate

Commercially instruments typically offer a wide range of scan rates (from 0.001 to 500°C·min^{-1}). The scan rate used may have the following impact on the measurements:

1. *Sensitivity*. The faster the scan rate the greater the sensitivity. The reason for this is that a DSC measures the *flow* of energy and during a fast scan the flow of energy is high. Faster scan rates should be used for small difficult-to-find transitions.

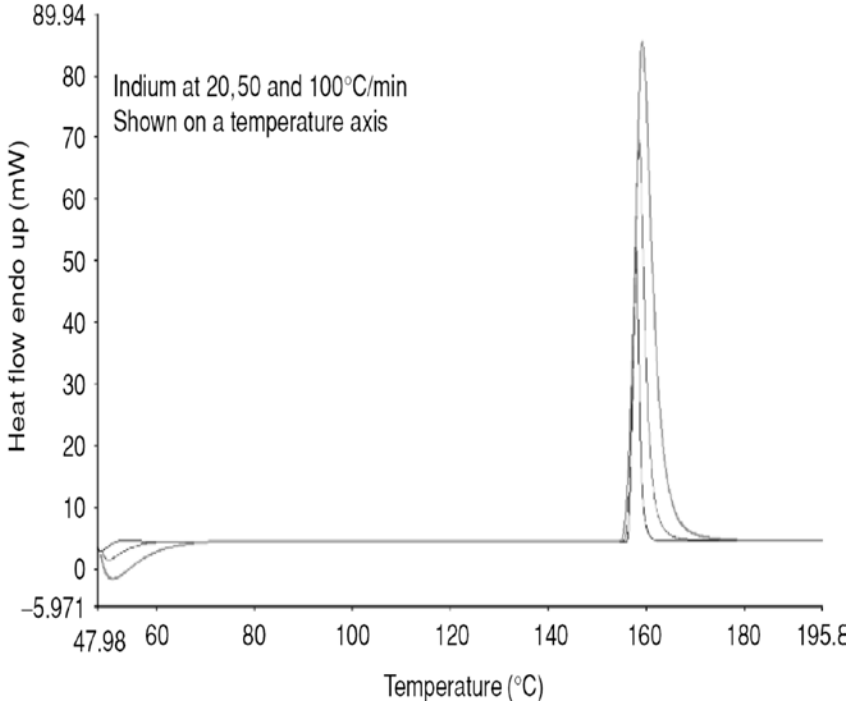

Figure 132. The effect of increasing scan rate on indium. The same energy flows faster in a shorter time period at the faster rates, giving larger peaks.[26]

2. *Temperature calibration*. Calibrations prior to analysis should be performed at the scan rate of the measurement.

3. *Resolution*. Faster scan rates produce lower resolution because of thermal gradients across a sample. Thermal gradients can be reduced by reducing sample size and improving thermal contact with the pan.

4. *Transition kinetics*. When measuring transitions or reactions, scan rates should be slower than kinetics of an event to ensure that it goes to completion.

3.1.5 Sample size

Sample size depends on the instrument and sample pans being used. Note that when considering accuracy of energy measurements the accuracy of the balance should be taken into account. For most work at least a five-figure balance is needed. More sample material means a more accurate weight measurement, however the use of too large a sample is one of the major causes of contamination.

3.1.6 Purge gas

Measurements are typically done using a purge gases to control the sample environment, purge volatiles from the system, and prevent contamination. Purging the system with gas reduces noise from internal convection currents, prevent ice formation in sub-ambient systems, and can provide an active atmosphere. The most common purge gas is nitrogen. Helium is used for work at very low temperatures where nitrogen and oxygen would condense. Sometimes argon is used when operating at higher temperatures (> 600°C). Argon's low thermal conductivity reduces heat loses, but at lower temperatures results in decreased resolution and sensitivity. Because air, nitrogen and oxygen have similar thermal conductivities, an instrument's calibration is unaffected when switching between these different purge gases. This is not true of helium or argon which requires separate calibrations to be performed. It is recommended to use high-purity gases and allow enough time for the sample area to be fully purged of air before beginning a run. Note that purge gas flow rates are normally low and should restricted or perturbed by the flow measurement equipment.

3.1.7 Sub-ambient operation

Low (cryogenic) temperature measurements are possible with many DSC's. The measurement of the heat capacity of physisorption storage materials should be done in

the range of operating temperatures (77K to room temperature) for the most complete results. DSC instruments using cryogenic liquids should be closely monitored for thermal stability and a constant supply of the cryogen during calibration and measurements. Refrigerated coolers (intracoolers) offer an alternative to cryogenic liquids.

3.1.8 Preparing the DSC instrument for measurements

Some general instrument preparation considerations are presented here; please refer to equipment manuals and the publication by Paul Gabbott for details.[26]

- Before starting and before turning on accessories, thoroughly inspect and clean the instrument. After physically cleaning the furnace, per manufacturer's instructions a furnace burn-off at about 600°C or above may be performed in air. Note that, although organics will burn off, metal and inorganic content may burn in, so make sure the furnaces are as clean as possible before a burn-off.
- Platinum furnace covers should also be clean. Do not mix up sample and reference furnace covers as they have slightly different heat capacities.
- Furnace covers should fit well. Incorrectly fitting covers will lead to significant slope on the baseline.
- Allow purge gas and cooling system to stabilize before starting measurements. Stable background temperatures and purge gas flow provide a controlled environment from which stable and reproducible performance can be obtained.

3.2 Calibration

Calibration is a process which is not complete until the instrument has been checked by running a standard to ensure that values obtained are acceptable. It is this verification that ensures that the equipment is ready to make accurate measurements, not the calibration procedure itself.

Calibrations should be performed following the manufacturers' instructions. In order to ensure accuracy and repeatability of data, a system must be calibrated and checked under the conditions of use. While calibrations adjust the instrument's response and output, its accuracy can only be determined by separately checking the instrument's measurement of accepted standards. A good overview of currently available standards for DSC with comments on accuracy and procedure is given in the publication by Giuseppe et al.[321]

3.2.1 Checking performance

The most common procedure for checking performance is to run an indium standard under the normal test conditions and measure the heat of fusion value and the melting onset temperature. These values are then compared with literature values to make sure the measurement is within acceptance limits. For many industries acceptance limits are ±0.5°C for temperature or 1% for heat of fusion, though tighter limits of ±0.3°C and 0.1% may also be adopted.[322] Use values supplied with the actual standards rather than literature values as different batches of standards may have different values.

3.2.2 When to calibrate

Instruments that are new, out of service for some time, have undergone some type of service, or are to be used under new conditions, most likely are in need a complete calibration. Instruments in regular use should also be checked regularly and calibrated when it is shown to be out of specification.

Frequent and consistent performance checks should be a part of standard operating procedures. If an instrument is only checked once every 6 months and then found to be in error, 6 months of work is then suspect. It is recommended that performance checks are done weekly.

3.2.3 Parameters to be calibrated

(a) *Heat flow or energy* is normally calibrated using the heat of fusion of a known standard such as indium or may be calibrated directly using a standard of known specific heat.

(b) *Temperature Measured* is calibrated using the melting point of known standards.

(c) *Temperature Control* is a calibration of the furnace.

Calibrations should be mad under the same conditions (or range of conditions) as the measurements to be performed. Calibrations should be checked and verified for each set of conditions and scan rates used.

Please refer to the manufacturer's instructions for the exact procedures on how to perform these calibrations. Additional information may be found in the publication by Paul Gabbott.[26]

3.2.4 Choice of standards

Table 13 lists details of commonly used reference materials. Materials should be used once and then discarded, with the exception of indium. Indium can be reheated many times with fusion values repeated to very high precision (0.1%) provided it is not overheated above 180°C. To ensure complete recrystallization Indium should be cooled to 50°C or below after each test. For temperature ranges where no metal transitions are appropriate other materials may be used as reference materials.

"Reference" materials possess a certificate of high purity allowing use of theoretical melting and heat of fusion values. "Certified" reference materials have a certificate giving values obtained after the material has been tested by a range of certified laboratories. These standards are regarded as the ultimate in reference materials.

3.2.5 Factors affecting calibration

Factors that if varied may require different calibration settings or a new calibration include:

- Instrument set-up and stability
- Use of cooling accessories
- Scan rate
- Purge gas and flow rate
- Pan type

Most instruments will have a slight drift as they warm up and, therefore, should be switched on for a while (typically at least an hour) before calibration. Cooling systems (if used) should be switched on and stable before calibration. If different scan rates are going to be used, ensure that the instrument is suitably calibrated for each scan rate. Purge gases such as air, oxygen and nitrogen have similar thermal effects and can be used interchangeably without recalibration. However, instruments should be recalibrated when switching to helium or argon.

Summary

It is our intent that this overview of measurements of the engineering properties of hydrogen storage materials will aid research and development of advanced systems for hydrogen storage. In particular we hope to have clarified some of the recommended practices and caveats in performing high-quality experiments to measure the hydrogen sorption and desorption kinetics properties of advanced materials.

Acknowledgements

We gratefully acknowledge assistance and financial support from the U.S. Department of Energy Office of Energy Efficiency and Renewable Energy Hydrogen Storage Program. This work supported the President's Hydrogen Fuel and Advanced Energy Initiatives. The authors also acknowledge technical advice and contributions from many experts in the field including Dr. Philip Parilla and Dr. Thomas Gennett of the National Renewable Energy Laboratory in Golden CO, Dr. Ned Stetson and Dr. Carole Read of the U.S. Department of Energy, Dr. Gary Sandrock, Dr. George Thomas, and Dr. Robert Bowman Jr. consultants to the U.S. Department of Energy, Professor Gavin Walker of the University of Nottingham, United Kingdom, Dr. Thomas Autrey of Pacific Northwest National Laboratory, Dr. Michael Miller of Southwest Research Institute in San Antonio TX, Dr. Anne Dailly, Dr. Frederick Pinkerton, Dr. Scott Jorgensen of General Motors GM R&D Center, Professor Ole Martin Løvvik of the Department of Physics, University of Oslo, Norway, Dr. Eric Poirier of General Motors/Optimal CAE Inc., Professor Channing Ahn of the California Institute of Technology in Pasadena CA, Dr. Kevin Ott, Dr. Anthony Burrell, and Dr. Troy Semelsberger of Los Alamos National Laboratory, Professor Richard Chahine and Dr. Renju Zacharia of the Université du Québec à Trois-Rivières, Canada, Dr. Andrea Sudik, Ford Motor Company, USA, Professor Klaus Yvon of the University of Geneva, Switzerland, Professor Sam Mao of the University of California Berkeley in Berkeley CA, and Dr. Nobuhiro Kuriyama and Dr. Tetsu Kiyobayashi of the National Institute of Advanced Industrial Science and Technology in Osaka, Japan, Dr. Ewa Rönnebro, Pacific Northwest National Laboratories, Dr. Bart van Hassel, United Technologies Research Center, Dr. Lars Röntzsch, Fraunhofer Institute for Manufacturing Technology and Advanced Materials, Dresden, Germany, Dr. Michel Latroche, Institut de Chimie et des Matériaux de Paris Est CNRS, France, Dr. Patricia De Rango, Institut Néel CNRS, Grenoble, France, Dr. Mike Veenstra and Dr. Jun Yang of Ford Motor Co., USA, Professor David Grant and Dr. Alastair Stuart, of the University of Nottingham, United Kingdom, Daniel Dedrick, Sandia National Laboratories, Livermore, CA.

Disclaimer

"This report was prepared as an account of work sponsored by an agency of the United States Government. Neither the United States Government nor any agency thereof, nor any of their employees, nor the authors of this work, nor their respective employers nor the institutions they represent make any warranty, express or implied, or assumes any legal liability or responsibility for the accuracy, completeness, or usefulness of any information, apparatus, product, or process disclosed, or represents that its use would not infringe privately owned rights. Reference herein to any specific commercial product, process, or service by trade name, trademark, manufacturer, or otherwise does not necessarily constitute or imply its endorsement, recommendation, or favoring by the authors, the United States Government or any agency thereof."

References

1 Walker, G.S. (editor), "Solid-state hydrogen storage: materials and chemistry", Woodhead Publishing Ltd, **(2008)**, Cambridge, UK.

2 Barnes, R.G. (editor), "Hydrogen Storage Materials." *Trans Tech Publications*, **(1988)**.

3 Schlapbach, L., and Züttel, A., "Hydrogen-storage materials for mobile applications." *Nature*, 414 **(2001)** p.353-358.

4 Broom D.P., "Hydrogen Sorption Measurements on Potential Storage Materials". *JRC Scientific and Technical Reports* (**2008**), JRC 43223, EUR 23242 EN, ISBN 978-92-79-08345-7 ISSN 1018-5593 DOI: 10.2790/86100.

5 Wiberg, E., and Amberger, E., "Hydrides of the Elements of Main Groups". Z-ZV. Elsevier, Amsterdam, **(1971)**, 2. D. A. Armitage.

6 Muller, W.M., Blackledge, J.P., Libowitz, G.G. editors, "Metal Hydrides". Academic Press, **(1968)**, New York.

7 Dedieu, A., "Transition Metal Hydrides", **(1991)**, Wiley-VCH.

8 Sandrock, G., "A panoramic overview of hydrogen storage alloys from a gas reaction point of view." *J. Alloys and Compounds*, 293-295, **(1999)**, p. 877-888.

9 Sandrock, G., "State-of-the-art Review of Hydrogen Storage in Reversible Metal Hydrides for Military Fuel Cell Applications." Report for the Department of the Navy, Office of Naval Research, **(1997)**, NTIS Report # AD-A328073/2INZ.

10 Stephens, F.H., Vincent Pons, V., and Baker, R.T., "Ammonia–borane: the hydrogen source par excellence?", *Dalton Trans.*, **(2007)**, p. 2613–2626.

11 Zidan, R., "Aluminum Hydride" in "Handbook of hydrogen storage: New Materials for Future Energy Storage", eds. Hirscher, M., Hirose, K., Weinheim : Wiley-VCH, **(2009)** p. 249.

12 Thomas, K.M., "Hydrogen adsorption and storage on porous materials." *Catalysis Today*, 120 **(2007)**, p. 389–398.

13 Van den Berg, A.W.C., Arean, C.O. "Materials for hydrogen storage: current research trends and perspectives." *Chemical Communications*, **(2008)**, p. 668–681.

14 Schmitz, B., Muller, U., Trukhan, N., Schubert, M., Ferey, G., and Hirscher, M. "Heat of Adsorption for Hydrogen in Microporous High-Surface-Area Materials." *Chem Phys Chem*, 9 **(2008)**, p. 2181–2184.

15 Perry, R. H. and Green, D. W. "Perry's Chemical Engineers Handbook", McGraw-Hill. **(1984)**, ISBN 0-07-049479-7.

16 Roy, B. N. "Fundamentals of Classical and Statistical Thermodynamics", **(2002)**, John Wiley & Sons. ISBN 0-470-84313-6.

17 Reif, F. "Chapter 5 – Simple applications of macroscopic thermodynamics". Fundamentals of Statistical and Thermal Physics. McGraw-Hill, **(1965)**, ISBN 0070518009.

18 Özişik, M. Necati, "Heat Transfer: A Basic Approach", (**1984**), Mcgraw-Hill College, ISBN-10: 0070479828.

19 J.H. Lienhard IV, U. Houston and J.H. Lienhard V, MIT, "A Heat Transfer Textbook", 4th edition (2012), Phlogiston Press, Cambridge, MA, U.S.A. http://web.mit.edu/lienhard/www/downloadform1.html.

20 McLaughlin, E. "The thermal conductivity of liquids and dense gases," 64, (**1964**), *Chem. Rev.*, p. 389-428.

21 Eckert,, R.J. Goldstein, E.R.G., Pfender, E., Ibele, W.E., Ramsey, J.W., Simon, T.W., Decker, N.A., Kuehn, T.H., Lee, H.O., S.L. Girshick, "Heat transfer—a review of 1985 literature", *Int. J. of Heat and Mass Transfer*, 29, Issue 12 **(1986)**, p. 1767–1842.

22 Eckert, E.R.G., Goldstein, R.J., Ibele, W.E., Patankar, S.V., Simon, T.W., Strykowski, P.J., Tamma, K.K., Kuehn, T.H., Bar-Cohen, A., Heberlein, J.V.R., Hofeldt, D.L., Stelson, K.A. and Davidson, J.H., "Heat: transfer-a review of 1993 literature", *J. Heat Mass Transfer*, 39, No. 5, (**1996**) p. 885-963,

23 Eckert, E.R.G., Goldstein, R.J., Ibele, W.E., Patankar, S.V., Simon, T.W., Strykowski, P.J., Tamma, K.K., Kuehn, T.H., Bar-Cohen, A., Heberlein, J.V.R., Hofeldt, Davidson, J.H., Bishof, J., Kulacki, F., and Kortshagen, U., "Heat transfer—a review of 1995 literature", *Int*. *J. of Heat and Mass Transfer*, 42, **(1999)** p. 2717-2797.

24 Nield, Donald A. and Bejan, Adrian, "Convection in Porous Media", Springer Science+Business Media Inc., **(2006)**, New York, NY.

25 Buck, Wolfgang and Rudtsch, Steffen. "Springer Handbook of Metrology and Testing", Editors Czichos, H., Saito, T., and Smith, L.M. (**2011**), Springer-Verlag, Berlin Heidelberg, Chapter 8 "Thermal Properties", p. 435-484.

26 Gabbott, P. "A Practical Introduction to Differential Scanning Calorimetry, in Principles and Applications of Thermal Analysis". (ed P. Gabbott), (**2008**) Blackwell Publishing Ltd, Oxford, UK. doi: 10.1002/9780470697702.ch1

27 Hardy, B.J., "Geometry, Heat Removal and Kinetics Scoping Models for Hydrogen Storage Systems", Report prepared for US DOE, **(2007)**, WSRC-TR-2007-00439, http://www1.eere.energy.gov/hydrogenandfuelcells/pdfs/bruce_hardy_srnl-2007-0043_part1.pdf .

28 Hardy, B.J., "Integrated Hydrogen Storage System Model", Report prepared for US DOE, **(2007)**, WSRC-TR-2007-00440, http://www1.eere.energy.gov/hydrogenandfuelcells/pdfs/bruce_hardy_srnl-2007-0043_part2.pdf

29 Gross, K.J., Carrington, R.K. Barcelo, S., Karkamkar, A. Purewal, J., Ma, S., Zhou, H.-C., Dantzer, P., Ott, K., Burrell, T., Semeslberger, T., Pivak, Y., Dam, B., and Chandra, D., "Recommended Best Practices for the Characterization of Storage Properties of Hydrogen Storage Materials", DOE publication: http://www1.eere.energy.gov/hydrogenandfuelcells/storage/test_analysis.html

30 Wikipedia, "Thermal Conductivity", http://en.wikipedia.org/wiki/Thermal_conductivity, http://creativecommons.org/licenses/by-sa/3.0 .

31 Welty, J.R. and Wicks, C.E., "Fundamentals of momentum, heat, and mass transfer", Ed. John Wiley, 4th ed. **(2001)**, New York, U.S.A.

32 Cverna, F. "Thermal Properties of Metals", Introduction to Thermal Properties ASM Ready Reference: (#06702G), (**2002**), Technical Editor.

33 Parrott, J . E., and Stuckes, A. D., "Thermal Conductivity of Solids", **(1975)**, Pion Ltd., London, UK.

34 Do, C.T., Bentz, D.P., and Stutzman, P.E., "Microstructure and Thermal Conductivity of Hydrated Calcium Silicate Board Materials", *J. Building Physics* 31 no. 1, **(2007)**, p. 55-67.

35 Russell, H.W. "Principles of Heat Flow in Porous Insulators", *J. American Ceramic Society*, 18(1) **(1935)** p. 1-5.

36 Frey, S. "Ueber Die Elektrische Leitfahigkeit Binarer Aggregate", *Zeitschrift Fuer Elektrochemie*, 38 **(1932)** p. 260-274.

37 Bruggeman, D., "Dielectric Constant and Conductivity of Mixtures of Isotropic Materials", *Annalen Der Physik* 24(7) **(1935)** p. 636-664.

38 Loeb, A.L., "Thermal Conductivity: VIII, A Theory of Thermal Conductivity of Porous Materials", *J. American Ceramic Society* 37(2): **(1954)** p. 96-99.

39 Dedrick, D.E., "Solid-state hydrogen storage system design", in "Solid-state hydrogen storage: materials and chemistry", Walker, G.S. (editor), Woodhead Publishing Ltd, (**2008**), Cambridge, UK, p. 82-103. Figures reproduction by permission of Woodhead Publishing Limited, ISBN 9 1 84569 270 4.

40 Oi, T., Makia, K., and Sakakib, Y., " Heat transfer characteristics of the metal hydride vessel based on the plate-fin type heat exchanger ", *J. Power Sources*, 125, Issue 1, 2 (2004), Pages 52–61.

41 Yagi, S., and Kunii, S., "Studies on effective thermal conductivities in packed beds.", *A.I.ch.E. Journal* (3) (**1957**) p.373-381.

42 Sun, D., "A theoretical model predicting the effective thermal conductivity in powdered metal hydride beds", Int. J. Hydrogen Energy, 15(5) (**1990**) p. 331-336.

43 Ishido, Y., Kawamura, M., Ono, S., "Thermal conductivity of magnesium-nickel hydride powder beds ina hydrogen atmosphere*", Int. J. Hydrogen Energy*, 7(2) (**1982**) p. 173-182.

44 Suissa, E., Jacob, I., Hadari, Z.," Experimental measurements and general conclusions on the effective thermal conductivity of powdered metal hydrides", *J. Less-Common Met*, 104 **(1984)** p. 287-295.

45 Isselhorst, A., "Heat and mass transfer in coupled hydride reaction beds", *J. Alloys and Compounds*, Vol. 231, (**1995**) p. 871-879.

46 Kapischke, J., Hapke, J. *"*Measurement of the effective thermal conductivity of a Mg–MgH2 packed bed with oscillating heating*", Experimental Thermal and Fluid Science*, 17 (**1998**), p. 347-355.

47 Tstsas, E., and Martin, H., "Thermal conductivity of packed beds: A review", *Chemical Engineering and Processing*, 22 (**1987**) p. 19-37.

48 Rodriguez Sanchez, A., et al., " Expanded graphite as heat transfer matrix in metal hydride beds ", *Int. J. Hydrogen Energy*, 28 (**2003**) p. 515-527.

49 Created by Ido Perelmutter, Wikipedia article "Thermal contact conductance", http://en.wikipedia.org/wiki/Thermal_contact_resistance.

50 Holman, J.P., "Heat Transfer", 8th Edition. (**1997**) McGraw-Hill.

51 Asakuma, Y., Miyauchi, S., Yamamoto, T., Aoki, H., Miura, T., "Homogenization method for effective thermal conductivity of metal hydride bed", *Int. J. of Hydrogen Energy*, 29 (**2004**) p.209 – 216.

52 Hahne, D., Kallweit, J., "Thermal conductivity of metal hydride materials for storage of hydrogen: experimental investigation", *Int. J. Hydrogen Energy* **(1998**) 23(2) p.107–14.

53 Griesinger A, Spindler K, and Hahne E., "Measurement and theoretical modeling of the effective thermal conductivity of zeolites", *Int J. Heat Mass Transfer*, 42 **(1999)** p. 4363–74.

54 Kaviany M. Principles of Heat Transfer in Porous Media. Second Edition, Springer, New York, New York, ISBN 0-387-94550-4 (**1995**)

55 Wakao N., Kaguei S. Heat and mass transfer in Packed Beds. Gordon and Breach Science Publishers, New York, New York, ISBN 0-677-05860-8, (**1982**).

56 Péclet, E., "Traité de la chaleur", Fourth Edition, Paris, **1878**.

57 Poensgen, R., "Ein technisches Verfahren zur Ermittlung der Wärmeleitgfähigkeit plattenförmiger Stoffe", *Zeitschrift des Vereines Deutscher Ingenieure*, (**1912**) p. 56.

58 Adapted from: Evitherm.org article, "Measurement Methods", http://www.evitherm.org/, http://www.evitherm.org/default.asp?ID=308, and Wikipedia article "Thermal Conductivity", http://en.wikipedia.org/wiki/Thermal_conductivity. http://en.wikipedia.org/wiki/Thermal_conductivity.

59 Tye, R. P., Compendium of Thermophysical Properties Measurement Methods Vol. 2 , Eds. K. Maglic et al, (**1994**), Plenum Press New York, 77-97.

60 Sweet, J. N., Moss, and M., Sisson, C. E.,. Thermal Conductivity 18 , Eds T Ashworth, D R Smith, Plenum Press, (**1985**) New York, 43-59.

61 Brandt, R., and Neuer, G., "Measurement of the Electric Resistivity of Metals up to and Above the Melting Temperature", *Advanced Engineering Materials* 5 (**2003**), p. 52-55.

62 Szelagowski, H., and Taylor, R. "Measurement of thermal diffusivity of liquid metals", *High Temp.-High Press.* 30 (**1998**), 343-350.

63 Iida, T., and Guthrie, R., The Physical Properties of Liquid Metals Clarendon Press, Oxford (**1988**), 232.

64 Coumou, K. G., and Tye, R. P., *High Temp. High Press.*, 13 (**1981**), 695.

65 Agari, Y., Tanaka, M., and Nagai, S. (**1987**), Thermophysical Properties 8, Japanese Society of Thermophysical Properties, Tokyo.

66 ASTM E1530-04, Standard Test Method for Evaluating the Resistance to Thermal Transmission of Materials by the Guarded Heat Flow Meter Technique, ASTM Stand. Philadelphia.

67 Klarsfield, S. (**1984**), Compendium of Thermophysical Properties Measurement Methods, Eds K Maglic et al, 169—230.

68 Pratt, W. (**1969**), Thermal Conductivity Vol.2, ed. R P Tye, p. 301-404.

69 Guarded Hot Plate and Heat-Flow Meter Technology, Eds C. J. Shirtliffe and R. P. Tye (**1985**), ASTM STP 879, ASTM, Philadelphia.

70 Verschoor, J. D., and Wilber, A., *Trans Am Soc Heat Vent Engrs*, 60 (**1954**).

71 Pelanne, C. M., and Bradley, C. B., *Mats Res Stand*, 2 (**1962**), p. 549.

72 Tye, R. P., Coumou, K. G., Desjarlais, A. O., and Haines, D. M. (**1987**), Thermal Insulation: Materials and Systems, ASTM STP 922, ASTM Philadelphia.

73 Solvason, K. R., **1965**, ASHRAE Transactions, Vol. 65.

74 Mumaw, J. R., Heat Transmission Measurements in Thermal Insulations, ASTM STP 544, **1974,** Ed R P Tye, ASTM International, West Conshohocken, PA, p. 193-211.

75 Mumaw, J. R., Thermal Insulation Performance, ASTM STP 718, **1980,** Eds D. L. McElroy and R. P. Tye, ASTM International, West Conshohocken, PA, p. 195-207.

76 Perrine, E. L., Linehan, P. W., Howanski, J. W., and Shu, L. S., **1981**, Thermal Performance of the Exterior Envelopes of Buildings, ASHRAE SP28, American Society of Refrigeration and Air-Conditioning Engineers, Inc, New York, NY, p. 237-249 (see also P R Achenbach, ibid, p. 308-319 and J L Rucker and J R Mumaw, ibid, p. 237-249).

77 Lavine, A. G., Rucker, J. L., Wilkes, K. E., **1983**, Thermal Insulations, Materials, and Systems for Energy Conservation in the 80s, ASTM STP 789, Eds F. A. Govan, D. M. Greason, J. D. McAllister, ASTM International, West Conshohocken, PA, p. 234-247.

78 Van Geem, M. G., "Overview of the Workshop for Hot Box Operators*", J Testing and Evaluation* 15, **1987**, p. 178-184.

79 Bales, E., **1988**, ASTM, Hot box round-robin, ORNL/Sub/84/97333/2, Oak Ridge National Laboratory, Oak Ridge, TN.

80 Kubicar, L., Bohac, V., "A step-wise method for measuring thermophysical parameters of materials*", Meas Sci Tech* 11 (**2000**), p. 252-259.

81 Kubicar, L., *High Temp-High Press*, 23 (**1991**), p. 40.

82 Gustafsson, S. E., "Transient plane source techniques for thermal conductivity and thermal diffusivity measurements of solid materials", *Rev Sci Instrum*. 62, (**1991**) p. 797-804M.

83 Log, T., Gustafsson, S. E., "Transient plane source (TPS) technique for measuring thermal transport properties of building materials*", Fire and Materials*, 19, (**1995**) p. 43-49.

84 Hammerschmidt, U., and Sabuga, W., "Transient Hot Wire THW. Method: Uncertainty Assessment", *Int. J. Thermophys.* 21, (**2000**) p. 217, and 21, p. 1255 –1278.

85 Parker, W. J., Jenkins, R. J., Butler, C. P., and Abbot, G. L., "Flash Method of Determining Thermal Diffusivity, Heat Capacity, and Thermal Conductivity", *J. Appl. Phys.* 32, (**1961**), p. 1679-1684.

86 Maglic, K. D., and Taylor, R. E., (**1992**), Compendium of Thermophysical Properties Measurement Methods Vol 2, Eds K Maglic et al, Plenum Press New York, p. 281-314. Also Vol1 (**1984**), p. 299-336.

87 Cezairliyan, A., Baba, T., and Taylor, R. E., "A high-temperature laser-pulse thermal diffusivity apparatus "*Int. J. Thermophys.*, 15 (**1994**), p. 317-341.

88 Angstrom, A. J., *Annal Phys.* 64, (**1861**), p. 513.

89 Sidles, P. H., and Danielson, G. C., "Thermal Diffusivity of Metals at High Temperatures"**,** *J. App. Phys.*, 25 (**1954**), p. 58-66.

90 Abeles, B., Cody, G. D., and Beers, D. S. , "Apparatus for the Measurement of the Thermal Diffusivity of Solids at High Temperatures", *J. App. Phys.*, 31, (**1960**), p.1585-1591.

91 Hatta, I., Sasuga, Y., Kato, R. and Maesono, A., "Thermal diffusivity measurement of thin films by means of an ac calorimetric method", *Rev. Sci. Instrum.*, 56, (**1985**) p. 1643-1647.

92 Gu, Y., Tang, X., Xu, Y., and Hatta, I., "Ingenious Method for Eliminating Effects of Heat Loss in Measurements of Thermal Diffusivity by ac Calorimetric Method", *Jpn. J. Appl. Phys.* 32, (**1993**) , p.L1365-L1367.

93 Kato, R., Maesono, A., and Tye, R. P., Thermal Conductivity 22, (**1994**) Ed T. Tong, p. 473—485.

94 De Coninck, R., and Peletsky, V. E., (**1984**). Compendium of Thermophysical Property Measurement Methods, Eds K. D. Maglic et al., p.367-428.

95 Wheeler, M. J., *J. Sci. Technol.*, 38 (**1971**), p.10.

96 Cowan, R. D. "Proposed Method of Measuring Thermal Diffusivity at High Temperatures", *J. Appl. Phys.* 32, (**1961**) p. 1363-1370.

97 Brandt, R. and Neuer, G., "Thermal diffusivity of solids – analysis of a modulated heating-beam technique", *High Temp-High Press* 11 (**1979**), p. 59-68.

98 Rosencwaig, A., "Photo-acoustic spectroscopy of solids", *Rev Sci Instr*, 48, (**1977**) p. 1133-1137.

99 Tam, A. C., "Applications of photoacoustic sensing techniques *", Rev Mod Phys*, 58, (**1986**) p.381-431.

100 Rohde, M., "Photoacoustic characterization of thermal transport properties in thin films and microstructures*", Thin Solid Films*, 238, (**1994**) p. 199-206.

101 McElroy, D. L., and Moore, J. P. (**1969**), Thermal Conductivity Vol 1, Ed R. P. Tye, Academic Press, London and New York, 186-239.

102 Flynn, D. R., (**1994**), Compendium of Thermophysical Properties Measurement Methods Vol 2 , Eds K Maglic et al, Plenum Press New York, 33-75.

103 Powell, R. W., and Tye, R. P., "New measurements on thermal conductivity reference materials". *Int. J. Heat and Mass Transfer*, 10, (**1967**) p. 581.

104 Cezairliyan, A. (**1992**), Compendium of Thermophysical Properties.

105 Measurement Methods Vol 2 , Eds K. Maglic et al, Plenum Press New York, p. 483-517. See also Vol 1 (**1984**), p.643-668.

106 Righini, F., Rosso, A., "A pulse technique for the measurement of thermophysical properties", *Measurement*, 1, (**1983**) p.79-84.

107 Righini, F., Rosso, A., Ruffino, G. "System for fast high temperature measurement." *High Temp High Press* 4, (**1972**), p.597-603.

108 Adapted from: Evitherm.org article, "Measurement Methods", http://www.evitherm.org/, http://www.evitherm.org/default.asp?ID=308.

109 Adapted from: Evitherm.org, http://www.evitherm.org/default.asp?ID=676&menu1=676

110 Dedrick, D.E., Kanouff, M.P., Replogle, B.C. and Gross, K.J., "Thermal properties characterization of sodium alanates", *J. Alloys and Compounds*, Vol. 389, (**2005**) p. 299–305.

111 Communication with Dr. Mike Veenstra and Dr. Jun Yang Ford Motor Co.

112 Image from National Physical Laboratory, Hampton Road, Teddington, Middlesex, TW11 0LW, UK, web page: "Axial Heat Flow Meter", http://www.npl.co.uk/science-technology/thermal-performance/areas/thermal-conductivity/axial-heat-flow-meter.

113 Fesmire, J.E., Augustynowicz, S.D., Heckle, K.W., and Scholtens, B.E., "Equipment and Methods for Cryogenic Thermal Insulation Testing", *Advances in Cryogenic Engineering*, 710 (1) **(2004)**, p. 579-586.

114 Zarr R.R., "A History of Testing Heat Insulators at the National Institute of Standards and Technology",©ASHRAE www.ashrae.org , *ASHRAE Transactions*, V.107, Pt. 2, June **(2001)**.

115 Van Dusen, M.S. "A simple apparatus for comparing the thermal conductivity of metals and very thin specimens of poor conductors", *J. Optical Society of America and Review of Scientific Instruments*, 6 **(1922)**, p. 739- 743.

116 Reprinted, with permission, from ASTM C1044-98(2003) Standard Practice for Using a Guarded-Hot-Plate Apparatus or Thin-Heater Apparatus in the Single-Sided Modes, copyright ASTM International, 100 Barr Harbor Drive, West Conshohocken, PA 19428. A copy of the complete standard may be obtained from ASTM International, www.astm.org.

117 Flynn, D.R., "A radial-flow apparatus for determining the thermal conductivity of loose-fill insulations to high temperatures", Bureau of Standards Journal of Research, 67C **(1962)**, p. 129-137.

118 Flynn, D.R., "Thermal conductivity of loose-fill materials by a radial-heat-flow method, Compendium of thermophysical property measurement methods", Volume 2, Recommended measurement techniques and practices, K. D. Maglic, A. Cezairliyan, and V. E. Peletsky, eds., **(1992)** New York: Plenum Press., p. 33-75.

119 Barrios, M., "Measuring Thermal Conductivity of Powder Insulation at Cryogenic Temperatures", M.S. Thesis, **(2006)** Florida State University, College of Engineering.

120 Choi, Y.S., Barrios, M.N., Chang, H.M., and Van Sciver, S.W., "Thermal Conductivity of Powder Insulations for Cryogenic Storage Vessels", *Advances in Cryogenic Engineering*, 823 (1), **(2006)**, p. 480.

121 Aberdeen, J. and Laby, T.H., "Conduction of heat through Powders and Its Dependence on the Pressure and Conductivity of the Gaseous Phase", *Proceedings of the Royal Society of London* , Series A, Vol. 113, No. 764, **(1926)** p. 459-477.

122 Nayak, A.L. and Tien C.L., "Thermal Conductivity of Microsphere Cryogenic Insulation", *Advances in Cryogenic Engineering* 22 **(1977)**, p. 251-262.

123 Figure adapted from **"**Thermal Conductivity - Different Methods for Measurement of Thermal Conductivity" AZoM Editors, http://www.azom.com/article.aspx?ArticleID=5615 .

124 Figure adapted from **"**Principal Methods of Thermal Conductivity Measurements", Technical Note #67, http://www.anter.com/technotes/TPN-67%20Principal%20Methods%20of%20Thermal%20Conductivity%20Measurement.pdf .

125 Van Dusen, M., and Shelton, S., , "Apparatus for measuring thermal conductivity of metals up to 600 C". *Bureau of Standards Journal of Research*, 12, (**1934),** p. 429-440.

126 Ballard, S., McCarthy, K., and Davis, W. "A Method for Measuring the Thermal Conductivity of Small Samples of Poorly Conducting Materials such as Optical Crystals". *Review of Scientific Instruments*, 21, (**1950),** p. 905.

127 Morris, R., and Hust, J. "Thermal Conductivity Measurements of Silicon from 30 to 425 C". *Physical Review*, 124(5), (**1961),** p. 1426-1430.

128 Francl, J., and Kingery, W. D. "Apparatus for Determining Thermal Conductivity by a Comparative Method," *J. American Ceramic Society*, 37 (**1954)**.

129 Mirkovich, V. "Comparative Method and Choice of Standards for Thermal Conductivity Determinations," *J. American Ceramic Society*, 48(8), (**1965),** p. 387-391.

130 Sweet, J., Roth, E., Moss, M., Haseman, G., and Anaya, J. "Comparative Thermal Conductivity Measurements at Sandia National Laboratories," (**1986),** No. SAND86-0840, Sandia National Laboratory, Albuquerque, NM.

131 Pillai, C., and George, A. "An Improved Comparative Thermal Conductivity Apparatus for Measurements at High Temperatures," *Int. J. Thermophysics*, 12(3), (**1991),** p. 563-576.

132 ASTM Standard E1225, 1987 (**2004**), "Standard Test Method for Thermal Conductivity of Solids by Means of the Guarded-Comparative-Longitudinal Heat Flow Technique," ASTM International, West Conshohocken, PA.

133 Babelot, J., Gaal, P., Van Geel, J., and Schmidt, H., **1994**, "A Heat Flow Comparator for Measuring the Thermal Conductivity of Highly Radioactive Specimens," Proc. International Thermal Conductivity Conference 22, T. W. Tong, ed., Tecnomic Publishing Company, p. 913-919.

134 Jensen, C., Xing, C., Ban, H., and Phillips, J. "Validation of a Thermal Conductivity Measurement System for Fuel Compacts", Proceedings of the ASME/JSME **2011** 8th Thermal Engineering Joint Conference, AJTEC2011, March 13-17, 2011, Honolulu, HI, USA.

135 Didion, D., **1968**, "An Analysis and Design of a Linear Guarded Cut-bar Apparatus for Thermal Conductivity Measurements," No. AD-665789, National Technical Information Service, Springfield, VA.

136 ASTM D5334, "Determination of Thermal Conductivity of Soil and Soft Rock by Thermal Needle Probe Procedure", **(2000)**, originally published as D 5334 – 92, ASTM International, West Conshohocken, PA, DOI: 10.1520/D5334-08 , www.astm.org.

137 Blackwell, J.H. "A Transient-Flow Method for Determination of Thermal Constants of Insulating Materials in Bulk, Part I – Theory", *J. Applied Physic*s, 25 **(1954)** p. 2.

138 Wechsler, A.E., "The Probe Method for Measurement of Thermal Conductivity". in Maglić K.D., Cezairliyan A., Peletsky V.E., (Eds.) *Compendium of Thermophysical Property Measurement Methods*, Vol. 2, Recommended Measurement Techniques and Practices **(1992)** New York, London, Plenum Press, p. 281.

139 Manohar, K., Yarbrough, D. W., Booth, J.R., "Measurement of Apparent Thermal Conductivity by the Thermal Probe Method", *J. Testing and Evaluation*, **(2000)** p. 345-352.

140 Jones, B. W. "Thermal conductivity probe: development of method and application to a coarse granular medium", *J. Phys. E: Sci. Instrum.* 21 **(1988)** p. 832-839.

141 Batty, W.J. "Assessment of the Thermal-probe Technique for Rapid, Accurate Measurements of Effective Thermal Conductivities", *J. Applied Energy* 16 **(1984)** p. 83-113.

142 Gustafsson, S.E. "Device for measuring thermal properties of a test substance – the transient plane source (TPS) method." **(1991)**, U.S. Patent No. 5,044,767.

143 Gustafsson, S.E. "Transient plane source techniques for thermal conductivity and thermal diffusivity measurements of solid materials", *Rev. Sci. Instrum.* 62, **(1991)**, p.797–804.

144 Gustafsson, S.E., Karawacki, E. and Khan, M.N. "Determination of the thermal-conductivity tensor and the heat capacity of insulating solids with the transient hot-strip method", *J. Applied Physics*, 52, **(1981)**, p. 2596-2600.

145 Gustafsson, S.E., Karawacki, E. and Khan, M.N. "Transient hot-strip method for simultaneously measuring thermal conductivity and thermal diffusivity of solids and fluids". *J. Physic. D: Applied Physics*, 12 **(1979)**, p. 1411-1421.

146 Suleiman, B.M. "Thermal Conductivity of Saturated Samples Using the Hot-Disk Technique", Proceedings of the 4th WSEAS Int. Conf. on Heat Transfer, Thermal Engineering and Environment, Elounda, Greece, **(2006)**, p140-145.

147 Gustavsson, M., Karawacki, E., and Gustafsson, S.E. "Thermal conductivity, thermal diffusivity and specific heat of thin samples from transient measurement with Hot Disk sensors*." Rev. Sci. Instru.,* 65 (12), (**1994**) p. 3856.

148 Log, T. and Gustafsson, S.E. "Transient Plane Source (TPS) Technique for Measuring Thermal Transport Properties of Building Materials", *Fire and Materials* 19(1), **(1995)** p. 43.

149 Bohac, V., Gustafsson, M.K., Kubicar, L. and Gustafsson, S.E. "Parameter estimations for measurements of thermal transport properties with the hot disk thermal constants analyzer ", *Rev. Sci. Instru.*, 71(6), **(2000)** p. 2452.

150 Carslaw, H. and Jaeger, J. "Conduction of Heat in Solids", 2 ed. **(1959)** Oxford, Clarendon Press.

151 He, Y. "Rapid thermal conductivity measurement with a hot disk sensor: Part 1. Theoretical considerations", *Thermochimica Acta*, 436, (1–2), **(2005)**, p. 122–129.

152 Beattie, S.D., Harris, A., Levchenko, A., Rudolph, J., Christopher D. Willson, C.D., and McGrady, G.S. "Thermal conductivity and specific heat measurements of metal hydrides", *ITCC Proceedings*, **(2009)** - unb.ca.

153 Harris, S. "Thermal Conductivity Testing of Minimal Volumes of Energetic Powders", *International Thermal Conductivity Conference* **(2005)**.

154 Flueckiger, S.M. "Thermal Properties Measurements of High Pressure Metal Hydrides: Master of Science Thesis in Mechanical Engineering, Purdue University, May **2009**, UMI Number: 1469847.

155 Suleiman, B. M. "Transient Plane Source Method Thesis : Chapter 4", Physics Department, Chalmers University of Technology, Gothenburg, Sweden **1994**, p. 37-58.

156 Gustavsson, M. & Gustafsson, S.E. "On the use of transient plane source sensors for studying materials with directions dependent properties", proceedings 26th ITCC, **(2001)** Boston, USA, p. 195-199.

157 Incropera, F., Dewitt, D., Bergman, T., and Lavine, A. "Fundamentals of Heat and Mass Transfer", 6 ed. **(2007)**: John Wiley & Sons.

158 Davis, W.R. "Hot-Wire Method for the Measurement of the Thermal Conductivity of Refractory Materials", in Maglić, K.D., Cezairliyan A., Peletsky V.E., (Eds.) *Compendium of Thermophysical Property Measurement Methods*, Vol. 1 Survey of Measurement Techniques **(1984)** New York, London, Plenum Press, p. 161.

159 Vozár, L.. **"**Hot wire method apparatus - the thermal conductivity measurement of solids, powders and granulate materials in the temperature range from 20 to 1000° C", http://www.tpl.fpv.ukf.sk/engl_vers/hot_wire.htm , Constantine the Philosopher University.

160 Vozár, L., "A Computer-Controlled Apparatus for Thermal Conductivity Measurement by the Transient Hot Wire Method", *J. of Thermal Analysis*, 46, **(1996),** p. 495-505.

161 NIST, Experimental Properties of Fluids Group, *"Thermal Conductivity of Liquids and Gases"*, http://fluidproperties.nist.gov/thermal.html .

162 The results of the transient hot-wire measurements are available for a many fluids in a series of NBS/NIST reports. Copies of these publications can be obtained by contacting Dr. Richard A. Perkins, NIST, Physical and Chemical Properties Division, Experimental Properties of Fluids Group, Mail Stop 838.07, 325 Broadway, Boulder, CO 80305-3328 USA, perkins@boulder.nist.gov.

163 Roder, H.M., *"Experimental Thermal Conductivity Values for Hydrogen, Methane, Ethane and Propane"*, **(1984)**, Chemical Engineering Sciences Division, National Engineering Laboratory, National Bureau of Standards, prepared for NASA-Lewis Research Center, NBSIR 84-3006.

164 [Image by Marilyn Yetzbacher], NIST, Experimental Properties of Fluids Group, *"Thermal Conductivity of Liquids and Gases"*, http://fluidproperties.nist.gov/thermal.html .

165 ASTM Standard E1461-01, "Standard Test Method for Thermal Diffusivity of Solids by the Flash Method", ASTM International, West Conshohocken, PA, DOI: 10.1520/E1461-07, www.astm.org.

166 Parker, W.J., Jenkins, R.J., Butler, C.P., and Abbott, G.L., "A Flash Method of Determining Thermal Diffusivity, Heat Capacity, and Thermal Conductivity", *J. Applied Physics*, 32 (9), **(1961)**, p. 1679-1684.

167 Smith, S.E. and Campbell, R.C., "Flash Diffusivity Method: A Survey of Capabilities", May (**2002**) Article in Electronic Cooling: http://www.electronics-cooling.com/2002/05/flash-diffusivity-method-a-survey-of-capabilities .

168 Hohenauer, W., in "A today's philosophy to determine the Thermal Conductivity", presentation, ExtreMat: Thermophysical Workshop, http://www.phox.at/upload/Methods%20in%20Thermophysics.pdf , Thermophysik & Thermokinetik am Austrian Institute of Technology – AIT, http://www.phox.at .

169 Adapted from figure by Hohenauer, W., in "A today's philosophy to determine the Thermal Conductivity", presentation, ExtreMat: Thermophysical Workshop, http://www.phox.at/upload/Methods%20in%20Thermophysics.pdf , Thermophysik & Thermokinetik am Austrian Institute of Technology – AIT, http://www.phox.at .

170 ASTM E1269-11, "Standard Test Method for Determining Specific Heat Capacity by Differential Scanning Calorimetry", ASTM International, West Conshohocken, PA, DOI: 10.1520/E1269-11, www.astm.org.

171 Campbell, R.C, Smith, S.E., and Dietz, R.L., "Measurements of Adhesive Bondline Effective Thermal Conductivity and Thermal Resistance Using the Laser Flash Method", *Proceedings of IEEE SEMI-THERM* XV, **(1999)**, p. 83-97.

172 Donaldson, A.B., "Two-Dimensional Thermal Attenuation of a Laser Pulse in a Solid", *J. the Franklin Institute*, 294(4), **(1972)**, p. 275-281.

173 Donaldson, A.B., "Radial Conduction Effects in the Pulse Method of Measuring Thermal Diffusivity", *J. Applied Physics*, 43(10), **(1972)**, p. 4226-4228.

174 Donaldson, A.B., and Taylor, R.E., "Thermal Diffusivity Measurement by a Radial Heat Flow Method", *J. Applied Physics*, 46(10), **(1975)**, p. 4584.

175 Zhang, J., Fisher, T.S., Ramachandran, P.V., and Gore, J.P., "A Review of Heat Transfer Issues in Hydrogen Storage Technologies*", J. of Heat Transfer*, Vol. 127 (**2005)** p. 1391-1399.

176 Sanchez**,** R.A., Klein, H.-P., and Groll, M., "Expanded Graphite as Heat Transfer Matrix in Metal Hydride Beds," *Int. J. Hydrogen Energy*, 28 (5) **(2003)**, p. 515–527.

177 Kim, K. J., Montoya, B., Razani, A., and Lee, K.-H., "Metal Hydride Compacts of Improved Thermal Conductivity," *Int. J. Hydrogen Energy*, 26 (6) **(2001)**, p. 609–613.

178 Oi, T., Maki, K., and Sakaki, Y., "Heat Transfer Characteristics of the Metal Hydride Vessel Based on the Plate-Fin Type Heat Exchanger," *J. Power Sources*, 125 (1) **(2004)**, p. 52–61.

179 Kaviany, K., (**1995)**, Principles of Heat Transfer in Porous Media, Springer, New York.

180 Asakuma, Y., Miyauchi, S., Yamamoto, T., Aoki, H., and Miura, T., "Homogenization Method for Effective Thermal Conductivity of Metal Hydride Bed*," Int. J. Hydrogen Energy*, 29, (**2004),** p. 209–216.

181 Wang, J., (**2004)**, "Hydride Development for Hydrogen Storage," Proceedings of the 2004 Annual U.S. DOE Hydrogen Program Review.

182 Heung, L. K., (**2003)**, Using Metal Hydride to Store Hydrogen, DOE report: WSRC-MS-2003-00172.

183 Askri, F., Jemni, A., and Ben Nasrallah, S., "Study of Two-Dimensional and Dynamic Heat and Mass Transfer in a Metal-Hydrogen Reactor*," Int. J. Hydrogen Energy*, 285, (**2003),** p. 537–557

184 Klein, H.-P., and Groll, M., "Heat Transfer Characteristics of Expanded Graphite Matrices in Metal Hydride Beds*", Int. J. Hydrogen Energy*, 29 14, (**2004),** p. 1503–1511.

185 Asakum, Y., Miyauchi, S., Yamamoto, T., Aoki, H., and Miura, T., "Numerical Analysis of Absorbing and Desorbing Mechanism for the Metal Hydride by Homogenization Method.", *Int. J. Hydrogen Energy*, 285, (**2003),** p. 529–536.

186 Nakagawa, T., Inomata, A., Aoki, H., and Miura, T., "Numerical Analysis of Heat and Mass Transfer Characteristics in the Metal Hydride Bed.", *Int. J. Hydrogen Energy*, 254, (**2000),** p. 339–350

187 Gadre, S. A., Ebner, A. D., Al-Muhtaseb, S. A., and Ritter, J. A., , "Practical Modeling of Metal Hydride Hydrogen Storage Systems," *Ind. Eng. Chem. Res.,* 42, (**2003),** p. 1713–1722.

188 Askri, F., Jemni, A., and Nasrallah, S. B., , "Prediction of Transient Heat and Mass Transfer in a Closed Metal-Hydrogen Reactor.", *Int. J. Hydrogen Energy,* 29, (**2004),** p. 195–208.

189 Guo, Z., and Sung, H. J., "Technical Note Conjugate Heat and Mass Transfer in Metal Hydride Beds in the Hydriding Process.", *Int. J. Heat Mass Transfer*, 42, (**1999),** p. 379–382.

190 Georgiadis, J. G., "Future Research Needs in Convective Heat and Mass Transport in Porous Media," Convective Heat and Mass Transfer in Porous Media, Kakac, S., Kilkis, B., Kulacki, F. A., and Arinc, F., Eds., Kluwer Academic Publishers, Boston, (**1990)** p. 1073–1088.

191 Visaria, M., Mudawar, I., Pourpoint, T., Kumar, S., "Study of heat transfer and kinetics parameters influencing the design of heat exchangers for hydrogen storage in high-pressure metal hydrides", *Int. J. Heat and Mass Transfer*, 53 **(2010),** p. 2229–2239.

192 Suda, S., Komazaki, Y., Kobayashi, N. "Effective thermal conductivity of metal hydride beds", *J. Less-Common Met*, 89 **(1983)** p. 317–324.

193 Botzung, M., Chaudourne, S., Gillia, O., Perret, C., Latroche, M., Percheron-Guegan, A., and Marty, P., "Simulation and experimental validation of a hydrogen storage tank with metal hydrides", *Int. J. Hydrogen Energy* 33 **(2008)** p. 98–104.

194 Challet, S., Latroche, M., Heurtaux, F., "Development of a La0.55Y0.45Ni5 metal hydride pilot buffer tank for fuel cell car", WHEC 16 / 13-16 June **(2006)** – Lyon France.

195 Botzung, M., Chaudourne, S., Gilliaa, O., Perret, C., Latroche, M., Percheron-Guegan, A., and Marty, P., "Simulation and experimental validation of a hydrogen storage tank with metal hydrides", *Int. J. Hydrogen Energy*, 33 (**2008**) p. 98 – 104.

196 Pons M., "Heat transfers in the LaNi5 powder coupled with hydrogenation reaction", Thesis, PARIS VI University, (**1991**).

197 Private communication with Dr. Patricia De Rango, Institute Néel /CRETA in Grenoble France.

198 Gross, K.J., Majzoub, E., Thomas, G.J., and Sandrock, G., "Hydride development for hydrogen storage", (**2002**) *Proceedings U.S. DOE Hydrogen Program Review,* NREL/CP-610-32405. Golden, CO.

199 Carslaw, H. S., Jaeger, J. C., "Conduction of heat in solids", Oxford University Press **(1959)**, p. 345.

200 Jones, B.W., "Thermal conductivity probe: development of method and application to a coarse granular medium", *J. Phys. E: Sci. Instrum.* 21 **(1988)** p. 832-839.

201 Gartling, D.K., Hogan, R.E. and Glass, M.W., "COYOTE- A finite element computer program for nonlinear heat conduction problems", Sandia National Laboratories Report, SAND94-1179, Albuquerque NM, February **(2003)**.

202 Pons, M., Dantzer, P. and Guilleminot, J.J., "A measurement technique and a new model for the wall heat transfer coefficient of a packed bed of (reactive) powder without gas flow", *Int. J. Heat Mass Transfer*, 36, No. 10, **(1993)**, p. 2635-2646.

203 Zhang, H., Report on: "Metal Hydride Composite Pellet Development", **2008**, General Motors.

204 McGaughey, A.J.H., Kaviany, M. "Thermal conductivity decomposition and analysis using molecular dynamics simulations part II. Complex silica structures". *Int. J. Heat and Mass Transfer* 47, (**2004**), p.1799e816.

205 McGaughey, A.J.H., Kaviany, M. "Thermal conductivity decomposition and analysis using molecular dynamics simulations part II. Complex silica structures". *Int. J. Heat and Mass Transfer* , 47 (**2004**), p. 1799e816.

206 Griesinger, A., Spindler, K., Hahne, E. "Measurements and theoretical modeling of the effective thermal conductivity of zeolites". *Int. J. Heat and Mass Transfer* 42 (**1999)**, p. 4363e74.

207 Greenstein, A., Hudiono, Y., Graham, S., Nair, S. "Effects of nonframework metal cations and phonon scattering mechanisms on the thermal transport properties of polycrystalline zeolite LTA films". *J. Applied Physics* 107 (**2010)**; Art. No. 063518.

208 Murashov, V.V., White, M.A. "Thermal properties of zeolites: effective thermal conductivity of dehydrated powdered zeolite 4A". *Materials Chemistry and Physics* 75, (**2002),** p.178e80.

209 Wyckoff, R.W.G. Crystal structures. 2 ed. New York: John Wiley and Sons, Interscience; **1963**.

210 Huang, B.L., Ni, Z., Millward, A., McGaughey, A.J.H., Uher, C., Kaviany, M., et al. "Thermal conductivity of a metal-organic framework (MOF-5): part II. Measurement". *Int. J. Heat and Mass Transfer,* 50, (**2007),** p. 405e11.

211 Liu, D., Purewal, J.J., Yang, J., Sudik, A., Maurer, S., Mueller, U., Ni, J., Siegel, D.J., "MOF-5 composites exhibiting improved thermal conductivity", *Int. J. of Hydrogen Energy*, 37 (**2012**) p. 6109-6117.

212 Fulk, M.M. "Evacuated powder insulation for low temperatures", *Progress in Cryogenics* 1, **(1959)**, p. 65-84.

213 Kropschot, R.H., "Cryogenic Insulation", *ASHRAE Journal*, **(1959)**, p. 48-54.

214 Fesmire, J.E., Augustynowicz, S.D., Heckle, K.W., and Scholtens, B.E. "Equipment and Methods for Cryogenic Thermal Insulation Testing", *Advances in Cryogenic Engineering*, 710, Issue 1, **(2004)**.

215 Fesmire, J.E., Augustynowicz, S.D., and Rouanet, S. , "Aerogel Beads as Cryogenic Thermal Insulation System", *Advances in Cryogenic Engineering: Proceedings of the CEC*, 47, **(2002)**.

216 Figure from: Barrios, M., "Measuring Thermal Conductivity of Powder Insulation at Cryogenic Temperatures", M.S. Thesis, (2006) Florida State University, College of Engineering. Aerogel powder data in figure from: Rettelbach, T., Säuberlich, J., Korder, S.,

Fricke, J. “Thermal conductivity of silica aerogel powders at temperatures from 10 to 275 K.”, *J. Non-Crystalline Solids* 186, (**1995)**, p. 278-284.

217 Huang, B.L., Ni, Z., Millward, A., McGaughey, A.J.H., Uher, C., Kaviany, M., et al. “Thermal conductivity of a metal-organic framework (MOF-5): part II. Measurement”. *Int. J. Heat and Mass Transfer,* 50, (**2007),** p. 405e11. The MD predicted result from: Huang, B.L., McGaughey, A.J.H., Kaviany, M., “Thermal conductivity of a metal-organic framework (MOF-5). Part I: Molecular dynamics simulations”, *Int. J. Heat Mass Transfer*, this issue, doi:10.1016/ j.ijheatmasstransfer.2006.10.002.

218 Ott, K.C., “2010 Overview and Wrapup: DOE Chemical Hydrogen Storage Center of Excellence (CHSCoE)”, DOE Hydrogen Program **(2010)** Annual Progress Report, http://www.hydrogen.energy.gov/pdfs/progress10/iv_b_1a_ott.pdf.

219 Mohajeri, N., T-Raissi, A., Ramasamy, K., Adebiyi, O., and Bokerman, G., “Ammonia-Borane Complex for Hydrogen Storage”, Florida Solar Energy Center, Research Summary, Period: June 2002 to December 2007, http://www.fsec.ucf.edu/en/publications/pdf/FSEC-CR-1745-08/summaries.pdf**.**

220 ASTM C177–10 Standard, “Method for Steady-State Heat Flux Measurements and Thermal Transmission Properties by Means of the Guarded Hot Plate Apparatus”, **2004**, *ASTM International*, West Conshohocken, PA, DOI: 10.1520/C0177-10, www.astm.org.

221 ISO 8302:1991, “Thermal Insulation —Determination of Steady-State Thermal Resistance and Related Properties—Guarded Hot Plate Apparatus”, **1991**.

222 ASTM C 518–10 Standard, “Test Method for Steady-State Thermal Transmission Properties by Means of the Heat Flow Meter Apparatus”, *ASTM International*, West Conshohocken, PA, DOI: 10.1520/C0518-10, www.astm.org.

223 ISO 8301:1991, “Thermal Insulation —Determination of Steady-State Thermal Resistance and Related Properties —Heat Flow Meter Apparatus”, **1991**.

224 Miller, R.A. and Kuczmarski, M.A. “Method for Measuring Thermal Conductivity of Small Samples Having Very Low Thermal Conductivity”, NASA Report, TM (**2009)** 215460.

225 Dehouche, Z., Grimard, N., Laurencelle, F., Goyette, J., Bose, T.K., **“**Hydride alloys properties investigations for hydrogen sorption compressor*”, J. Alloys and Compounds* 399 **(2005)**, p. 224–236.

226 Radwanski, R. J., Kim-Ngan, N. H., Kayzel, F. E., Franse, J. J. M., Gignoux, D., Schmitt, D. and Zhang, F. Y.*,”* The specific heat of $ErNi_5$ and $LaNi_5$*”, J. Phys.: Condens. Matter* 4 (**1992**) p.8853–8862.

227 Chaise, A., de Rango, P., Marty, Ph., Fruchart, D., Miraglia, S., Olivès, R., and Garrier, S., “Enhancement of hydrogen sorption in magnesium hydride using expanded natural graphite”, *Int. J. Hydrogen Energy* 34 **(2009)**, p. 8589-8596.

228 Fedchenia, I.I., and van Hassel, B.A., “Solution of Inverse Thermal Problem for Assessment of Thermal Parameters of Engineered H2 Storage Materials”, paper, Comsol Conference, Boston **(2011)**.

229 Beck, J.V., “Transient determination of thermal properties”, *Nuclear Engineering and Design*, 3, **(1966)**, p.373-381.

230 Schisler, I. P, and Beck J.V., “Estimation of thermal parameters from transient temperature measurements containing correlated ARIMA errors”, *Letters in Heat and Mass Transfer,* 6, **(1979)**, p.181-188.

231 Yi, H., "Rapid thermal conductivity measurement with a hot disk sensor", Part 1&2, *Thermochimica Acta*, 436 (**2005**), p.122–134.

232 van Hassel, B.A., Pasini, J.M., Mosher, D., Gorbounov, M., Holowczak, J., Fedchenia, I., Khalil, J., Sun, F., Tang, X., Brown, R., Laube, B., and Pryor, L., "Advancement of Systems Designs and Key Engineering Technologies for Materials Based Hydrogen Storage", DOE Hydrogen Program Annual Merit Review, Washington, DC May 11, **(2011)**.

233 Pohlmann, C., Röntzsch, L., Hu, J., Weißgärber, T., Kieback, B., and Fichtner, M. "Tailored heat transfer characteristics of pelletized $LiNH_2$–MgH_2 and $NaAlH_4$ hydrogen storage materials", *J. Power Sources* 205 (**2012**), p. 173– 179.

234 Pohlmann, C., Röntzsch, L., Kalinichenka, S., Hutsch, T., Weißgärber, T., and Kieback, B., "Hydrogen storage properties of compacts of melt-spun $Mg_{90}Ni_{10}$ flakes and expanded natural graphite", *J. Alloys and Compounds,* 509S (**2011**), p.625– 628.

235 Pohlmann, C., Röntzsch, L., Kalinichenka, S., Hutsch, T., and Kieback, B., "Magnesium alloy-graphite composites with tailored heat conduction properties for hydrogen storage applications", *Int. J. Hydrogen Energy,* 35 (**2010**), p. 12829-12836.

236 Mamunya, Ye.P., Davydenko, V.V., Pissis, P., and Lebedev, E.V., "Electrical and thermal conductivity of polymers filled with metal powders", *European Polymer Journal*, 38 (**2002**) p. 1887-1897.

237 Figure provided by Dr. Renju Zacharia of the Université du Québec à Trois-Rivières, Canada.

238 DOE Technical Targets for Onboard Hydrogen Storage Systems for Light Duty Vehicles. Website as of 7/16/2012 : http://www1.eere.energy.gov/hydrogenandfuelcells/storage/pdfs/targets_onboard_hydro_storage.pdf

239 Corgnale, C., Hardy, B.J., Tamburello, D.A., Garrison, S.L., Anton, D.L. "Acceptability envelope for metal hydride-based hydrogen storage systems". *Int. J. Hydrogen Energy*, 37 (**2012**), p. 2812-2824.

240 Hardy, B.J., Anton, D.L. "Hierarchical methodology for modeling hydrogen storage systems. Part II: Detailed models". *Int. J. of Hydrogen Energy,* 34 (**2009**), p. 2992-3004.

241 Hardy, B., Corgnale, C., Chahine, R., Richard, M.-A., Garrrison, S., Tamburello, D., Cossement, D., Anton, D. " Modeling of adsorbent based hydrogen storage systems." *Int. J. Hydrogen Energy*, 37 (**2012**) p. 5691-5705.

242 Mosher, D., Tang, X., Arsenault, S., Laube, B., Cao, M., Brown, R. and Saitta, S. "High Density Hydrogen Storage System Demonstration Using NaAlH4 Complex Compound Hydrides". DOE Hydrogen Program Annual Peer Review, Arlington, VA, **2007**.

243 Bird, R.B., Stewart, W.E., Lightfoot, E.N. "Transport Phenomena." *John Wiley & Sons*, New York, **1960**.

244 Bhouri, M., Goyette, J., Hardy, B., Anton, D.L., "Honeycomb metallic structure for improving heat exchange in hydrogen storage system". *Int. J. Hydrogen Energy*, 36 (11) (**2011**) p. 6723-6738.

245 Richard, M.-A., Bénard, P.,Chahine, R. "Gas adsorption process in activated carbon over a wide temperature range above the critical point. Part 1: modified dubinin-astakhov model." *Adsorption* 15 (**2009**), p. 43-51

246 Richard, M.-A., Bénard, P., Chahine, R. "Gas adsorption process in activated carbon over a wide temperature range above the critical point. Part 2: conservation of mass and energy". *Adsorption* 15, (**2009**), p.53-63.

247 Lemmon, E.W., Huber, M.L., McLinden, M.O. NIST Standard Reference Database 23: Reference Fluid Thermodynamic and Transport Properties-REFPROP, Version 8.0, National Institute of Standards and Technology, Standard Reference Data Program, Gaithersburg, **2007**.

248 Richard, M.-A., Cossement, D., Chandonia, P.-A., Chahine, R., Mori, D., Hirose, K. "Preliminary Evaluation of the Performance of an Adsorption-Based Hydrogen Storage System." *AIChE Journal* 11 (**2009),** p.2985-2996.

249 Paggiaro, R., Michl, F., Bénard, P., Polifke, W. "Cryo-adsorptive hydrogen storage on activated carbon, II: Investigation of the thermal effects during filling at cryogenic temperatures." *Int. J. Hydrogen Energy* 35 (**2010**), p.648-59.

250 Kumar, V.S., Raghunatahan, K., Kumar, S. "A lumped-parameter model for cryo-adsorber hydrogen storage tank." *Int. J. Hydrogen Energy* 34, (**2009**), P.5466-75.

251 Schütz, W., Michl, F., Polifke, W., Paggiaro, R. " Storage systems for storing a medium and method for loading a storage system with a storage medium an emptying the same therefrom." Patent(WO/2005/044454), http://www.wipo.int/pctdb/en/wo.jsp?wo=2005044454;. **2005**

252 Hermosilla-Lara, G., Momen, G., Marty, P.H., Le Neindre, B., Hassouni, K. " Hydrogen storage by adsorption on activated carbon: Investigation of the thermal effects during the charging process*." Int. J. Hydrogen Energy,* 32 (**2007)**, p.1542-53.

253 Momen, G., Hermosilla, G., Michau, A., Pons, M., Firdaus, M., Marty, P.H., Hassouni, K. "Experimental and numerical investigation of the thermal effects during hydrogen charging in a packed bed storage tank." *Int. J. Hydrogen Energy,* 52 (**2009)**, p.1495-1503.

254 Klein, H.P., Groll, M. "Heat transfer characteristics of expanded graphite matrices in metal hydride beds. "*Int. J. Hydrogen Energy*,29 (**2004**) p. 3-11.

255 Sanchez, A.R., Klein, H.P., Groll, M. "Expanded graphite as heat transfer matrix in metal hydride beds." *Int. J. Hydrogen Energy*, 28 (**2003**) p. 515-527.

256 Ichikawa, T., Chen, D.M., Isobe, S., Gomibuchi, E., Fujii, H. "Hydrogen storage properties on mechanically milled graphite." *Materials Science and Engineering B: Solid-State Materials for Advanced Technology*, 108, (**2004**) p. 138-142.

257 Chaise, A., de Rango, P., Marty, P., Fruchart, D., Miraglia, S., Olives, R., et al. "Enhancement of hydrogen sorption in magnesium hydride using expanded natural graphite." *Int. J. Hydrogen Energy*, 34, (**2009**) p. 8589-8596.

258 Kim, K.J., Montoya, B., Razani, A., Lee, K.H. "Metal hydride compacts of improved thermal conductivity." *Int. J. Hydrogen Energy*, 26 (**2001**) p. 609-613.

259 Heung, L. K. "On-board Hydrogen Storage System Using Metal Hydride". HYPOTHESIS II Hydrogen Power, Theoretical and Engineering Solutions, International Symposium. **1997**.

260 Mat, M. D., Kaplan, Y. "Numerical Study of Hydrogen Absorption in an Lm-Ni5 Hydride Reactor." *Int. J. Hydrogen Energy* 26, (**2001**), p. 957-963.

261 Levesque, S., Ciureanu, M., Roberge, R., Motyka, T. "Hydrogen Storage for Fuel Cell Systems with Stationary Applications I. Transient Measurement Technique for Packed Bed Evaluation*". Int. J. Hydrogen Energy* 25 (**2000**), p. 1095-1105.

262 Klein, J. E., Brenner, J. R., Dye, E. F. "Development of a Passively Cooled, Electrically Heated (PACE) Bed." *Fusion Technol*. 41 (**2002**), p.782-787.

263 Kurosaki, K., Maruyama, T., Takahashi, K., Muta, H., Uno, M., and Yamanaka, S. "Design and development of MH actuator system", *Sensors and Actuators A*, 113 (**2004**) p. 118-123.

264 Kim, K.J.**,** Lloyd, G.K., Razani, A., and Feldman, K.T. Jr, "Development of LaNi5/Cu/Sn Metal Hydride Powder Composites"**.** *Powder Technology*, 99 (**1998**) p. 40-45.

265 Ishikawa, H., Oguro, K., Kato, A., Suzuki, H., and Ishii, E., *"*Preparation and properties of hydrogen storage alloys microencapsulated by copper*", J. Less-Common Metals,* 120 (**1986**) p. 123-133.

266 Chen, Y., Sequeira, C. A. C., Chen, C., Wang, X., and Wang, Q., "Metal hydride beds and hydrogen supply tanks as minitype PEMFC hydrogen sources", *Int. J. of Hydrogen Energy*, 28 (**2003**), p. 329-333.

267 Eaton, E, Olsen, C.E., Sheinberg, H., and Steyert, W. A., "Mechanically stable hydride composites designed for rapid cycling", *Int. J. of Hydrogen Energy*, 6(6) (**1981**), p. 609-623.

268 Ron, M., Gruen, D., Mendelsohn, M., and Sheet, I., "Preparation and properties of porous metal hydride compacts", *J. Less-Common Metals*, 74 (**1980**) p. 445-448.

269 Bershadski, E., Josephy, Y., and Ron, M. "Permeability and thermal conductivity of porous metallic matrix hydride compacts", *J. Less-Common Metals*, 153 (**1989**) p. 65-78.

270 Josephy, Y., Eisenberg, Y., Perez. S., Ben-David, A., Ron, M., "Hydrogen and thermal yields of porous matrix hydride compacts of $MmNi_{4:15}Fe_{0:85}H_x$.", *J. Less-Common Metals*, 104 (**1984**) p. 297-305.

271 Nagel, M., Komazaki, Y., and Suda, S. "Effective thermal conductivity of a metal hydride bed augmented with a copper wire matrix*", J. Less-Common Metals*, 120 (**1986**) p. 35-43.

272 Sun, D-W, "Designs of metal hydride reactors", *Int. J. of Hydrogen Energy*, 17(12) (**1992**), p. 945-949.

273 Groll, M., Supper, W., Mayer, U., Brost, O., "Heat and mass transfer limitations in metal hydride reaction beds", *Int. J. of Hydrogen Energy*, Volume 12, Issue 2, (**1987**), p. 89-97

274 Couturier, K., Joppich, F., Wörner, A., and Tamme, R., "Tank Design for On-Board Hydrogen Storage in Metal Hydrides", Proceedings of ES (**2008**), Energy Sustainability 2008, August 10-14, Jacksonville, FL.

275 Johnson, T. and Kanouff, M.P., "Parameter Study of a Vehicle-scale Hydrogen Storage System", SANDIA REPORT, (**2010**), SAND2010-2140, Unlimited Release.

276 Dedrick, D.E., et al., "Heat and mass transport in metal hydride based hydrogen storage systems", **(2009)** *Proceedings of the ASME Summer Heat Transfer Conference*, July 19-23, 2009, San Francisco, California USA.

277 Sanchez, A. R., Klein, H. P., and Groll, M., "Expanded graphite as heat transfer matrix in metal hydride beds", *Int. J. of Hydrogen Energy*, 28, (**2003**), p. 515–527,

278 Definition of "Standard Pressure", IUPAC Compendium of Chemical Terminology. Nic, M., Jirat, J., Kosata, B., eds. (**2006**). DOI:10.1351/goldbook.S05921. ISBN 0-9678550-9-8.

279 Gaskell, D. R., "Introduction to the thermodynamics of materials", Fifth Edition, **(2008)** Taylor & Francis. ISBN 1-59169-043-9.

280 Reprinted with permission from: White, G.K. and Collocott, S.J., "Heat Capacity of Reference Materials: Cu and W", *J. Phys. Chem. Ref. Data*, 13, No. 4, **(1984)** p. 1251-1257. Copyright1984, American Institute of Physics.

281 Wikipedia, "Heat Capacity", http://en.wikipedia.org/wiki/Specific_heat_capacity#Extensive_and_intensive_quantities

282 Article, Chemwiki "The Dynamic Chemistry Textbook", website, University of California, Davis, "Heat Capacity of Solids", http://chemwiki.ucdavis.edu/Physical_Chemistry/Quantum_Mechanics/Heat_Capacity_of_Solids

283 Frenkel, J., "Kinetic Theory of Liquids", Oxford University Press, Oxford, (**1946**).

284 Ziman, J.M., "Models of Disorder", Cambridge University Press, Cambridge, UK, (**1979**).

285 Boon, J.P. and Yip, S., "Molecular Hydrodynamics", Dover, NewYork, (**1980**).

286 March, N.H., "Liquid Metals", Cambridge University Press, Cambridge, UK, (**1990**).

287 Barrat, J.L. and Hansen, J.P., "Basic Concepts for Simple and Complex Liquids" Cambridge University Press, Cambridge, (**2003**).

288 Hansen, J.P. and McDonald, I.R., "Theory of Simple Liquids", Amsterdam, Boston, Elsevier, (**2007**).

289 Landau, L. D. and Lifshitz, E. M., "Statistical Physics" Nauka, Moscow, **(1964)**.

290 Bolmatov, D. and Trachenko, K., "Liquid heat capacity in the approach from the solid state: An harmonic theory", *Physical Rev. B* 84, **(2011)** p. 054106/1-7.

291 Grimvall, G., "The Heat Capacity of Liquid Metals", *Phys. Scr.* 11, **(1975)** p. 381.

292 Wallace, D.C., "Liquid dynamics theory of high-temperature specific heat", *Phys. Rev.* E 57, **(1998)** p. 1717.

293 Dexter, A.R. and Matheson, A.J., "Temperature dependence of heat capacity and viscosity of non-associated liquids", *Trans. Faraday Soc.* 64, **(1968)** p. 2632.

294 Born, M. and Green, H. S. "A General Kinetic Theory of Liquids. I. The Molecular Distribution Functions ", *Proc. R. Soc. London, Ser. A* 188, (**1946**), p. 10.

295 Henderson, D. "The Theory of Liquids and Dense Gases", *Annu. Rev. Phys. Chem.* 15, (**1964**), p. 31.

296 Trachenko, K. "Heat capacity of liquids: An approach from the solid phase ***",*** *Phys. Rev. B* 78, (**2008**), p. 104201.

297 Smith, C.G. "Quantum Physics and the Physics of large systems", *Part 1A Physics*, **(2008)**, University of Cambridge.

298 Diagram from: http://hyperphysics.phy-astr.gsu.edu/hbase/kinetic/shegas.html

299 Davis, C.O. and Johnston, H.L., "Heat Capacity Curves of the Simpler Gases. V. The Heat Capacity of Hydrogen at High Temperatures. The Entropy and Total Energy. A Corrected Table of the Free Energy above 2000°" *J. Am. Chem. Soc.* 56, **(1934)** p. 1045.

300 Woolley, H.W., Scott, R.B., and Brickwedde, F.G., "Compilation of Thermal Properties of Hydrogen in Its Various Isotopic and Ortho-Para Modifications", *J. of Research of the National Bureau of Standards Research*, Paper HP1932, 41, **(1948)** p.379-47, Contribution of the National Institute of Standards and Technolog.

301 Lemmon, E.W., Huber, M.L., McLinden, M.O. NIST Standard Reference Database 23: Reference Fluid Thermodynamic and Transport Properties-REFPROP, Version 9.0, National Institute of Standards and Technology, Standard Reference Data Program, Gaithersburg, **2010**.

302 Younglove, B.A., and Diller, D.E., "The Specific Heat at Constant Volume of Para-Hydrogen at Temperatures from 15 to 90K and Pressures to 340 atm", *Cryogenics* 2(6) (**1962**) p. 348-52.

303 Calculated for normal hydrogen, using "miniREFPROP" software, NIST Standard Reference Database 23, Version 9.1, Authors Lemmon, E.W., Huber, M.L., and McLinden, M.O. (**2012**).

304 "Hydrogen Vehicle Fueling Station," D. E. Daney, F. J. Edeskuty, M. A. Daugherty, F. C. Prenger, and D. D. Hill, Los Alamos National Laboratory, presented at the 17-21 July 95 Cryogenic Engineering Conference in Columbus, OH.

305 James, B.D., Baum, G.N., Lomax, FD. Jr., Thomas, C.E. (Sandy), Kuhn, I.R. Jr. **"**Comparison of Onboard Hydrogen Storage for Fuel Cell Vehicles", (**1996**), Task 4.2 Final Report prepared for Ford Motor Co. under contract DE-AC02-94CE50389, "Direct Hydrogen-Fueled Proton-Exchange-Membrane (PEM) Fuel Cell System for Transportation Applications" to the U.S. Department of Energy.

306 ASTM E1269 – 11, "Standard Test Method for Determining Specific Heat Capacity by Differential Scanning Calorimetry", ASTM International, West Conshohocken, PA, 2003, DOI: 10.1520/E1269-11, www.astm.org.

307 ASTM E967 – 08, "Standard Practice for Temperature Calibration of Differential Scanning Calorimeters and Differential Thermal Analyzers", ASTM International, West Conshohocken, PA, 2003, DOI: 10.1520/E0968-02R08, www.astm.org.

308 Minges, M.L., "Thermal Conductivity", edited by Hust, J.G., **(1983)**, Plenum, New York, Vol. 17, p. 73.

309 White, G.K. and Collecott, S.J., "Heat Capacity of Reference Materials: Cu and W", *J. Phys. Chem. Ref. Data*, 13, No. 4 **(1984)**, p. 1251-1257.

310 Pjpers, T.F.J., Mathot, V.B.F., Goderis, B., et al. "High-speed calorimetry for the study of the kinetics of (de)vitrification, crystallization, and melting of macromolecules." *Macromolecules* 35 (**2002**), p. 3601– 3613.

311 Cerdeirina, C.A., Miguez, J.A., Carballo, E., Tovar, C.A., de la Puente, E., Romani, L., "Highly precise determination of the heat capacity of liquids by DSC: calibration and measurement", *Thermochimica Acta* 347 (**2000**) p. 37-44.

312 Hoehne, G.W.H., Cammenga, H.K., Eysel, W., Gmelin, E., Hemminger, W., "The temperature calibration of scanning calorimeters" *Thermochim. Acta* 160 (**1990**) p.1-12.

313 Cammenga, H.K., Eysel, W., Gmelin, E., Hemminger, W., Hoehne, G.W.H., Sarge, S.M., "The temperature calibration of scanning calorimeters**:** Part 2. Calibration substances" *Thermochim. Acta* 219 (**1993**) p. 333-342.

314 Sarge, S.M., Gmelin, E., Hoehne, G.W.H., Cammenga, H.K., Hemminger, W., Eysel, W. , "The caloric calibration of scanning calorimeters" *Thermochim. Acta* 247 (**1994**) p. 129-168.

315 Sarge, S.M., Hemminger, W., Gmelin, E., Hoehne, G.W.H., Cammenga, H.K., Eysel, W., "Metrologically based procedures for the temperature, heat and heat flow rate calibration of DSC" *J. Therm. Anal.* 49 (**1997**) p. 1125-1134.

316 Gates, J.A., Wood, R.H., Cobos, J.C., Casanova, C., Roux, A.H., Roux-Desgranges, G., and Grolier, J.-P.E., "Densities and heat-capacities of 1-butanol+decane from 298 K to 400 K"., *Fluid Phase Equilibria* 27 (**1986**) p. 137-151.

317 Cobos, J.C., Garcia, I., Casanova, C., Roux, A.H., Roux- Desgranges, G., and Grolier, J.-P.E., *"*Excess heat capacities of 1-butanol + toluene from 298 to 368 K*". Fluid Phase Equilibria* 69 (**1991**) p. 223-233.

318 Tovar, C.A., Carballo, E., Cerdeirina, C.A., Legido, J.L., Romani, L., " Effect of temperature on W-shaped excess molar heat capacities and volumetric properties: Oxaalkane-nonane systems" . *Int. J. Thermophys.* 18 (**1997**) p. 761-777.

319 Benoist, L., Mercier, J., Roux, A.H., Roux-Desgranges, G., Grolier, J.-P.E., V Convegno Nazionale di Calorimetria e di Analisi Termica, Trieste (Italy), 14-16 December **1983**, p. 240.

320 Roux, A.H., Roux-Desgranges, G., Grolier, J.-P.E., Viallard, A., Journal de Calorimetrie et Analyse Thermique, La Gaillarde (France), 16-17 May **1983**, Vol. XIV, p. 142.

321 Giuseppe, D.G., Della Gatta, G., Richardson, M.J., Sarge, S.M., and Stølen, S. "Standards, calibration, and guidelines in microcalorimetry: Part 2. Standards for DSC", Pure Appl. Chem , 78 (7) (**2006**), p. 1455– 1476.

322 Giuseppe, D.G., Della Gatta, G., Richardson, M.J., Sarge, S.M., and Stølen, S. "Standards, calibration, and guidelines in microcalorimetry: Part 2. Standards for DSC", Pure Appl. Chem , 78 (7) (**2006**), p. 1455– 1476.